

# **Chemical Micro Preconcentrators Development for Micro Gas Chromatography Systems**

Bassam Alfeeli

Dissertation submitted to the faculty of the Virginia Polytechnic Institute and State  
University in partial fulfillment of the requirements for the degree of

Doctor of Philosophy

In

Electrical Engineering

Masoud Agah, Chair

Kathleen Meehan

Anbo Wang

Robert W. Hendricks

Larry T. Taylor

October 06 2010

Blacksburg, Virginia

Keywords: Handheld Chemical Analysis, Micro Analytical Systems, Breath Analysis,  
Sample Pretreatment, Tenax TA Films, Microfabrication, DRIE, MEMS

Copyright 2010, Bassam Alfeeli

# Chemical Micro Preconcentrators Development for Micro Gas Chromatography Systems

Bassam Alfeeli

## ABSTRACT

Microelectromechanical systems (MEMS) technology allows the realization of mechanical parts, sensors, actuators and electronics on silicon substrate. An attractive utilization of MEMS is to develop micro instruments for chemical analysis. An example is gas chromatography (GC) which is widely used in food, environmental, pharmaceutical, petroleum/refining, forensic/security, and flavors and fragrances industries. A MEMS-based micro GC ( $\mu$ GC) provides capabilities for quantitative analysis of complex chemical mixtures in the field with very short analysis time and small amounts of consumables.

The aim of this research effort is to enhance the sensitivity and selectivity of  $\mu$ GC instruments by implementing chemical amplification method known as preconcentration. A micro preconcentrator ( $\mu$ PC) extracts the target analytes from the sample matrix, concentrates them, and injects them into the separation column for analysis.

This work resulted in the development of silicon-glass bonded chips consisting of  $7\text{ mm} \times 7\text{ mm} \times 0.38\text{ mm}$  multiport cavity with thousands of embedded 3D microstructures (to achieve high surface-to-volume ratio) coated with polymeric thin film adsorbents. Deep reactive ion etching (DRIE) was the enabling technology for the realization of  $\mu$ PCs. Several coating methods, such as inkjet printing of polymers and polymer precipitation from solution have been utilized to coat complex geometrical structures. One major outcome was the development of cobweb adsorbent structure. Moreover, the porous polymeric adsorbent Tenax TA in the film form was characterized, for the first time, for  $\mu$ PC application and shown to have similar properties to that of the granular form.

Several  $\mu$ PC designs were experimentally evaluated for their performance in concentrating volatile organic compounds, including cancer biomarkers, Propofol (anesthetic agent), environmental pollutants, and chemical warfare simulants. The possibility of utilizing the  $\mu$ PCs in practical applications such breath analysis was also demonstrated.

# **To My Family and The State of Kuwait**

## Acknowledgements

Scientific research is a collaborative work based on accumulated knowledge from previous work, inspiration, and influences from superiors and peers. There have been many people who have helped me achieve my goals, and for that I am forever grateful to them.

None of this work would have borne fruit without the trust, faith and guidance of my adviser, Associate Professor Masoud Agah. His mentorship and support have been invaluable, and his infinite patience is greatly appreciated. I also owe a huge debt of gratitude to the rest of my esteemed Doctorate Committee, Clayton Ayre Professor Anbo Wang (ECE), Professor Emeritus Larry Taylor (Chemistry), Associate Professor Kathleen Meehan (ECE), and Professor Robert Hendricks (ECE/MSE). They have provided various insights into my research and made the major milestones throughout my educational career memorable.

I am eternally grateful to Dr. Mehdi Ashraf-Khorassani of the Analytical Services at the Department of Chemistry for imparting the wealth of his experience in analytical chemistry to me; Mr. Donald Leber of the Center for Microelectronics, Optoelectronics, and Nanotechnology (MicrON) for his availability and readiness to help whenever needed when it come equipment malfunction in the clean room; Mr. Amin Zareian and Mr. Syed Ali, former graduate students of VT MEMS laboratory for being in lockstep with me throughout the most trying of times, working day and night to obtain results; five former undergraduate students of VT MEMS laboratory: Mr. Daniel Cho for his innovative crisscross design and simulation work; Mr. Richard Wilson for his assistance in creating the mask layout for second generation devices; Mr. Daniel Moodie for his assistance in the experimental evaluations, especially his patience in satisfying any request of repeating tests I may have made of him; Mr. Sajan Sharma and Mr. Abhishke Kapoor for building and characterizing the homemade anodic bonder which was invaluable in fabricating the devices. Two current students of VT MEMS laboratory deserve special acknowledgement for accepting to carry the “MEMS-based chemical sensing” baton when it was passed to them: Mr. Shree Narayanan a doctoral student who insists that every problem has a solution and Mr. Daniel Hogg, an undergraduate student who exhibit high level of professionalism; and last but in no way least the rest of VT MEMS group members: Mr. Mehdi Nikkiah, Mr. Phillip Zellner, Mr. Alperen Ketene, Ms. Vaishnavi Srinivasaraghavan, and Dr.

Jeannine Strobl for the enjoyable conversations, scientific or not. Words cannot begin to express my appreciation and gratitude felt towards all members of VT MEMS group, both past and present, for creating a completely unforgettable graduate school experience.

I would also like to thank Mr. Franck Torres-Miguel of Tegal Corp. for his endless technical support to resolve DRIE problems; Mr. Stephen McCartney and Mr. John McIntosh both of the Nanoscale Characterization and Fabrication Laboratory (NCFL) of Virginia Tech Institute for Critical Technology and Applied Science (ICTAS) for providing training and support to electron microscopy; Prof. Gary Pickrell of the Department of Materials Science and Engineering for giving me the privilege to use the materials characterization laboratory to conduct surface area analysis; Prof. Andrea Dietrich of the Department of Civil and Environmental Engineering for letting me use the GC-MS equipment in her lab; Also her research group members Ms. Heather Vereb who courageously took the pledge of evaluating the devices for possible deployment in practical application and Mrs. Jody Smiley who knew everything about GC-MS.

I owe special thanks to the individuals who performed some of the analysis on my behalf or provided me with samples or consultancy: Mr. Frank Cromer of the Analytical Services at the Department of Chemistry for XPS analysis; Dr. Frederick Beyer of the U.S. Army Research Laboratory for XRD analysis; Mr. Richard Johnson of the Macromolecular Science and Engineering for TGA analysis; Mr. Vikas Meka of Convergent Engineering for providing Propofol sample; Mr. Edward Buurman of Buchem B.V. for providing historical background information on Tenax TA; Prof. Randy Heflin of the Department of Physics for many stimulating discussions on coating materials; Also his reach group member Dr. Vaibhav Jain for coating devices with self-assembled nanoparticles; Prof. Gary Rice of the College of William and Mary and his research group for evaluating the performance of devices; Dr. Ron Manginell of Sandia National Laboratories, Prof. Mark Shannon of the University of Illinois, Prof. Edward Zellers of University of Michigan, and Mr. Patrick Lewis of Defiant Technologies for many valuable discussions on micro preconcentration technology.

Another thank you goes to the Department of Electrical and Computer Engineering staff, specifically Ms. Kim Medley, Ms. Becky Semones, and Mr. John Harris, for their administrative support throughout my research. I would like to also thank all the faculty and staff I interacted

with during my residency at Virginia Tech for making this experience a gratifying, enjoyable and highly educational one.

Special thanks also go to the staff at the Kuwait Cultural Attaché Office of the Kuwait Embassy in Washington, DC, especially Mr. Aderson Exumé, Ms. Anneke Chy, and Ms. Stacy Dellinger for their professionalism and stalwart support throughout the duration of my study in the United States.

I would like to profusely thank the Kuwait Institute for Scientific Research for giving me the opportunity to continue of my postgraduate education, which has culminated in my pursuit of a Doctoral Degree. I thank Mr. Hani Qasem, Manager of the Department of Advanced Systems (DAS), whose faith in my abilities and fervent support in procuring my scholarship has my infinite gratitude; DAS staff members for believing in me from the very beginning; Dr. Najj Al-Mutairi, KISR's Director General whom I hope this work will make proud and whose leadership I eagerly look forward to experiencing.

I would also like to extend my sincerest and warmest appreciation to Ms. Mona Al-Failakawi and Mr. Ahmad Al-Failakawi of the Scholarship and Training Department for always being there to represent me in my absence. My heartiest thanks goes to the scholarship committee members: Dr. Mohammad Al-Ramadhan, Mr. Ghanem Al-Shemmari, Dr. Mohmoud Abdul Jawad, Dr. Salah Al-Mazidi, Dr. Abdul Adheem Marafie, Dr. Mohammad Al-Bahou, Dr. Lulwa Ali, Dr. Fatemah Haidar, Ms. Suad Al-Houti, and Ms. Maha Al-Jaser for supporting my scholarship program until the end of this very difficult journey.

Finally, I would like to thank all my friends in Blacksburg and elsewhere for their friendship and emotional support especially Maj. Abdullah Zakariya.

To everyone else who has helped me in anyway but was overlooked, Thank You!

This work has been supported by the National Science Foundation under Award No. CBET-0854242, the Kuwait Institute for Scientific Research, and the Kuwait Foundation for the Advancement of Science.

# Table of Contents

<b>CHAPTER ONE: INTRODUCTION.....</b>	<b>1</b>
<b>1.1 OVERVIEW .....</b>	<b>1</b>
<b>1.2 GAS CHROMATOGRAPHY .....</b>	<b>1</b>
<b>1.3 MICRO GAS CHROMATOGRAPHY .....</b>	<b>3</b>
<b>1.4 PRECONCENTRATION .....</b>	<b>4</b>
<b>1.5 PROBLEM STATEMENT.....</b>	<b>8</b>
<b>1.6 TECHNICAL OBJECTIVES .....</b>	<b>8</b>
<b>REFERENCES .....</b>	<b>9</b>
<b>CHAPTER TWO: TECHNICAL BACKGROUND .....</b>	<b>13</b>
<b>2.1 INTRODUCTION.....</b>	<b>13</b>
<b>2.2 EQUILIBRIUM VS. EXHAUSTIVE PRECONCENTRATION .....</b>	<b>13</b>
<b>2.3 THERMAL DESORPTION .....</b>	<b>14</b>
<b>2.4 ADSORBENT MATERIALS .....</b>	<b>15</b>
<b>2.5 EVOLUTION OF MICRO PRECONCENTRATORS .....</b>	<b>16</b>
<b>2.6 CONCLUSIONS.....</b>	<b>19</b>
<b>REFERENCES .....</b>	<b>20</b>
<b>CHAPTER THREE: MEMS-BASED MULTI-INLET/OUTLET PRECONCENTRATOR COATED BY INKJET PRINTING OF POLYMER ADSORBENTS.....</b>	<b>25</b>
<b>3.1 INTRODUCTION.....</b>	<b>25</b>
<b>3.2 DESIGN AND FABRICATION .....</b>	<b>26</b>
<b>3.3 EXPERIMENTAL SETUP.....</b>	<b>32</b>
<b>3.4 RESULTS AND DISCUSSION .....</b>	<b>34</b>
<b>3.5 CONCLUSIONS.....</b>	<b>38</b>
<b>REFERENCES .....</b>	<b>39</b>
<b>CHAPTER FOUR: MEMS-BASED SELECTIVE PRECONCENTRATION OF TRACE LEVEL BREATH ANALYTES .....</b>	<b>44</b>

4.1	INTRODUCTION.....	44
4.2	PRECONCENTRATION TECHNOLOGY.....	45
4.3	EXPERIMENTAL .....	49
4.4	RESULTS AND DISCUSSION .....	51
4.4.1	PERFORMANCE EVALUATION .....	51
4.4.2	PRECONCENTRATOR BEHAVIOR.....	53
4.4.3	TWO-STEP PRECONCENTRATION.....	55
4.5	CONCLUSION .....	61
	REFERENCES .....	62
	<b>CHAPTER FIVE: EFFECT OF SHAPE, SPACING, AND ARRANGEMENT OF PILLARS ON THE PERFORMANCE OF <math>\mu</math>PCS.....</b>	<b>66</b>
5.1	INTRODUCTION.....	66
5.2	ROLE OF SURFACE AREA AND FLOW PATTERN ON $\mu$ PC PERFORMANCE .....	66
5.3	EXPERIMENTAL SETUP.....	68
5.4	RESULTS AND DISCUSSION .....	69
	REFERENCES .....	71
	<b>CHAPTER SIX: LOW PRESSURE DROP MICRO PRECONCENTRATORS WITH A COBWEB TENAX-TA FILM .....</b>	<b>73</b>
6.1	INTRODUCTION.....	73
6.2	LOW PRESSURE DROP $\mu$ PC DESIGN .....	74
6.3	FABRICATION AND COBWEB COATING.....	77
6.4	EXPERIMENTAL RESULTS .....	78
6.5	CONCLUSIONS.....	81
	REFERENCES .....	81
	<b>CHAPTER SEVEN: EVALUATION OF TENAX TA THIN FILMS AS ADSORBENT MATERIAL FOR MICRO PRECONCENTRATION APPLICATIONS.....</b>	<b>83</b>
7.1	INTRODUCTION.....	83
7.2	MATERIALS AND METHODS .....	86



7.2.1	μPCs DEVELOPMENT .....	86
7.2.2	MATERIALS AND EQUIPMENT .....	87
7.3	RESULTS AND DISCUSSION .....	89
7.3.1	TENAX TA PHYSICAL CHARACTERISTICS.....	89
7.3.1.1	PHYSICAL CHARACTERISTICS OF GRANULAR TENAX TA.....	89
7.3.1.2	PHYSICAL CHARACTERISTICS OF TENAX TA FILMS .....	91
7.3.1.2.1	SCANNING ELECTRON MICROSCOPY ANALYSIS.....	91
7.3.1.2.2	TENAX TA CRYSTALLOGRAPHIC STUDY .....	95
7.3.1.2.3	TENAX TA THERMAL CHARACTERISTICS .....	97
7.3.2	TENAX TA ADSORBENT FILMS EVALUATION .....	97
7.3.2.1	MODES OF UPTAKE IN TENAX TA .....	97
7.3.2.2	TENAX TA FILMS DESORPTION EFFICIENCY .....	101
7.3.2.3	TENAX TA FILMS AFFINITY TO REPRESENTATIVE VOLATILE ORGANIC COMPOUNDS .....	102
7.3.2.4	TENAX TA FILMS CAPACITY .....	103
7.3.2.5	ANALYTE STORAGE TIME ON TENAX TA FILMS .....	104
7.3.2.6	COMPETITIVE ADSORPTION ON TENAX TA FILMS.....	105
7.4	CONCLUSIONS.....	106
	REFERENCES .....	107

**CHAPTER EIGHT: SOLID-PHASE MICROEXTRACTION USING SILICA FIBERS  
COATED WITH TENAX-TA FILMS..... 112**

8.1	INTRODUCTION.....	112
8.2	EXPERIMENTAL SECTION.....	115
8.2.1	CHEMICALS AND INSTRUMENTATION.....	115
8.2.2	TENAX TA FIBERS PREPARATION .....	115
8.2.3	EXTRACTION PROCEDURE .....	115
8.3	RESULTS AND DISCUSSION .....	116
8.3.1	TENAX TA FIBERS.....	116
8.3.2	TENAX TA FILM STABILITY .....	117

8.3.3	CHROMATOGRAPHIC ANALYSIS .....	119
8.4	CONCLUSIONS.....	122
	REFERENCES .....	122
CHAPTER NINE: SUMMARY AND FUTURE DIRECTIONS.....		125
9.1	SUMMARY .....	125
9.2	SIGNIFICANCE OF THE WORK .....	125
9.3	VALIDATION AND SCIENTIFIC PRODUCTION .....	127
9.4	FUTURE DIRECTIONS.....	128
9.4.1	GENERAL REMARKS.....	128
9.4.2	NEW AVENUES.....	129
9.4.2.1	ADSORBENT MATERIAL .....	131
9.4.2.1.1	CONVENTIONAL ADSORBENT .....	131
9.4.2.1.1.1	TENAX TA.....	131
9.4.2.1.1.2	OTHER ADSORBENT MATERIALS.....	131
9.4.2.1.2	UNCONVENTIONAL ADSORBENT FILMS .....	131
9.4.2.2	ENHANCING $\mu$ PC CAPABILITIES.....	132
9.4.2.3	INTEGRATION .....	132
9.4.2.4	APPLICATIONS .....	132
APPENDIX.....		134
A-I ELECTIVE MICRO PRECONCENTRATION OF PROPOFOL FOR ANESTHETIC DEPTH		
MONITORING BY USING SEEDLESS ELECTROPLATED GOLD AS ADSORBENT .....		134
A-II MICRO PRECONCENTRATOR FOR HANDHELD MONITORING OF WATER QUALITY ....		144
A-III ADSORBENT MATERIAL SELECTION .....		149

# List of Figures

<b>FIGURE 1 BLOCK DIAGRAM OF THE MAIN COMPONENTS OF MICROFABRICATED GAS CHROMATOGRAPHY SYSTEM.....</b>	<b>3</b>
<b>FIGURE 2 GC ANALYSIS OF SAMPLE INJECTED USING CONVENTIONAL INJECTOR OF A COMMERCIAL GC SYSTEM.....</b>	<b>5</b>
<b>FIGURE 3 GC ANALYSIS OF SAMPLE INJECTED USING <math>\mu</math>PC DEVELOPED AT VT MEMS, VIRGINIA TECH .....</b>	<b>5</b>
<b>FIGURE 4 AN OVERVIEW OF THE ADSORPTION SYSTEM WITH DEFINITIONS OF THE DIFFERENT TERMS: ADSORPTION, DESORPTION, ADSORPTIVE, ADSORBATE, AND ADSORBENT .....</b>	<b>7</b>
<b>FIGURE 5 COMMERCIAL THERMAL DESORPTION PRECONCENTRATION TUBES.....</b>	<b>16</b>
<b>FIGURE 6 NUMBER OF REPORTS ON <math>\mu</math>PC DEVELOPMENT AS A FUNCTION OF PUBLICATION YEAR .....</b>	<b>17</b>
<b>FIGURE 7 3-D RENDERING OF THE MICROPILLARS BASED <math>\mu</math>PC .....</b>	<b>27</b>
<b>FIGURE 8 CFD SIMULATION OF THE FLOW IN (A) ORDERED SQUARE PILLARS, (B) CRISSCROSS PILLARS, (C) CRISSCROSS PILLARS WITH SINGLE INLET/OUTLET SHOWING THE FLOW PATH, (D) CRISSCROSS PILLARS WITH MULTIPLE INLET/OUTLET SHOWING THE FLOW PATH.....</b>	<b>29</b>
<b>FIGURE 9 STEP BY STEP PROCESSING OF THE WAFER IN CROSS-SECTIONAL VIEW .....</b>	<b>30</b>
<b>FIGURE 10 OPTICAL IMAGE OF THE <math>\mu</math>TPC SHOWING THE FRONT AND BACK SIDES OF THE DEVICE, INSETS ARE SEM MICROGRAPHS OF THE ETCHED 3D STRUCTURES AND THE FLUIDIC PORTS .....</b>	<b>31</b>
<b>FIGURE 11 SEM MICROGRAPHS OF TENAX TA COATED PILLARS .....</b>	<b>32</b>
<b>FIGURE 12 <math>\mu</math>PC TEST SETUP WITH (A) VALVES SET IN THE LOADING POSITION, (B) VALVES SET IN DESORPTION POSITION .....</b>	<b>33</b>
<b>FIGURE 13 DESORPTION PEAKS OF TENAX TA AND PDMS .....</b>	<b>35</b>
<b>FIGURE 14 HEIGHT AND AREA OF THE DESORPTION PEAK AS A FUNCTION OF PRESSURE .....</b>	<b>36</b>
<b>FIGURE 15 SERIES OF <math>\mu</math>PC GENERATED DESORPTION PULSES .....</b>	<b>37</b>
<b>FIGURE 16 HYDROCARBON MIXTURE SAMPLE INJECTION CHROMATOGRAMS (SAMPLE VOLUME 1 <math>\mu</math>L), (A) REPRESENT THE SAMPLE INJECTED THROUGH THE GC'S CONVENTIONAL INJECTION</b>	

PORT WITH A ZOOMED-IN VERSION BELOW IT, (B) REPRESENT THE SAMPLE INJECTED BY THE $\mu$ TPC FAST THERMAL DESORPTION WITH A ZOOMED-IN VERSION BELOW IT .....	38
FIGURE 17 (A) PHOTOLITHOGRAPHY (B) DEEP REACTIVE-ION ETCHING (DRIE) (C) COATING THE PILLARS WITH ADSORBENT POLYMER BY INKJET PRINTING (D) SEALING THE DEVICE WITH PYREX BY ANODIC BONDING (E) PATTERNING OF THIN-FILM RESISTIVE HEATERS AND TEMPERATURE SENSORS OVER PECVD OXIDE AT THE BACK OF THE DEVICE.....	46
FIGURE 18 SEM MONOGRAPHS SHOWING THE COVERAGE AND UNIFORMITY OF TENAX TA COATING TECHNIQUE .....	47
FIGURE 19 OPTICAL IMAGE OF THE $\mu$ PC SHOWING THE FRONT AND BACK SIDES OF THE DEVICE, INSETS ARE SEM MONOGRAPHS OF THE ETCHED 3D STRUCTURES AND THE FLUIDIC PORTS .....	48
FIGURE 20 $\mu$ PC TEST SETUP WITH THE VALVES SET IN THE (A) LOADING POSITION, (B) INJECTION POSITION, AND (C) SEPARATION POSITION .....	50
FIGURE 21 $\mu$ PC SAMPLE PRECONCENTRATION FACTOR AS A FUNCTION OF TIME AT CONSTANT CONCENTRATION OF PURE ISOPROPANOL VAPOR .....	52
FIGURE 22 (A) DESORPTION VS. FLOW RATE AT 35 °C AND (B) DESORPTION VS. TEMPERATURE AT 2 mL/MIN FOR THE FIVE COMPOUNDS USED IN THE EXPERIMENT.....	54
FIGURE 23 SELECTIVE PRECONCENTRATION OF TARGET VOC (BLACK), (A-B) LOW-BOILERS REDUCTION (BLUE & GREEN), (C) HIGH-BOILERS REDUCTION BY FLOW REVERSAL, (D) RELEASE OF CONCENTRATED TARGET VOCs.....	56
FIGURE 24 CHROMATOGRAMS PRODUCED BY DIFFERENT TEMPERATURE CONFIGURATIONS DURING ADSORPTION OF TWO $\mu$ PCs CONNECTED IN SERIES, BOTH DEVICES ARE DESORBED AT THE SAME TIME AND TEMPERATURE, SAMPLE WAS A STANDARD CHROMATOGRAPHIC TEST MIXTURE CONSISTING OF POLAR AND NONPOLAR COMPOUNDS IN DICHLOROMETHANE .....	57
FIGURE 25 CHROMATOGRAM OF THE VOCs MIX WITHOUT $\mu$ PC SHOWING THE LARGE AMOUNT OF 1-PROPANO, INSET IS ZOOM-IN OF THE SEPARATED VOCs .....	58
FIGURE 26 CHROMATOGRAM OF SELECTIVE PRECONCENTRATION OF PROPOFOL. (A) SHOWS THE MAGNITUDE OF THE PEAK, (B) ZOOM-IN OF THE UNPRECONCENTRATED VOCs. REDUCTION IN THE 1-PROPANOL CONTENT IS EVIDENT .....	59
FIGURE 27 ANALYSIS OF INDOOR AIR STANDARD MIXTURE USING SINGLE $\mu$ PC .....	60

<b>FIGURE 28 SELECTIVE PRECONCENTRATION BY TEMPERATURE MANIPULATION ALONE USING SINGLE <math>\mu</math>PC .....</b>	<b>61</b>
<b>FIGURE 29 SELECTIVE PRECONCENTRATION OF N-DECANE, N-UNDECANE, AND N-DODECANE FROM THE INDOOR AIR STANDARD MIXTURE USING THE TWO-STEP PRECONCENTRATION METHOD .....</b>	<b>61</b>
<b>FIGURE 30 3D RENDERING OF THE SILICON-GLASS <math>\mu</math>PC.....</b>	<b>67</b>
<b>FIGURE 31 SEM MICROGRAPHS OF THE FABRICATED SQUARE AND MALTESE-CROSS PILLARS .....</b>	<b>67</b>
<b>FIGURE 32 SIMULATED FLOW VELOCITY PROFILE FOR SQUARE AND MALTESE-CROSS PILLAR DESIGNS, BLUE REGION REPRESENT ZERO VELOCITY .....</b>	<b>68</b>
<b>FIGURE 33 N-NONANE DESORPTION CONCENTRATION FOR THE SQUARE AND MALTESE-CROSS PILLAR DESIGNS AT DIFFERENT PILLAR SPACING (10, 50, AND 100 <math>\mu</math>m), ALL HAVE ORDERED PILLAR ARRANGEMENT, EMPTY RESEMBLES A PILLARS-FREE CAVITY .....</b>	<b>69</b>
<b>FIGURE 34 DESORPTION CONCENTRATION FOR THE MALTESE-CROSS DESIGN AT DIFFERENT PILLAR SPACING (10<math>\mu</math>m AND 100<math>\mu</math>m) AND DIFFERENT PILLAR ARRANGEMENT (ORDERED AND STAGGERED) .....</b>	<b>70</b>
<b>FIGURE 35 GC SEPARATION (RED CHROMATOGRAM) OF 1PPB CANCER BIOMARKERS MIXTURE: (1) PENTANE, (2) BENZENE, (3) HEPTANE, (4) TOLUENE, (5) OCTANE, (6) NONANE, (7) DECANE, (8) UNDECANE, (9) DODACENE, (10) TETRADECANE IN NITROGEN, BLACK CHROMATOGRAM REPRESENTS THE PRECONCENTRATED SAMPLE .....</b>	<b>71</b>
<b>FIGURE 36 THE <math>\mu</math>PC UNIT CELL. ARROWS INDICATE THE FLOW DIRECTION.....</b>	<b>74</b>
<b>FIGURE 37 COMPARISON OF CALCULATED AND EXPERIMENTAL FLOW RATES TO ESTABLISH CONFIDENCE IN THE CFD MODEL.....</b>	<b>75</b>
<b>FIGURE 38 PRESSURE-DROP PROFILE IN THE <math>\mu</math>PC .....</b>	<b>75</b>
<b>FIGURE 39 SIMULATION OF THE FLOW PROFILE THROUGH DIFFERENT DESIGN SPACING ARRANGEMENTS .....</b>	<b>76</b>
<b>FIGURE 40 <math>\mu</math>PC FABRICATION PROCESS FLOW .....</b>	<b>77</b>
<b>FIGURE 41 OPTICAL IMAGE OF THE COBWEB TENAX TA.....</b>	<b>77</b>
<b>FIGURE 42 3D RENDERING OF THE <math>\mu</math>PC, INSETS ARE SEM MICROGRAPHS OF THE FABRICATED MICROSTRUCTURES .....</b>	<b>78</b>

<b>FIGURE 43 SEM IMAGE OF COBWEB TENAX TA ON THE MICRO PARABOLIC REFLECTORS .....</b>	<b>78</b>
<b>FIGURE 44 BENZENE DESORPTION CONCENTRATION FOR THE THREE DESIGNS AS WELL AS THE FIRST GENERATION DESIGN .....</b>	<b>79</b>
<b>FIGURE 45 REPRODUCIBILITY OF <math>\mu</math>PC DESORPTION PULSES.....</b>	<b>80</b>
<b>FIGURE 46 PRECONCENTRATION AND SEPARATION OF A MIXTURE OF (1) TOLUENE, (2) NONANE, (3) DECANE, (4) UNDECANE, (5) DODECANE, (6) TRIDECANE, (7) TETRADECANE, AND (8) PENTADECANE DILUTED IN PENTANE BELOW THE FID DETECTION LIMIT. ....</b>	<b>80</b>
<b>FIGURE 47 A PHOTOGRAPH OF THE <math>\mu</math>PC SHOWING BOTH FRONT AND BACK SIDE WHERE THE HEATERS AND SENSORS ARE LOCATED.....</b>	<b>87</b>
<b>FIGURE 48 SEM MICROGRAPH SHOWING THE STRUCTURE OF THE <math>\mu</math>PC. INSET SHOWS THE UNIFORMITY OF THE INKJET COATING OF TENAX TA .....</b>	<b>87</b>
<b>FIGURE 49 SEM MICROGRAPHS OF TENAX TA BEADS AS RECEIVED, INSETS ARE HIGHER MAGNIFICATION MICROGRAPHS .....</b>	<b>90</b>
<b>FIGURE 50 SEM MICROGRAPHS SHOWING THE NATURE OF POROUS BEADS STRUCTURE, INSET IS HIGHER MAGNIFICATION MICROGRAPH .....</b>	<b>90</b>
<b>FIGURE 51 SEM MICROGRAPHS SHOWING THE DIFFERENT TOPOGRAPHIES OF TENAX TA FILMS. SAMPLES (A-D) WERE PREPARED FROM FROZEN SOLUTION AND DEPOSITED UNDER VACUUM. SAMPLES (E-H) WERE PREPARED FROM SOLUTION AT ROOM TEMPERATURE AND DEPOSITED UNDER AMBIENT ATMOSPHERE .....</b>	<b>92</b>
<b>FIGURE 52 SEM MICROGRAPHS SHOWING TENAX TA FILMS OUTER SURFACE AND INNER STRUCTURE. SAMPLES WERE PREPARED FROM SOLUTION AT ROOM TEMPERATURE AND DEPOSITED UNDER AMBIENT ATMOSPHERE .....</b>	<b>93</b>
<b>FIGURE 53 SEM MICROGRAPHS SHOWING TENAX TA FILM TOPOGRAPHIES AT HIGH MAGNIFICATION. SAMPLES WERE PREPARED FROM FROZEN SOLUTION AND DEPOSITED UNDER VACUUM .....</b>	<b>94</b>
<b>FIGURE 54 XRD PATTERN FOR A TENAX TA FILM DEPOSITED AT 20 °C (PEAK INTENSITIES HAVE BEEN REDUCED FOR CLARITY) .....</b>	<b>96</b>
<b>FIGURE 55 XRD PATTERNS FROM GRANULAR TENAX TA AND FILMS DEPOSITED AT 100 °C... 96</b>	<b>96</b>
<b>FIGURE 56 THERMAL GRAVIMETRIC ANALYSIS OF TENAX FILMS FROM 0 °C TO 1000 °C.....</b>	<b>97</b>
<b>FIGURE 57 MECHANISMS OF ORGANIC COMPOUND UPTAKE BY POLYMERS .....</b>	<b>98</b>

<b>FIGURE 58 BET SURFACE AREA ANALYSIS OF DIFFERENT TENAX TA CONCENTRATION FILMS PREPARED UNDER THE SAME CONDITIONS.....</b>	<b>99</b>
<b>FIGURE 59 FID ANALYSIS OF DESORBED ALKANE SAMPLES FROM TENAX TA FILMS MADE FROM DIFFERENT TENAX TA SOLUTIONS AT CONCENTRATIONS OF 1 mg/mL, 5 mg/mL, AND 10 MG/ML .....</b>	<b>100</b>
<b>FIGURE 60 DESORPTION EFFICIENCY OF ALKANE SAMPLES FROM TENAX TA FILMS MADE FROM DIFFERENT TENAX TA SOLUTIONS AT CONCENTRATIONS OF 1 MG/ML, 5 mg/mL, AND 10 MG/ML .....</b>	<b>101</b>
<b>FIGURE 61 FID ANALYSIS OF DESORBED VOC REPRESENTATIVE SAMPLES ON TENAX TA FILMS .....</b>	<b>102</b>
<b>FIGURE 62 FID ANALYSIS OF COMPETITIVE ADSORPTION BETWEEN 1-PROPANOL AND TOLUENE, N-OCTANE, N-DECANE, N-DODECANE, AND N-TRIDECANE RESPECTIVELY BY ELUTION ORDER .....</b>	<b>106</b>
<b>FIGURE 63 SCHEMATIC DIAGRAM OF STANDARD SPME IN HEADSPACE SAMPLING MODE.....</b>	<b>113</b>
<b>FIGURE 64 SEM MICROGRAPHS OF (A) SILICA FIBER COATED WITH TENAX TA, (B) HIGHER MAGNIFICATION MICROGRAPH SHOWING TENAX TA FILM THICKNESS RESULTED FROM DIPPING THE FIBER IN 100MG/ML SOLUTION .....</b>	<b>116</b>
<b>FIGURE 65 SEM MICROGRAPH SHOWING SIDE VIEW OF TENAX TA COATED FIBER.....</b>	<b>117</b>
<b>FIGURE 66 HIGHER MAGNIFICATION SEM MICROGRAPH OF TENAX TA FILM ON A SILICA FIBER.....</b>	<b>117</b>
<b>FIGURE 67 THERMAL GRAVIMETRIC ANALYSIS OF TENAX TA FILM, 98% WEIGHT LOSS OCCURRED AT 540°C.....</b>	<b>118</b>
<b>FIGURE 68 HEADSPACE ANALYSIS OF N-ALKANES EXTRACTED BY TENAX TA COATED SILICA FIBER.....</b>	<b>119</b>
<b>FIGURE 69 SPME ADSORPTION TIME PROFILE OF 3 μM TENAX TA AND 65 μM PDMS/DVB FILMS FOR UNDECANE SHOWING UPTAKE SATURATION TIME AFTER 25 MIN FOR PDMS/DVB AND 40 MIN FOR TENAX TA .....</b>	<b>120</b>
<b>FIGURE 70 AN OVERVIEW DIAGRAM MAPPING THE DIFFERENT CONTRIBUTIONS OF THIS WORK TO THE μPC TECHNOLOGY .....</b>	<b>126</b>

<b>FIGURE 71 AN OVERVIEW DIAGRAM MAPPING NEW AVENUES TO FURTHER IMPROVE <math>\mu</math>PC TECHNOLOGY .....</b>	<b>130</b>
<b>FIGURE 72 (A) PHOTOLITHOGRAPHY (B) DEEP REACTIVE-ION ETCHING (DRIE) (C) ELECTRODEPOSITION AND PATTERNING OF THE ADSORBENT MATERIAL (D) SEALING THE DEVICE WITH PYREX BY ANODIC BONDING (E) PATTERNING OF RESISTIVE HEATERS AND TEMPERATURE SENSORS OVER PECVD OXIDE AT THE BACK OF THE DEVICE.....</b>	<b>137</b>
<b>FIGURE 73 OPTICAL IMAGES SHOWING THE THE UNIFORM AND CONFORMAL COVERAGE COATING OF ELECTROPLATED GOLD. THE TOP FLAT SURFACES INCLUDING THE TOP OF THE POSTS ARE POLISHED AND SMOOTH FOR ANODIC BONDING. THE POROUSE SURFACE TEXTURE OF THE GOLD LAYER MAXIMIZES THE ADSORBENT SURFACE AREA .....</b>	<b>137</b>
<b>FIGURE 74 OPTICAL IMAGES OF THE <math>\mu</math>PC SHOWING THE FRONT AND BACK SIDES OF THE DEVICE, INSETS ARE SEM MONOGRAPHS OF THE ETCHED MICROSTRUCTURES AND THE FLUIDIC PORTS .....</b>	<b>138</b>
<b>FIGURE 75 <math>\mu</math>PC TEST SETUP WITH THE VALVES SET IN THE (A) LOADING OR SEPERATION POSITION (B) INJECTION POSITION.....</b>	<b>139</b>
<b>FIGURE 76 CHROMATOGRAM OF BREATH REPRESENTATIVE MIXTURE WITHOUT <math>\mu</math>PC SHOWING THE LARGE AMOUNT OF 1-PROPANO, INSET IS ZOOM-IN OF THE SEPARATED VOCs .....</b>	<b>140</b>
<b>FIGURE 77 CHROMATOGRAM OF SELECTIVE PRECONCENTRATION OF PROPOFOL. VOCs WERE NOT PRECONCENTRATED IN THE <math>\mu</math>PC .....</b>	<b>141</b>
<b>FIGURE 78 3D RENDERING OF THE SILICON-GLASS <math>\mu</math>PC.....</b>	<b>144</b>
<b>FIGURE 79 <math>\mu</math>PC FABRICATION PROCESS FLOW, (A) PHOTOLITHOGRAPHY ON SILICON WAFER USING PR9260 FOLLOWED BY ETCHING USING DRIE (B) ADSORBENT DEPOSITION, (C) FORMATION OF COBWEB, (D) ANODIC BONDING, RIGHT, SEM MICROGRAPHS OF THE FABRICATED <math>\mu</math>PC SHOWING THE SQUARE SHAPED <math>\mu</math>-PILLARS .....</b>	<b>145</b>
<b>FIGURE 80 OPTICAL IMAGE OF THE COBWEB TENAX TA, (A) AND (B) ARE A DIFFERENT FOCAL POINTS SHOWING THAT THE COBWEB EXTENDS IN ALL DIRECTION BETWEEN THE <math>\mu</math>-PILLARS</b>	<b>146</b>
<b>FIGURE 81 FID RESPONSE TO THE CONCENTRATED BENZENE FROM THE 10ML WATER SAMPLE. ....</b>	<b>147</b>
<b>FIGURE 82 FID RESPONSE (PEAK AREA) TO THE THREE DIFFERENT SAMPLE VOLUMES ALONG WITH THE 1<math>\mu</math>L SAMPLE OF UNPRECONCENTRATED WATER SAMPLE.....</b>	<b>147</b>



# List of Tables

<b>TABLE 1 PRECONCENTRATION FACTOR FOR DIFFERENT DESIGNS OF UNCOATED <math>\mu</math>PC .....</b>	<b>34</b>
<b>TABLE 2 CALCULATED PILLARS SURFACE AREA AND DENSITY .....</b>	<b>48</b>
<b>TABLE 3 PRECONCENTRATION FACTOR FOR DIFFERENT DESIGNS .....</b>	<b>52</b>
<b>TABLE 4 CALCULATED PILLAR FOOTPRINT AND TOTAL SURFACE AREA PER PILLAR.....</b>	<b>67</b>
<b>TABLE 5 DIFFERENT SPACING ARRANGEMENTS AND THEIR CORRESPONDING SYMMETRY RATIO ALONG WITH THE SIMULATED PRESSURE DROPS AT 1.5mL/MIN FLOW RATE. ....</b>	<b>74</b>
<b>TABLE 6 PERFORMANCE OF DIFFERENT ADSORBENTS UNDER SIMILAR ADSORPTION/DESORPTION CONDITIONS .....</b>	<b>104</b>
<b>TABLE 7 SOME CHARACTERISTICS OF PDMS/DVB AND TENAX-TA FIBERS USED IN THIS WORK .....</b>	<b>120</b>
<b>TABLE 8 STATIC HEADSPACE EXTRACTION OF OCTADECANE SHOWING EXTRACTION REPRODUCIBILITY OF TENAX TA FIBER AT A DESORPTION TEMPERATURE OF 325 °C.....</b>	<b>121</b>
<b>TABLE 9 STATIC HEADSPACE EXTRACTION OF UNDECANE USING A COMMERCIAL CARBOXEN/PDMS/DVB FIBER .....</b>	<b>121</b>
<b>TABLE 10 STATIC HEADSPACE EXTRACTION OF PENTACOSANE USING TENAX TA FIBER AT A DESORPTION TEMPERATURE OF 400 °C .....</b>	<b>122</b>
<b>TABLE 11 OVERVIEW OF THE MAJOR SCIENTIFIC PRODUCTION OF THIS RESEARCH EFFORT.</b>	<b>127</b>
<b>TABLE 12 POROUS POLYMER ADSORBENT SELECTION CHART.....</b>	<b>149</b>

# Chapter One: Introduction

## *1.1 Overview*

Gas phase chemical analysis plays an important role in environmental monitoring, public safety, and process control in manufacturing [1]. Several gas analysis technologies such as spectroscopy, mass-spectrometry, and chromatography have been developed to identify chemical species (analytes) and quantify their concentration. The performance of a chemical analysis is usually evaluated in terms of reversibility, sensitivity, selectivity, response time, and reproducibility [1]. It is necessary to make trade-offs among these various factors when designing an analytical system. While the performance of the detection method is critical to the performance of the complete system, the system itself makes a substantial contribution to the final results obtained. Sensitivity and selectivity, in particular, can be greatly enhanced by a system approach [2]. In this work, we undertake such an approach to enhance the performance of the micro gas chromatography under development.

## *1.2 Gas Chromatography*

Gas chromatography (GC) is a popular analytical chemistry tool commonly employed in the laboratory setting to analyze volatile and semi-volatile organic compounds in the gas phase [3]. GC is a physical method of separating a gaseous mixture without decomposition of the separated analytes. In GC, a moving gas (referred to as mobile phase or carrier) sweeps through a tube (known as separation column) containing an immobilized solid or liquid phase material (referred to as stationary phase). Solid phase material could be inorganic or polymeric material, whereas, liquid phase is gum or gelatin like polymeric material. In the separation column, the mixture is distributed between two phases (mobile and stationary). The part of the mixture in the mobile phase is transported by a carrier gas through the column and the other part of mixture is adsorbed onto the stationary phase. Based upon the kinetics of the adsorption-desorption process in the gas-solid interface in the column, different analytes achieve different moving speeds in the carrier gas to become separated from one another and their matrix. Within a column length, the chemical mixture can be separated into its various analytes and recorded by the detector. The

analytes are identified through their retention times, the traverse time for each of them as they pass through the separation column [3]. GC systems typically include the following key components: flow controller, a sample introduction device (injector), separation column, oven, detectors, and data handling system.

Gas chromatography utilizes a wide variety of detectors. The selection of a detector depends on the target analytes, concentration range and whether qualitative identification or quantitative analysis is desired. Flame ionization detector (FID), mass spectrometer (MS), and electron capture detector (ECD) are the most popular GC detectors with approximate percent uses of 37%, 27% and 21%, respectively [4]. While traditionally ECD has been the method of choice for halogenated compounds, FID is the predominant method for light hydrocarbon analysis. MS is a universal organic compound detector that positively identifies the actual presence of a particular substance in a given sample. Such capability has led to the gradual increase of MS detection in this field [4].

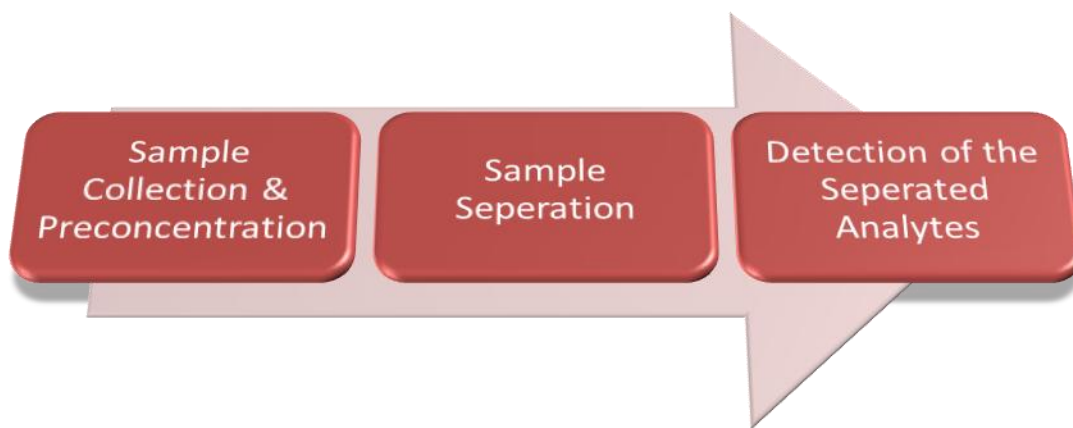
Conventional GC systems are heavy, power-hungry, table-top instruments preventing their use for on-site analysis. Moreover, long analysis time is a major disadvantage of these systems which makes real-time analysis unattainable. Furthermore, there exists a risk of contamination, decomposition, degradation, and loss of analytical sample during storage and transport from the collection site to the laboratory for analysis. This has initiated growing efforts to bring the lab to the sample instead of taking the sample to the lab [5]. The concept of GC miniaturization was introduced in late 1970s [6]. However, it should be noted that only recent advancements in microfabrication technologies have enabled significant development towards realizing micro GCs ( $\mu$ GC) as sophisticated handheld chemical analyzers.

The function of a  $\mu$ GC is to provide capabilities for quantitative analysis of complex chemical mixtures in the field with very short analysis time and small amounts of consumables. For example, in environmental applications, portable  $\mu$ GCs can be used in monitoring process emissions from incinerators and strippers and for detecting emissions that can migrate off site.  $\mu$ GC can also be used during chemical emergencies to provide data for effective public safety decisions. As the threats from terrorists grow,  $\mu$ GC can find applications in detection of explosives and chemical agents in various public facilities and buildings. Noninvasive medical

diagnostic testing can employ  $\mu$ GC systems for the detection of metabolites, such as breath volatiles. Similar handheld systems may find application in medical screening for certain diseases like cancer or diabetes. Moreover, as the petrochemical industry strives to be more efficient and gain competitive edges, rapid process monitoring and early detection of deviations from normal compositions in feed streams can be used in a plant operational feedback control system. Thus,  $\mu$ GC can become an integral part of the plant control system, providing higher operating efficiency that requires analyses of samples at the process stream rather than in a centralized laboratory [7].

### *1.3 Micro Gas Chromatography*

The  $\mu$ GC system consistent with a conventional GC system consists of three main components (shown in Figure 1) which enables the capture, injection, separation, and detection of gaseous mixtures.



**Figure 1 Block diagram of the main components of microfabricated gas chromatography system**

The first component serves as the sample collection and injection device, commonly referred to in the  $\mu$ GC community as the preconcentrator, which is the focus of this dissertation. The second component is the separation column which is responsible for the separation of the chemical mixture to be analyzed. The last component is the detector, which could be a single or

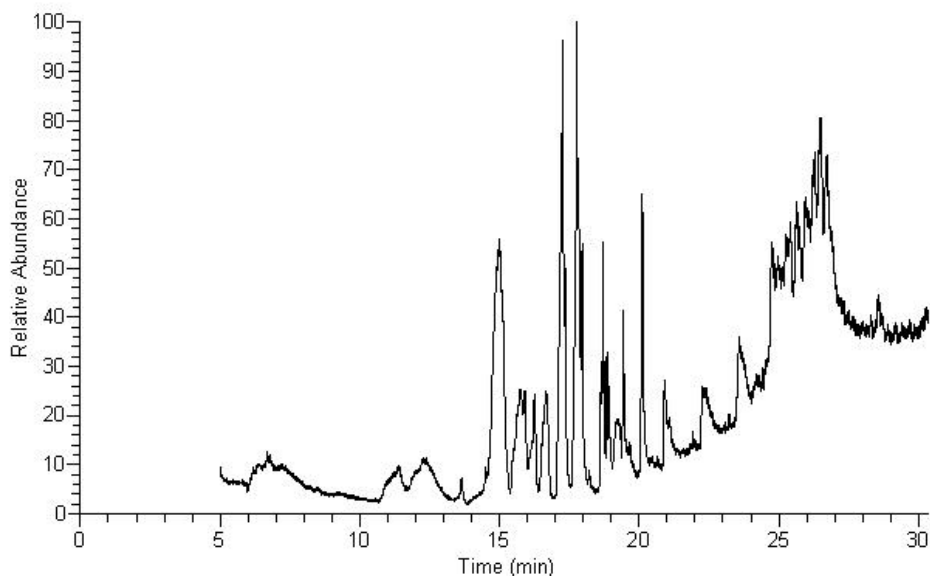
an array of detectors that would resolve the eluted analytes. Through the utilization of silicon micromachining technology, preconcentrators [8-21], separation columns [22-32], and detectors, such as micro thermal conductivity detector, micro flame ionization detector, surface acoustic wave, chemiresistors, and micro differential mobility spectrometer [33-40] for chromatographic gas analysis have been developed.

Although substantial reduction in size has been achieved, the potential for increases in analysis speed and detection performance have not yet been fully realized. Attempting to analyze concentration levels in the parts-per-billion (ppb) to parts-per-trillion (ppt) range of the target analytes in a matrix is difficult regardless of the analytical method used. Thus, to achieve detection limits in this concentration range, preconcentration is required. Preconcentration methods do not only improve the limits of detection of the system, thereby facilitating analysis of trace compounds, but can also bridge the gap that exists between the sample collection and analysis. Moreover, target analytes never exist alone. They exist as part of a sample matrix which contains other analytes not of interest, but can interfere with the instrumentation or analysis. For example, samples taken from the ambient environment contain air, water vapor, background pollutants, and particulate matter. Thus, in general, analytical methods involve a sample preparation step to separate the target analytes from the matrix and concentrate them before analyzing them. This is necessary to get the sample into a form compatible with the analytical instrument. Sample preparation is typically done in a laboratory setting by a trained technician. Well over 80% of the analysis time is spent on sample preparation [41]. Also, since humans are involved in this step, sample preparation is the most error-prone and labor-intensive task in the analytical laboratory. A preconcentrator in a micro analytical system takes the role of the laboratory technician in analytical laboratory. It extracts the target analytes from the sample matrix, concentrates them, and injects them into the separation column.

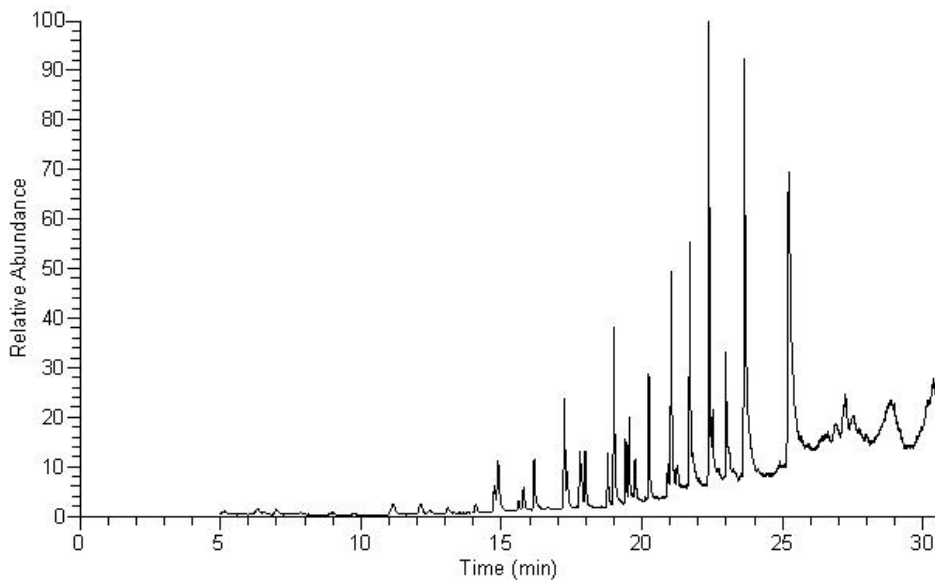
#### *1.4 Preconcentration*

Preconcentration, the process of target analyte enrichment and reduction of interferences, can be achieved by collecting (or trapping) the target analytes over a period of time and then releasing them in the form of a narrow, highly concentrated plug for subsequent chemical analysis. It is noteworthy that narrow injection plugs enhance chromatographic separation

performance. To illustrate, a comparison of GC analysis done by two injection methods is shown in Figure 2 and Figure 3. The first analysis was done by injecting the sample into the separation column using a conventional injector of a commercial GC system and the second one using a  $\mu$ PC developed at Virginia Tech MEMS Laboratory. The sharp plug injection of the  $\mu$ PC resulted in chromatogram with sharper and distinctively resolved peaks.



**Figure 2 GC analysis of sample injected using conventional injector of a commercial GC system**

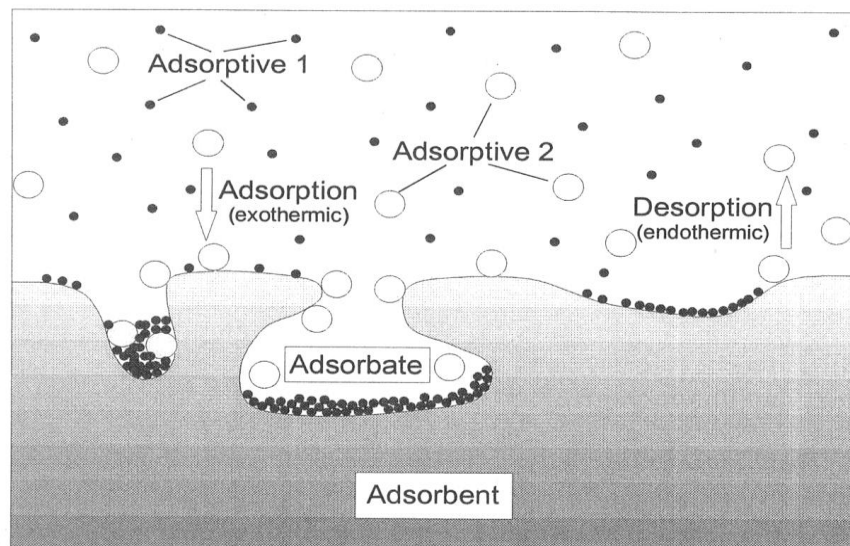


**Figure 3 GC analysis of sample injected using  $\mu$ PC developed at VT MEMS, Virginia Tech**

Two main preconcentration methods are mostly used when dealing with gas-phase samples: cryogenic or sorption trapping. The word “sorption” is used as a general term for indicating adsorption and absorption, which could take place simultaneously. Other methods such as solvent or membrane extraction are also used [42]. Trapping by cryogenic condensation is done by passing the sample through a cooled tube, usually filled with glass beads to provide large surface area. The cooling is done with cryogenic fluids, with which trapping temperatures between  $-150\text{ }^{\circ}\text{C}$  to  $-170\text{ }^{\circ}\text{C}$  are achieved [43]. This method is not currently practical for  $\mu\text{GC}$  systems. However, pseudo- cryogenic trapping using microfabricated thermoelectric coolers [44] can be implemented (see Section 9.4.2.2). Temperatures reached with these systems are typically within the  $+10\text{ }^{\circ}\text{C}$  to  $-30\text{ }^{\circ}\text{C}$  range. In those circumstances, cryogenic preconcentration is only possible in combination with sorbent agents. Sorption trapping relies on sorption phenomena, which include [45]:

- Adsorption
- Absorption
- Chemical adsorption
- Capillary condensation of gaseous analytes
- Dissolved substances on solid or liquid adsorbent

Adsorption is a phenomenon that depends on surface properties and the amount of surface available for adsorption is critical. Figure 4 gives an overview of the adsorption system and defines the terms adsorption, desorption, adsorptive, adsorbate, and adsorbent. The entire adsorbent surface may not be available for adsorption, particularly when the surface of the adsorbent is microporous (less than 2 nm pore size), as molecules might be too large to enter the pores [46]. Because the amount of surface is related to the porosity of a material, adsorbents with very high surface areas are desirable.



**Figure 4 An overview of the adsorption system with definitions of the different terms: adsorption, desorption, adsorptive, adsorbate, and adsorbent [47], Used under the Fair-Use Provision of Copyright Law**

Trapping onto sorbents, either by active or passive sampling, is a well established sample preparation technique. Active sampling is performed by pumping air through a bed of sorbent(s), at a rate typically in the 10-100 mL/min range for a period in the order of minutes. In passive (diffusive) sampling, sorbent material is exposed to air for a period in the order of days [48]. Once enough analytes have been obtained, it is necessary to desorb them for injection into the separation column. When preconcentrating using the sorption method, the sorbent can be thermally desorbed directly into the carrier gas. Conventional thermal desorption preconcentration has disadvantages when compared to cryogenic methods, including analyte residuals and poor heat transfer, which results in high power consumption. These shortcomings result in inefficient desorption and necessitate refocusing of the analytes prior to separation to obtain high peak resolution. Therefore, miniaturization of such devices is highly desirable. Miniature preconcentrators provide high peak resolution at the GC stage and even offer on-line automation [42]. This dissertation focuses on the design, fabrication, and evaluation of a microfabricated preconcentrator ( $\mu$ PC) for  $\mu$ GC systems. It is noteworthy that  $\mu$ PCs can also be used with various micro and macro detection systems to enhance their performance.



### *1.5 Problem Statement*

There are technical barriers that must be overcome before realizing high performance  $\mu$ PCs. The first barrier is the trade-off between miniaturization and sample capacity. Reducing the device size limits the available surfaces for adsorption, which in turn limits the amount of analytes that can be trapped by the  $\mu$ PCs. High density packing of porous granular adsorbent into the  $\mu$ PCs enhances the surface-to-volume ratio but it comes at the cost of large pressure drop and poor heat transfer from the  $\mu$ PC walls to granules. Furthermore, entraining and packing relatively large adsorbent particles within microfabricated structures is not a trivial task. The harsh conditions of granular adsorbent packing, such as high pressure and the application of ultrasonication to achieve good packing density usually cannot be tolerated by microstructures within the  $\mu$ PC or chip packaging technology. Coating  $\mu$ PCs with film based adsorbents is also not a straight forward task especially with the dilemma of finding a coating method that is compatible with both the adsorbent material and the microfabrication process.

Another challenge is to develop and package a robust microfabricated device capable of handling harsh thermal cycling (rapid heating and cooling between 20-300 °C) using the available microfabrication tools on campus. Moreover, interfacing such a micro device with macro world for performing chromatographic evaluations are not easy tasks.

### *1.6 Technical Objectives*

The specific technical objectives for this research are given below:

- Design and fabricate high surface-to-volume-ratio  $\mu$ PCs
- Develop a suitable coating method to cover the micro structures with adsorbent material
- Evaluate experimentally the performance of the device
- Demonstrate the utility of  $\mu$ PCs in practical applications

A detailed discussion of  $\mu$ PC development evolution, fabrication, and research accomplishments is given in the following chapters. **It should be noted that all reported results in this dissertation are within 10-15% accuracy unless mentioned otherwise.**

## References

- [1] J. Fraden, *Handbook of Modern Sensors : Physics, Designs, and Applications*, 2nd ed. ed. vol. xiv, 556 p. .: Woodbury, N.Y. .: American Institute of Physics, 1996.
- [2] J. W. Grate, S. L. Rose-Pehrsson, D. L. Venezky, M. Klusty, and H. Wohltjen, "Smart Sensor System for Trace Organophosphorus and Organosulfur Vapor Detection Employing a Temperature-Controlled Array of Surface Acoustic Wave Sensors, Automated Sample Preconcentration, and Pattern Recognition," *Analytical Chemistry*, vol. 65, 1993, pp. 1868-1881.
- [3] R. L. Grob and E. F. Barry, *Modern Practice of Gas Chromatography*, 4th ed. Hoboken: Wiley-Interscience, 2004.
- [4] D. Helmig, "Air Analysis by Gas Chromatography," *Journal of Chromatography A*, vol. 843, 1999, pp. 129-146.
- [5] F. L. Dorman, J. J. Whiting, J. W. Cochran, and J. Gardea-Torresdey, "Gas Chromatography," *Analytical Chemistry*, vol. 82, 2010, pp. 4775-4785.
- [6] S. C. Terry, J. H. Jerman, and J. B. Angell, "A Gas Chromatographic Air Analyzer Fabricated on a Silicon Wafer," *IEEE Transactions on Electron Devices*, vol. 26, 1979, pp. 1880-1886.
- [7] E. B. Overton, H. P. Dharmasena, U. Ehrmann, and K. R. Carney, "Trends and Advances in Portable Analytical Instrumentation," *Field Analytical Chemistry & Technology*, vol. 1, 1996, pp. 87-92.
- [8] M. Kim and S. Mitra, "A Microfabricated Microconcentrator for Sensors and Gas Chromatography," *Journal of Chromatography A*, vol. 996, 2003, pp. 1-11.
- [9] C. E. Davis, C. K. Ho, R. C. Hughes, and M. L. Thomas, "Enhanced Detection of M-Xylene Using a Preconcentrator with a Chemiresistor Sensor," *Sensors and Actuators B: Chemical*, vol. 104, 2005, pp. 207-216.
- [10] R. R. Lima, R. A. M. Carvalho, A. P. N. Filho, M. L. P. Silva, and N. R. Demarquette, "Production and Deposition of Adsorbent Films by Plasma Polymerization on Low Cost Micromachined Non-Planar Microchannels for Preconcentration of Organic Compound in Air," *Sensors and Actuators B: Chemical*, vol. 108, 2005, pp. 435-444.
- [11] W.-C. Tian, H. K. L. Chan, L. Chia-Jung, S. W. Pang, and E. T. Zellers, "Multiple-Stage Microfabricated Preconcentrator-Focuser for Micro Gas Chromatography System," *Journal of Microelectromechanical Systems*, vol. 14, 2005, pp. 498-507.
- [12] E. W. Simoes, S. G. de Souza, M. L. P. da Silva, R. Furlan, and H. E. Maldonado Peres, "Study of Preconcentration of Non-Polar Compounds in Microchannels with Constrictions," *Sensors and Actuators B: Chemical*, vol. 115, 2006, pp. 232-239.
- [13] C. Pijolat, M. Camara, J. Courbat, J. P. Viricelle, D. Briand, and N. F. de Rooij, "Application of Carbon Nano-Powders for a Gas Micro-Preconcentrator," *Sensors and Actuators B: Chemical*, vol. 127, 2007, pp. 179-185.

- [14] M. Martin, M. Crain, K. Walsh, R. A. McGill, E. Houser, J. Stepnowski, S. Stepnowski, H.-D. Wu, and S. Ross, "Microfabricated Vapor Preconcentrator for Portable Ion Mobility Spectroscopy," *Sensors and Actuators B: Chemical*, vol. 126, 2007, pp. 447-454.
- [15] A. M. Ruiz, I. Gracia, N. Sabate, P. Ivanov, A. Sanchez, M. Duch, M. Gerboles, A. Moreno, and C. Cane, "Membrane-Suspended Microgrid as a Gas Preconcentrator for Chromatographic Applications," *Sensors and Actuators A: Physical*, vol. 135, 2007, pp. 192-196.
- [16] S. Li, J. C. Day, J. J. Park, C. P. Cadou, and R. Ghodssi, "A Fast-Response Microfluidic Gas Concentrating Device for Environmental Sensing," *Sensors and Actuators A: Physical*, vol. 136, 2007, pp. 69-79.
- [17] Y. Junghoon, C. R. Field, B. Byunghoon, R. I. Masel, and M. A. Shannon, "The Design, Fabrication and Characterization of a Silicon Microheater for an Integrated Mems Gas Preconcentrator," *Journal of Micromechanics and Microengineering*, vol. 18, 2008, p. 125001 (125012 pp.).
- [18] I. Gràcia, P. Ivanov, F. Blanco, N. Sabaté, X. Vilanova, X. Correig, L. Fonseca, E. Figueras, J. Santander, and C. Cané, "Sub-Ppm Gas Sensor Detection Via Spiral M-Preconcentrator," *Sensors and Actuators B: Chemical*, vol. 132, 2008, pp. 149-154.
- [19] R. P. Manginell, D. R. Adkins, M. W. Moorman, R. Hadizadeh, D. Copic, D. A. Porter, J. M. Anderson, V. M. Hietala, J. R. Bryan, D. R. Wheeler, K. B. Pfeifer, and A. Rumpf, "Mass-Sensitive Microfabricated Chemical Preconcentrator," *Journal of Microelectromechanical Systems*, vol. 17, 2008, pp. 1396-1407.
- [20] I. Voiculescu, M. Zaghoul, and N. Narasimhan, "Microfabricated Chemical Preconcentrators for Gas-Phase Microanalytical Detection Systems," *TrAC Trends Anal. Chem.*, vol. 27, 2008, pp. 327-343.
- [21] B. Alfeeli, D. Cho, M. Ashraf-Khorassani, L. T. Taylor, and M. Agah, "Mems-Based Multi-Inlet/Outlet Preconcentrator Coated by Inkjet Printing of Polymer Adsorbents," *Sensors and Actuators B, Chemical*, vol. 133, 2008, pp. 24-32.
- [22] S. Zampolli, I. Elmi, J. Stürmann, S. Nicoletti, L. Dori, and G. C. Cardinali, "Selectivity Enhancement of Metal Oxide Gas Sensors Using a Micromachined Gas Chromatographic Column," *Sensors and Actuators B: Chemical*, vol. 105, 2005, pp. 400-406.
- [23] M. Agah, G. R. Lambertus, R. Sacks, and K. Wise, "High-Speed Mems-Based Gas Chromatography," *Journal of Microelectromechanical Systems*, vol. 15, 2006, pp. 1371-1378.
- [24] M. Agah and K. D. Wise, "Low-Mass Pecvd Oxynitride Gas Chromatographic Columns," *Journal of Microelectromechanical Systems*, vol. 16, 2007, pp. 853-860.
- [25] J. A. Potkay, G. R. Lambertus, R. D. Sacks, and K. D. Wise, "A Low-Power Pressure- and Temperature-Programmable Micro Gas Chromatography Column," *Journal of Microelectromechanical Systems*, vol. 16, 2007, pp. 1071-1079.

- [26] A. Bhushan, D. Yemane, D. Trudell, E. Overton, and J. Goettert, "Fabrication of Micro-Gas Chromatograph Columns for Fast Chromatography," *Microsystem Technologies*, vol. 13, Feb. 2007, pp. 361-368.
- [27] S.-I. Ohira and K. Toda, "Micro Gas Analyzers for Environmental and Medical Applications," *Analytica Chimica Acta*, vol. 619, 2008, pp. 143-156.
- [28] M. A. Zareian-Jahromi, M. Ashraf-Khorassani, L. T. Taylor, and M. Agah, "Design, Modeling, and Fabrication of Mems-Based Multicapillary Gas Chromatographic Columns," *Journal of Microelectromechanical Systems*, vol. 18, 2009, pp. 28-37.
- [29] S. Ali, M. Ashraf-Khorassani, L. T. Taylor, and M. Agah, "Mems-Based Semi-Packed Gas Chromatography Columns," *Sensors and Actuators B, Chemical*, vol. 141, 2009, pp. 309-315.
- [30] G. Serrano, H. Chang, and E. T. Zellers, "A Micro Gas Chromatograph for High-Speed Determinations of Explosive Vapors," in *International Conference on Solid-State Sensors, Actuators and Microsystems, TRANSDUCERS'09*, 2009, pp. 1654-1657.
- [31] A. D. Radadia, A. Salehi-Khojin, R. I. Masel, and M. A. Shannon, "The Fabrication of All-Silicon Micro Gas Chromatography Columns Using Gold Diffusion Eutectic Bonding," *Journal of Micromechanics and Microengineering*, 2010, p. 015002.
- [32] M. A. Zareian-Jahromi and M. Agah, "Microfabricated Gas Chromatography Columns with Mono-Layer Protected Gold Stationary Phases," *Journal of Microelectromechanical Systems*, vol. 19, 2010, pp. 294-304.
- [33] I. Simon and M. Arndt, "Thermal and Gas-Sensing Properties of a Micromachined Thermal Conductivity Sensor for the Detection of Hydrogen in Automotive Applications," *Sensors and Actuators A: Physical*, vol. 97-98, 2002, pp. 104-108.
- [34] G. R. Lambertus, C. S. Fix, S. M. Reidy, R. A. Miller, D. Wheeler, E. Nazarov, and R. Sacks, "Silicon Microfabricated Column with Microfabricated Differential Mobility Spectrometer for Gc Analysis of Volatile Organic Compounds," *Analytical Chemistry*, vol. 77, 2005, pp. 7563-7571.
- [35] D. Cruz, J. P. Chang, S. K. Showalter, F. Gelbard, R. P. Manginell, and M. G. Blain, "Microfabricated Thermal Conductivity Detector for the Micro-Chemlab," *Sensors and Actuators B: Chemical*, vol. 121, 2007, pp. 414-422.
- [36] W. J. Kuipers and J. Muller, "A Planar Micro-Flame Ionization Detector with an Integrated Guard Electrode," *Journal of Micromechanics and Microengineering*, 2008, p. 064015.
- [37] B. C. Kaanta, H. Chen, G. Lambertus, W. H. Steinecker, O. Zhdaneev, and X. Zhang, "High Sensitivity Micro-Thermal Conductivity Detector for Gas Chromatography," in *International Conference on Micro Electro Mechanical Systems, MEMS'09*, 2009, pp. 264-267.
- [38] F. I. Bohrer, E. Covington, C. Kurdak, and E. T. Zellers, "Nanoscale Chemiresistor Arrays with Patterned Nanoparticle Interface Layers for Micro Gas Chromatography," in *International Solid-State Sensors, Actuators and Microsystems Conference, TRANSDUCERS'09*, 2009, pp. 148-151.

- [39] S. Narayanan, B. Alfeeli, and M. Agah, "A Micro Gas Chromatography Chip with an Embedded Non-Cascaded Thermal Conductivity Detector," *Procedia Engineering*, vol. 5, 2010, pp. 29-32.
- [40] G. C. Frye-Mason, R. P. Manginell, E. J. Heller, C. M. Matzke, S. A. Casalnuovo, V. M. Hietala, R. J. Kottenstette, P. R. Lewis, and C. C. Wong, "Microfabricated Gas Phase Chemical Analysis Systems," in *Microprocesses and Nanotechnology Conference*, Yokohama, Japan, 1999, pp. 60-61.
- [41] G. Vas and K. Vékey, "Solid-Phase Microextraction: A Powerful Sample Preparation Tool Prior to Mass Spectrometric Analysis," *Journal of Mass Spectrometry*, vol. 39, 2004, pp. 233-254.
- [42] K. Demeestere, J. Dewulf, B. De Witte, and H. Van Langenhove, "Sample Preparation for the Analysis of Volatile Organic Compounds in Air and Water Matrices," *Journal of Chromatography A*, vol. 1153, 2007, pp. 130-144.
- [43] B. Kolb, "Headspace Sampling with Capillary Columns," *Journal of Chromatography A*, vol. 842, 1999, pp. 163-205.
- [44] D. Koester, R. Venkatasubramanian, B. Conner, and G. J. Snyder, "Embedded Thermoelectric Coolers for Semiconductor Hot Spot Cooling," in *Intersociety Conference on Thermal and Thermomechanical Phenomena in Electronics Systems, IThERM'06*, 2006, pp. 491-496.
- [45] Z. B. Alfassi and C. M. Wai, Eds., *Preconcentration Techniques for Trace Elements*. Boca Raton :: CRC Press, 1992.
- [46] M. Harper, "Sorbent Trapping of Volatile Organic Compounds from Air," *Journal of Chromatography A*, vol. 885, 2000, pp. 129-151.
- [47] J. U. Keller and R. Staudt, *Gas Adsorption Equilibria: Experimental Methods and Adsorptive Isotherms*. New York: Springer, 2005.
- [48] M. R. Ras, F. Borrull, and R. M. Marcé, "Sampling and Preconcentration Techniques for Determination of Volatile Organic Compounds in Air Samples," *TrAC Trends in Analytical Chemistry*, vol. 28, 2009, pp. 347-361.

## Chapter Two: Technical Background

### 2.1 Introduction

As mentioned in chapter one, the usefulness of  $\mu$ GC systems relies on their ability to identify and quantify very low concentrations (or trace analytes). In general, the term “trace analytes” refers to concentration below 100  $\mu\text{g/g}$  or 100 ppm and ultra-trace analytes at concentration below 10 ng/g or 10 ppb [1]. A 1 ppm amount of hydrocarbon in air is equivalent to about 3 ng/mL [2]. Based on the sensitivity of current GC detectors one needs to introduce at least 10 mL of air to the detector to obtain a measurable signal. This is a rather large volume in the micro world. A preconcentration step is therefore necessary, in which the captured analytes are desorbed into a much smaller volume. The highly concentrated and reduced volume would be compatible for  $\mu$ GC analysis. The performance of any preconcentration technique is generally characterized by the term known as the preconcentration factor (PF). If before the preconcentration step we have a sample with analytes at concentration  $C_0$ , and after the procedure of the preconcentration the concentration of analytes is  $C_f$ , then the preconcentration factor is given by:

$$PF = \frac{C_f}{C_0}$$

This chapter provides some technical background to aid with understanding of this research work.

### 2.2 Equilibrium vs. Exhaustive Preconcentration

Preconcentration can be categorized into exhaustive preconcentration and equilibrium based (or non-exhaustive) preconcentration [3]. Exhaustive based preconcentrators, as the name indicates, are designed to capture all of the analyte from a given sample volume. This is achieved by passing the sample through a tube packed with a granular adsorbent material. Here, all analytes are transferred from the sample matrix to the adsorbent and nothing, except carrier gas, is allowed to pass through during the collection stage. Thus, care should be taken during operation not to exceed the predetermined maximum sample volume (also known breakthrough

volume). Exhaustive based preconcentrators are advantageous as one can obtain quantitative trapping of the analytes onto the adsorbent. However, this configuration suffers from large pressure drop (requires large backpressure) and poor heat transfer from the heating element to center of the packed bed. Desorption difficulties may also arise when analytes have high affinity to the adsorbent [3].

In equilibrium based preconcentration, analytes are not completely extracted from the sample matrix. The analytes are absorbed or adsorbed by the sorbent film until equilibrium is reached in the system [4, 5]. There is no need to measure the volume of the sample; therefore, this method can be used directly for quantification of target analytes. This configuration has the advantages of low pressure drop and good heat transfer from the heating element to the adsorbent film. The lower power requirements of this category make it more suitable for microsystems. The work in this dissertation falls under the category of equilibrium based preconcentration.

### *2.3 Thermal Desorption*

Thermal desorption is achieved by rapidly heating the sorbent to release the trapped analytes. When compared to other desorption methods, it is simple to implement, provides high concentration factors, and is suitable for  $\mu$ GC analysis. It is true that thermal desorption can decompose the trapped analytes or degrade the sorbent over time. However, the increase in sensitivity achieved with this method outweighs the potential disadvantage [2, 6]. There are several factors that could influence the sharpness of the injection plug and/or the efficiency of desorption (analyte recovery). These factors include heating rate, final temperature, time duration at this temperature, and flow rate [6, 7]. One should note that the sorbent material can also affect how efficiently the trapped analytes can be recovered. The efficiency of desorption is defined as the ratio of the desorbed analyte mass to the adsorbed mass [8]. The final temperature is dictated by thermal stability of the adsorbent and its impacts on the adsorbed analytes [6, 9]. Exceeding the maximum temperature of the analytes and/or the sorbent can result in the decomposition of the analytes and loss of sorbent material. Optimizing desorption conditions for both narrow injection plugs and high desorption efficiency should be considered when designing and operating  $\mu$ PCs. However, this topic is outside the scope of this dissertation.

## 2.4 Adsorbent Materials

There is a great variety of commercially available materials that can be used as adsorbents. The user is often faced with the difficulty of selecting an appropriate adsorbent. In general, the adsorbent used should meet the following criteria [10]:

- The ability to trap analytes of interest. The specific surface area and the porous structure give a rough indication of the adsorption strength of a material.
- Complete and fast desorption of the analytes.
- Homogenous and inert surface to avoid artifact formation, irreversible adsorption, and catalytic effects during sampling, storage of the loaded adsorbent tubes, and desorption.
- Low affinity to water to avoid displacement and hydrolysis reactions and to minimize disturbances of the gas chromatographic analysis (damage of the stationary phase).
- Low affinity for other inorganic constituents of air such as nitrogen oxide, sulfur dioxide, carbon dioxide, or ozone.
- High inertness against reactive species, such as ozone.
- High mechanical and thermal stability.
- Reusability.

Adsorbents can be classified into three categories: inorganic materials, carbon based adsorbents, and organic polymers. Inorganic and carbon based materials are out of the scope of this research and are not discussed further. However, Supelco, a subsidiary of Sigma Aldrich Inc., one of the leading enterprises serving the commercial adsorbents market provides a technical report which lists the available adsorbents and their properties. The report also includes retention and desorption data for 43 different VOCs to aid in choosing the right adsorbent for a given application. These materials include graphitized carbons, carbon molecular sieves, porous polymers, and other adsorbents, including glass beads and charcoal [11]. Porous organic polymers are a large group of adsorbents with different surface areas and polarities. Many of these adsorbents have their origin as stationary phase in packed GC columns. A characterization of common porous polymers is given in Table 12 in the appendix [12-14]. It should be noted that



polydimethylsiloxane (PDMS) is not an adsorbent material since analyte trapping in this material is based on an absorption process [10].

Due to the controllable manufacturing process, porous polymers are mostly very pure materials. A serious drawback is the limited temperature stability of several adsorbents restricting the application of thermal desorption. The polymer poly-(2,6-diphenyl-p-phenylene oxide) or Tenax TA is the most important material for air analysis among the porous polymers and will be discussed in Chapter 7.

### 2.5 Evolution of Micro Preconcentrators

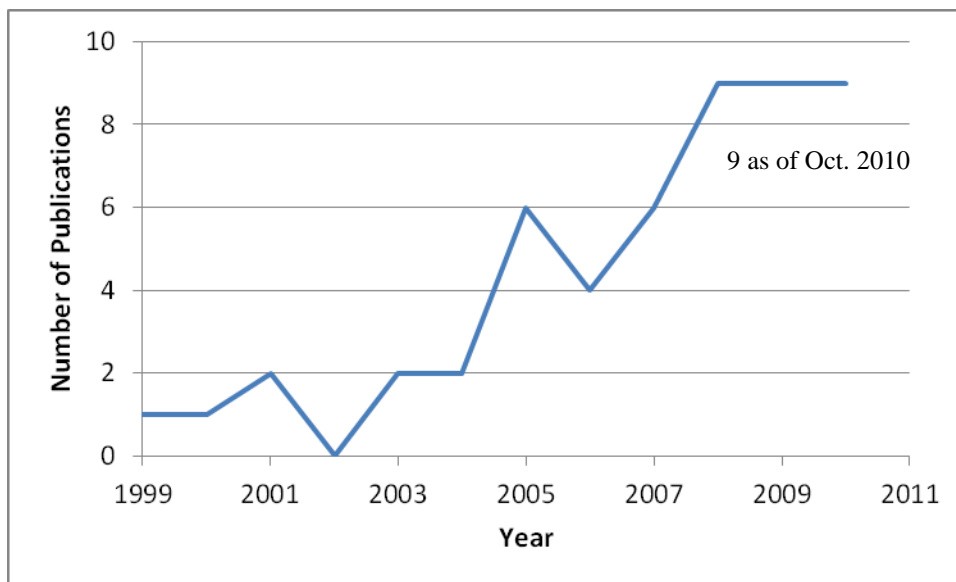
Development of preconcentrators started in the 1970s for air sampling applications [15-17]. A conventional preconcentrator consists of a tube, made of stainless steel or precision bore borosilicate glass (shown in Figure 5), to hold the adsorbent material. The tubes are made with very precise dimensions to ensure leak-free connection to the desorption apparatus, and they are packed with one or multiple adsorbent materials. Typically, the cost of these tubes is around \$100/tube. In addition, there is the capital outlay for the desorption apparatus, typically between \$15,000 to \$40,000 depending on whether the unit is single tube or has automated multi-tube capability. A typical air sampling procedure for personal exposure calls for 10 L of air passed through a standard preconcentrator using a personal air sampling pump operating at 200 mL/min.



**Figure 5 Commercial thermal desorption preconcentration tubes [18], Courtesy of CAMSCO Inc., Used with permission**

Various  $\mu$ PC designs utilizing wide range of adsorbent materials have been reported in the past ten years. Interest in  $\mu$ PCs continues to grow in response to ever increasing demand for more sensitive and selective micro sensing systems. Evidence of this is shown in Figure 6 which

shows the number of reports on  $\mu$ PC development as a function of publication year. It should be noted that not all reported  $\mu$ PCs are necessarily intended for  $\mu$ GC application. In fact, some are manufactured to be used in conjunction with standalone sensors. This research development continues to aim toward reducing size, power requirements, enhancing performance, and the promise of batch manufacturing to reduce costs.



**Figure 6** Number of reports on  $\mu$ PC development as a function of publication year

Most  $\mu$ PC designs follow the same two categories of preconcentration discussed above, exhaustive and equilibrium based devices. Exhaustive  $\mu$ PCs consist of microcavities or microchannels packed with granular adsorbent [19, 20]. Equilibrium  $\mu$ PCs consist of planar surfaces, microchannels, or complex 3D microstructures coated with a thin film of sorbent material. Due to MEMS technology, these micro structures are made with extreme uniformity in terms of geometric properties (size, shape, and distribution) resulting in good control over fluid flow through the device [21]. Coating of  $\mu$ PCs is done by either spin coating [22], plasma deposition [23], inkjet printing [24], electroplating [25], or conventional methods used to coat chromatographic open tubular capillary column such as the one reported in [26].

Sandia National Laboratories reported the first  $\mu$ PC in 1999 as part of their  $\mu$ ChemLab program for real-time monitoring of dangerous gases in public areas [27]. The Sandia team made

notable developments in  $\mu$ PC technology. Their design consists of 2.5 mm  $\times$  2.5 mm membrane micro hotplate coated with surfactant templated sol gel polymer. This device achieved 200 °C in 4 msec, using roughly 100 mW. The ultra fast temperature ramping enabled sample thermal desorption pulse widths as narrow as 200 ms at 5 mL/min. However, the low surface area of the device limited its sample capacity [28]. Several research groups also reported similar devices in which a polymeric sorbent is deposited atop a micro heater [22, 29-32]. Sandia also showed the possibility of monolithic integration of  $\mu$ PC, separation column, and micro detector on a single chip using their “surface micromachining with integrated fluidic technology” (a 5-layer polysilicon MEMS process) [33]. Although they demonstrate the fabricated device, they did not report experimental results on the performance of this monolithically integrated system. Sandia’s most recent development was what they called “smart preconcentrator”. The device combined mass sensing and preconcentration to determine when the  $\mu$ PC has collected sufficient analyte for analysis [34].

In 2003, the Center for Wireless Integrated Microsystems at the University of Michigan reported the development of exhaustive  $\mu$ PCs [35]. Their device consisted of a microfabricated compartment (3 mm  $\times$  3 mm) filled with 1.8 mg granular Carbopack X at 0.4 g/cm<sup>3</sup> packed-bed density. Their  $\mu$ PC achieved 250 °C in 15 sec using 15 °C/sec ramp rate at 2.25 W. The device provided sample thermal desorption pulse widths of 6.5 sec with 3.3 mL/min flow. They managed to reduce the pulse width by implementing what they call “stop-flow” time into the  $\mu$ PC operation. To help sharpen the desorption profile, they stop the carrier flow at the start of the heating cycle. During the stop-flow period, the trapped analytes will be desorbed from the adsorbent to the free volume inside the device. Then, the gas flow is resumed to sweep the desorbed analytes out of the free volume to the detector. Pulse width of 0.8 sec was achieved using a stop-flow time of 25 sec to reach 280 °C at 2.25 W and 3.3 mL/min flow. They improved the analytes trapping range of their device by extending their design to three compartments, consisting of 1.6 mg Carbopack B, 1.0 mg Carbopack X, and 0.6 mg Carboxen 1000. The overall dimensions of the chip were 13 mm  $\times$  4 mm. Heating rate and power consumption of the three stage  $\mu$ PC were 100 °C/sec and 0.8 W per stage, respectively, to reach a desorption temperature of 250 °C. Pulse width information were not provided for this design. The improvements in

heating efficiency were achieved by reducing the conductive heat loss to the underlying package substrate. Moreover, the thermal masses of the heater and cover plate were reduced from 28.6 mg to 10.1 mg per stage [19]. Other exhaustive  $\mu$ PC designs were also reported in the literature [20, 36].

In 2005, the Center of Advanced Materials for the Purification of Water with Systems at the University of Illinois introduced a hybrid (or mixed) design that combined Sandia's and Michigan's designs to achieve large surface area and small flow restriction. This was done by embedding micro posts coated with adsorbent films within a microcavity [37]. It is noteworthy that the concept of embedding micro posts within a microcavity has been utilized in 1998 for liquid chromatography [38] and in 2002 to promote multiphase mixing and reaction [21]. Other applications of such configurations that appeared in 2005 and later include pin fin heat sinks [39], hydrophobic surfaces [40], study of DNA dynamics [41], and GC columns [42]. The Illinois device had a 5 mm  $\times$  2.5 mm footprint, achieved a heating rate of 200 °C/sec and produced 20 sec desorption plus width. However, they were faced with the coating challenges. It is difficult to attain uniform and full coverage coating on such structures using conventional coating methods due to channeling of the coating solution in the cavity. That is, the solution will not flow uniformly around all posts. This would result in partial coverage coating. The Institute of Microengineering at Ecole Polytechnique Fédérale de Lausanne (EPFL) in Switzerland also took similar approach in 2009 by embedding "Zigzag" micro structures in a microcavity [43]. They were also faced with the same coating challenges as Illinois.

## ***2.6 Conclusions***

In both preconcentration categories, the device performance varies based on operating parameters and adsorbent materials used. Nevertheless, only preliminary results were reported with limited details on operational parameters and fundamental factors affecting  $\mu$ PC performance. Reports on the influence of adsorbent mass, sample concentration, and fluid dynamics are also scarce with a few studies being found in the literature [19, 44-46]. Exhaustive  $\mu$ PC performance is simpler to analyze using the modified Wheeler model. Zellers et. al. [47] have tweaked the model to make it applicable to the equilibrium based preconcentrators. This was done by averaging the adsorbent bulk density over the entire inner volume of the

preconcentrator to make an effective packing density value. Although this approach provided reasonable estimates of breakthrough times, the use of the modified Wheeler model in characterizing equilibrium preconcentrators is criticized because this model was developed assuming packed adsorbent bed. Furthermore, the concept of breakthrough does not hold as the adsorbent material does not pose restrictions on the sample molecules passing through the preconcentrator. That is, there would always be molecules breaking through the preconcentrator whether the adsorbent film is saturated or not.  $\mu$ PC performance characterization becomes most challenging in equilibrium based designs having complex 3D microstructures. Here, the performance is convoluted by geometric properties (or surface-to-volume ratio), flow dynamics, and sorbent material. Yeom, et. al. [45] have recently proposed a figure of merit based on their flow resistance model, which they called adsorption compliance. It depends on surface-to-volume ratio, blockage ratio, and number of 3D microstructures. This figure of merit is based only on geometrical factors and does not take into account the effect of adsorbent material.

The preconcentration factor (PF) has been commonly used as a metric to estimate the performance of  $\mu$ PCs. It denotes the enrichment or gain in sample concentration. However, there is no standard definition for PF. The most common definition is the concentration of the preconcentrated sample relative to the original concentration [20, 28, 29, 45, 48-51]. Other definitions include sample container volume to desorption volume [35] and breakthrough time difference [52]. It should be noted that PF on its own is ambiguous. This is because PF depends on the analyte concentration, how long one collects them, and at what flow rate and, thus, is not strictly an intrinsic property of the preconcentrator itself [53].

## **References**

- [1] C. Vandecasteele, *Modern Methods for Trace Element Determination* vol. xi, 330 p. :. Chichester ; New York :: Wiley, 1993.
- [2] M. Harper, "Sorbent Trapping of Volatile Organic Compounds from Air," *Journal of Chromatography A*, vol. 885, 2000, pp. 129-151.
- [3] R. Veeneman, "Design and Characterization of a Multi-Vapor Preconcentrator for a Micro-Scale Gas Chromatograph," Doctor of Philosophy Dissertation, Department of Chemistry, University of Michigan, Ann Arbor, MI, 2009.

- [4] O. B. Egorov, M. J. O'Har, and J. W. Grate, "Equilibration-Based Preconcentrating Minicolumn Sensors for Trace Level Monitoring of Radionuclides and Metal Ions in Water without Consumable Reagents," *Analytical Chemistry*, vol. 78, 2006, pp. 5480-5490.
- [5] G. Ouyang and J. Pawliszyn, "A Critical Review in Calibration Methods for Solid-Phase Microextraction," *Analytica Chimica Acta*, vol. 627, 2008, pp. 184-197.
- [6] J. Namiesnik, "Preconcentration of Gaseous Organic Pollutants in the Atmosphere," *The International Journal of Pure and Applied Analytical Chemistry*, vol. 35, 1988, pp. 567-587.
- [7] J. J. Whiting and R. D. Sacks, "Evaluation of Split/Splitless Operation and Rapid Heating of a Multi-Bed Sorption Trap Used for Gas Chromatography Analysis of Large-Volume Air Samples," *Journal of Separation Science*, vol. 29, 2006, pp. 218-227.
- [8] Z. B. Alfassi and C. M. Wai, Eds., *Preconcentration Techniques for Trace Elements*. Boca Raton :: CRC Press, 1992.
- [9] J. M. Sanchez and R. D. Sacks, "On-Line Multi-Bed Sorption Trap for Voc Analysis of Large-Volume Vapor Samples: Injection Plug Width, Effects of Water Vapor and Sample Decomposition," *Journal of Separation Science*, vol. 28, 2005, pp. 22-30.
- [10] K. Dettmer and W. Engewald, "Adsorbent Materials Commonly Used in Air Analysis for Adsorptive Enrichment and Thermal Desorption of Volatile Organic Compounds," *Analytical and Bioanalytical Chemistry*, vol. 373, 2002, pp. 490-500.
- [11] J. Brown and B. Shirey, "A Tool for Selecting an Adsorbent for Thermal Desorption Applications," Sigma-Aldrich Co., Bellefonte, PA2001.
- [12] A. J. Núñez, L. F. González, and J. Janáček, "Pre-Concentration of Headspace Volatiles for Trace Organic Analysis by Gas Chromatography," *Journal of Chromatography A*, vol. 300, 1984, pp. 127-162.
- [13] V. Camel and M. Caude, "Trace Enrichment Methods for the Determination of Organic Pollutants in Ambient Air," *Journal of Chromatography A*, vol. 710, 1995, pp. 3-19.
- [14] Camsco Inc., "Camsco Sorbent Selection Chart," ed. Houston, TX: Camsco, Inc., 2009.
- [15] J. W. Russell, "Analysis of Air Pollutants Using Sampling Tubes and Gas Chromatography," *Environmental Science & Technology*, vol. 9, 1975, pp. 1175-1178.
- [16] R. H. Brown and C. J. Purnell, "Collection and Analysis of Trace Organic Vapour Pollutants in Ambient Atmospheres : The Performance of a Tenax-Gc Adsorbent Tube," *Journal of Chromatography A*, vol. 178, 1979, pp. 79-90.
- [17] E. D. Pellizzari, J. E. Bunch, R. E. Berkley, and J. McRae, "Collection and Analysis of Trace Organic Vapor Pollutants in Ambient Atmospheres. The Performance of a Tenax Gc Cartridge Sampler for Hazardous Vapors," *Analytical Letters*, vol. 9, 1976, pp. 45 - 63.
- [18] Camsco Inc., "Product Catalog," ed. Houston, TX: Chemical Agent Monitoring Supply Company Inc., 2010.

- [19] W.-C. Tian, H. K. L. Chan, L. Chia-Jung, S. W. Pang, and E. T. Zellers, "Multiple-Stage Microfabricated Preconcentrator-Focuser for Micro Gas Chromatography System," *Journal of Microelectromechanical Systems*, vol. 14, 2005, pp. 498-507.
- [20] I. Gràcia, P. Ivanov, F. Blanco, N. Sabaté, X. Vilanova, X. Correig, L. Fonseca, E. Figueras, J. Santander, and C. Cané, "Sub-Ppm Gas Sensor Detection Via Spiral M-Preconcentrator," *Sensors and Actuators B: Chemical*, vol. 132, 2008, pp. 149-154.
- [21] M. W. Losey, R. J. Jackman, S. L. Firebaugh, M. A. Schmidt, and K. F. Jensen, "Design and Fabrication of Microfluidic Devices for Multiphase Mixing and Reaction," *Journal of Microelectromechanical Systems*, vol. 11, 2002, pp. 709-717.
- [22] M. Kim and S. Mitra, "A Microfabricated Microconcentrator for Sensors and Gas Chromatography," *Journal of Chromatography A*, vol. 996, 2003, pp. 1-11.
- [23] R. R. Lima, R. A. M. Carvalho, A. P. N. Filho, M. L. P. Silva, and N. R. Demarquette, "Production and Deposition of Adsorbent Films by Plasma Polymerization on Low Cost Micromachined Non-Planar Microchannels for Preconcentration of Organic Compound in Air," *Sensors and Actuators B: Chemical*, vol. 108, 2005, pp. 435-444.
- [24] B. Alfeeli, D. Cho, M. Ashraf-Khorassani, L. T. Taylor, and M. Agah, "Mems-Based Multi-Inlet/Outlet Preconcentrator Coated by Inkjet Printing of Polymer Adsorbents," *Sensors and Actuators B, Chemical*, vol. 133, 2008, pp. 24-32.
- [25] B. Alfeeli, M. A. Zareian-Jahromi, and M. Agah, "Micro Preconcentrator with Seedless Electroplated Gold as Self-Heating Adsorbent," in *8th IEEE Conference on Sensors*, Chirstchurch, New Zealand, 2009, pp. 1947-1950.
- [26] S. Reidy, G. Lambertus, J. Reece, and R. Sacks, "High-Performance, Static-Coated Silicon Microfabricated Columns for Gas Chromatography," *Analytical Chemistry*, vol. 78, 2006, pp. 2623-2630.
- [27] G. C. Frye-Mason, R. P. Manginell, E. J. Heller, C. M. Matzke, S. A. Casalnuovo, V. M. Hietala, R. J. Kottenstette, P. R. Lewis, and C. C. Wong, "Microfabricated Gas Phase Chemical Analysis Systems," in *Microprocesses and Nanotechnology Conference*, Yokohama, Japan, 1999, pp. 60-61.
- [28] R. P. Manginell, G. C. Frye-Mason, R. J. Kottenstette, P. R. Lewis, and C. Channy Wong, "Microfabricated Planar Preconcentrator," in *Solid-State Sensors, Actuators, and Microsystems Workshop, Hilton Head'00*, 2000, pp. 179-182.
- [29] I. Voiculescu, R. A. McGill, M. E. Zaghoul, D. Mott, J. Stepnowski, S. Stepnowski, H. Summers, V. Nguyen, S. Ross, K. Walsh, and M. Martin, "Micropreconcentrator for Enhanced Trace Detection of Explosives and Chemical Agents," *IEEE Sensors Journal*, vol. 6, 2006, pp. 1094-1104.
- [30] M. Martin, M. Crain, K. Walsh, R. A. McGill, E. Houser, J. Stepnowski, S. Stepnowski, H.-D. Wu, and S. Ross, "Microfabricated Vapor Preconcentrator for Portable Ion Mobility Spectroscopy," *Sensors and Actuators B: Chemical*, vol. 126, 2007, pp. 447-454.

- [31] C. E. Davis, C. K. Ho, R. C. Hughes, and M. L. Thomas, "Enhanced Detection of M-Xylene Using a Preconcentrator with a Chemiresistor Sensor," *Sensors and Actuators B: Chemical*, vol. 104, 2005, pp. 207-216.
- [32] P. Ivanov, F. Blanco, I. Gracia, N. Sabate, A. Ruiz, X. Vilanova, X. Correig, L. Fonseca, E. Figueras, J. Santander, and C. Cane, "Improvement of the Gas Sensor Response Via Silicon M-Preconcentrator," *Sensors and Actuators B: Chemical*, vol. 127, 2007, pp. 288-294.
- [33] P. R. Lewis, P. Manginell, D. R. Adkins, R. J. Kottenstette, D. R. Wheeler, S. S. Sokolowski, D. E. Trudell, J. E. Byrnes, M. Okandan, J. M. Bauer, R. G. Manley, and C. Frye-Mason, "Recent Advancements in the Gas-Phase Microchemlab," *IEEE Sensors Journal*, vol. 6, 2006, pp. 784-795.
- [34] R. P. Manginell, D. R. Adkins, M. W. Moorman, R. Hadizadeh, D. Copic, D. A. Porter, J. M. Anderson, V. M. Hietala, J. R. Bryan, D. R. Wheeler, K. B. Pfeifer, and A. Rumpf, "Mass-Sensitive Microfabricated Chemical Preconcentrator," *Journal of Microelectromechanical Systems*, vol. 17, 2008, pp. 1396-1407.
- [35] W.-C. Tian, S. W. Pang, L. Chia-Jung, and E. T. Zellers, "Microfabricated Preconcentrator-Focuser for a Microscale Gas Chromatograph," *Journal of Microelectromechanical Systems*, vol. 12, 2003, pp. 264-272.
- [36] H. K. L. Chan, S. W. Pang, R. A. Veeneman, E. T. Zellers, and M. Takei, "Microfabricated Preconcentrator for Quantitative Analysis of Low Concentration Volatile Organic Compounds," in *International Conference on Solid-State Sensors, Actuators and Microsystems, TRANSDUCERS'07*, Korea, 2005, pp. 2091-2094.
- [37] Y. Tang, J. Yeom, J. Han, B. Bae, R. I. Masel, and M. A. Shannon, "A Micro-Post Preconcentrator for a Microscale Gas Chromatography System," in *International Conference on Miniaturized Systems for Chemistry and Life Sciences, MicroTAS'05*, Boston, MA, 2005, pp. 660-662.
- [38] B. He and F. Regnier, "Microfabricated Liquid Chromatography Columns Based on Collocated Monolith Support Structures," *Journal of Pharmaceutical and Biomedical Analysis*, vol. 17, 1998, pp. 925-932.
- [39] Y. Peles, A. Kosar, C. Mishra, C.-J. Kuo, and B. Schneider, "Forced Convective Heat Transfer across a Pin Fin Micro Heat Sink," *International Journal of Heat and Mass Transfer*, vol. 48, 2005, pp. 3615-3627.
- [40] Y. Jihoon and et al., "Robust Hydrophobic Surfaces with Various Micropillar Arrays," *Journal of Micromechanics and Microengineering*, vol. 20, 2010, p. 025028.
- [41] N. P. Teclerian, V. A. Beck, E. S. G. Shaqfeh, and S. J. Muller, "Dynamics of DNA Polymers in Post Arrays: Comparison of Single Molecule Experiments and Simulations," *Macromolecules*, vol. 40, 2007, pp. 3848-3859.
- [42] S. Ali, M. Ashraf-Khorassani, L. T. Taylor, and M. Agah, "Mems-Based Semi-Packed Gas Chromatography Columns," *Sensors and Actuators B, Chemical*, vol. 141, 2009, pp. 309-315.



- [43] E. H. M. Camara, P. Breuil, D. Briand, L. Guillot, C. Pijolat, and N. F. de Rooij, "A Micro Gas Preconcentrator with Improved Performances for Environmental Monitoring," in *International Conference on Solid-State Sensors, Actuators and Microsystems, TRANSDUCERS'09*, 2009, pp. 983-986.
- [44] R. P. Manginell, S. Radhakrishnan, M. Shariati, A. L. Robinson, J. A. Ellison, and R. J. Simonson, "Two-Dimensional Modeling and Simulation of Mass Transport in Microfabricated Preconcentrators," *IEEE Sensors Journal*, vol. 7, 2007, pp. 1032-1041.
- [45] J. Yeom, D. D. Agonafer, J.-H. Han, and M. A. Shannon, "Low Reynolds Number Flow across an Array of Cylindrical Microposts in a Microchannel and Figure-of-Merit Analysis of Micropost-Filled Microreactors," *Journal of Micromechanics and Microengineering*, vol. 19, 2009, p. 065025.
- [46] E. H. M. Camara, P. Breuil, and C. Pijolat, "Preconcentration Modeling for the Optimization of a Micro Gas Preconcentrator Applied to Environmental Monitoring," *Procedia Chemistry*, vol. 1, 2009, pp. 662-665.
- [47] E. T. Zellers, M. Morishita, and Q.-Y. Cai, "Evaluating Porous-Layer Open-Tubular Capillaries as Vapor Preconcentrators in a Microanalytical System," *Sensors and Actuators B: Chemical*, vol. 67, 2000, pp. 244-253.
- [48] H. Pham Tuan, H.-G. Janssen, and C. A. Cramers, "Novel Preconcentration Technique for on-Line Coupling to High-Speed Narrow-Bore Capillary Gas Chromatography: Sample Enrichment by Equilibrium (Ab)Sorption: I. Principles and Theoretical Aspects," *Journal of Chromatography A*, vol. 791, 1997, pp. 177-185.
- [49] C. Thammakhet, P. Thavarungkul, R. Brukh, S. Mitra, and P. Kanatharana, "Microtrap Modulated Flame Ionization Detector for on-Line Monitoring of Methane," *Journal of Chromatography A*, vol. 1072, 2005, pp. 243-248.
- [50] K. Song and S.-K. Lee, "Development of a Compact Sample Pre-Concentration System for the Detection of a Trace Amount of Volatile Organic Compounds (Vocs)," *Sensors and Actuators B: Chemical*, vol. 125, 2007, pp. 173-179.
- [51] F. Blanco, X. Vilanova, V. Fierro, A. Celzard, P. Ivanov, E. Llobet, N. Cañellas, J. L. Ramírez, and X. Correig, "Fabrication and Characterisation of Microporous Activated Carbon-Based Pre-Concentrators for Benzene Vapours," *Sensors and Actuators B: Chemical*, vol. 132, 2008, pp. 90-98.
- [52] C. Pijolat, M. Camara, J. Courbat, J. P. Viricelle, D. Briand, and N. F. de Rooij, "Application of Carbon Nano-Powders for a Gas Micro-Preconcentrator," *Sensors and Actuators B: Chemical*, vol. 127, 2007, pp. 179-185.
- [53] J. W. Grate, N. C. Anheier, and D. L. Baldwin, "Progressive Thermal Desorption of Vapor Mixtures from a Preconcentrator with a Porous Metal Foam Internal Architecture and Variable Thermal Ramp Rates," *Analytical Chemistry*, vol. 77, Mar 2005, pp. 1867-1875.

## Chapter Three: MEMS-Based Multi-Inlet/Outlet Preconcentrator Coated by Inkjet Printing of Polymer Adsorbents

This chapter was reproduced from [1] with permission from Elsevier B. V.

*B. Alfeeli, D. Cho, M. Ashraf-Khorassani, L. T. Taylor, and M. Agah, "MEMS-Based Multi-Inlet/Outlet Preconcentrator Coated by Inkjet Printing of Polymer Adsorbents," Sensors and Actuators B, Chemical, vol. 133, 2008, pp. 24-32.*

### 3.1 Introduction

Law enforcement, national security, environmental compliance, industrial process monitoring, and biomedicine are some of the applications that require the capabilities of chemical agent detection. These applications need sensitive, selective, and rapid detection as well as quantification of the chemicals of interest. Most chemical detection methods are either time consuming, expensive, or they have limited sampling frequency and detection range [2].

The advancement of micro electromechanical systems (MEMS) technology has enabled the realization of miniaturized analytical instruments or so called "Lab-on-a-chip" devices. The first microfabricated component for gas analysis was reported in 1979 [3], and in 1999, the concept of a complete microscale chemical analysis system was introduced [4]. A microsystem based on chromatography is a promising approach to low- power, low-cost, and (near) real-time analysis of complex gaseous mixtures which is moving toward small portable micro instruments [5-16].

Sample pretreatment plays a major role in the analysis of gas mixtures. It is an important factor in the performance of many analytical techniques such as gas chromatography (GC). A comprehensive review on air analysis using gas chromatography has been reported by Helmig [17]. The author comments that one of the most common procedures required for high sensitivity and excellent selectivity is sample preconcentration. Conventional thermally desorbed preconcentrators (PCs) consist of a short-length microbore tubing packed with an adsorbent which is heated by means of an electrically conducting wire coiled around it [6, 18-29]. The use of MEMS technology has led to the development of PCs with smaller sizes, lower pressure drops, lower power consumptions, and higher efficiencies compared to conventional counterparts

[12]. Different configurations such as packed compartments, and coated planar surface, micro channels, and micro 3D structures have been reported [7, 8, 10, 15, 30-40]. The main challenge in the development of MEMS-based PC is limited sample capacity. One effective method to enhance sample capacity without significant pressure drop is to utilize embedded pillars that result in a hybrid configuration that combines packed (large surface area) and equilibrium based (small flow restrictions) structures [41].

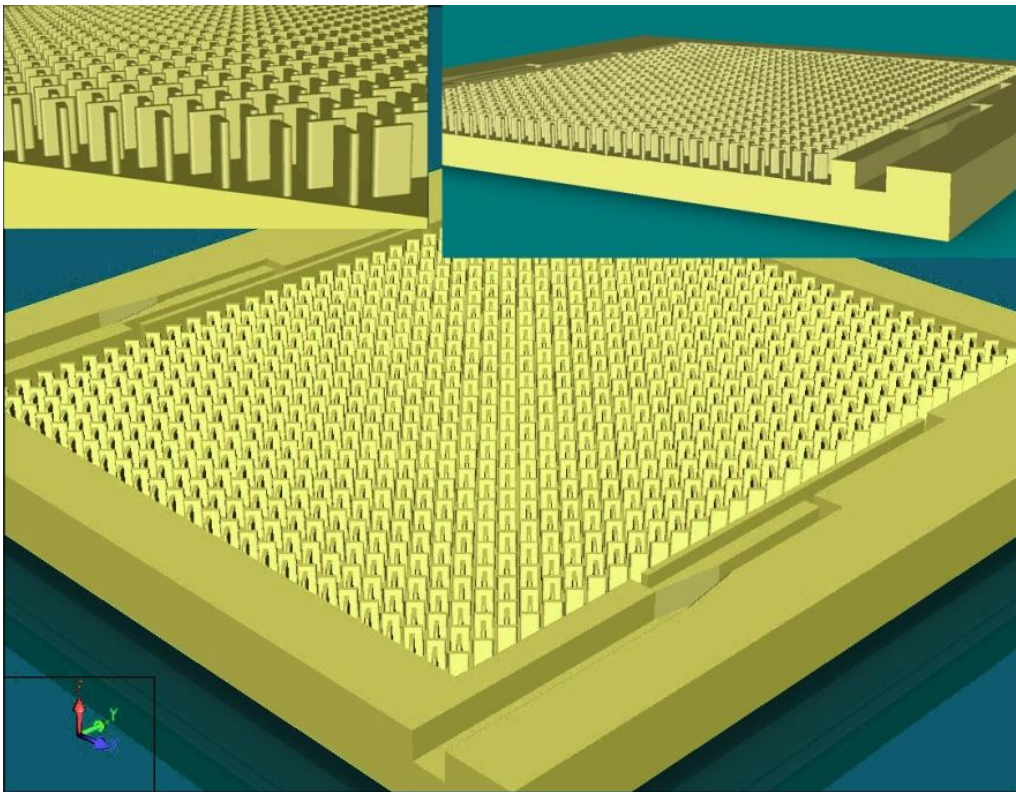
Adsorbent materials are used in  $\mu$ PCs to trap volatile organic compounds (VOCs). There is no universal trapping method as different VOCs require different methods of trapping. According to reference [17], VOCs are classified into three groups: light ( $C_2$ - $C_5$ ) which requires cryogenic trapping, mid-range ( $C_5$ - $C_{12}$ ) whose typical adsorbents include activated charcoal, Tenax, Carbotrap, and Carbosieve, and semi-volatile ( $> C_{12}$ ) that can be adsorbed by either a polyurethane foam (PUF) plug or silica gel. In addition to conventional granular adsorbents, the use of an adsorbent film such as surfactant templated sol gel layer for adsorbing dimethyl methyl phosphonate (DMMP), xylene, and methyl ethyl ketone (MEK) [30], a hyperbranched polycarbosilane functionalized with hexafluoroisopropanol (HFIP) pendant groups for adsorbing DMMP and TNT [35], and a 50% polymethyl-50% phenyl polymer for adsorbing benzene and toluene [31] have been reported.

This chapter reports a  $\mu$ PC device consisting of multiple inlets and outlets having novel embedded crisscross pillars which are coated with a Tenax TA thin film by using an inkjet printing technique. High surface-to-volume ratio, low thermal mass (rapid heating), small flow resistance (low pressure drop), high capacity, acceptable repeatability, and easy integration with a GC instrument are characteristics of this microfabricated preconcentrator.

### ***3.2 Design and Fabrication***

Our design goal was to achieve high capacity preconcentration using high-aspect-ratio fabrication techniques. To meet this goal, the design of a  $\mu$ PC should satisfy the following requirements: large surface area, low pressure drop, low thermal mass, robust structure, and simplicity for the purpose of effective integration and packaging. Micro preconcentrators can be classified into exhaustive and equilibrium designs. Exhaustive designs have the advantage of

large surface area, but they suffer from limitations such as large pressure drop, high dead volume, gas residuals, and poor heat transfer. Equilibrium based designs overcome these disadvantages but their surface area is limited. One way to overcome the current challenge of increased surface area without obstruction of the flow in a  $\mu$ PC is to fabricate micropillars within the preconcentrator structure as shown in Figure 7.

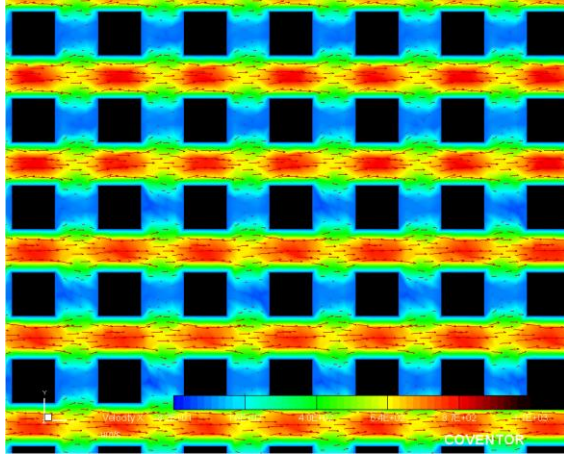


**Figure 7 3-D rendering of the micropillars based  $\mu$ PC**

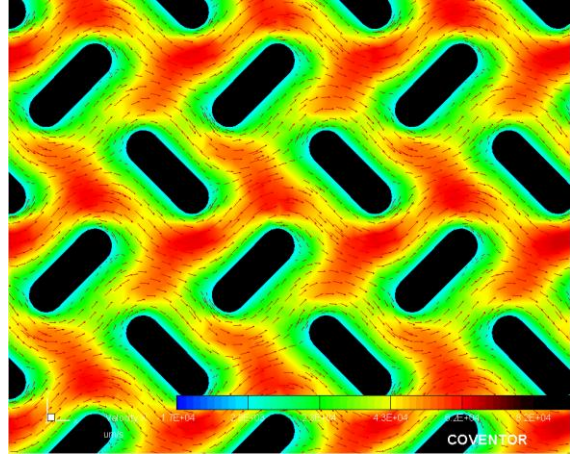
Using computational fluid dynamics (CFD) simulation in the CoventorWare package, the flow through this configuration with crisscross and square pillars (for comparison purposes) was simulated. A 2-D geometry of the device was defined as shown in Figure 8. In order to provide the simulation model with the same surface area and flow rates as that of the real device, the dimensions of the pillars and inlet pressure were scaled accordingly. Simulation of the gas flow through the device was performed at steady state. The velocity vectors for the square and crisscross pillars are shown in Figure 8 (a) and (b). Due to the sharp corners of the square pillars, the flow stagnates between the pillars in a direction perpendicular to the flow to satisfy the Kutta

condition, a principle in fluid dynamics [42]. Furthermore, since the flow in the perpendicular direction cannot pass through to the other side due to the relatively fast flow in the parallel direction, the fluid must come to rest at that region creating a stagnation point. This flow pattern indicated that the sample molecules do not reach half of the pillar surfaces, thus decreasing the adsorption surface by two fold. In the crisscross design, the sharp corners have been smoothed out and the flow is directed in a zigzag pattern ensuring non-zero velocity in all direction and maximizing the adsorption surface. It should be also noted that there is no backflow at the outlet region. The simulation analysis also showed that the multiple inlet/outlet design spreads the flow more evenly among the pillars as shown in Figure 8 (c) and (d). Although the zigzag pattern helps distribute the flow, the flow velocity is highest at the line of sight between the inlet and outlet which gives rise to an undesired flow concentration in the middle of the device in the case of a single inlet/outlet design. The use of a double inlet/outlet lessened this effect which allowed more interaction between the pillars and the sample flowing through the device. Based on the simulation results, the crisscross design with double inlet/outlet proved to be a better design for the  $\mu$ PC.

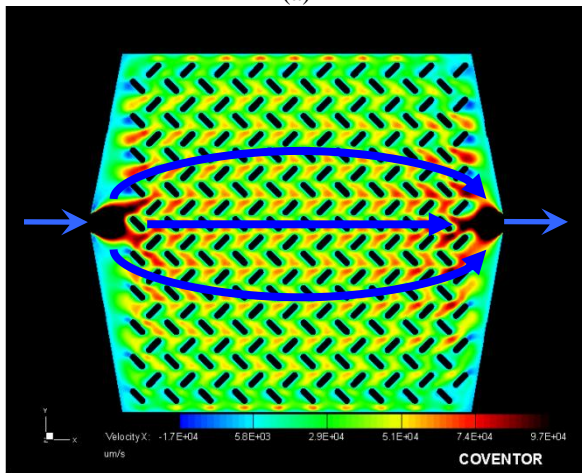
Most of the previously reported  $\mu$ PC structures require multiple masks for the fabrication process. Nevertheless, our fabrication approach meets the simplicity requirement as it requires only two masks, one for patterning the microstructures and one for patterning onboard heaters and sensors. Using high-resolution, superior aspect ratio thick film photoresist (PR9260), the micropillars and the fluidic ports were patterned on a 100 mm silicon wafer (See Figure 9 (a), (b)). The pattern was then etched using deep reactive ion etching (DRIE) to form 240  $\mu$ m-deep 3D structures, Figure 9 (c). To seal the structure, the etched wafer was bonded to a Pyrex glass wafer. Anodic bonding which is more robust than a polymer adhesive has been used to make the bond, Figure 9 (d). To fabricate the thin-film resistive heaters and temperature sensors, PECVD oxide was deposited on the backside of the wafer and then 20/40 nm Ti/Pt was evaporated and patterned by the lift-off technique, Figure 9 (e). The wafer containing 140 chips was diced into individual devices. Each device was connected on both sides with 240  $\mu$ m-OD, 100  $\mu$ m-ID deactivated fused silica tubing using a high temperature silica based bonding agent, Figure 9 (f).



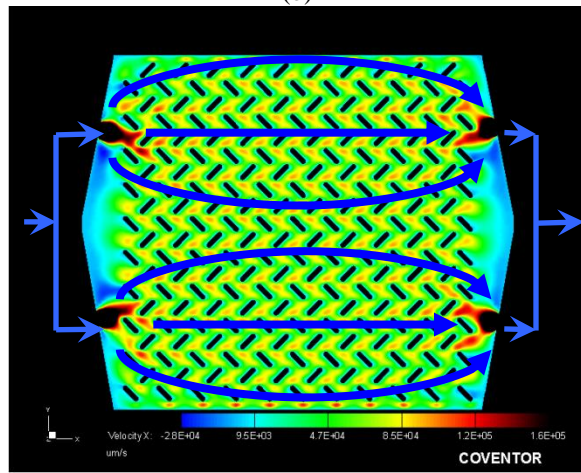
(a)



(b)

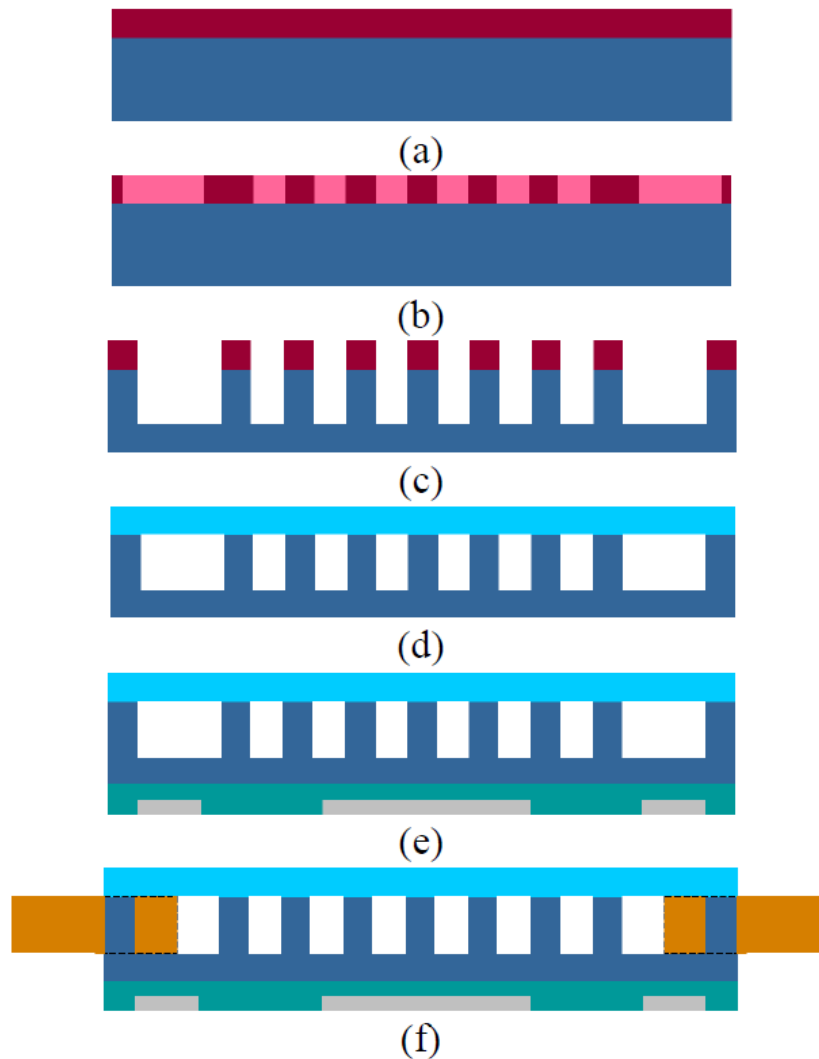


(c)



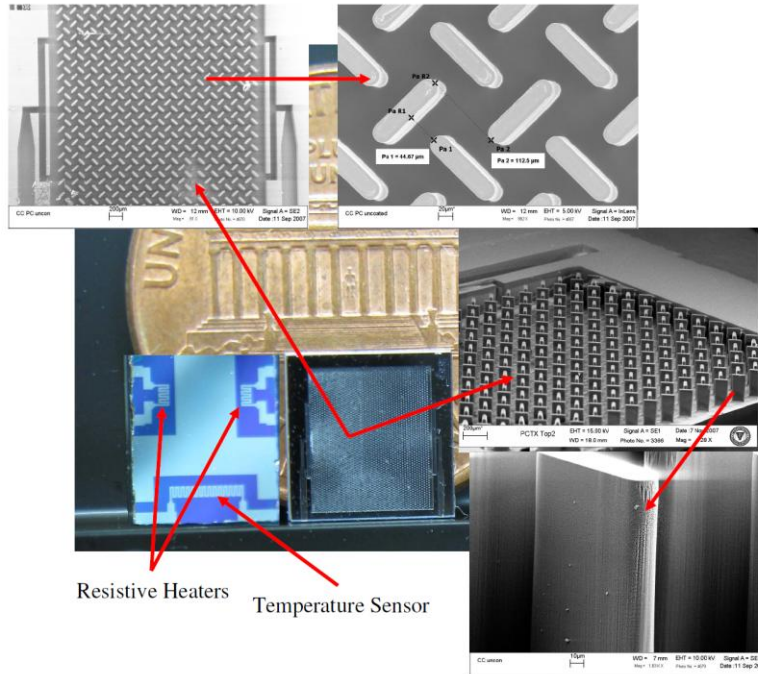
(d)

**Figure 8** CFD simulation of the flow in (a) ordered square pillars, (b) crisscross pillars, (c) crisscross pillars with single inlet/outlet showing the flow path, (d) crisscross pillars with multiple inlet/outlet showing the flow path



**Figure 9 Step by step processing of the wafer in cross-sectional view**

Figure 10 shows an optical image of the device and scanning electron microscopic (SEM) micrographs of the etched 3D structures. The silicon-glass chip has outer dimensions of 7 mm × 7 mm and a total inner surface area of about 200 mm<sup>2</sup> and a volume of about 6.5 μL. The pillars have high-aspect-ratio with dimensions of 27 μm × 115 μm × 240 μm. The flow splits 1:1 at the inlet port and then recombines again at the outlet port with the same ratio. The fluidic ports were tapered to make the silica tubing fit snugly into the port and to reduce dead volume.

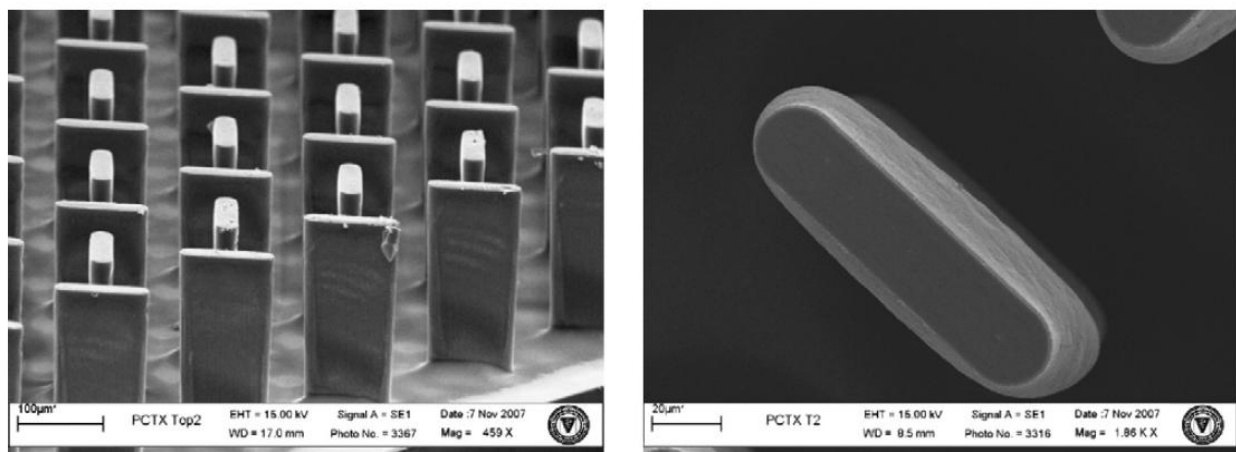


**Figure 10** Optical image of the  $\mu$ TPC showing the front and back sides of the device, insets are SEM micrographs of the etched 3D structures and the fluidic ports

In our experiments, we used Tenax TA dissolved in dichloromethane to coat the 3D structures with film adsorbent. Conventional static and dynamic coating techniques failed to produce good coverage coating due to a channeling effect. Furthermore, both techniques were only capable of depositing very thin films ( $\leq 250$  nm). Using the principle of inkjet printing technology, the micro structures were coated before anodic bonding by installing micro droplets of diluted Tenax TA solution. The droplets were created by pushing the solution at low pressure through small micro bore capillary tubing. This method ensured high coverage coating. We also used polydimethylsiloxane (PDMS) dissolved in *n*-pentane (also coated by inkjet method) as an alternative adsorbent film to study the influence of the adsorbent material on chip performance.

Figure 11 shows SEM monographs of the Tenax TA coated pillars. As can be seen, the coating method produced high coverage and uniform adsorbent film on the pillars.



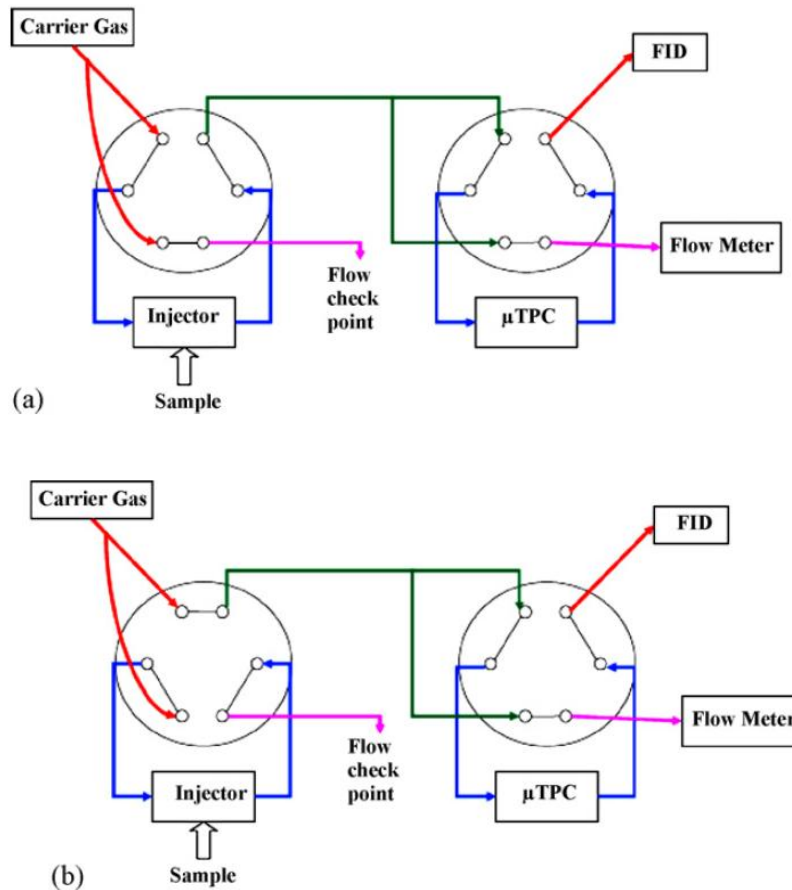


**Figure 11 SEM micrographs of Tenax TA coated pillars**

### **3.3 Experimental Setup**

All adsorption/desorption tests were carried out using an HP 6890 GC system (Agilent Technologies, Inc., Palo Alto, CA). The testing setup was installed inside the GC oven in order to maintain isothermal temperature conditions. Helium carrier gas was supplied to the setup via the GC split/splitless inlet. This allowed the built-in gas flow controller to control the carrier gas entering the setup. The built-in flame ionization detector (FID) was also connected to the device. This enabled signal detection and data collection through the built-in signal processing unit of the GC system. The experimental setup consisted of two six-port zero-dead-volume valves, deactivated silica-lined TEE connectors, and deactivated fused silica transfer lines.

Figure 12 (a) shows the test setup for  $\mu$ PC with the valves set in the “loading position”. In this configuration, the carrier gas continuously flowed through the injector,  $\mu$ PC device, and FID. The sample was manually withdrawn from the sample vial by a precision sampling syringe and then injected into the injector port. Figure 12 (b) resembles the valves set in the “desorption position”. In this configuration, the injector is taken off-line and flushed out of any residual sample. The isolation of the injector from the main flow prevented any residual vapor from reaching the FID during desorption. The device was then heated to start the desorption process. The inertness of the setup was tested by replacing the device with a 10 cm-long, 100  $\mu$ m-ID, deactivated fused silica tube. This test showed insignificant adsorption throughout the setup transfer line and valves. This configuration was also used to calibrate the FID.



**Figure 12  $\mu$ PC test setup with (a) valves set in the loading position, (b) valves set in desorption position**

Device testing consisted of a series of three different runs: blank, loading, and heating. In the blank run, the device was heated to 250 °C at 100 °C/sec in order to establish a baseline. In the loading run a sample of nonane ( $C_9$ ) was injected into the injector at an isothermal temperature of 35 °C. Finally, in the heating run, the preconcentrator was heated to 250 °C at 100 °C/sec in order to desorb the sample. An off-board high performance ceramic heater (ultra fast ramp rate) was used in the experiments. The on-board resistive heaters and temperature sensor required a customized temperature controller which was not available at the time of the experiment. In future work, the on-chip thermal desorption capability will be used.

### 3.4 Results and Discussion

Using the fabrication process described above, high quality  $\mu$ PC devices with high-aspect-ratio structures (240 $\mu$ m) were produced. As mentioned earlier, the 7 mm  $\times$  7 mm chip has a total inner surface area of about 200 mm<sup>2</sup> and a total inner volume of about 6.5  $\mu$ L resulting in an approximately 31 mm<sup>-1</sup> surface area to volume ratio (S/V). For comparison, a 25 cm-long, 250  $\mu$ m-ID capillary tube yields the same surface area but has an inner volume of 12.5  $\mu$ L, and S/V of 16 mm<sup>-1</sup>, which results in a lower adsorption (concentration) capacity.

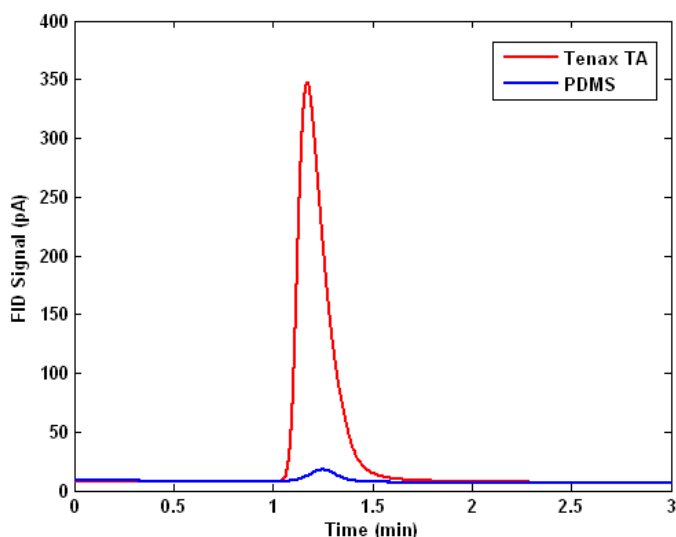
The effect of the multiple inlet/outlet on the  $\mu$ PC performance was studied by testing the performance of the uncoated devices. This enabled us to study the distributed inlet/outlet effect on the performance of the  $\mu$ PC without interference of the adsorbent material. Table 1 lists the preconcentration factor for single and multiple inlet/outlet. This factor is the ratio between the areas under the peak of the generated FID signal with/without the  $\mu$ PC. The double inlet/outlet device produced a higher concentration factor than the single inlet/outlet. This could be attributed to the effective dispersing of the sample among pillars which resulted in more vapor/surface interaction. Moreover, although the overall flow rate is the same for both single and double inlet/outlet devices, the inside flow is not. This is because the double inlet/outlet splits the flow into two flows with half the magnitude of the incoming flow (See Table 8 (d)). This resulted in a slower flow within the device compared to the flow in the single inlet/outlet device. Table 1 also illustrates the effect of pillar packing density. The  $\mu$ PCs with 40  $\mu$ m spacing showed a higher PC factor than the ones with 80  $\mu$ m spacing. Decreasing the spacing between the pillars increased the number of pillars in the device which resulted in an increased S/V ratio and thus increased the PC factor.

**Table 1 Preconcentration factor for different designs of uncoated  $\mu$ PC**

<i>Number of inlet/outlet</i>	<i>Spacing between posts (<math>\mu</math>m)</i>	<i>PC factor<sup>a</sup></i>
1	40	23 $\pm$ 2
2	40	32 $\pm$ 1
1	80	15 $\pm$ 3
2	80	22 $\pm$ 1

<sup>a</sup> Determined by saturating the  $\mu$ TPC with pure nonane

The capacity of the two adsorbents used in this study was evaluated by testing two devices, one coated with PDMS and the other with Tenax TA. Figure 13 compares the desorption peaks under identical test conditions showing the superior capacity of Tenax TA over PDMS. For nonane (C<sub>9</sub>), the PC factor for PDMS and Tenax TA was 100 and 1000, respectively. The results demonstrate the major preconcentration enhancement of  $\mu$ PCs by the adsorbent material. PDMS and Tenax TA enhanced the performance of the  $\mu$ PC by ~5-fold and ~50-fold, respectively, compared to the uncoated one. Tenax TA-coated chip was expected to produce a larger PC factor since it has a higher adsorption capacity than PDMS.



**Figure 13 Desorption peaks of Tenax TA and PDMS**

The height of the desorption peak and its area as a function of the inlet pressure were plotted in Figure 14. For this experiment, we used the same pressure (flow rate) during adsorption and thermal desorption cycles. It is seen that the height of the desorption peak increased linearly with inlet pressure. Increased pressure (flow rate) forced the desorbed molecules to exit the device faster resulting in a narrower peak. The constant peak area indicated that the peak was only getting sharper with increased pressure. This allowed us to determine the optimal inlet pressure that would result in the sharpest desorption pulse. Furthermore, the height of the desorption peak reached a maximum value then decreased along with the peak's area when the pressure exceeded 25 psi. At high pressure (flow rate) the molecule residence time within the device was shortened

during the adsorption cycle, which decreased the interaction of vapor molecules with the device inner surface, thus reducing the adsorption efficiency. The device operation was found to be optimal at an inlet pressure of 25 psi. It is worth mentioning that the device can operate under two different flow rates. A low flow rate during adsorption and a high flow rate during desorption. In this case, the inlet pressure can exceed 25 psi during desorption to produce a sharper peak without affecting the amount of adsorbed sample (peak area).

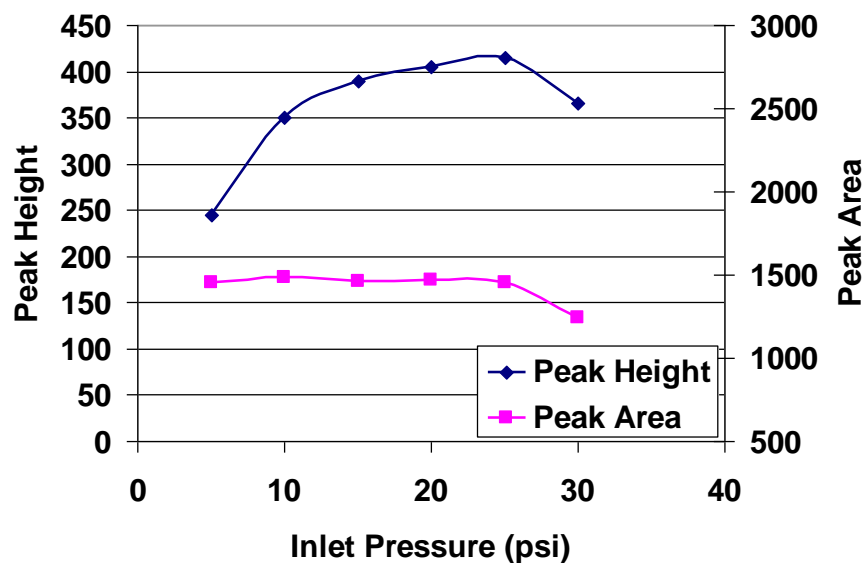
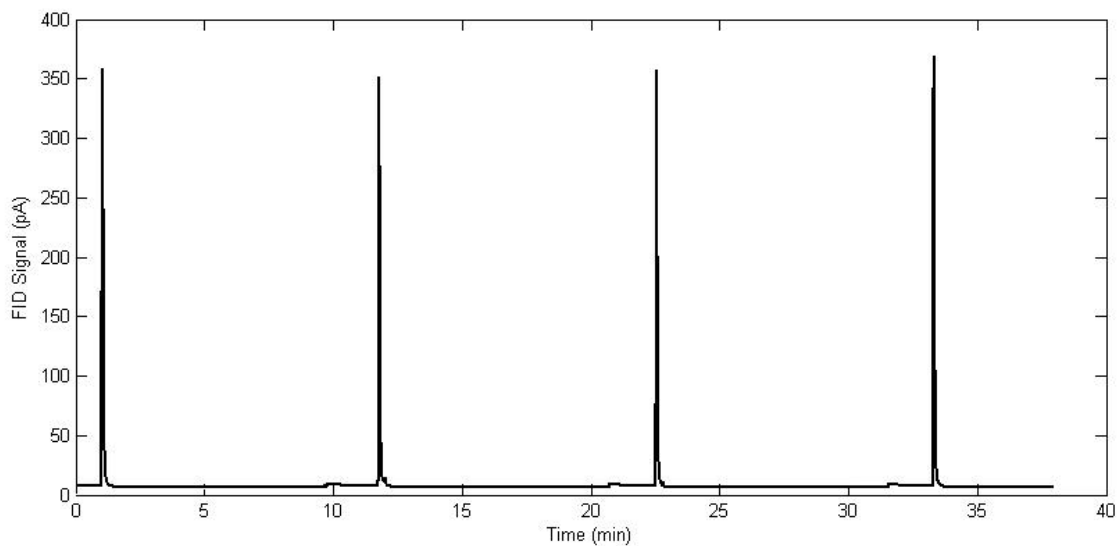


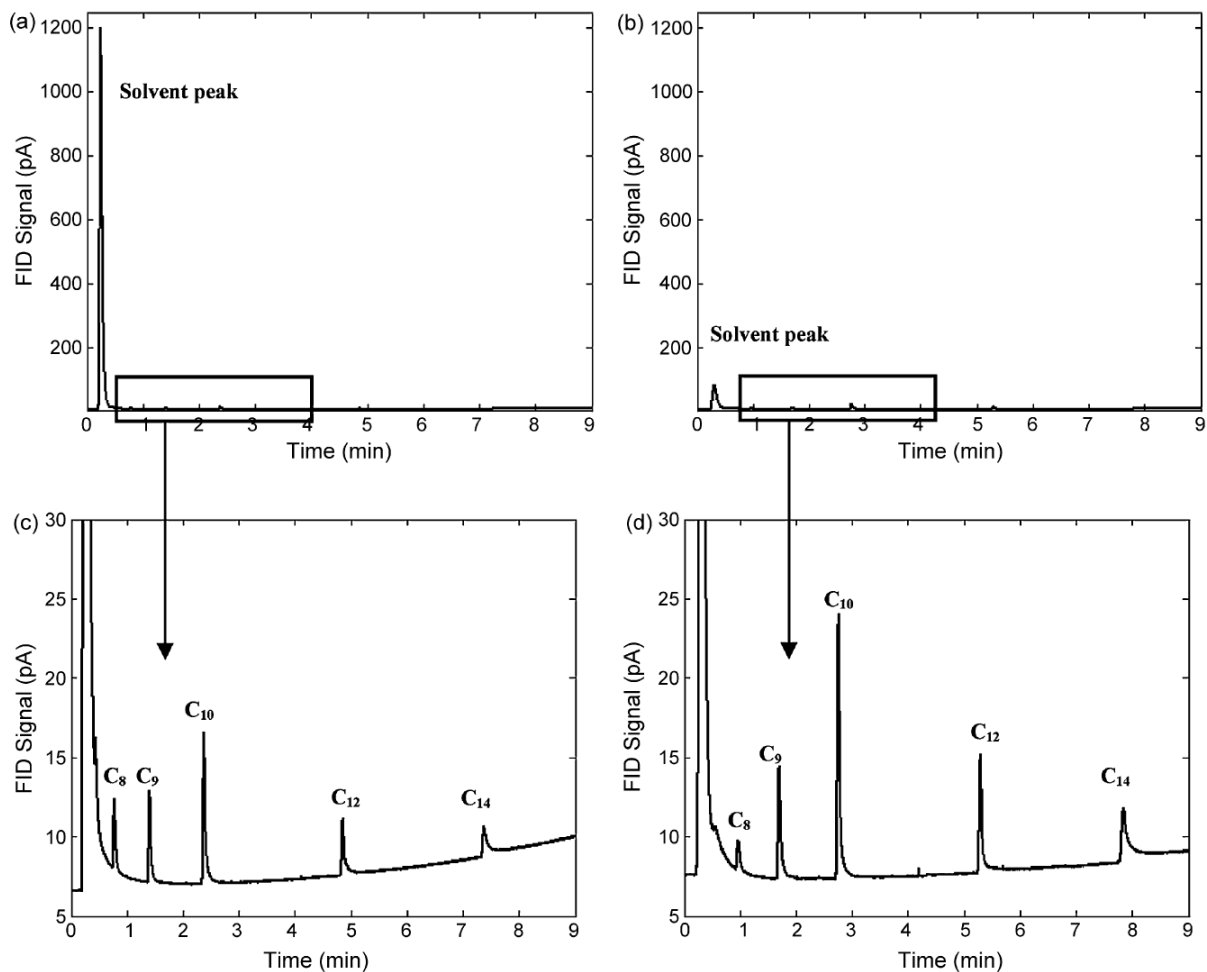
Figure 14 Height and area of the desorption peak as a function of pressure

Figure 15 demonstrates a series of desorption pulses generated by the  $\mu$ PC coated by Tenax TA. Reproducibility in terms of peak height and area was excellent, and the adsorption/desorption process could be continued indefinitely. To further demonstrate the capability of our device, the  $\mu$ PC was used as a GC injector. The device was put on-line with a 2 m-long, 100  $\mu$ m-ID fused silica capillary column coated in-house with a methylpolysiloxane stationary phase. The  $\mu$ PC was loaded with a diluted sample, a mixture of 5 hydrocarbon compounds: n-octane ( $C_8$ ), n-nonane ( $C_9$ ), n-decane ( $C_{10}$ ), n-dodecane ( $C_{12}$ ), and n-tetradecane ( $C_{14}$ ). The fast thermal desorption enabled sharp peak injection comparable to what could be produced by the GC injection port as shown in Figure 16. The initial and final temperatures of the column were 35  $^{\circ}$ C and 150  $^{\circ}$ C with temperature programming of 10  $^{\circ}$ C/min and an inlet

pressure of 20 psi. Figure 16 (a) and (b) represent the chromatogram obtained by injecting the sample through the GC conventional injector and the  $\mu$ PC, respectively. The solvent peak is significantly smaller in the  $\mu$ PC injection pulse indicating that the device did not concentrate most of the solvent (dichloromethane). Yet, most of the separated compounds show a higher peak when injected through the  $\mu$ PC as clearly demonstrated in the zoomed-in chromatograms. This indicates that the  $\mu$ PC was successful in preconcentrating the compounds in the diluted sample. The shift in the peaks' elution time resulted from the change in the flow in the system due to the placement of the  $\mu$ PC. It should be noted that only a fraction of the sample introduced to the  $\mu$ PC is trapped as some of it will pass through without being adsorbed. As mentioned earlier, this can be suppressed if a lower flow rate is employed during adsorption.



**Figure 15 Series of  $\mu$ PC generated desorption pulses**



**Figure 16 Hydrocarbon mixture sample injection chromatograms (sample volume 1  $\mu\text{L}$ ), (a) represent the sample injected through the GC's conventional injection port with a zoomed-in version below it, (b) represent the sample injected by the  $\mu\text{TPC}$  fast thermal desorption with a zoomed-in version below it**

### 3.5 Conclusions

The quality of gas mixture analysis relies on the sample pretreatment. MEMS technology could lead to the development of  $\mu\text{PCs}$  having smaller sizes, lower pressure drops, lower power consumptions, and higher efficiencies compared to conventional counterparts (microtraps). By utilizing embedded pillars, we have demonstrated a hybrid configuration combining exhaustive (large surface area) and equilibrium (small flow restrictions) designs. The high-aspect-ratio structures needed for the  $\mu\text{PC}$  design were produced using deep reactive ion etching of silicon. A concentration factor of 1000 was achieved using the presented microfabricated preconcentrators

which were coated by Tenax TA using the inkjet printing principle. Work is under way to explore different structural possibilities including the size and spacing of micropillars and to evaluate their effects on the uniform coating of the pillar array using the aforementioned technique.

CFD analysis verified by experimental results has shown the effect of the distributed inlet/outlet as well as the pillars geometry and configuration on the  $\mu$ PC performance. The increase in the PC factor for the uncoated devices is attributed to the effective dispersing of the sample among the pillars during the adsorption process. Future work will aim to better understand and model the behavior of the  $\mu$ PC under different conditions.

The performance of the presented  $\mu$ PC was evaluated in terms of the adsorption capacity (different adsorbent material), pillar packing density (distance between pillars), and inlet pressure. The  $\mu$ PC demonstrated very sharp reproducible desorption peaks needed for fast on-field analytical analysis. For proof of concept, the  $\mu$ PC was used as a GC injector. The device was successful in concentrating diluted multi-compound hydrocarbon mixture and in delivering the concentrated sample into a separation column by producing a sharp pulse suitable for GC analysis.

## References

- [1] B. Alfeeli, D. Cho, M. Ashraf-Khorassani, L. T. Taylor, and M. Agah, "Mems-Based Multi-Inlet/Outlet Preconcentrator Coated by Inkjet Printing of Polymer Adsorbents," *Sensors and Actuators B, Chemical*, vol. 133, 2008, pp. 24-32.
- [2] C. K. Ho, A. Robinson, D. R. Miller, and M. J. Davis, "Overview of Sensors and Needs for Environmental Monitoring," *Sensors*, vol. 5, 2005, pp. 4-37.
- [3] S. C. Terry, J. H. Jerman, and J. B. Angell, "A Gas Chromatographic Air Analyzer Fabricated on a Silicon Wafer," *IEEE Transactions on Electron Devices*, vol. 26, 1979, pp. 1880-1886.
- [4] G. A. Thomas, G. C. Frye-Mason, C. Bailey, M. E. Warren, J. A. Fruetel, K. Wally, J. Wu, R. J. Kottenstette, and E. J. Heller, "Microchemlabtm -an Integrated Microanalytical System for Chemical Analysis Using Parallel Gas and Liquid Phase Microseparations," in *SPIE Conference on Unattended Ground Sensor Technologies and Applications*, Orlando, FL, 1999, pp. 66-76.
- [5] E. S. Kolesar, Jr. and R. R. Reston, "Silicon Micromachined Gas Chromatography System," in *Second Annual IEEE International Conference on Innovative Systems in Silicon*, Austin, TX, 1997, pp. 117-125.



- [6] H. Pham Tuan, H.-G. Janssen, and C. A. Cramers, "Novel Preconcentration Technique for on-Line Coupling to High-Speed Narrow-Bore Capillary Gas Chromatography: Sample Enrichment by Equilibrium (Ab)Sorption: I. Principles and Theoretical Aspects," *Journal of Chromatography A*, vol. 791, 1997, pp. 177-185.
- [7] W. C. Tian, H. K. L. Chan, S. W. Pang, C. J. Lu, and E. T. Zellers, "High Sensitivity Three-Stage Microfabricated Preconcentrator-Focuser for Micro Gas Chromatography," in *International Conference on Solid-State Sensors, Actuators and Microsystems, TRANSDUCERS'03*, 2003, pp. 131-134.
- [8] W.-C. Tian, S. W. Pang, L. Chia-Jung, and E. T. Zellers, "Microfabricated Preconcentrator-Focuser for a Microscale Gas Chromatograph," *Journal of Microelectromechanical Systems*, vol. 12, 2003, pp. 264-272.
- [9] M. Agah, J. A. Potkay, G. Lambertus, R. Sacks, and K. D. Wise, "High-Performance Temperature-Programmed Microfabricated Gas Chromatography Columns," *Journal of Microelectromechanical Systems*, vol. 14, 2005, pp. 1039-1050.
- [10] W.-C. Tian, H. K. L. Chan, L. Chia-Jung, S. W. Pang, and E. T. Zellers, "Multiple-Stage Microfabricated Preconcentrator-Focuser for Micro Gas Chromatography System," *Journal of Microelectromechanical Systems*, vol. 14, 2005, pp. 498-507.
- [11] M. Agah, G. R. Lambertus, R. Sacks, and K. Wise, "High-Speed MemS-Based Gas Chromatography," *Journal of Microelectromechanical Systems*, vol. 15, 2006, pp. 1371-1378.
- [12] P. R. Lewis, P. Manginell, D. R. Adkins, R. J. Kottenstette, D. R. Wheeler, S. S. Sokolowski, D. E. Trudell, J. E. Byrnes, M. Okandan, J. M. Bauer, R. G. Manley, and C. Frye-Mason, "Recent Advancements in the Gas-Phase Microchemlab," *IEEE Sensors Journal*, vol. 6, 2006, pp. 784-795.
- [13] R. W. Cernosek, A. L. Robinson, D. Y. Cruz, D. R. Adkins, J. L. Barnett, J. M. Bauer, M. G. Blain, J. E. Byrnes, S. M. Dirk, G. R. Dulleck, J. A. Ellison, J. G. Fleming, T. W. Hamilton, E. J. Heller, S. W. Howell, R. J. Kottenstette, P. R. Lewis, R. P. Manginell, M. W. Moorman, C. D. Mowry, R. G. Manley, M. Okandan, K. Rahimian, G. J. Shelmidine, R. J. Shul, R. J. Simonson, S. S. Sokolowski, J. J. Spates, A. W. Staton, D. E. Trudell, D. R. Wheeler, and W. G. Yelton, "Micro-Analytical Systems for National Security Applications," in *Micro (MEMS) and Nanotechnologies for Space Applications*, Orlando (Kissimmee), FL, USA, 2006, pp. 622306-622313.
- [14] M. Agah and K. D. Wise, "Low-Mass Pecvd Oxynitride Gas Chromatographic Columns," *Journal of Microelectromechanical Systems*, vol. 16, 2007, pp. 853-860.
- [15] A. M. Ruiz, I. Gracia, N. Sabate, P. Ivanov, A. Sanchez, M. Duch, M. Gerboles, A. Moreno, and C. Cane, "Membrane-Suspended Microgrid as a Gas Preconcentrator for Chromatographic Applications," *Sensors and Actuators A: Physical*, vol. 135, 2007, pp. 192-196.

- [16] J. A. Potkay, G. R. Lambertus, R. D. Sacks, and K. D. Wise, "A Low-Power Pressure- and Temperature-Programmable Micro Gas Chromatography Column," *Journal of Microelectromechanical Systems*, vol. 16, 2007, pp. 1071-1079.
- [17] D. Helmig, "Air Analysis by Gas Chromatography," *Journal of Chromatography A*, vol. 843, 1999, pp. 129-146.
- [18] J. W. Grate, S. L. Rose-Pehrsson, D. L. Venezky, M. Klusty, and H. Wohltjen, "Smart Sensor System for Trace Organophosphorus and Organosulfur Vapor Detection Employing a Temperature-Controlled Array of Surface Acoustic Wave Sensors, Automated Sample Preconcentration, and Pattern Recognition," *Analytical Chemistry*, vol. 65, 1993, pp. 1868-1881.
- [19] S. Mitra and C. Yun, "Continuous Gas Chromatographic Monitoring of Low Concentration Sample Streams Using an on-Line Microtrap," *Journal of Chromatography A*, vol. 648, 1993, pp. 415-421.
- [20] S. Mitra, Y. H. Xu, W. Chen, and A. Lai, "Characteristics of Microtrap-Based Injection Systems for Continuous Monitoring of Volatile Organic Compounds by Gas Chromatography," *Journal of Chromatography A*, vol. 727, 1996, pp. 111-118.
- [21] W. A. Groves, E. T. Zellers, and G. C. Frye, "Analyzing Organic Vapors in Exhaled Breath Using a Surface Acoustic Wave Sensor Array with Preconcentration: Selection and Characterization of the Preconcentrator Adsorbent," *Analytica Chimica Acta*, vol. 371, 1998, pp. 131-143.
- [22] T. Nakamoto, Y. Isaka, T. Ishige, and T. Moriizumi, "Odor-Sensing System Using Preconcentrator with Variable Temperature," *Sensors and Actuators B: Chemical*, vol. 69, 2000, pp. 58-62.
- [23] C. J. Lu and E. T. Zellers, "A Dual-Adsorbent Preconcentrator for a Portable Indoor-Voc Microsensor System," *Analytical Chemistry*, vol. 73, July 15, 2001 2001, pp. 3449-3457.
- [24] A. Kroupa, J. Dewulf, H. Van Langenhove, and I. Viden, "Breakthrough Characteristics of Volatile Organic Compounds in the -10 to +170 Oc Temperature Range on Tenax Ta Determined by Microtrap Technology," *Journal of Chromatography A*, vol. 1038, 2004, pp. 215-223.
- [25] S. Mitra, M. Karwa, and Z. Iqbal, "Self-Assembly of Nano-Particles for Preconcentration in Environmental Sensing Platforms," in *227th ACS National Meeting*, Anaheim, CA, 2004.
- [26] T. Nakamoto, K. Sukegawa, and E. Sumitomo, "Higher Order Sensing Using Qcm Sensor Array and Preconcentrator with Variable Temperature," *IEEE Sensors Journal*, vol. 5, 2005, pp. 68-74.
- [27] C. Thammakhet, P. Thavarungkul, R. Brukh, S. Mitra, and P. Kanatharana, "Microtrap Modulated Flame Ionization Detector for on-Line Monitoring of Methane," *Journal of Chromatography A*, vol. 1072, 2005, pp. 243-248.
- [28] F. Zheng, D. L. Baldwin, L. S. Fifield, N. C. Anheier, C. L. Aardahl, and J. W. Grate, "Single-Walled Carbon Nanotube Paper as a Sorbent for Organic Vapor Preconcentration," *Analytical Chemistry*, vol. 78, 2006, pp. 2442-2446.

- [29] M. Libardoni, P. T. Stevens, J. H. Waite, and R. Sacks, "Analysis of Human Breath Samples with a Multi-Bed Sorption Trap and Comprehensive Two-Dimensional Gas Chromatography (Gc X Gc)," *Journal of Chromatography B*, vol. 842, 2006, pp. 13-21.
- [30] R. P. Manginell, G. C. Frye-Mason, R. J. Kottenstette, P. R. Lewis, and C. Channy Wong, "Microfabricated Planar Preconcentrator," in *Solid-State Sensors, Actuators, and Microsystems Workshop, Hilton Head'00*, 2000, pp. 179-182.
- [31] M. Kim and S. Mitra, "A Microfabricated Microconcentrator for Sensors and Gas Chromatography," *Journal of Chromatography A*, vol. 996, 2003, pp. 1-11.
- [32] H. K. L. Chan, S. W. Pang, R. A. Veeneman, E. T. Zellers, and M. Takei, "Microfabricated Preconcentrator for Quantitative Analysis of Low Concentration Volatile Organic Compounds," in *International Conference on Solid-State Sensors, Actuators and Microsystems, TRANSDUCERS'07*, Korea, 2005, pp. 2091-2094.
- [33] C. E. Davis, C. K. Ho, R. C. Hughes, and M. L. Thomas, "Enhanced Detection of M-Xylene Using a Preconcentrator with a Chemiresistor Sensor," *Sensors and Actuators B: Chemical*, vol. 104, 2005, pp. 207-216.
- [34] E. W. Simoes, S. G. de Souza, M. L. P. da Silva, R. Furlan, and H. E. Maldonado Peres, "Study of Preconcentration of Non-Polar Compounds in Microchannels with Constrictions," *Sensors and Actuators B: Chemical*, vol. 115, 2006, pp. 232-239.
- [35] I. Voiculescu, R. A. McGill, M. E. Zaghoul, D. Mott, J. Stepnowski, S. Stepnowski, H. Summers, V. Nguyen, S. Ross, K. Walsh, and M. Martin, "Micropreconcentrator for Enhanced Trace Detection of Explosives and Chemical Agents," *IEEE Sensors Journal*, vol. 6, 2006, pp. 1094-1104.
- [36] S. M. Cho, Y. J. Kim, G. S. Heo, and S.-M. Shin, "Two-Step Preconcentration for Analysis of Exhaled Gas of Human Breath with Electronic Nose," *Sensors and Actuators B: Chemical*, vol. 117, 2006, pp. 50-57.
- [37] M. Martin, M. Crain, K. Walsh, R. A. McGill, E. Houser, J. Stepnowski, S. Stepnowski, H.-D. Wu, and S. Ross, "Microfabricated Vapor Preconcentrator for Portable Ion Mobility Spectroscopy," *Sensors and Actuators B: Chemical*, vol. 126, 2007, pp. 447-454.
- [38] P. Ivanov, F. Blanco, I. Gracia, N. Sabate, A. Ruiz, X. Vilanova, X. Correig, L. Fonseca, E. Figueras, J. Santander, and C. Cane, "Improvement of the Gas Sensor Response Via Silicon M-Preconcentrator," *Sensors and Actuators B: Chemical*, vol. 127, 2007, pp. 288-294.
- [39] S. Li, J. C. Day, J. J. Park, C. P. Cadou, and R. Ghodssi, "A Fast-Response Microfluidic Gas Concentrating Device for Environmental Sensing," *Sensors and Actuators A: Physical*, vol. 136, 2007, pp. 69-79.
- [40] C. Pijolat, M. Camara, J. Courbat, J. P. Viricelle, D. Briand, and N. F. de Rooij, "Application of Carbon Nano-Powders for a Gas Micro-Preconcentrator," *Sensors and Actuators B: Chemical*, vol. 127, 2007, pp. 179-185.
- [41] Y. Tang, J. Yeom, J. Han, B. Bae, R. I. Masel, and M. A. Shannon, "A Micro-Post Preconcentrator for a Microscale Gas Chromatography System," in *International Conference*

*on Miniaturized Systems for Chemistry and Life Sciences, MicroTAS'05*, Boston, MA, 2005, pp. 660-662.

[42] B. R. Munson, D. F. Young, and T. H. Okiishi, *Fundamentals of Fluid Mechanics*, 5th Edition ed. New York: Wiley, 2006.

## Chapter Four: MEMS-based Selective Preconcentration of Trace Level Breath Analytes

Part of this chapter was reproduced from [1] with permission from IEEE

*B. Alfeeli and M. Agah, "MEMS-Based Selective Preconcentration of Trace Level Breath Analytes," IEEE Sensors Journal, vol. 9, 2009, pp. 1068-1075.*

### 4.1 Introduction

Human breath contains a complex mixture of volatile organic compounds (VOCs) at very low concentrations typically in the parts per billion (ppb) range [2]. The VOCs content in breath is derived mainly from blood by passive diffusion across the pulmonary alveolar membrane [3]. The identification and quantification of VOCs in human breath can lead to early diagnosis or evaluation of several common disorders such as lung cancer, pneumonia, heart disease, rheumatoid arthritis, inflammatory bowel disease, malnutrition, and exposure to environmental toxins [4].

The long-term objective of our work is to develop a self-contained handheld instrument that would offer sensitive, accurate, reliable, and easy-to-use breath analysis at low cost to facilitate its use in physicians' offices. However, breath analysis is not a trivial task for several reasons. First, the trace level concentrations of VOCs in breath are difficult to detect by conventional sensors. Second, the interfering species in the breath sample such as water vapor, carbon dioxide, and methane [5] can hinder the detection sensitivity or the analysis accuracy [6]. Third, is the high level of breath complexity containing more than 1200 VOCs [4] which include alcohols, ketones and aldehydes [7] which makes it difficult to identify breath biomarkers.

The current breath analysis is carried out in an analytical laboratory by highly trained technicians. The breath sample is collected from the patient in an inert gas sample bag (Tedlar bag) [8]. Then, the laboratory technician performs sample preconcentration procedure followed by chromatographic separation and mass spectrometry detection (GC-MS) in order to analyze the

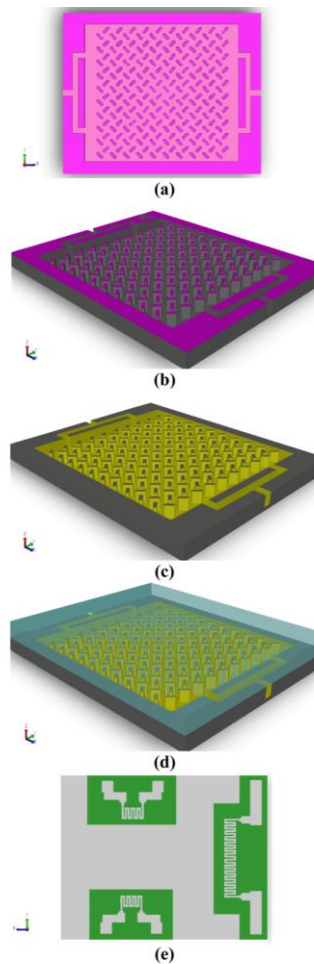
breath sample [9, 10]. This procedure is inconvenient, time consuming, and prone to sample contamination and/or its loss.

In addition, current gas chromatography (GC) systems are large, require intensive maintenance, and are expensive table-top instruments with high power consumptions [11]. Microelectromechanical systems (MEMS) technology has made it possible to miniaturize GC components such as preconcentrators (PC) and separation columns for various sensing and monitoring applications [12-27]. This chapter addresses the three abovementioned technical challenges through the utilization of MEMS-based preconcentrators. The presented high performance device improves the detection limit of breath components. It can selectively preconcentrate the analytes of interest in breath which can later be processed by a short  $\mu$ GC column. Moreover, by cascading multiple devices, the influence of the interfering species (mainly water vapor) can be significantly reduced.

## ***4.2 Preconcentration Technology***

Traditional PCs consist of tubing packed with granular adsorbent. Packing these tubes with small particles could result in significant pressure drops and poor heat transfer. Moreover, excessive peak broadening may occur if their volume is large relative to the detector cell. Their size also limits the sampling speed (duty cycle) since additional time is needed for cooling prior to subsequent sample collection. Equilibrium based PCs consist of tubing in which the inner wall is coated with an adsorbent material. They overcome some of the disadvantages of exhaustive PCs but their sample capacity is limited due to their small adsorption surface area. This limitation becomes most dominant in equilibrium based  $\mu$ PCs due to their small dimensions. Nevertheless,  $\mu$ PCs offer lower pressure drop, lower power consumptions, and higher efficiencies compared to their conventional counterparts [14]. To date, different  $\mu$ PC configurations such as packed compartments, and coated planar surface, micro channels, and 3D microstructures have been reported in literature [18-25, 28-31]. In general PCs are characterized by a figure of merit known as the preconcentration factor (PF). The preconcentration factor is defined as the ratio of the area under the detector's signal with and without the presence of the  $\mu$ PC [32]. The reported  $\mu$ PCs have PF values that range from 6 to 6000.

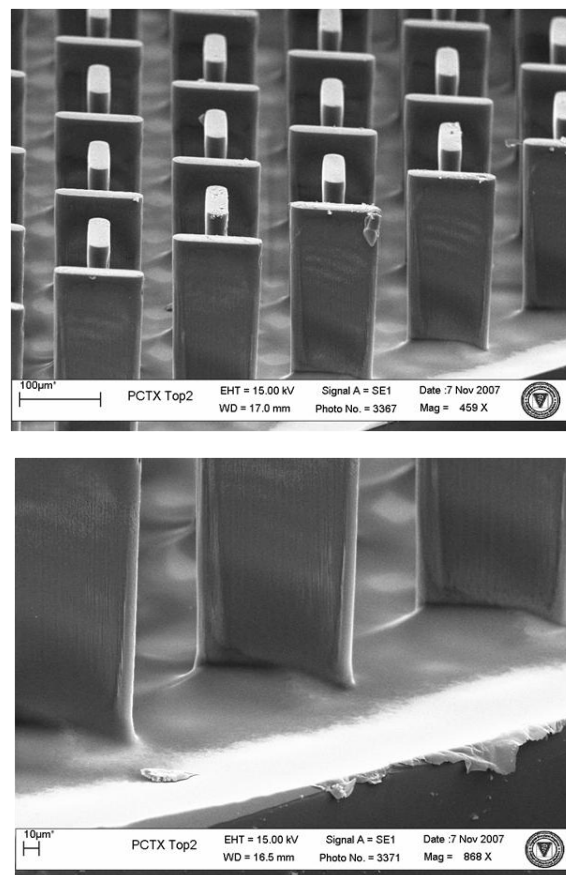
The  $\mu$ PCs used in this study contain an array of 3D micro pillars and is similar to our previously reported work [11]. Figure 17 summarizes the fabrication process of the  $\mu$ PC.



**Figure 17 (a) Photolithography (b) Deep reactive-ion etching (DRIE) (c) Coating the pillars with adsorbent polymer by inkjet printing (d) Sealing the device with Pyrex by anodic bonding (e) Patterning of thin-film resistive heaters and temperature sensors over PECVD oxide at the back of the device, © [2009] IEEE. Reprinted, with permission, from [1]**

First, the design pattern was transferred to a silicon wafer via standard photolithography as shown in Figure 17 (a). Second, the silicon wafer was etched by a single step deep reactive ion etching (Figure 17 (b)) followed by oxygen plasma clean step to remove any residual fluorocarbon on the etched surface. The devices were then coated with 2,6-diphenylene oxide

polymer (Tenax TA) by inkjet printing as shown in Figure 17 (c). Inkjet printing technique produced excellent coverage and uniform coating as shown in Figure 18. The wafer was then sealed with Pyrex wafer by anodic bonding process (Figure 17 (d)) at 1250 V and 300 °C instead of conventional 350-400 °C bonding temperature to avoid damaging the polymer. The maximum recommended operating temperature by the manufacturer for Tenax TA is 350 °C. The final step was patterning thin film Ti/Pt resistive heaters and temperature sensors over plasma enhanced chemical vapor deposition (PECVD) oxide on the back side of the silicon wafer as shown in Figure 17 (e).




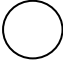
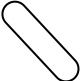
**Figure 18 SEM monographs showing the coverage and uniformity of Tenax TA coating technique, © [2009] IEEE. Reprinted, with permission, from [1]**

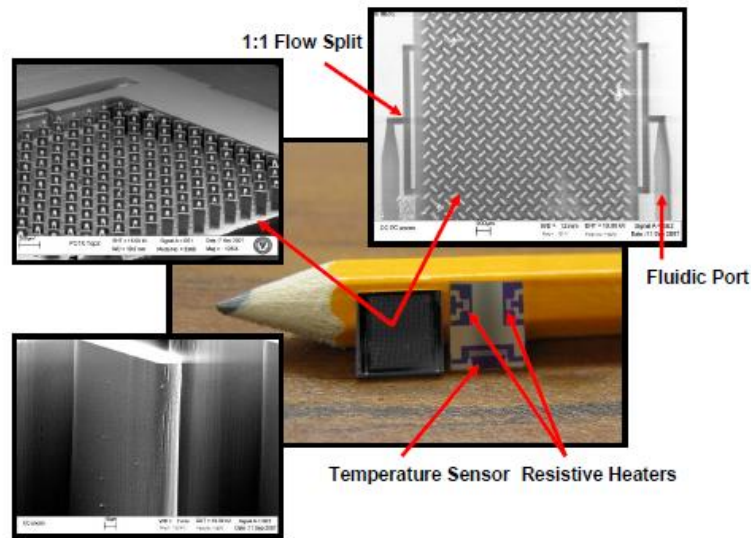
The outer dimensions of the silicon-glass chip were 7 mm × 7 mm × 1 mm. The µPC specific surface area was measured to be 10 m<sup>2</sup>/g (gas sorption method) with a volume of about 6.5 µL.



The dimensions of the high-aspect-ratio pillars were  $30\ \mu\text{m} \times 120\ \mu\text{m} \times 240\ \mu\text{m}$ . For this work, different pillar geometries and configurations have been designed and fabricated to evaluate their effectiveness for sample preconcentration. The available surface area and density of the pillars which are indicators of the microchip sample capacity are summarized in Table 2. Figure 19 illustrates the top and bottom views of the  $\mu\text{PC}$  placed in front of a pencil to give a size prospective.

**Table 2 Calculated Pillars Surface Area and Density, © [2009] IEEE. Reprinted, with permission, from [1]**

<i>Pillar Shape</i>	<i>Pillar Surface Area (mm<sup>2</sup>)</i>	<i>Pillars/mm<sup>3</sup></i>
	0.048	100
	0.038	100
	0.066	90



**Figure 19 Optical image of the  $\mu\text{PC}$  showing the front and back sides of the device, insets are SEM monographs of the etched 3D structures and the fluidic ports, © [2009] IEEE. Reprinted, with permission, from [1]**

### 4.3 Experimental

The testing setup was installed inside a commercial GC oven in order to maintain isothermal temperature conditions. Moreover, the built-in auxiliary systems such as a gas flow controller and flame ionization detector (FID) were also utilized to ensure consistent testing parameters. Carrier gas was supplied via the GC inlet and controlled by the flow controller. The testing setup consisted of two six-port zero-dead-volume valves, and deactivated fused silica transfer lines configured as shown in Figure 20. The inertness of the setup was tested. Figure 20 (a) shows the test setup with the valves set in the “loading position”. The sample was injected by a precision sampling syringe into the GC injector. The GC column was kept offline to prevent the sample from reaching it at this stage. Figure 20 (b) portrays the valves set in the “injection position.” In this configuration, the GC column was connected to the preconcentrator. The  $\mu$ PC was heated rapidly to 250 °C at 100 °C/sec to inject the collected sample into the column. The inlet pressure was adjusted to achieve 1 mL/min flow rate through the  $\mu$ PC and column. Figure 20 (c) illustrates the valves set in the “separation position.” Here, the  $\mu$ PC was taken offline and the column was heated to 150 °C from 35 °C at 30 °C/min.

The sample adsorption/desorption and the chromatographic separation were measured by the FID. The on-board resistive heaters and temperature sensors were not used in this experiment. Instead, an off-board high-performance ceramic heater (ultra-fast ramp rate) was used for thermal desorption along with a K-type thermocouple for manual temperature monitoring and control. In future work, the on-chip thermal desorption capability will be used. For two-step preconcentration, the single  $\mu$ PC was replaced with two  $\mu$ PCs connected in series.

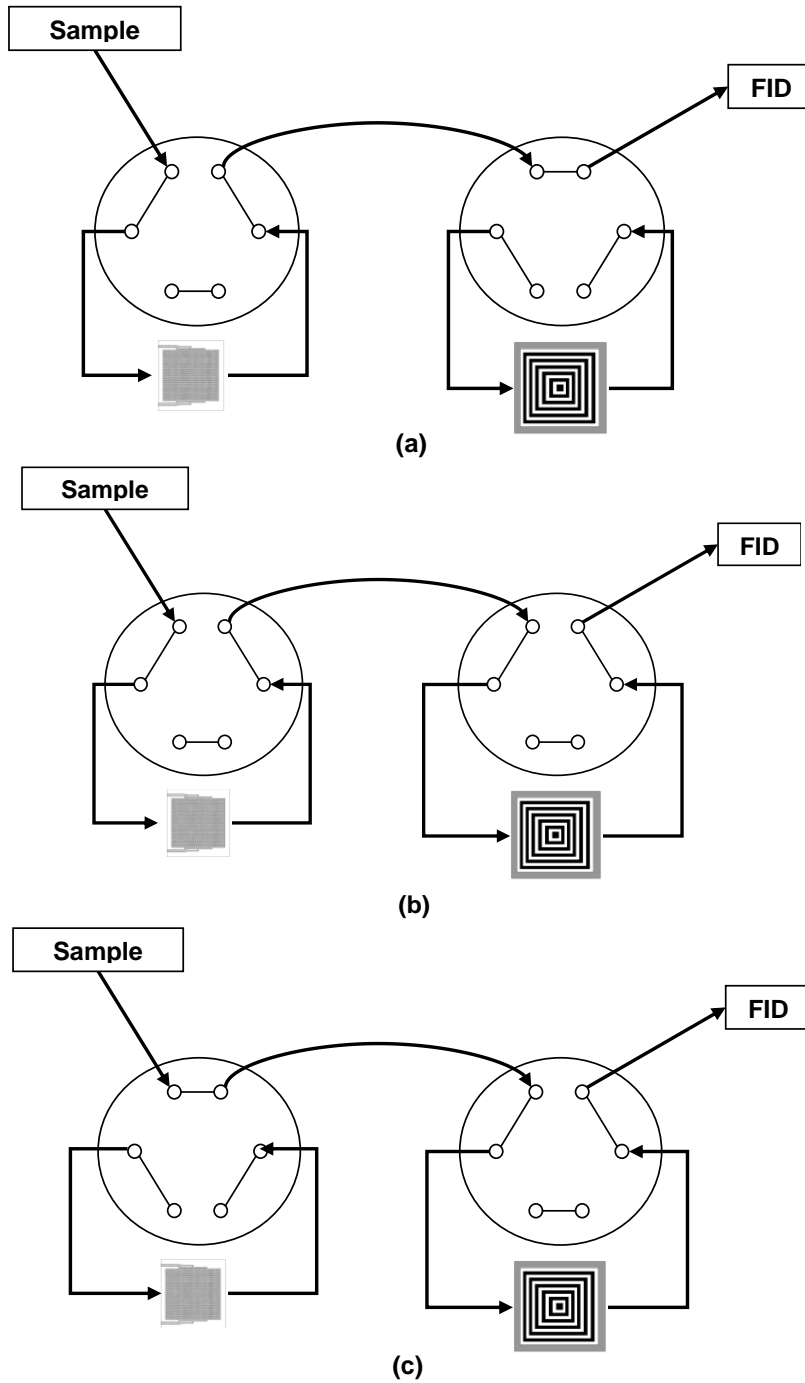


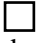






Figure 20  $\mu$ PC test setup with the valves set in the (a) loading position, (b) injection position, and (c) separation position, © [2009] IEEE. Reprinted, with permission, from [1]

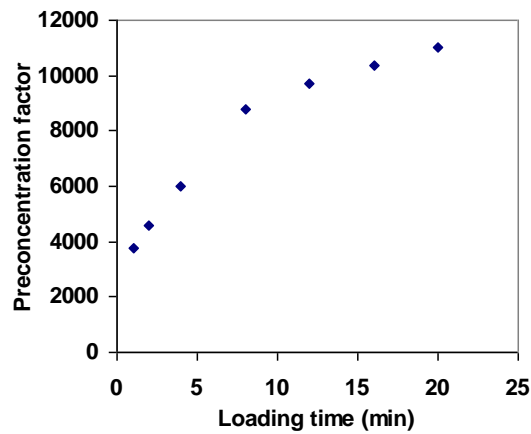
## *4.4 Results and Discussion*

### *4.4.1 Performance Evaluation*

Table 3 summarizes the preconcentration factor measured on both coated and uncoated  $\mu$ PCs under similar conditions by loading the chip with 1  $\mu$ L of n-nonane ( $C_9$ ) and then thermally desorbing it at 100 °C/sec up to 250 °C. The area under the FID curve was used to determine the preconcentration factor. In the ordered pillar design, the flow in the perpendicular direction cannot pass to the other side due to the relatively fast flow in the parallel direction, thus creating a stagnation point. This flow pattern indicated that the sample molecules do not effectively collide with half of the pillar surfaces, thus decreasing the adsorption surface and resulting in a low PF of 7. This shortcoming was minimized in the circular staggered and crisscross designs which resulted in the doubling of PF. Moreover, significant increase in the preconcentration factor was observed when the microfluidic ports connecting the inner cavity with the outside world were branched into two channels at each side of the cavity instead of a single channel. This is attributed to the flow pattern created by these fluidic ports within the cavity. In the single channel design, the flow velocity was highest in the middle of the cavity giving rise to an undesired flow concentration. The branching of the single channel into two lessened this effect allowing more interaction between the pillars and the gaseous sample, thus increasing the PF from 22 to 32 in the case of crisscross design. All subsequent tests were performed on the coated crisscross design. The maximum concentration factor for the crisscross design with double inlet/outlet and 80  $\mu$ m spacing between pillars was also determined by varying the loading time at a continuous and constant concentration of isopropanol vapor as shown in Figure 21 and it was determined to be more than 10,000.

**Table 3 Preconcentration Factor for Different Designs, © [2009] IEEE. Reprinted, with permission, from [1]**

<i>Design</i>	<i>Number of Inlet/Outlets</i>	<i>Spacing Between Pillars</i>	<i>PF</i>
No Pillars	1	-	4
 Ordered	1	50	7
 Staggered	1	50	20
 Staggered	2	50	28
 Crisscross	1	80	22
 Crisscross	2	80	32
 Crisscross	1	80 + Tenax TA	700
 Crisscross	2	80 + Tenax TA	1000



**Figure 21  $\mu$ PC sample preconcentration factor as a function of time at constant concentration of pure isopropanol vapor, © [2009] IEEE. Reprinted, with permission, from [1]**

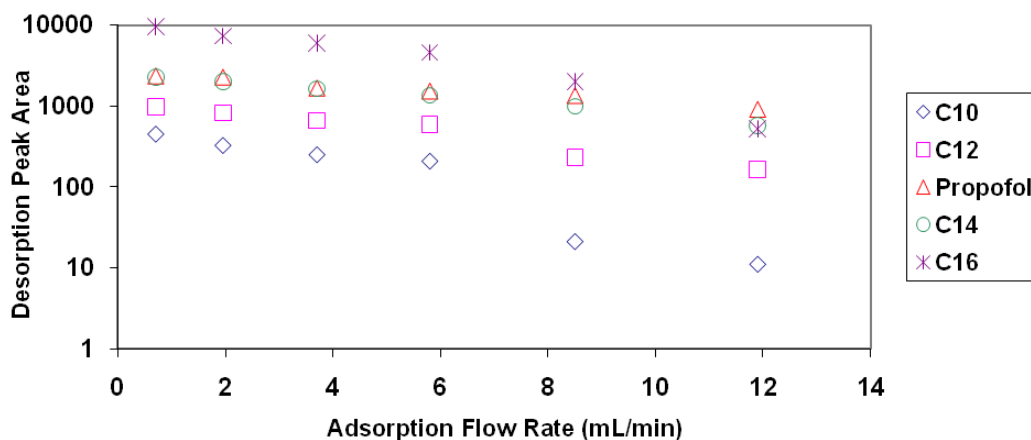
#### 4.4.2 Preconcentrator Behavior

For preliminary evaluation, we used several compounds found in human breath undergoing anesthesia [4] such as n-decane ( $C_{10}$ ), n-dodecane ( $C_{12}$ ), 2,6-diisopropylphenol (Propofol), n-tetradecane ( $C_{14}$ ), and n-hexadecane ( $C_{16}$ ) diluted in 1-propanol at a concentration of 500  $\mu\text{g/mL}$ . Propofol is widely used substance for anesthesia and sedation in various clinical settings. Continuous assessment of depth of anesthesia (Propofol content in breath) is important to prevent accidental awaking of patients during surgery. 1-propanol was chosen instead of water vapor present in breath mainly because the available detector (FID) was water insensitive. It should be noted that the retention volume of solvents such as dichloromethane and 1-propanol on the adsorbent (Tenax TA) is larger than water by a factor of 19 and 26, respectively [33]. Water and 1-propanol share similar boiling point and polarity. As a model for a portable  $\mu\text{GC}$ , the  $\mu\text{PC}$  was put in series with a 1 m fused silica column coated with methylpolysiloxane to resemble a MEMS column.

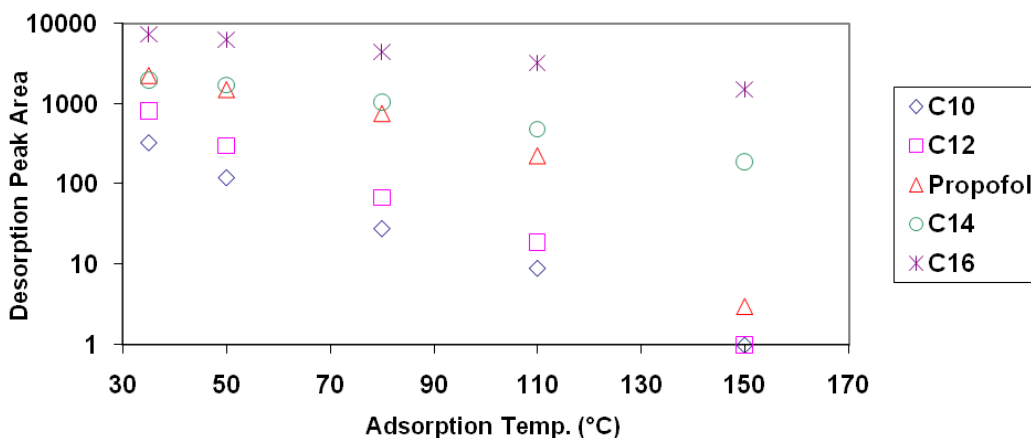
The adsorption time ( $\tau_a$ ), the time needed for a gas molecule to be trapped once the gas sample enters the preconcentrator, depends on the physical and chemical properties of both the gas molecule and the adsorbent surface. The residence time ( $\tau$ ), which is the time needed for a molecule to pass through the preconcentrator at a specific linear velocity, is equivalent to the maximum time that a non-adsorbed molecule can reside in the preconcentrator. In order to achieve high preconcentration efficiency, the residence time should be greater than the adsorption time,  $\tau \gg \tau_a$ . In other words, the sample molecule should reside within the preconcentrator much longer than the time needed for the molecule to be adsorbed. The molecule residence time, however, is inversely proportional to the flow rate and the adsorbent temperature. To evaluate the effects of these two important controllable parameters on VOC adsorption in the  $\mu\text{PC}$ , calibrations (desorption peak area vs. parameter of interest) for VOCs used in this study were conducted. This was done by using adsorption flow rates ranging from 0.7 mL/min to 12 mL/min and adsorption temperatures ranging from 35 °C to 150 °C.

Figure 22 shows the inverse relationship between adsorption versus flow rate and temperature. As expected, adsorption decreases with increasing flow rate and/or temperature. At higher flow rates, the molecule residence time shortens decreasing the interaction of molecules with the

adsorbent surface and, thus, reducing the adsorption efficiency. Likewise, at higher temperatures, the molecules are less likely to stay on the surface due to their high thermal energy. Propofol desorption peak area dropped by approximately 50% as the flow rate increased from 2 mL/min to 12 mL/min. At an adsorption temperature of 80 °C, the desorption peak areas of C<sub>10</sub> and C<sub>12</sub> dropped significantly suggesting that these two compounds are hardly adsorbed at this temperature.



(a)



(b)

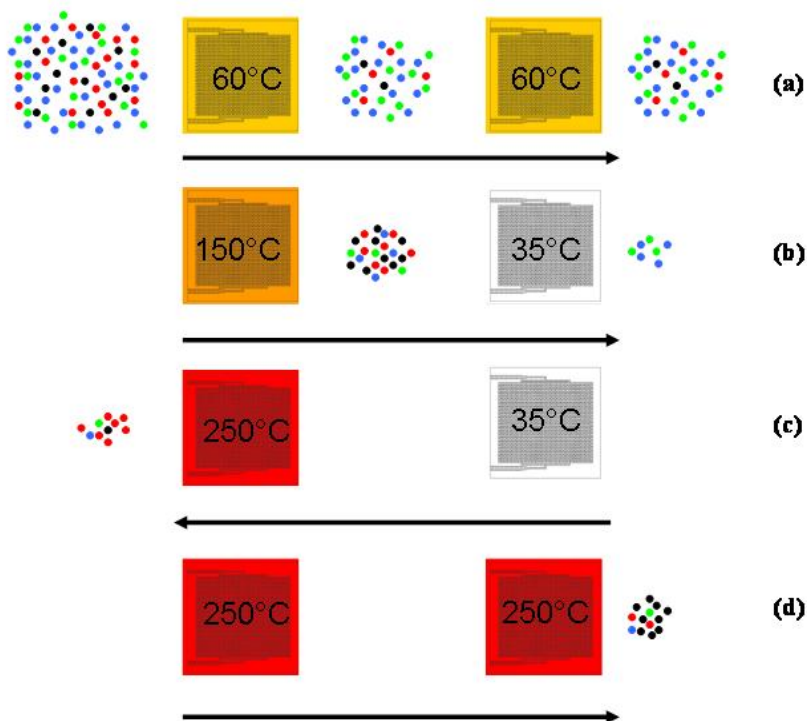
**Figure 22 (a) Desorption vs. flow rate at 35 °C and (b) desorption vs. temperature at 2 mL/min for the five compounds used in the experiment, © [2009] IEEE. Reprinted, with permission, from [1]**

At 150 °C, desorption peak areas of Propofol dropped to a low level. This means that this temperature was too high for an effective adsorption process for this compound. The results showed correlation between the amounts of compounds adsorbed and their boiling point. Hexadecane being a compound with a boiling point of 287 °C shows a larger desorption peak area compared to that of decane having a boiling point of 174 °C. The results shown in Figure 22 (b) also indicate that it is possible for the  $\mu$ PC to be tailored to concentrate certain gaseous compounds by controlling the device temperature. The above results prompted the idea of selective preconcentration and the elimination of unwanted compounds via two-step preconcentration.

#### *4.4.3 Two-step Preconcentration*

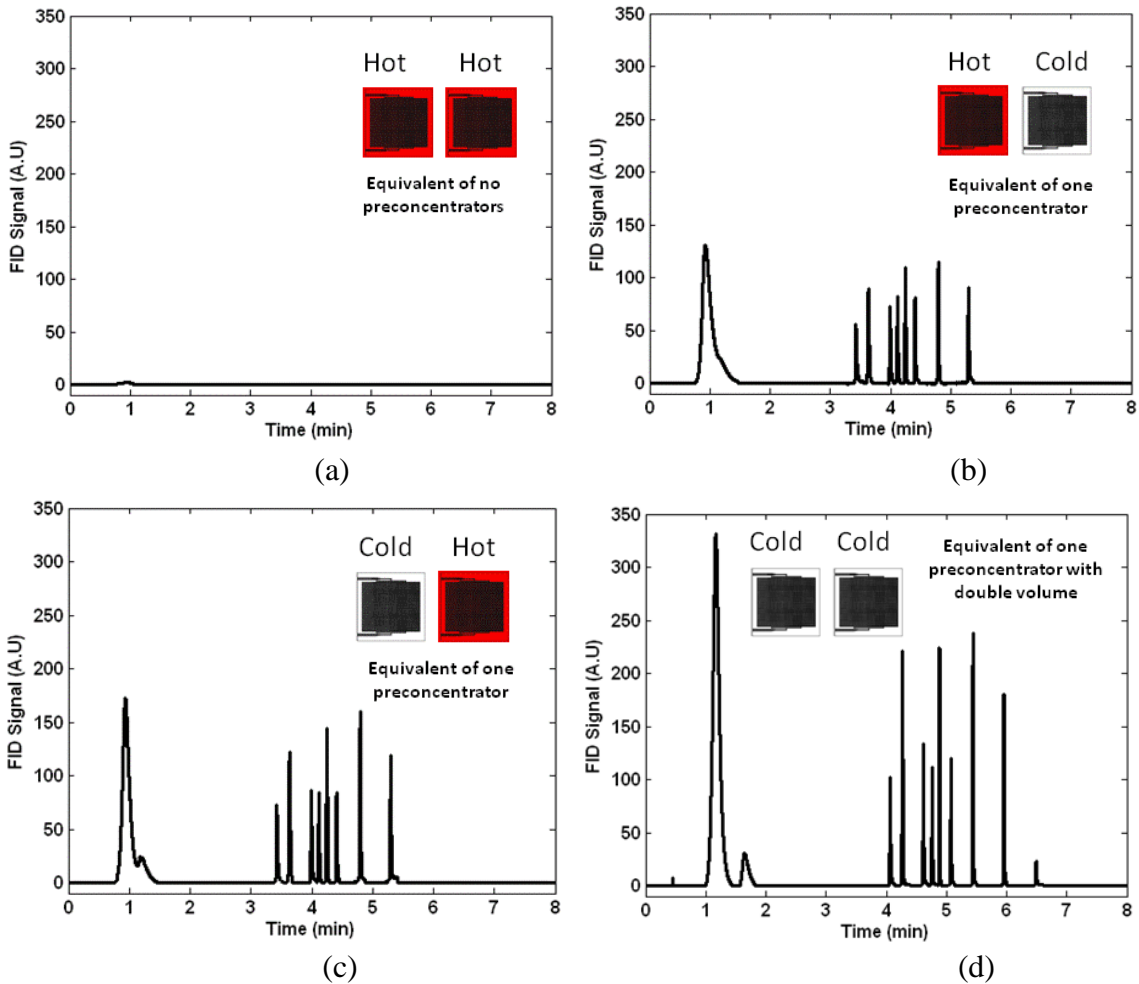
The novel concept of selective preconcentration of a target VOC (Propofol) over lower and higher boiling point compounds is demonstrated in Figure 23. The two cascaded  $\mu$ PCs ( $\mu$ PC1 and  $\mu$ PC2) are kept at 60 °C to minimize the adsorption of low-boilers as shown in Figure 23 (a). Next,  $\mu$ PC2 is cooled down to 35 °C and then  $\mu$ PC1 is heated to 150 °C to transfer the adsorbed mid-boilers from  $\mu$ PC1 to  $\mu$ PC2 as shown in Figure 23 (b). At this point, the flow is reversed and  $\mu$ PC1 is heated to 250 °C to release the high-boilers to waste as shown in Figure 23 (c). After cooling  $\mu$ PC1 to 35 °C,  $\mu$ PC2 is heated to 150 °C to transfer the adsorbed mid-boilers back to  $\mu$ PC1 (not shown in Figure 23). At this stage,  $\mu$ PC1 contains only mid-boilers and  $\mu$ PC2 contains only high-boilers. The flow is then reversed back and  $\mu$ PC2 is heated to 250 °C to release the high-boilers to waste (not shown in Figure 23). Finally,  $\mu$ PC1 is heated to the same temperature to release the mid-boilers to the GC column as shown in Figure 23 (d).





**Figure 23 Selective preconcentration of target VOC (black), (a-b) low-boilers reduction (blue & green), (c) high-boilers reduction by flow reversal, (d) release of concentrated target VOCs, © [2009] IEEE. Reprinted, with permission, from [1]**

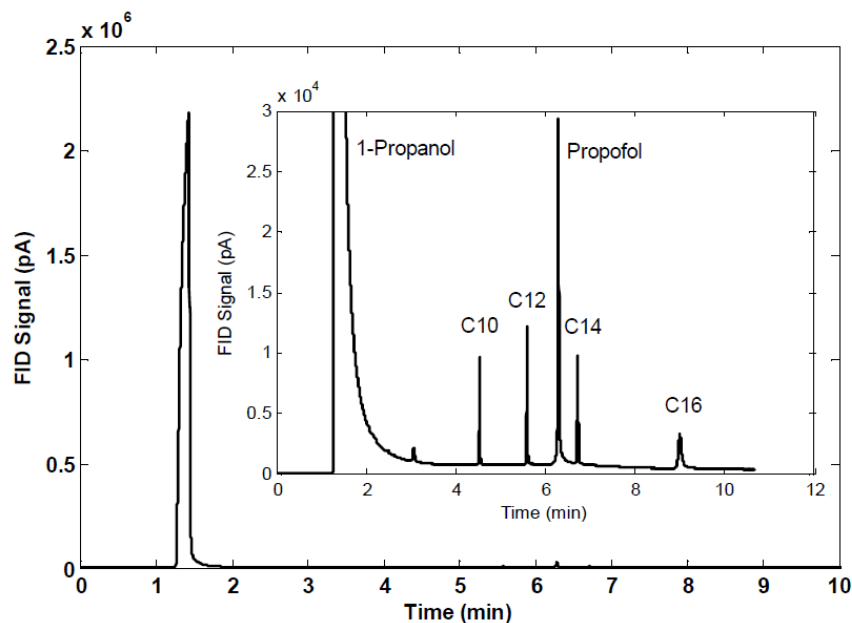
A list of chromatograms produced by different temperature configurations during adsorption of two cascaded  $\mu$ PCs is shown in Figure 24. In all cases, after species adsorptions, both microchips were heated rapidly to 250 °C at 100 °C/sec to desorb the concentrated components and inject them to the head of the GC column. The column was temperature programmed from 30 °C to 150 °C at 30 °C/min. The use of a single preconcentrator resulted in a chromatogram similar to those of Figure 24 (b) and (c).



**Figure 24 Chromatograms produced by different temperature configurations during adsorption of two  $\mu$ PCs connected in series, both devices are desorbed at the same time and temperature, sample was a standard chromatographic test mixture consisting of polar and nonpolar compounds in dichloromethane, © [2009] IEEE. Reprinted, with permission, from [1]**

Figure 25 shows the separation of the VOCs mixture without preconcentration and serves as a reference for the following discussion. The large 1-propanol content in injected sample is evident. The tailing of the large 1-propanol peak could overshadow other peaks and thus affects the accuracy of the analysis. Moreover, unwanted compounds in the sample, such as 1-propanol (and similarly water vapor in breath) could impose premature saturation in the collection process by saturating the adsorbent material. It can also be the case in the detection process by saturating

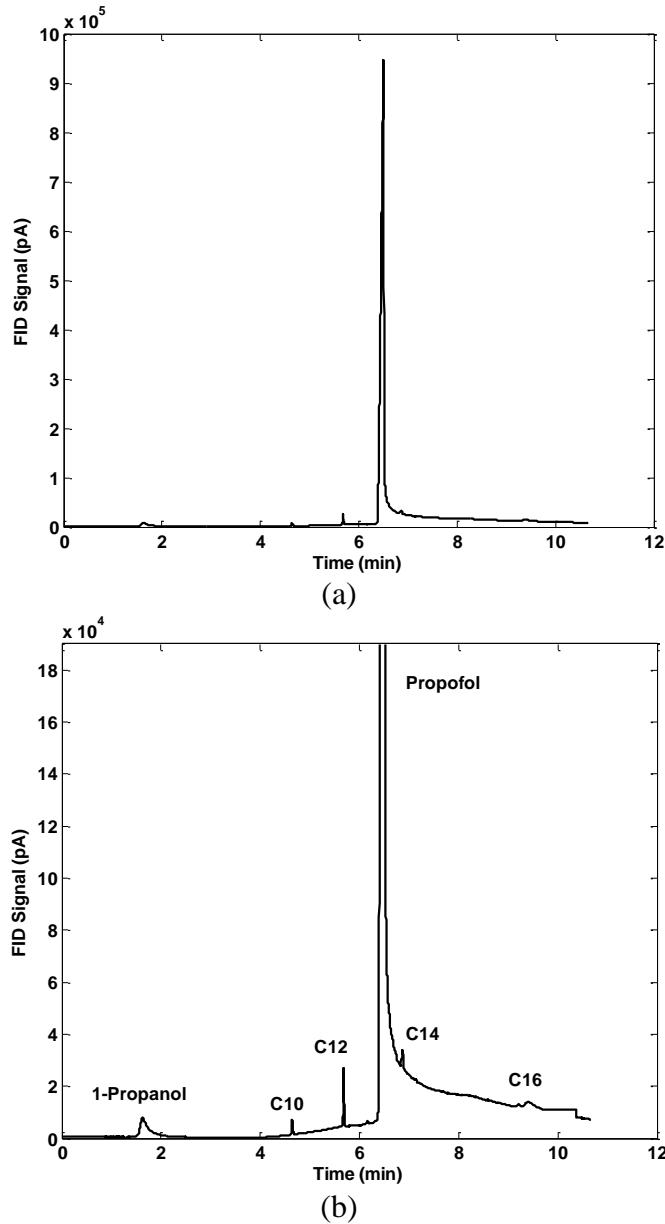
the detector. Most gas detector are sensitive to water [6]. Thus, eliminating the interfering compounds is essential for high performance analysis.



**Figure 25 Chromatogram of the VOCs mix without  $\mu$ PC showing the large amount of 1-Propanol, inset is zoom-in of the separated VOCs, © [2009] IEEE. Reprinted, with permission, from [1]**

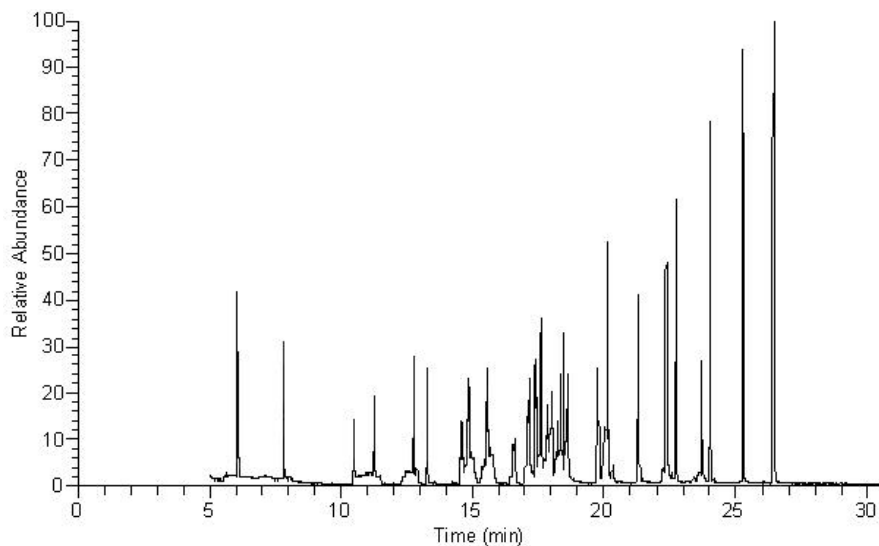
Figure 26 illustrates the results of selective preconcentration of Propofol mixed with other VOCs all diluted in water-like solvent (1-propanol). The elimination of unwanted species was performed by following the procedure explained in Figure 23. Selective preconcentration of high-boiler VOCs over low-boiler ones could be done simply by setting the  $\mu$ PCs at a temperature above the boiling point of the low-boiler VOCs. However, the challenge is to selectively preconcentrate mid-boilers over low and high-boilers. Two-step micro preconcentration was utilized to achieve this goal. The first step of this process was to eliminate 1-propanol, C<sub>10</sub>, and C<sub>12</sub> (low boilers) depicted by blue and green particles while adsorbing C<sub>14</sub>, Propofol, and C<sub>16</sub> depicted by red and black particles. After that, the carrier flow is reversed and the first  $\mu$ PC is heated to remove C<sub>14</sub> and C<sub>16</sub> from the preconcentration process (high boilers) depicted by red particles. This resulted in selective preconcentration of Propofol (depicted by black particles) and thus, the elimination of the interfering species. The process was able to

change the relative concentration of Propofol to C<sub>14</sub> from 50% (with one μPC) to 99.8% (with cascaded μPC). It also eliminated the solvent by 99.9%. It should be noted that two-step selective preconcentration comes at the cost of low preconcentration gain. This process is lossy and cannot be used in quantitative analysis.

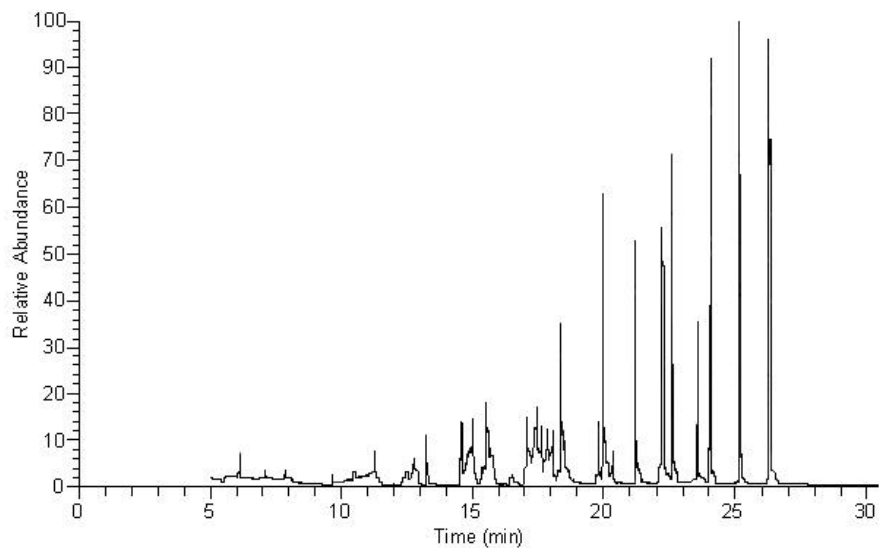


**Figure 26 Chromatogram of selective preconcentration of Propofol. (a) shows the magnitude of the peak, (b) zoom-in of the unpreconcentrated VOCs. Reduction in the 1-propanol content is evident, © [2009] IEEE. Reprinted, with permission, from [1]**

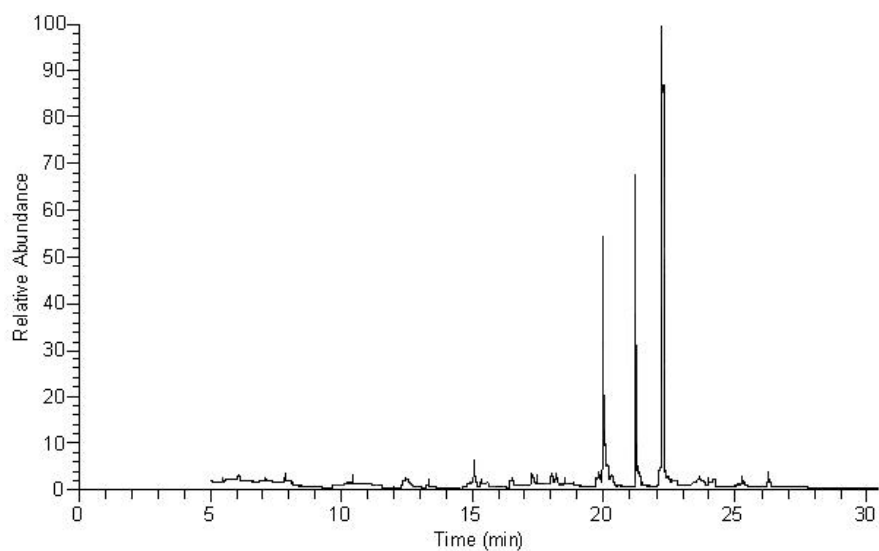
Selective preconcentration by temperature manipulation alone using single  $\mu$ PC was also carried out and compared to the cascaded  $\mu$ PCs method. The goal was to selectively preconcentrate n-decane, n-undecane, and n-dodecane among n-hexane, n-heptane, n-octane, n-nonane, n-tridecane, n-tetradecane, n-pentadecane, and n-hexadecane (other compounds in the mixture were not considered) from an indoor air standard mixture. The analysis of sample collection at 35 °C and desorption at 250 °C of a single device is shown in Figure 27. The analysis was performed with a GC-MS system with a DB-5 coated 30m fused-silica capillary column at an initial temperature of 35 °C, held for four minutes, followed by a ramp rate of 10 °C/min to 175°C. The flow was set to 1.2 mL/min. The analysis of sample collection at 60 °C and desorption at 150 °C of a single device is shown in Figure 28. It was possible to eliminate the low boiler alkanes when the  $\mu$ PC was maintained at elevated temperature. However, this temperature manipulation was not successful in eliminating the high boiler alkanes. This could be attributed to the multilayer adsorption of both mid and high boiler alkanes on the surface. Nevertheless, high boilers elimination was possible with the cascaded  $\mu$ PCs method as shown in Figure 29. It should be noted that the inherited absorbent selectivity also contribute to this process.



**Figure 27 Analysis of indoor air standard mixture using single  $\mu$ PC**



**Figure 28** Selective preconcentration by temperature manipulation alone using single  $\mu$ PC



**Figure 29** Selective preconcentration of n-decane, n-undecane, and n-dodecane from the indoor air standard mixture using the two-step preconcentration method

#### 4.5 Conclusion

Enabling hand-held breath analysis technology is essential for the following reasons:

- Noninvasive and painless testing
- Rapid results

- Minimal biohazard waste
- No special training
- Continuous monitoring

However, this technology is currently facing some technical difficulties that include:

- Trace level VOCs detection
- Elimination of interfering species in breath samples
- Simplification of complex mixtures

This chapter reported the utilization of MEMS technology to develop  $\mu$ PCs with 10,000 PF that would preconcentrate VOCs to detectable levels. The elimination of unwanted species by two-step preconcentration allowed more adsorption surface for the target compound on the adsorbent material and alleviated stringent requirements on the separation and detection stages. The demand for hand-held cost-effective Propofol monitoring devices is expected to increase as many surgical procedures are now being shifted from hospitals to outpatient surgical centers and physician's offices.

### *References*

- [1] B. Alfeeli and M. Agah, "Mems-Based Selective Preconcentration of Trace Level Breath Analytes," *IEEE Sensors Journal*, vol. 9, 2009, pp. 1068-1075.
- [2] P. Spanel, K. Dryahina, and D. Smith, "The Concentration Distributions of Some Metabolites in the Exhaled Breath of Young Adults," *Journal of Breath Research*, vol. 1, 2007, p. 026001.
- [3] W. A. Groves, E. T. Zellers, and G. C. Frye, "Analyzing Organic Vapors in Exhaled Breath Using a Surface Acoustic Wave Sensor Array with Preconcentration: Selection and Characterization of the Preconcentrator Adsorbent," *Analytica Chimica Acta*, vol. 371, 1998, pp. 131-143.
- [4] M. Phillips, "Method for the Collection and Assay of Volatile Organic Compounds in Breath," *Analytical Biochemistry*, vol. 247, 1997, pp. 272-278.
- [5] L. H. Hamilton. (1998). *Breath Testing and Gastroenterology (2 ed.)*.
- [6] S. M. Cho, Y. J. Kim, G. S. Heo, and S.-M. Shin, "Two-Step Preconcentration for Analysis of Exhaled Gas of Human Breath with Electronic Nose," *Sensors and Actuators B: Chemical*, vol. 117, 2006, pp. 50-57.

- [7] M. Libardoni, P. T. Stevens, J. H. Waite, and R. Sacks, "Analysis of Human Breath Samples with a Multi-Bed Sorption Trap and Comprehensive Two-Dimensional Gas Chromatography (Gc X Gc)," *Journal of Chromatography B*, vol. 842, 2006, pp. 13-21.
- [8] M. M. L. Steeghs, S. M. Cristescu, and F. J. M. Harren, "The Suitability of Tedlar Bags for Breath Sampling in Medical Diagnostic Research," *Physiological Measurement*, vol. 28, 2007, pp. 73-84.
- [9] D. Helmig, "Air Analysis by Gas Chromatography," *Journal of Chromatography A*, vol. 843, 1999, pp. 129-146.
- [10] A. Hengstenberg, M. Grossherr, T. Meier, and H. Gehring, "Breath Analysis and Artificial Ventilation: Chemical Identification and Classification of Volatile Substances in Exhaled Breath During I.V. Anesthesia," *Anesthesiology*, vol. 103, 2005, p. A808.
- [11] B. Alfeeli, D. Cho, M. Ashraf-Khorassani, L. T. Taylor, and M. Agah, "Mems-Based Multi-Inlet/Outlet Preconcentrator Coated by Inkjet Printing of Polymer Adsorbents," *Sensors and Actuators B: Chemical*, vol. 133, 2008, pp. 24-32.
- [12] S. C. Terry, J. H. Jerman, and J. B. Angell, "A Gas Chromatographic Air Analyzer Fabricated on a Silicon Wafer," *IEEE Transactions on Electron Devices*, vol. 26, 1979, pp. 1880-1886.
- [13] E. S. Kolesar Jr. and R. R. Reston, "Silicon Micromachined Gas Chromatography System," presented at the Second Annual IEEE International Conference on Innovative Systems in Silicon, Austin, TX, 1997.
- [14] P. R. Lewis, P. Manginell, D. R. Adkins, R. J. Kottenstette, D. R. Wheeler, S. S. Sokolowski, D. E. Trudell, J. E. Byrnes, M. Okandan, J. M. Bauer, R. G. Manley, and C. Frye-Mason, "Recent Advancements in the Gas-Phase Microchemlab," *IEEE Sensors Journal*, vol. 6, 2006, pp. 784-795.
- [15] M. Agah and K. D. Wise, "Low-Mass Pecvd Oxynitride Gas Chromatographic Columns," *Journal of Microelectromechanical Systems*, vol. 16, 2007, pp. 853-860.
- [16] I. Elmi, S. Zampolli, L. Masini, G. C. Cardinali, M. Severi, A. Barranco, L. Francioso, and P. Siciliano, "A Miniaturized Gas-Chromatographic System for the Evaluation of Fish Freshness," in *The 7th IEEE Conference on Sensors*, Lecce, Italy, 2008, pp. 1084-1087.
- [17] I. Gràcia, P. Ivanov, F. Blanco, N. Sabaté, X. Vilanova, X. Correig, L. Fonseca, E. Figueras, J. Santander, and C. Cané, "Sub-Ppm Gas Sensor Detection Via Spiral M-Preconcentrator," *Sensors and Actuators B: Chemical*, vol. 132, 2008, pp. 149-154.
- [18] C. E. Davis, C. K. Ho, R. C. Hughes, and M. L. Thomas, "Enhanced Detection of M-Xylene Using a Preconcentrator with a Chemiresistor Sensor," *Sensors and Actuators B: Chemical*, vol. 104, 2005, pp. 207-216.
- [19] M. Kim and S. Mitra, "A Microfabricated Microconcentrator for Sensors and Gas Chromatography," *Journal of Chromatography A*, vol. 996, 2003, pp. 1-11.



- [20] S. Li, J. C. Day, J. J. Park, C. P. Cadou, and R. Ghodssi, "A Fast-Response Microfluidic Gas Concentrating Device for Environmental Sensing," *Sensors and Actuators A: Physical*, vol. 136, 2007, pp. 69-79.
- [21] C. Pijolat, M. Camara, J. Courbat, J. P. Viricelle, D. Briand, and N. F. de Rooij, "Application of Carbon Nano-Powders for a Gas Micro-Preconcentrator," *Sensors and Actuators B: Chemical*, vol. 127, 2007, pp. 179-185.
- [22] E. W. Simoes, S. G. de Souza, M. L. P. da Silva, R. Furlan, and H. E. Maldonado Peres, "Study of Preconcentration of Non-Polar Compounds in Microchannels with Constrictions," *Sensors and Actuators B: Chemical*, vol. 115, 2006, pp. 232-239.
- [23] W.-C. Tian, H. K. L. Chan, L. Chia-Jung, S. W. Pang, and E. T. Zellers, "Multiple-Stage Microfabricated Preconcentrator-Focuser for Micro Gas Chromatography System," *Journal of Microelectromechanical Systems*, vol. 14, 2005, pp. 498-507.
- [24] F. Blanco, X. Vilanova, V. Fierro, A. Celzard, P. Ivanov, E. Llobet, N. Cañellas, J. L. Ramírez, and X. Correig, "Fabrication and Characterisation of Microporous Activated Carbon-Based Pre-Concentrators for Benzene Vapours," *Sensors and Actuators B: Chemical*, vol. 132, 2008, pp. 90-98.
- [25] A. M. Ruiz, I. Gracia, N. Sabate, P. Ivanov, A. Sanchez, M. Duch, M. Gerboles, A. Moreno, and C. Cane, "Membrane-Suspended Microgrid as a Gas Preconcentrator for Chromatographic Applications," *Sensors and Actuators A: Physical*, vol. 135, 2007, pp. 192-196.
- [26] M. A. Zareian-Jahromi, M. Ashraf-Khorassani, L. T. Taylor, and M. Agah, "Design, Modeling, and Fabrication of Mems-Based Multicapillary Gas Chromatographic Columns," *Journal of Microelectromechanical Systems*, vol. 18, 2009, pp. 28-37.
- [27] B. Alfeeli, S. Ali, V. Jain, R. Montazami, J. Heflin, and M. Agah, "Mems-Based Gas Chromatography Columns with Nano-Structured Stationary Phases," in *Sensors, 2008 IEEE*, 2008, pp. 728-731.
- [28] R. P. Manginell, G. C. Frye-Mason, R. J. Kottenstette, P. R. Lewis, and C. Channy Wong, "Microfabricated Planar Preconcentrator," presented at the Solid-State Sensors, Actuators, and Microsystems Workshop, Hilton Head'00, Hilton Head, SC, 2000.
- [29] H. K. L. Chan, S. W. Pang, R. A. Veeneman, E. T. Zellers, and M. Takei, "Microfabricated Preconcentrator for Quantitative Analysis of Low Concentration Volatile Organic Compounds," presented at the TRANSDUCERS, Korea, 2005.
- [30] I. Voiculescu, R. A. McGill, M. E. Zaghoul, D. Mott, J. Stepnowski, S. Stepnowski, H. Summers, V. Nguyen, S. Ross, K. Walsh, and M. Martin, "Micropreconcentrator for Enhanced Trace Detection of Explosives and Chemical Agents," *IEEE Sensors Journal*, vol. 6, 2006, pp. 1094-1104.
- [31] M. Martin, M. Crain, K. Walsh, R. A. McGill, E. Houser, J. Stepnowski, S. Stepnowski, H.-D. Wu, and S. Ross, "Microfabricated Vapor Preconcentrator for Portable Ion Mobility Spectroscopy," *Sensors and Actuators B: Chemical*, vol. 126, 2007, pp. 447-454.

- [32] B. Alfeeli and M. Agah, "Micro Preconcentrator with Embedded 3d Pillars for Breath Analysis Applications," presented at the The 7th IEEE Conference on Sensors, Lecce, Italy 2008.
- [33] M. F. I. Maier, "Retention Characteristics of Volatile Compounds on Tenax Ta," *Journal of High Resolution Chromatography*, vol. 11, 1988, pp. 566-576.

## Chapter Five: Effect of Shape, Spacing, and Arrangement of Pillars on the Performance of $\mu$ PCs

This chapter was reproduced from [1] with permission from IEEE

*B. Alfeeli and M. Agah, "Micro Preconcentrator for Handheld Diagnostics of Cancer Biomarkers in Breath," in 9th IEEE Conference on Sensors, Waikoloa, HI, November 1-4, 2010, pp. 2490-2493.*

### 5.1 Introduction

MEMS technology has enabled the realization micro structures with extreme uniformity in terms of geometric properties (size, shape, and distribution). Such capability allowed precise control over fluid flow through the device at the micro scale and enabled microfluidic devices [2]. As mentioned in chapter 2, the performance of  $\mu$ PCs is convoluted by geometric properties (or surface-to-volume ratio), flow dynamics, and sorbent material. Yeom, et. at. have recently proposed a figure of merit based on their flow resistance models which they called adsorption compliance [3]. It depends on surface-to-volume ratio, blockage ratio, and number of 3D microstructures. This chapter discusses new microstructure geometries that could enhance the performance of  $\mu$ PCs.

### 5.2 Role of Surface Area and Flow Pattern on $\mu$ PC Performance

Recently, 3D microstructures embedded within a microcavity of silicon-glass bonded chips, similar to the one shown in Figure 30, have been shown by our group to increase the performance of micro preconcentrators ( $\mu$ PCs) [3-5] by providing a large adsorption surface. Thus, new geometries are being sought to increase the surface-to-volume ratio in  $\mu$ PCs. In this section, we investigated the effect of shape, spacing, and arrangement of pillars on the performance of  $\mu$ PCs.

Square shaped pillars provide the largest surface area compared to other basic geometric shapes. However, the area of a square can be further increased by 72% when Maltese cross shape

is implemented. Table 4 compares pillar footprint and total surface area of the two designs. SEM micrographs of the square and Maltese-cross pillars are shown in Figure 31.

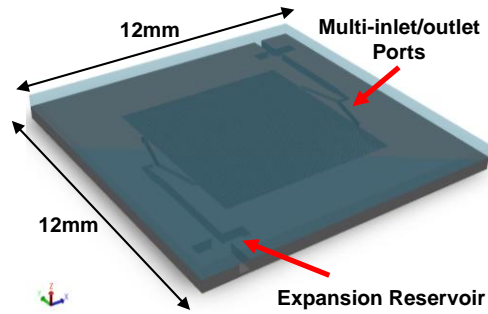




Figure 30 3D rendering of the silicon-glass  $\mu$ PC, © [2010] IEEE. Reprinted, with permission, from [1]

Table 4 Calculated pillar footprint and total surface area per pillar, © [2010] IEEE. Reprinted, with permission, from [1]

Shape	Footprint (mm <sup>2</sup> )	Surface Area (mm <sup>2</sup> )
	0.0025	0.070
	0.0008	0.120

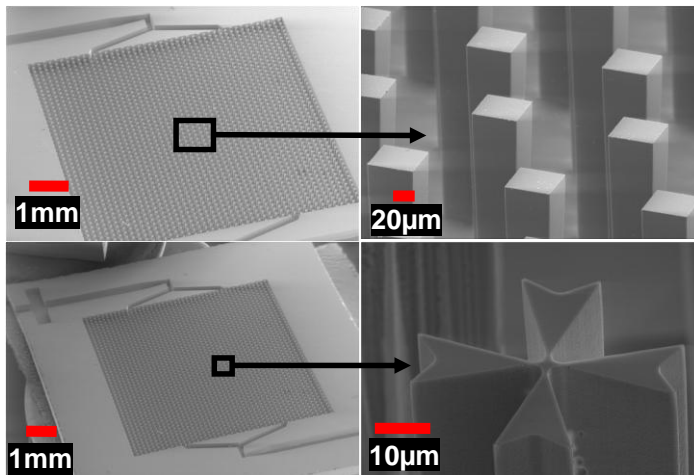
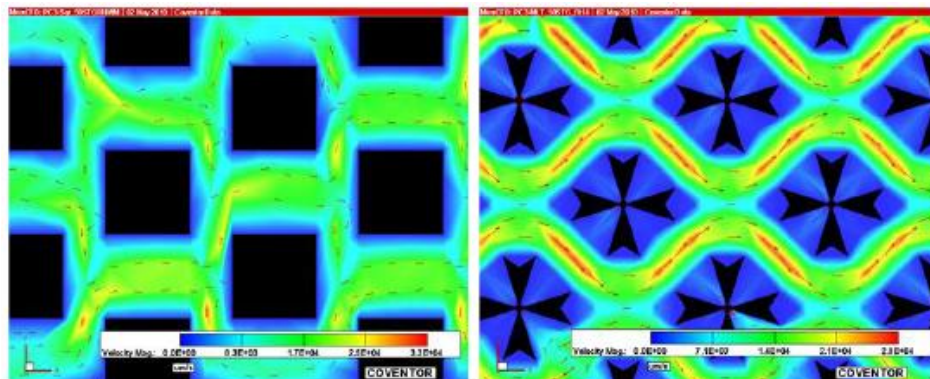


Figure 31 SEM micrographs of the fabricated square and Maltese-cross pillars, © [2010] IEEE. Reprinted, with permission, from [1]

Computational fluid dynamics was utilized to investigate the effectiveness of different micro pillar structures and their spacing configurations on the performance of the device. The steady state flow through the square and Maltese-cross pillar design in staggered arrangement was studied. Previous results indicated the existence of stagnation regions between the microstructures when arranged in ordered fashion [5]. However, stagnation region could exist especially in Maltese-cross design, even in staggered arrangement, as shown in Figure 32.



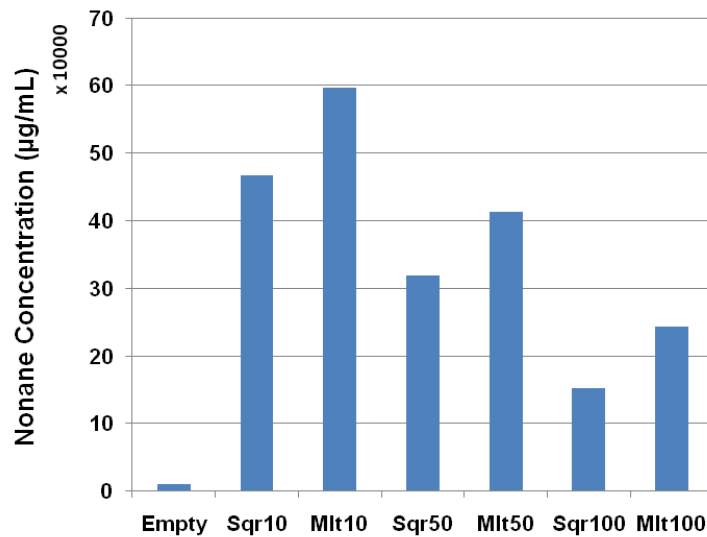
**Figure 32 Simulated flow velocity profile for square and Maltese-cross pillar designs, blue region represent zero velocity, © [2010] IEEE. Reprinted, with permission, from [1]**

### 5.3 Experimental Setup

The performance of the  $\mu$ PC was evaluated in terms of sample adsorption/desorption. The n-alkanes adsorption/ desorption was measured by a flame ionization detector (FID). To maintain isothermal temperature condition, the testing was carried out inside a commercial GC oven. The built-in gas flow controller was utilized to supply nitrogen carrier gas to the testing setup which consisted of a six-port zero-dead-volume valve, 10 m nonpolar methylpolysiloxane fused silica capillary column, and deactivated fused silica transfer lines. The valve was necessary to switch the flow to the separation column to perform the chromatographic analysis. The sample was injected by a precision sampling syringe into the GC injector. The GC column was kept offline during  $\mu$ PC loading stage to prevent the sample from poisoning the column. To determine the sample capacity of the  $\mu$ PCs, the devices were saturated with n-nonane at 40 °C and then desorbed at 100 °C/sec to 250 °C. The n-nonane concentration in the desorption peak reflects the sample amount collected by the device.

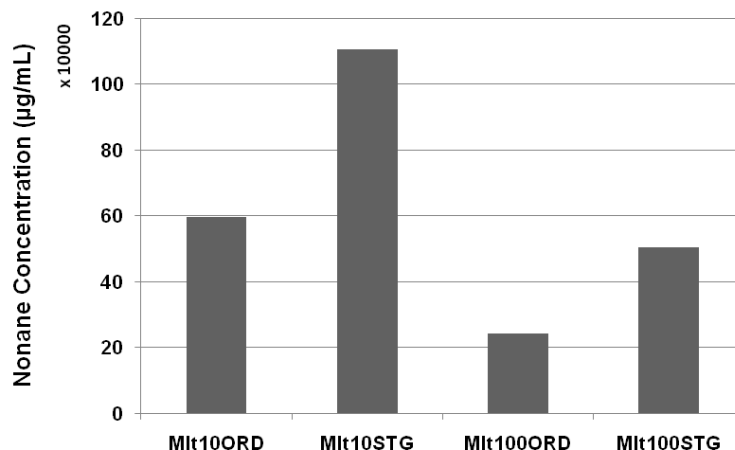
## 5.4 Results and Discussion

The bar chart in Figure 33 lists the n-nonane concentration in the desorption peaks for the square pillar design (Sqr) and Maltese-cross pillar design (Mlt). A  $\mu$ PC without pillars (Empty) was also included in this study for comparison purposes. The number that follows the design label indicates the spacing between the pillars in microns. The results demonstrated that the pillar spacing affects the capacity more than the pillar shape. Changing the shape from square to Maltese-cross resulted in 27% increase in performance. Reducing the spacing from 100  $\mu$ m to 10  $\mu$ m in Maltese-cross design resulted in 145% increase in performance.



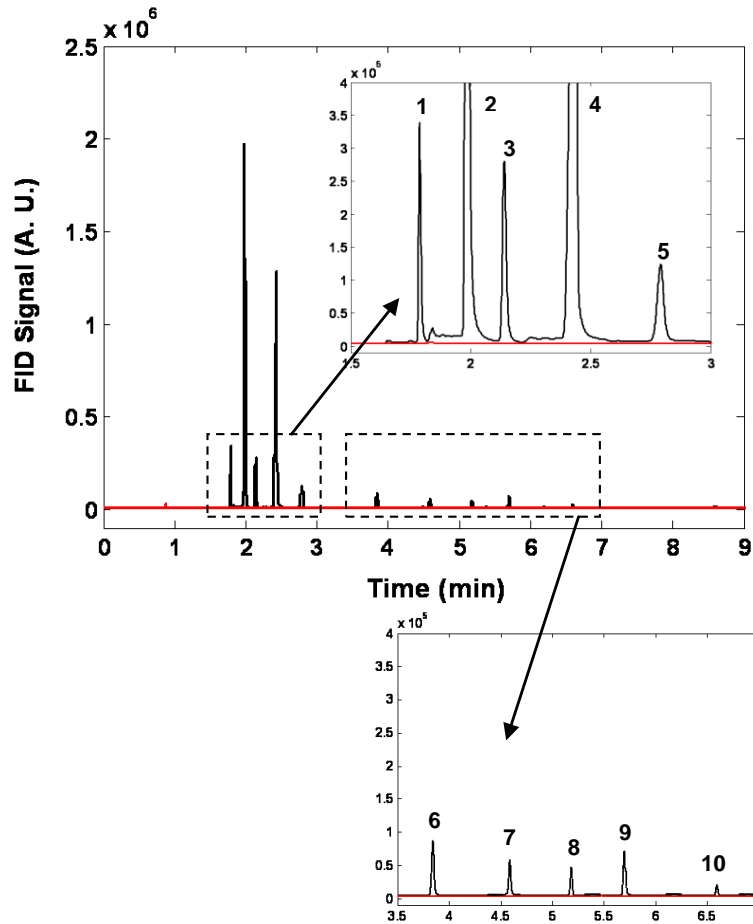
**Figure 33 n-nonane desorption concentration for the square and Maltese-cross pillar designs at different pillar spacing (10, 50, and 100  $\mu$ m), all have ordered pillar arrangement, empty resembles a pillars-free cavity, © [2010] IEEE. Reprinted, with permission, from [1]**

Figure 34 shows the effect of pillar arrangement on the device performance by comparing the n-nonane concentration in the desorption from  $\mu$ PCs with an ordered pillar arrangement (ORD) and from  $\mu$ PCs with a staggered pillar arrangement (STG). The staggered Maltese-cross performed better than the ordered arrangement as shown by the 85% increase in performance. These results allow us to conclude that in addition to the total surface area enhancement, the spacing and arrangement of the pillars which affect the flow pattern are also important.



**Figure 34 Desorption concentration for the Maltese-cross design at different pillar spacing (10µm and 100µm) and different pillar arrangement (ordered and staggered), © [2010] IEEE. Reprinted, with permission, from [1]**

The staggered Maltese-cross with 10 µm spacing design µPC was put in series with a GC column to demonstrate the successful preconcentration of volatile compounds identified as cancer biomarkers. The volatiles used in this work were n-pentane, benzene, n-heptane, toluene, n-octane, n-nonane, n-decane, n-undecane, n-dodacene, and n-tetradecane. The sample mixture was diluted to 1 ppb concentration in nitrogen. Tedlar bags were used to store the sample mixture. The chromatographic separations were done under column temperature program from 35 °C to 150 °C at 30 °C/min. The red chromatogram in Figure 35 belongs to the separation of the diluted sample whereas the black chromatogram is for the preconcentrated sample. It can be seen that the µPC made it possible to detect trace levels of volatile compounds that would be otherwise undetectable by the FID



**Figure 35 GC separation (red chromatogram) of 1ppb cancer biomarkers mixture: (1) pentane, (2) benzene, (3) heptane, (4) toluene, (5) octane, (6) nonane, (7) decane, (8) undecane, (9) dodacene, (10) tetradecane in nitrogen, black chromatogram represents the pre-concentrated sample, © [2010] IEEE. Reprinted, with permission, from [1]**

## References

- [1] B. Alfeeli and M. Agah, "Micro Preconcentrator for Handheld Diagnostics of Cancer Biomarkers in Breath," in *9th IEEE Conference on Sensors*, Waikoloa, HI, 2010, pp. 2490-2493.
- [2] M. W. Losey, R. J. Jackman, S. L. Firebaugh, M. A. Schmidt, and K. F. Jensen, "Design and Fabrication of Microfluidic Devices for Multiphase Mixing and Reaction," *Journal of Microelectromechanical Systems*, vol. 11, 2002, pp. 709-717.
- [3] J. Yeom, D. D. Agonafer, J.-H. Han, and M. A. Shannon, "Low Reynolds Number Flow across an Array of Cylindrical Microposts in a Microchannel and Figure-of-Merit Analysis of



Micropost-Filled Microreactors," *Journal of Micromechanics and Microengineering*, vol. 19, 2009, p. 065025.

- [4] B. Alfeeli and M. Agah, "Mems-Based Selective Preconcentration of Trace Level Breath Analytes," *IEEE Sensors Journal*, vol. 9, 2009, pp. 1068-1075.
- [5] B. Alfeeli, D. Cho, M. Ashraf-Khorassani, L. T. Taylor, and M. Agah, "Mems-Based Multi-Inlet/Outlet Preconcentrator Coated by Inkjet Printing of Polymer Adsorbents," *Sensors and Actuators B, Chemical*, vol. 133, 2008, pp. 24-32.

## Chapter Six: Low Pressure Drop Micro Preconcentrators with a Cobweb Tenax-TA Film

This chapter was reproduced from and [1] with permission from Transducer Research Foundation

*B. Alfeeli and M. Agah, "Low Pressure Drop Micro Preconcentrators with a Cobweb Tenax-TA Film," in Solid-State Sensors, Actuators, and Microsystems Workshop, Hilton Head Island, South Carolina, June 6-10, 2010, pp. 166-169.*

### 6.1 Introduction

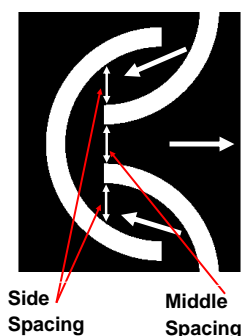
Generally speaking, preconcentrators (PCs) are concentration amplifiers used to improve the detection limit of analytical systems such as spectroscopy [2], mass-spectrometry [3], and chromatography [4]. They are also an integral part of handheld chemical detection systems. However, to meet the size and power constraints, handheld systems rely on microfabricated components (fluidic ports/channels, pumps, valves, etc.) which operate at low pressures. For example, a state-of-the-art micromachined pump designed for micro gas chromatographers can only provide a maximum back pressure of 7 kPa [5] whereas a typical MEMS-based  $\mu$ PC can introduce large pressure drop as high as 14 kPa [6]. Therefore, reducing the pressure drop in  $\mu$ PCs is a key development in handheld systems.

Conventional PCs are troubled by large pressure drop, dead volume, and high power consumption. Microfabrication technology has enabled high efficiency preconcentration in terms of sample capacity, device size, and the energy consumed. Recently, our group and others have utilized 3D microstructures embedded within a microcavity and coated with adsorbent films to realize low pressure drop  $\mu$ PC [7-9]. The microstructures provide large surface-to-volume ratio and low flow resistance compared to conventional microporous granular packing arrangement. This chapter discusses the design, simulation, and experimental evaluation of high performance low pressure drop  $\mu$ PC chips for micro analytical instruments including a micro gas chromatography system ( $\mu$ GC) [10]. In addition to our unique design enabling very low pressure drops, less than 100 Pa/cm, we present a new deposition method which results in a cobweb

structure of the adsorbent material, thereby significantly increasing the concentration efficiency without obstructing the gas flow.

## 6.2 Low Pressure Drop $\mu$ PC Design

The new design consists of an array of parabolic reflectors embedded within a  $7\text{ mm} \times 7\text{ mm} \times 0.38\text{ mm}$  cavity. The unit cell of the array consists of three reflectors as shown in Figure 36. The reflectors are arranged to split the flow in the forward direction and combine them back in the reverse direction. The spacing between the reflectors (side and middle spacing) was varied to investigate its effect on the device performance.



**Figure 36 The  $\mu$ PC unit cell. Arrows indicate the flow direction.**

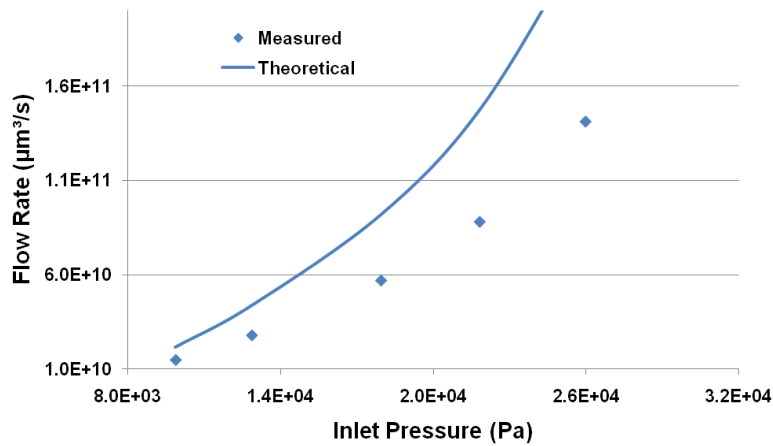
Table 5 list the different spacing values for both side and middle spacing along with the symmetry ratios (SR) of different designs. The SR was defined as the ratio of side to middle spacing. High SR represents narrow passage of flow which increases the probability of molecules scattering and interacting with the adsorption surface.

**Table 5 Different spacing arrangements and their corresponding symmetry ratio along with the simulated pressure drops at 1.5mL/min flow rate.**

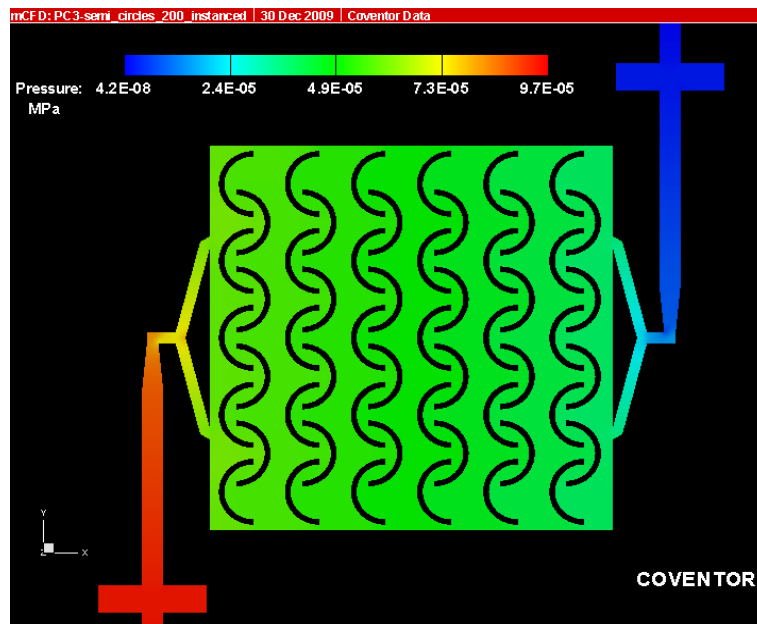
Design Label	Middle spacing ( $\mu\text{m}$ )	Side Spacing ( $\mu\text{m}$ )	SR	Pressure drop (Pa)
PC100	100	250	2.5	145
PC200	200	200	1	97
PC300	300	150	0.5	94

Full scale (actual chip size) computational fluid dynamics (CFD) simulation was consummated to investigate the flow behavior in such geometries. To establish confidence in the CFD model,

calculated flow rates were compared with experimental results as shown in Figure 37. The pressure drop profile is shown in Figure 38 indicates uniform pressure drop which is also desirable. The CFD results of the flow velocity profile showed high velocity in the middle spacing region of PC100 design as presented in Figure 39. The data suggested that high SR value is desirable. The CFD results confirmed the anticipated flow behaviors. The simulated pressure drops in the different designs are listed in Table 5.



**Figure 37 Comparison of calculated and experimental flow rates to establish confidence in the CFD model**



**Figure 38 Pressure-drop profile in the µPC**

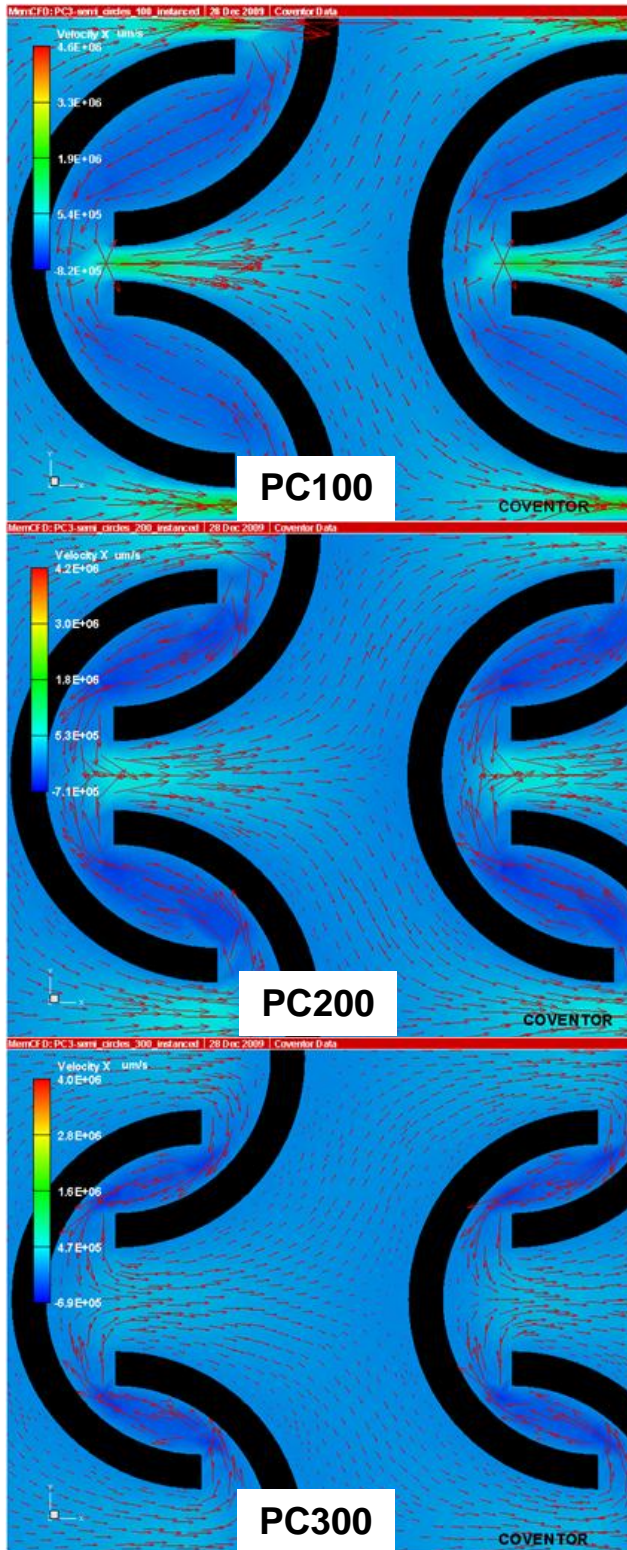


Figure 39 Simulation of the flow profile through different design spacing arrangements

### 6.3 Fabrication and Cobweb Coating

The microstructures were realized according to the process flow in Figure 40. The process starts with (a) photolithography of microstructures and fluidic ports on 100 mm test grade silicon wafer using high resolution, superior aspect ratio thick film photoresist (PR9260). This step was followed by (b) etching the patterned wafer using deep reactive ion etching (DRIE) to form 380  $\mu\text{m}$  deep 3D structures. Tenax TA particles were dissolved in dichloromethane at 50 mg/mL concentration to create a solution to fill the etched cavity with. Adsorbent deposition (c) was achieved by adding drops of 2-propanol into solution before it evaporates from the cavity. Cobweb Tenax TA evolves when 2-propanol contacts Tenax TA solution. The cobweb structure anchors to the sidewalls once the solvent evaporates as shown in Figure 41. The cavity was then sealed (d) by anodic bonding the silicon substrate to a Pyrex wafer at 1250 V and 300  $^{\circ}\text{C}$  instead of conventional 350-400  $^{\circ}\text{C}$  bonding temperature to avoid damaging the polymer.

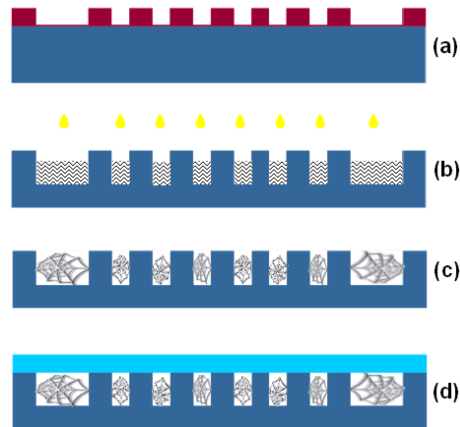


Figure 40 uPC fabrication process flow

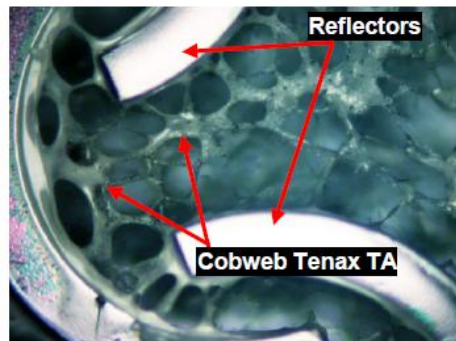
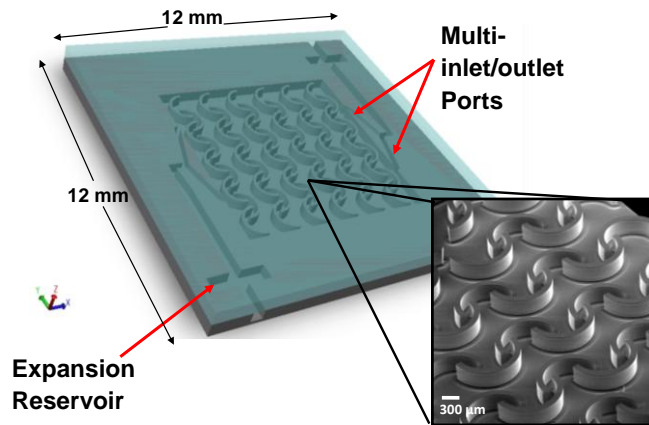
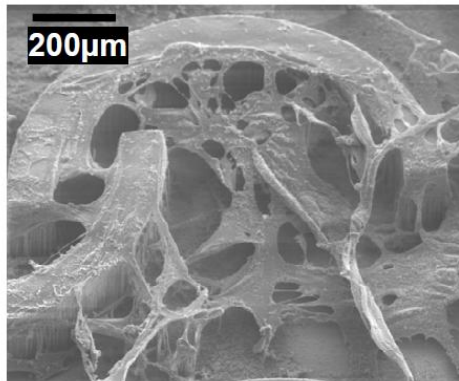


Figure 41 Optical image of the cobweb Tenax TA.

The expansion reservoirs shown in Figure 42 were incorporated into the inlet/outlet design to prevent the sealing adhesive from overflowing into the inner cavity. This was a new addition to the first generation design reported previously [8]. The silicon-Pyrex stack was then diced into individual devices like the one shown in Figure 42. Each device was connected on both sides with 300  $\mu\text{m}$ -OD, 170  $\mu\text{m}$ -ID deactivated fused silica tubing using high temperature ceramic based adhesive. The addition of Tenax TA did not create a measurable difference in the flow rate. Figure 43 presents a scanning electron microscopy (SEM) image of cobweb Tenax TA



**Figure 42 3D rendering of the  $\mu\text{PC}$ , insets are SEM micrographs of the fabricated microstructures**

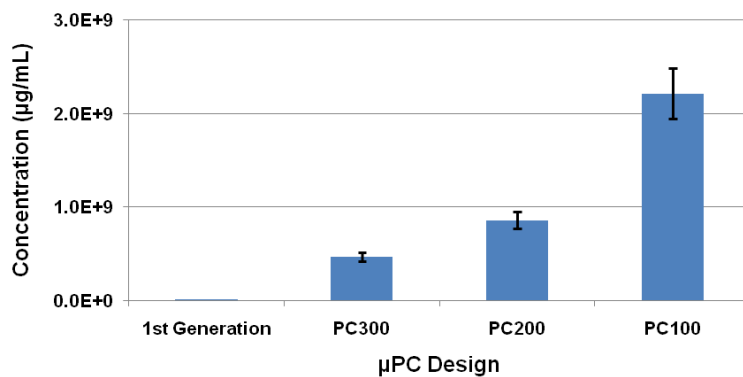


**Figure 43 SEM image of cobweb Tenax TA on the micro parabolic reflectors**

#### **6.4 Experimental Results**

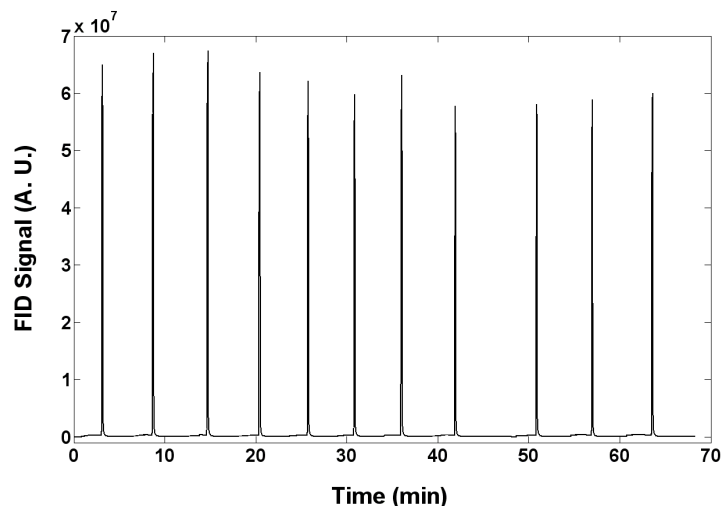
The  $\mu\text{PC}$ s were evaluated experimentally by using the adsorption capacity as a figure of merit. The testing was performed inside a temperature controlled chamber to accurately maintain the

testing temperature at 35 °C. An electronic gas flow controller was used to supply and control the carrier gas which was selected to be nitrogen to resemble actual field operation conditions. The flow rate through the  $\mu$ PC was set to constant 1 mL/min. A flame ionization detector (FID) was utilized to detect the hydrocarbon samples used in the experiments. An off-board high-performance ceramic heater (ultra-fast ramp rate) was used for thermal desorption along with K-type thermocouple for manual temperature monitoring and control. In future work, on-chip thermal desorption capability will be added to the  $\mu$ PCs. The chips were saturated with benzene at 35 °C and then desorbed at 100 °C/sec to 250 °C. The FID peak area is proportional to the analyte concentration. The benzene concentration in the desorption peak reflects the sample amount collected by the device. It is evident from Figure 44 that the SR parameter has a significant effect on the performance of the parabolic reflectors design. Moreover, Figure 44 shows that the performance of PC100 design is more than 2 orders of magnitude higher than the micro pillar design presented in HiltonHead'08 workshop [11]. In the first generation design inkjet printing of Tenax TA was used to provide uniform film deposition. Cobweb Tenax TA offers better utilization of the space between the microstructures with the  $\mu$ PC cavity. Reproducibility of the results in terms of peak area was 10% relative standard deviation (RSD) with more than 10 manual injections is shown in Figure 45.



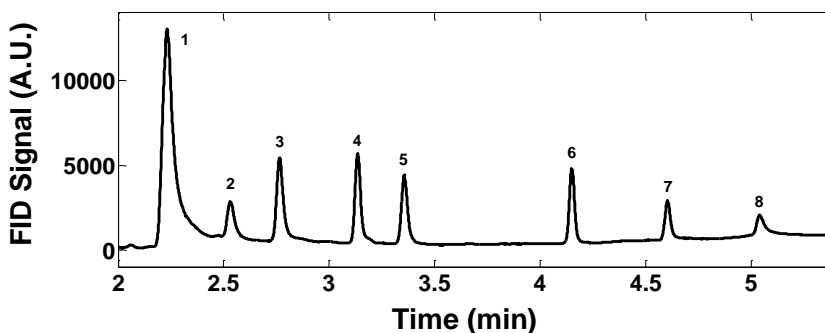
**Figure 44 Benzene desorption concentration for the three designs as well as the first generation design**





**Figure 45 Reproducibility of  $\mu$ PC desorption pulses**

For proof of concept, the  $\mu$ PC was put in series with a 1m 100% methylpolysiloxane microfabricated column [12] to demonstrate the possibility of  $\mu$ PC- $\mu$ GC integration. Under the same loading/desorbing conditions as the benzene test, the  $\mu$ PC was loaded with a mixture of toluene, n-nonane, n-decane, n-undecane, n-dodecane, n-tridecane, n-tetradecane, and n-pentadecane diluted in n-pentane at 1 ppm concentrations. The sample concentration was below the FID detection limit; thus, preconcentration was needed to make the sample detectable. Figure 46 illustrates a chromatogram of the preconcentrated sample injected into the micro column via thermal desorption. The initial and final temperatures of the column were 35 °C and 150 °C at 30 °C/min. The carrier flow rate was 1 mL/min.



**Figure 46 Preconcentration and separation of a mixture of (1) toluene, (2) nonane, (3) decane, (4) undecane, (5) dodecane, (6) tridecane, (7) tetradecane, and (8) pentadecane diluted in pentane below the FID detection limit.**

## 6.5 Conclusions

The performance of analytical instruments especially handheld systems can be improved with sample pretreatment techniques such as preconcentration. This chapter has demonstrated the possibility of developing lower pressure drops, small sizes, and high performance MEMS-based  $\mu$ PCs. This was realized by utilizing findings from previous designs, novel parabolic reflectors configuration, and cobweb Tenax TA. The simulation analyses verified by experimental results have shown the effect of the SR parameter in the parabolic reflectors design. Future work will aim to better understand and model the behavior of the  $\mu$ PCs under different conditions. The reproducible desorption peaks needed for fast on-field analytical analysis has been demonstrated by the  $\mu$ PC. The presented device was successful in concentrating a diluted multi-compound hydrocarbon mixture.

## References

- [1] B. Alfeeli and M. Agah, "Low Pressure Drop Micro Preconcentrators with a Cobweb Tenax-Ta Film," in *Solid-State Sensors, Actuators, and Microsystems Workshop, Hilton Head'10*, Hilton Head Island, South Carolina, 2010, pp. 166-169.
- [2] W. A. Groves, E. T. Zellers, and G. C. Frye, "Analyzing Organic Vapors in Exhaled Breath Using a Surface Acoustic Wave Sensor Array with Preconcentration: Selection and Characterization of the Preconcentrator Adsorbent," *Analytica Chimica Acta*, vol. 371, 1998, pp. 131-143.
- [3] C. Hornuss, S. Praun, J. Villinger, A. Dornauer, P. Moehnle, M. Dolch, E. Weninger, A. Chouker, C. Feil, J. Briegel, M. Thiel, and G. Schelling, "Real-Time Monitoring of Propofol in Expired Air in Humans Undergoing Total Intravenous Anesthesia," *Anesthesiology*, vol. 106, 2007, pp. 665-674.
- [4] K. Dettmer and W. Engewald, "Adsorbent Materials Commonly Used in Air Analysis for Adsorptive Enrichment and Thermal Desorption of Volatile Organic Compounds," *Analytical and Bioanalytical Chemistry*, vol. 373, 2002, pp. 490-500.
- [5] A. A. Astle, H. S. Kim, L. P. Bernal, K. Najafi, and P. D. Washabaugh, "Theoretical and Experimental Performance of a High Frequency Gas Micropump," *Sensors and Actuators A: Physical*, vol. 134, 2007, pp. 245-256.
- [6] W.-C. Tian, S. W. Pang, L. Chia-Jung, and E. T. Zellers, "Microfabricated Preconcentrator-Focuser for a Microscale Gas Chromatograph," *Journal of Microelectromechanical Systems*, vol. 12, 2003, pp. 264-272.
- [7] J. Yeom, D. D. Agonafer, J.-H. Han, and M. A. Shannon, "Low Reynolds Number Flow across an Array of Cylindrical Microposts in a Microchannel and Figure-of-Merit Analysis of

- Micropost-Filled Microreactors," *Journal of Micromechanics and Microengineering*, vol. 19, 2009, p. 065025.
- [8] B. Alfeeli, D. Cho, M. Ashraf-Khorassani, L. T. Taylor, and M. Agah, "Mems-Based Multi-Inlet/Outlet Preconcentrator Coated by Inkjet Printing of Polymer Adsorbents," *Sensors and Actuators B, Chemical*, vol. 133, 2008, pp. 24-32.
- [9] E. H. M. Camara, P. Breuil, D. Briand, L. Guillot, C. Pijolat, and N. F. de Rooij, "A Micro Gas Preconcentrator with Improved Performances for Environmental Monitoring," in *International Conference on Solid-State Sensors, Actuators and Microsystems, TRANSDUCERS'09*, 2009, pp. 983-986.
- [10] M. Agah, G. R. Lambertus, R. Sacks, and K. Wise, "High-Speed Mems-Based Gas Chromatography," *Journal of Microelectromechanical Systems*, vol. 15, 2006, pp. 1371-1378.
- [11] B. Alfeeli, M. Ashraf-Khorassani, L. T. Taylor, and M. Agah, "Multi-Inlet/Outlet Preconcentrator with 3-D M-Structures Coated by Inkjet Printing of Tenax Ta," in *Solid-State Sensors, Actuators, and Microsystems Workshop, Hilton Head'08*, Hilton Head Island, South Carolina, 2008, pp. 118-121.
- [12] M. Agah, J. A. Potkay, G. Lambertus, R. Sacks, and K. D. Wise, "High-Performance Temperature-Programmed Microfabricated Gas Chromatography Columns," *Journal of Microelectromechanical Systems*, vol. 14, 2005, pp. 1039-1050.

## Chapter Seven: Evaluation of Tenax TA Thin Films as Adsorbent Material for Micro Preconcentration Applications

Part of this chapter was reproduced from [1] with permission from Elsevier B. V.

*B. Alfeeli, L. T. Taylor, and M. Agah, "Evaluation of Tenax TA thin films as adsorbent material for micro preconcentration applications," Microchemical Journal, vol. 95, 2010, pp. 259-267.*

### 7.1 Introduction

Microelectromechanical systems (MEMS) technology has enabled the manufacturing of small-sized devices that are difficult to produce using conventional machining techniques. In the area of analytical chemistry, MEMS can offer the possibility of developing high-speed yet low-cost and low-power analytical devices that require small quantities of both sample and consumables such as solvents and reagents. The past few years have shown continuous developments in micro total analysis systems ( $\mu$ TAS) for field chemical analysis applications [2-6]. These micro systems typically consist of sample pretreatment, separation, and detection components. In general,  $\mu$ TAS applications are utilized for medical diagnostics, environmental monitoring, law enforcement forensics, and basic science and discovery.

Preconcentration is normally performed as part of the sample pretreatment step in various analytical techniques including micro gas chromatography. Preconcentration of volatile organic compounds (VOCs) should fulfill at least three conditions: (1) the sampled VOCs needs to be representative; (2) the procedure should be simple to enable field sampling; and (3) no analyte degradation or losses between sampling and analysis should occur [7]. Typically, VOCs are transferred from the adsorbent tube to the analytical column using rapid thermal desorption via heated transfer lines. This procedure does not always fulfill the third condition mentioned above because the sample interacts with, or condenses on the walls of the transfer lines. In addition, leaks from the connectors may result in partial sample loss. This shortcoming can be resolved with monolithic integration of the preconcentrator with the separation column. In other words, the need for connectors and transfer lines is eliminated by developing a preconcentrator and column on a single chip.

Miniaturization of preconcentrators (i.e.  $\mu$ PCs) allows for out-of-lab collection which subsequently enables in-field continuous monitoring. Miniaturization also provides high efficiency preconcentration in terms of sample capacity to device size. Moreover, the amount of energy needed to release the trapped chemical species is reduced.  $\mu$ PCs are made from micromachined silicon microstructures that can be coated or packed with adsorbent material [8-21]. On one hand, exhaustive  $\mu$ PCs consist of microcavities or microchannels packed with granular adsorbent. This packing is achieved by filling the  $\mu$ PC manually with adsorbent slurry using a syringe or with the help of pumps. However, the microstructures, fittings, and device packaging usually cannot tolerate the harsh conditions of granular adsorbent packing such as high pressures and the application of ultrasonication which is crucial to achieve good packing density [22]. On the other hand, equilibrium based  $\mu$ PCs consist of planar surfaces, microchannels, or 3D microstructures coated with a thin film of adsorbent material. Coating of  $\mu$ PCs is done by either spin coating [11], plasma deposition [23], inkjet printing [24], electroplating [24], or conventional methods used to coat chromatographic open tubular capillary column [25]. However, thin films have limited adsorption capacity and may be susceptible to degradation related to low surface adhesion and/or thermal instability.

The focus of this research was to evaluate adsorbent films (i.e. 2,6-diphenyl-*p*-phenylene oxide, commercially known as Tenax TA polymer) on 3D microstructures etched by a deep reactive ion etching (DRIE) process for  $\mu$ TAS applications. Understanding Tenax TA films would help improving the performance of  $\mu$ PCs which in turn improve the capabilities of  $\mu$ TAS technology especially for field analysis. The polymer of 2,6-diphenyl-*p*-phenylene oxide was patented by General Electric Co. in 1969 as an electrical insulation polymer [26]. The polymer was then developed by AKZO Research Laboratories, Netherlands, as a column packing material for chromatography [27]. It is commonly known by the trademark name “Tenax” with different suffixes. Tenax TA is an improved version of the original Tenax GC. Tenax GR is latest version containing 23% graphitized carbon [7]. The polymer was employed for the first time as an adsorbent for preconcentration of volatile organic compounds (VOCs) by the National Aeronautics and Space Administration (NASA) for monitoring cabin atmosphere in Skylab-4 [28]. Presently, the granular adsorbent is commonly used as a stationary phase in packed column gas chromatography [29] and as an adsorbent material in standard methods from the US EPA

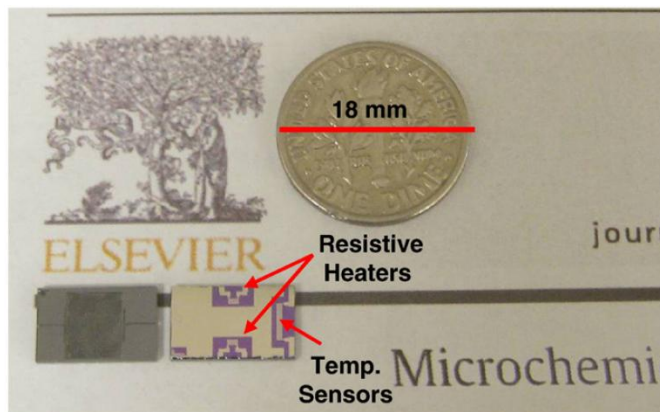
and the UK HSE for monitoring air quality and industrial emissions [30]. The adsorption properties of Tenax, in the granular form, have been studied extensively [31-39]. However, quantitative information regarding polymer's physical properties and VOCs adsorption mechanisms are rather scarce with a few studies being found in the literature [25, 40, 41]. Tenax TA falls under the category of porous organic polymers. Nonporous polymer adsorbents which rely on absorption of the solutes into the material also exist. Polydimethylsiloxane (PDMS) is an example of a nonporous polymer. It is mainly used in solid phase microextraction applications. The commercially available granular adsorbent, Tenax TA, is a partially crystalline glassy polymer [25]. It can also occur in crystalline form by crystallization from solution. In this case, the solvent is assumed to form an essential part of the crystal lattice [42]. In other words, Tenax TA forms an inclusion complex or clathrate compound. The linear polymer is soluble in lower chlorinated hydrocarbons. However, it is not soluble in alkanes, alcohols, ketones, etc. and it has been used as a stationary phase in gas chromatography [42]. It offers a variety of outstanding features such as high thermal stability (up to 350 °C) [42], relatively low water retention, and is relatively resistant to oxygen (does not require purification of carrier gas) [43].

Moreover, to the best of our knowledge, there are no reports of any systematic evaluation of Tenax TA thin films as an adsorbent material. Moreover, the film-based adsorbent is deposited on the microstructures from solution (Tenax TA in dichloromethane) under ambient conditions. However, it is not clear if the properties of the adsorbent are retained after this process. This chapter also describes the characterization of Tenax TA films deposited from solution at substrate temperature of 20 °C and 100 °C. The results presented here provide insight on the properties of the film-based polymer in comparison to the granular form. Such information is not only helpful for improving the performance of  $\mu$ PCs, but also in exploring other applications of the film-based polymer. Such applications include solid phase microextraction (SPME), capillary (also microfabricated) chromatography columns, and membrane separation technology. To the best of our knowledge, no systematic characterization of films deposited at different temperatures has been carried out previously.

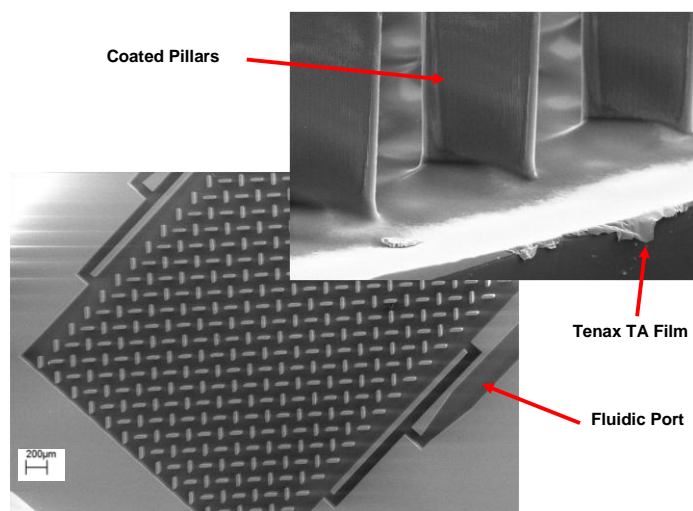
## 7.2 *Materials and Methods*

### 7.2.1 *μPCs Development*

The μPCs used in this study consisted of an array of 3D micro pillars and they were similar to our previously reported work [25]. The method for μPCs development can be described as follows: (1) the design pattern was transferred to a silicon wafer via standard photolithography, (2) the silicon wafer was etched by a single step deep reactive ion etching process followed by an oxygen plasma clean step to remove any residual fluorocarbon on the etched surface, and (3) μPC devices were then coated with Tenax TA thin film by inkjet printing. This technique gave the necessary precision needed to coat specific locations on the wafer. This was important as any spillover outside the device cavity would affect the integrity of the sealing process. The wafer was then sealed with a Pyrex wafer by anodic bonding. Finally, the last step consisted of patterning thin film Ti/Pt resistive heaters and temperature sensors over plasma enhanced chemical vapor deposition (PECVD) oxide on the back side of the silicon wafer. The wafer was then diced and fused silica (Polymicro Technologies, Phoenix, AZ) tubing 100μm-i.d., 240 μm-o.d. were inserted into the inlet/outlet ports. Gastight seals were formed around the inlet/outlet ports by using an inorganic high-temperature ceramic adhesive (Aremco Products, Inc., Valley Cottage, NY). Figure 47 provides a photograph of the μPC showing both front and backside where the heaters and sensors are located. Figure 48 shows micrographs of the μPC structure with an inset showing the uniformity of the inkjet coating of Tenax TA film. The outer dimensions of the silicon-glass chip were 7 mm × 7 mm × 1 mm. The μPC specific surface area was measured to be 10 m<sup>2</sup>/g (gas sorption method) with a volume of about 6.5 μL. The dimensions of the high-aspect-ratio pillars were 30 μm × 120 μm × 240 μm.



**Figure 47** A photograph of the  $\mu$ PC showing both front and back side where the heaters and sensors are located



**Figure 48** SEM micrograph showing the structure of the  $\mu$ PC. Inset shows the uniformity of the inkjet coating of Tenax TA

### *7.2.2 Materials and Equipment*

Tenax TA (80/100 mesh, Sigma-Aldrich, St. Louis, MO) was dissolved in dichloromethane at different concentrations and the solutions were used in all tests. All VOC samples used in this work were reagent grade (Sigma-Aldrich, St. Louis, MO). All adsorption/desorption tests were carried out using a Hewlett-Packard 5890 GC system (manufactured now by Agilent Technologies, Inc., Palo Alto, CA). The testing apparatus was installed inside the GC oven in order to maintain isothermal temperature conditions. The setup was supplied with nitrogen (zero



grade, AirGas Inc., Radnor, PA) as carrier gas via the GC inlet. This configuration enabled the use of the built-in gas flow controller to control the carrier gas entering the setup. The inlet pressure was adjusted to achieve 1 mL/min flow rate through the  $\mu$ PC. The setup was also connected to the built-in flame ionization detector (FID). This permitted signal detection and data collection through the built-in signal processing system of the GC instrument.

The testing apparatus consisted of a six-port zero-dead-volume valve (C6W, VICI Valco Instruments, Houston, TX), and two 250  $\mu$ m-ID deactivated fused silica transfer lines (Agilent Technologies, Inc., Palo Alto, CA). Using a precision sampling syringe (Pressure-Lok needle, VICI Valco Instruments, Houston, TX), the sample was manually withdrawn from the sample vial and then injected into the GC inlet.

Device testing consisted of a series of three different runs: blank, loading, and heating. In the blank run, the device was heated to 250 °C at a rate 100 °C/sec in order to establish a baseline. In the loading run, the sample was passed through  $\mu$ PC at an isothermal temperature of 60 °C to adsorb the sample. Finally, in the heating run, the  $\mu$ PC was heated to 250 °C at a rate of 100 °C/sec in order to desorb the sample. The inlet and FID temperatures were both kept at 280 °C. The on-board resistive heaters and temperature sensors were not used in this experiment. Instead, an off-board high-performance ceramic heater (ULTRAMIC 600, Watlow Electric Manufacturing Co., Chicago, IL) was used for thermal desorption along with a K-type thermocouple for manual temperature monitoring and control. In future work, the on-chip thermal desorption capability will be used.

Scanning electron microscopy (SEM) and optical microscopy were used to characterize film topography. Film thickness variations were measured using a profilometer (Dektak Veeco Instruments Inc., Plainview, NY). Film specific surface area was measured using a surface area analyzer (Autosorb-1, Quantachrome Instruments, Boynton Beach, FL). Most of the films were made from solution at room temperature and ambient air. However, films were made from frozen solution. That is, the solution was applied in the liquid phase and then frozen by cooling the back side of the substrate with liquid nitrogen. Once vacuum is reached, the coolant was removed and sample was allowed to melt at room temperature. It should be noted that the SEM imaging, BET

analysis, and the profilometric measurements were done on films deposited on flat crystalline silicon substrates.

For X-ray diffraction measurements, the films were deposited on Kapton at room temperature (20 °C) and at elevated temperature (100 °C). Film thicknesses were in the range of 100-150  $\mu\text{m}$ .

X-ray diffraction (XRD) patterns of the products were recorded using a powder-type X-ray diffractometer (Siemens D5005, Bruker AXS, Inc., Madison, WI) optimized for characterization of thin films. The instrument was operated at 40 kV and 40 mA, producing characteristic  $\text{Cu}_{\text{K}\alpha}$  radiation with an average wavelength of  $\lambda = 1.5418 \text{ \AA}$ . No background corrections were applied.

Thermal gravimetric analysis (TGA) was done using a research-grade thermogravimetric analyzer (Q 500, TA Instruments, New Castle, DE) for Tenax TA granular and films. The sample sizes for granular, 20 °C film, and 100 °C film were 22.4 mg, and 4.9 mg, and 6.5 mg respectively. The samples were heated from 0 °C to 1000 °C with a rate of 20 °C /min in the air atmosphere of 60 ml/min.

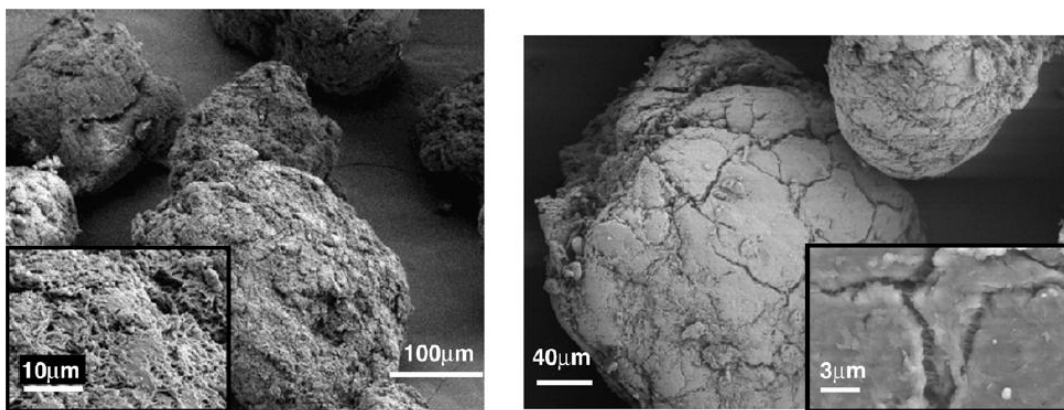
## ***7.3 Results and Discussion***

### ***7.3.1 Tenax TA Physical Characteristics***

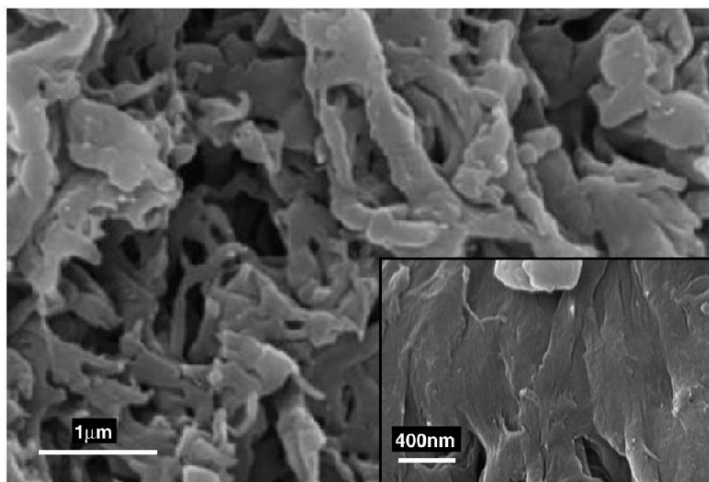
#### ***7.3.1.1 Physical Characteristics of Granular Tenax TA***

It was necessary to explore the nature of the polymer as received before investigating the physical characteristics of Tenax TA films since data on the nature of Tenax TA is rather scarce. This information will help in compare the physical characteristics of Tenax TA films to those of the granular form. The granular adsorbent (80/100 mesh) consist of highly porous particles with an average size of 200  $\mu\text{m}$ . The advertised specific surface area of the Tenax TA is 35  $\text{m}^2/\text{g}$ . However, a lower value was measured (19  $\text{m}^2/\text{g}$ ) by other researchers using the Brunauer, Emmett and Teller (BET) gas sorption method [30, 40, 44]. Our BET analysis reported specific surface area of 20  $\text{m}^2/\text{g}$ . Moreover, the adsorbent has a density of 0.25  $\text{g}/\text{cc}$ , pore volume of 2.4  $\text{cc}/\text{g}$ , and an average pore size of 200 nm [43]. Scanning electron microscopy analysis confirmed that the polymer particles had an average size of 200  $\mu\text{m}$  as shown in Figure 49. Most particles were highly porous but some were found to be partially porous. In fact, the particles consist of highly elongated and entangled solid material with spacing that ranges from 100 nm to 300 nm

as shown in Figure 50. The spacing, on average, is consistent with the pore size indicated by the manufacturer. It is notable that Zhao et al. [25] described Tenax TA particles as an assemblage of porous microspheres with an estimated radius of 1  $\mu\text{m}$  and with an average intraparticle pore size of 200 nm. The pore area within each microsphere was estimated by them to be approximately 20  $\text{nm}^2$ .



**Figure 49 SEM micrographs of Tenax TA beads as received, insets are higher magnification micrographs**

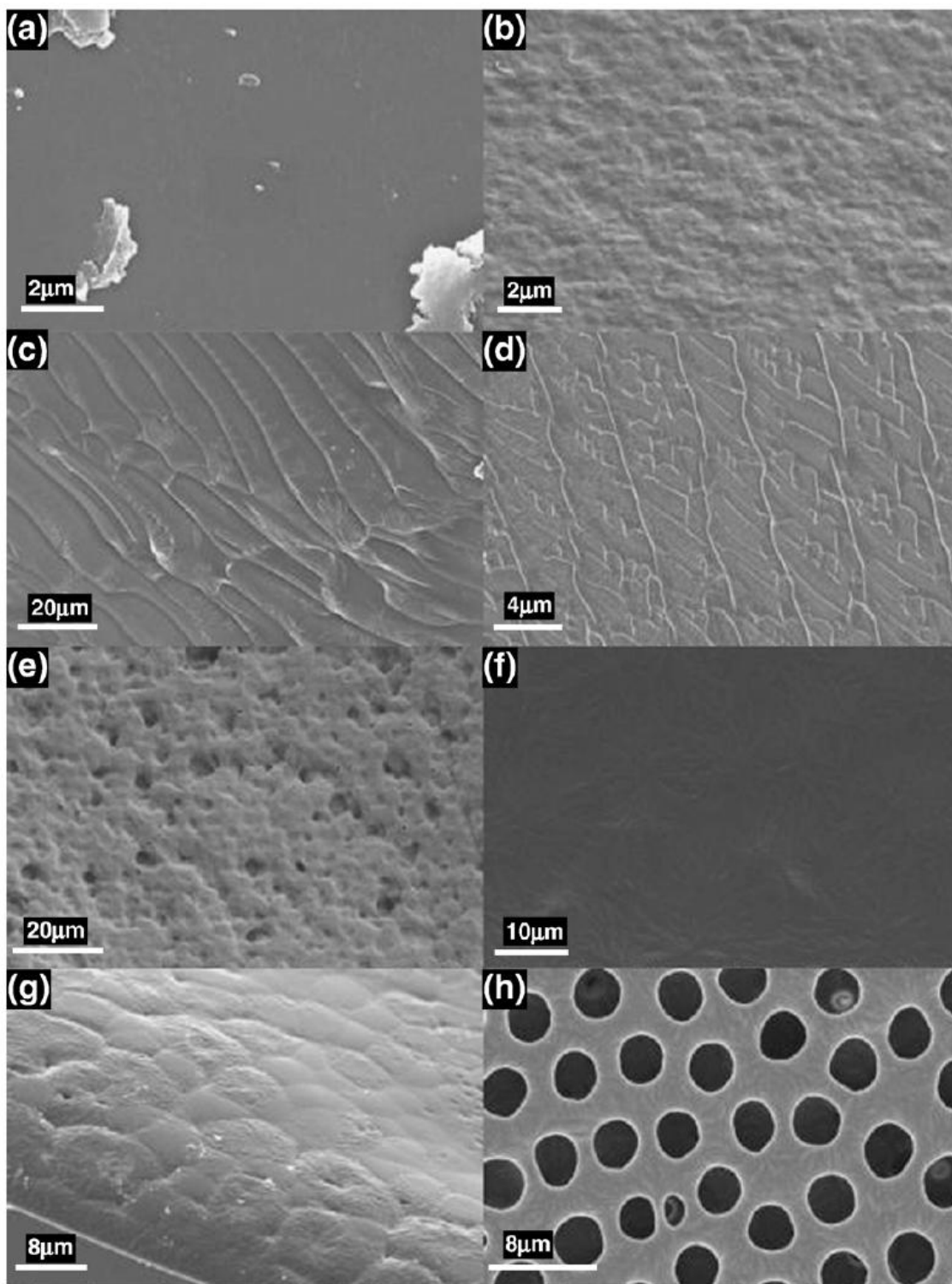


**Figure 50 SEM micrographs showing the nature of porous beads structure, inset is higher magnification micrograph**

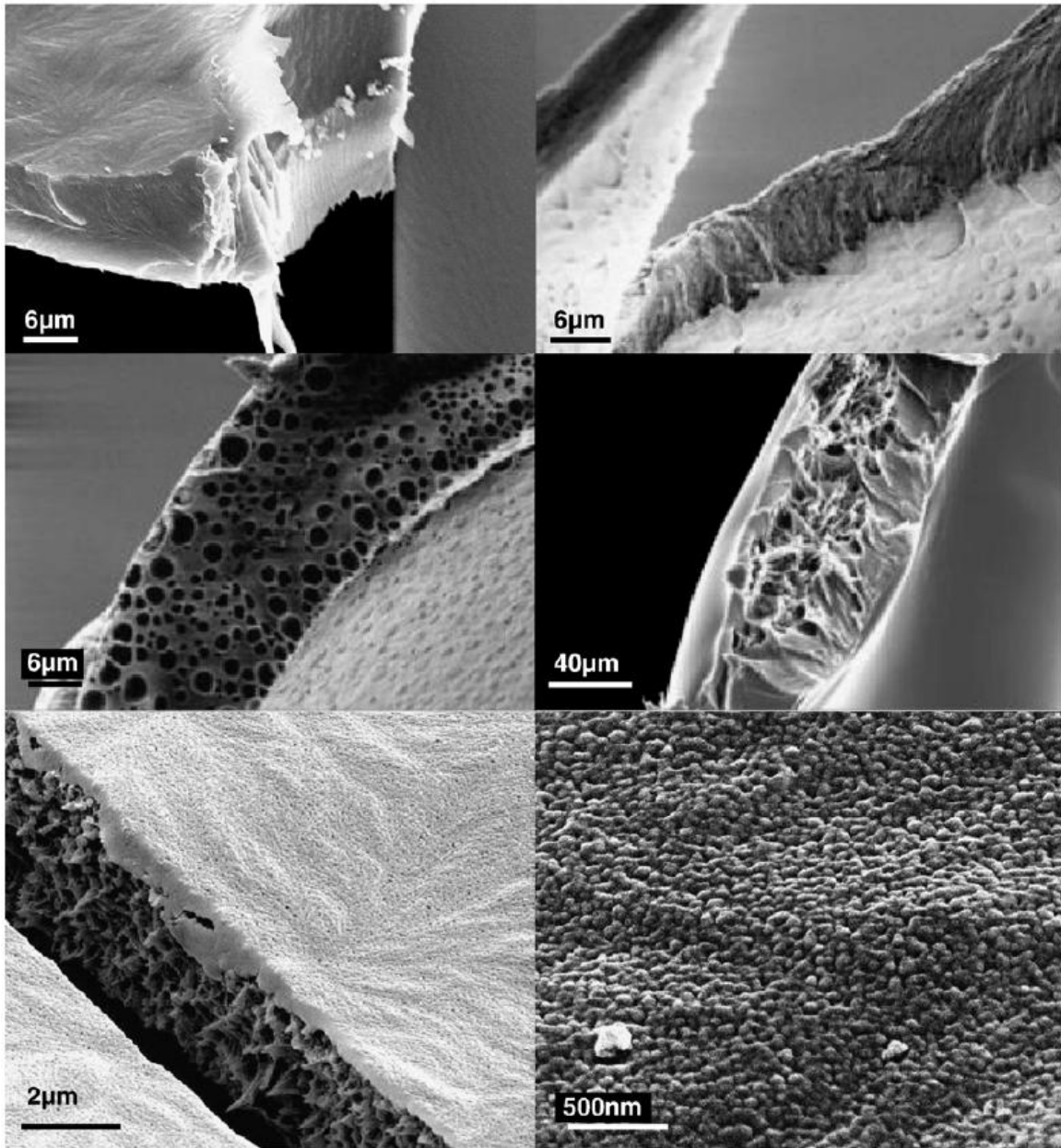
### *7.3.1.2 Physical Characteristics of Tenax TA Films*

#### *7.3.1.2.1 Scanning Electron Microscopy Analysis*

Tenax TA films were also examined by SEM. It was found that depending on the film deposition conditions, the film topography can vary within a wide range. Even under the same deposition conditions the film topography can vary. Alentiev et al. [41] raised the question, which remains unanswered, of why films of different phase composition are obtained under similar film casting conditions. It is believed that the variation in films topographies is related to the formation of inclusion complexes or clathrate compounds. Therefore, to minimize the formation of such compounds, some film solutions were frozen and placed in vacuum. The vacuum environment removed the solvent as it melted thus preventing the crystallization process. Some of the observed film topographies are shown in Figure 51. According to the SEM imaging investigation, it was revealed that some Tenax TA films had varying topographies such that some films showed an absence of patterns while others exhibited repeated spherulitic patterns. Furthermore, some films had a combination of patterned and non-patterned regions that were contained within hexagonal cells. The repeated patterns indicate the crystallization of Tenax TA. In Addition the structure of each specimen film varied in porosity. In other words some surfaces were shown to be solid or porous externally, while the inner structure could be either solid or porous, Figure 52. It is believed that the film porosity and surface area might play a significant role in the adsorption performance of the film.



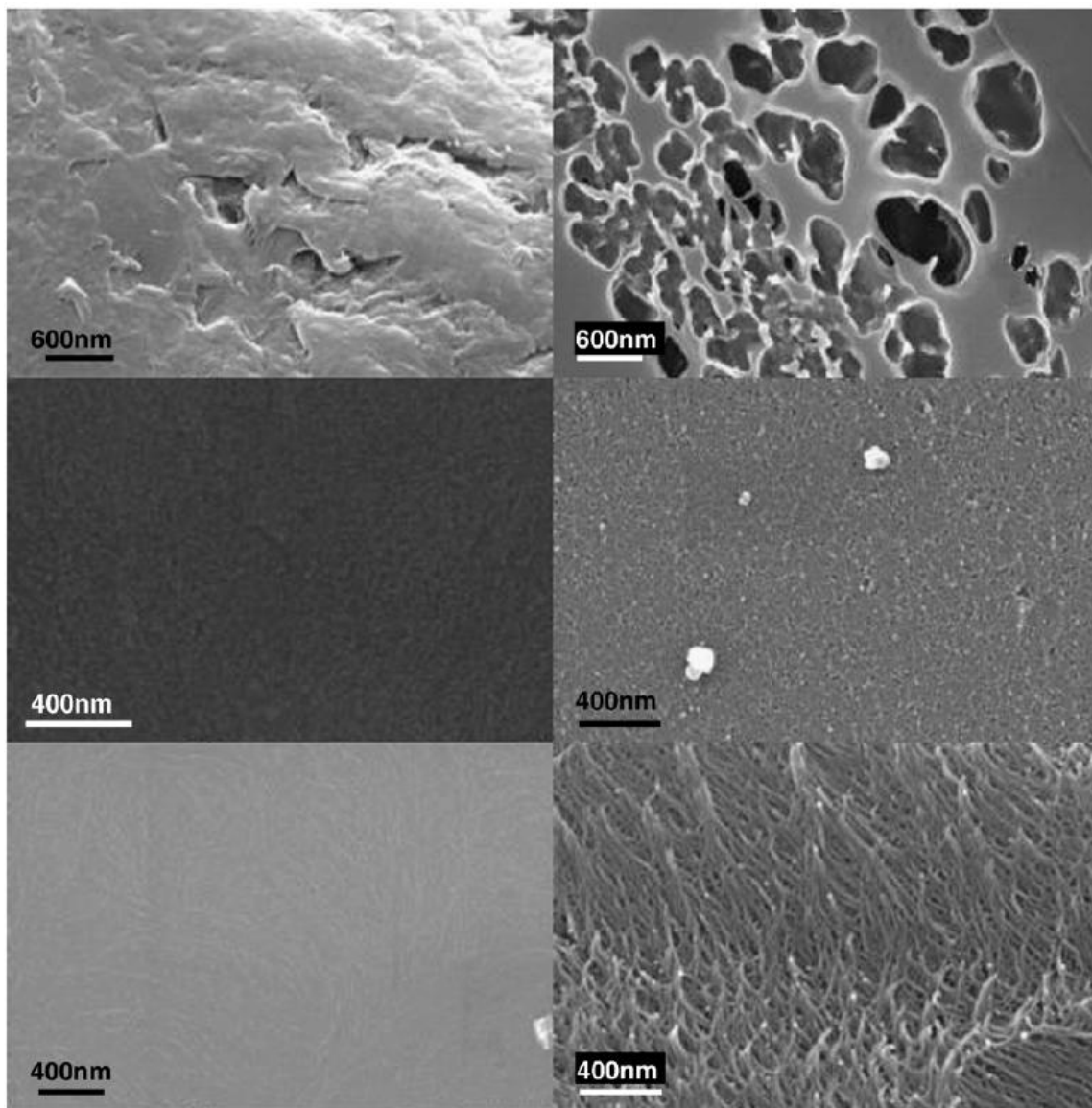
**Figure 51 SEM micrographs showing the different topographies of Tenax TA films. Samples (a-d) were prepared from frozen solution and deposited under vacuum. Samples (e-h) were prepared from solution at room temperature and deposited under ambient atmosphere**



**Figure 52 SEM micrographs showing Tenax TA films outer surface and inner structure. Samples were prepared from solution at room temperature and deposited under ambient atmosphere**

Upon closer examination it was revealed, from collection of images in Figure 53, that the Tenax TA film surface can vary. The resulting specimens were found to exhibit configurations that were solid, flat, or flat with interconnected pores. An additional configuration consisted of nano spheres which had the capacity to be closely packed together, with spacing in-between or

arranged in a row to form a wire-like configuration. The film could also consist of solid wires that formed a grass-like configuration.



**Figure 53 SEM micrographs showing Tenax TA film topographies at high magnification. Samples were prepared from frozen solution and deposited under vacuum**

It is worth noting that Boon et al. have done a detailed study on the crystalline structure of one of the two crystalline modifications of poly(2,6-diphenyl *p*-phenylene oxide), specifically  $\alpha$ -PPPO modifications obtained by thermal crystallization at 440 °C [45]. However, films under investigation here are believed to have a different phase compositions that consists of a medley

of  $\alpha$ -PPPO and  $\beta$ -PPPO crystalline phases as well as an amorphous phase. According to Boon *et al.*,  $\beta$ -PPPO can only be obtained by crystallization from solution whereas  $\alpha$ -PPPO can be obtained by either thermal crystallization of undiluted polymer or crystallization from solution.

### 7.3.1.2.2 Tenax TA Crystallographic Study

The X-ray diffraction patterns of Tenax TA granular and films were recorded in terms of intensity as a function of scattering angle,  $2\theta$ . Diffraction from crystalline materials is described by Bragg's law:

$$2d \sin\theta = n\lambda$$

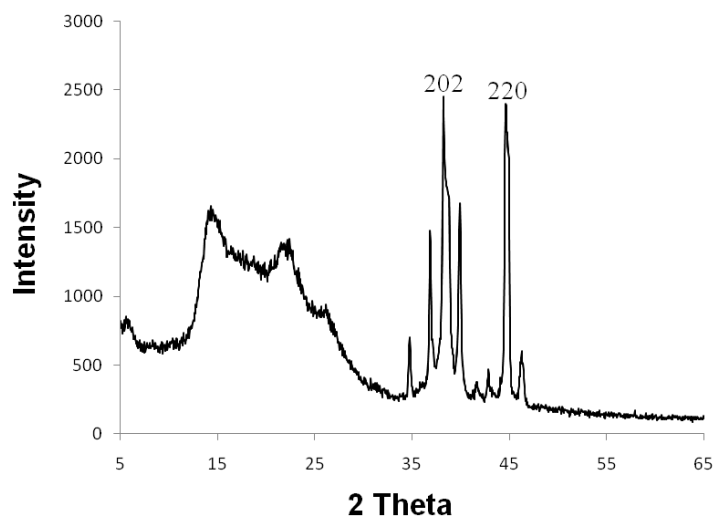
where  $d$  is the spacing between the planes,  $n$  is an integer determined by the order given, and  $\lambda$  is the wavelength of the X-rays. The diffraction patterns presented here were collected for the granular material, films deposited at 20 °C, and films deposited at 100 °C. Figure 54 shows the XRD data collected for films of Tenax TA deposited at 20 °C, while the XRD data collected for the granular material and for the films deposited at 100 °C are shown in Figure 55.

Tenax films formed at 20 °C showed a high level of crystallinity, as illustrated by the sharp diffraction maxima in Figure 54. Intense, narrow Bragg reflections were observed at 34.7, 38.2, 38.9, and 44.7 ° $2\theta$ . Tenax was previously studied with similar peaks and detailed characterization identified a tetragonal unit cell of  $a = b = 12.51 \text{ \AA}$  and  $c = 17.08 \text{ \AA}$  [41, 45]. Consistent with this previous work, the observed Bragg maxima correspond to 202 lattice plane in the peak that illustrate the tetragonal unit cell in Figure 54 at 38.2 ° $2\theta$ , which is also confirmed by Boon *et al.* with  $d$ -spacing values of 2.5 Å [45]. Broader, less intense scattering maxima were observed near 14 and approximately 22 ° $2\theta$ . These weaker scattering maxima are superimposed on the scattering from the amorphous polymer material, the “amorphous halo”, in the semi-crystalline sample and are most likely not related to the structure of the crystalline phase.

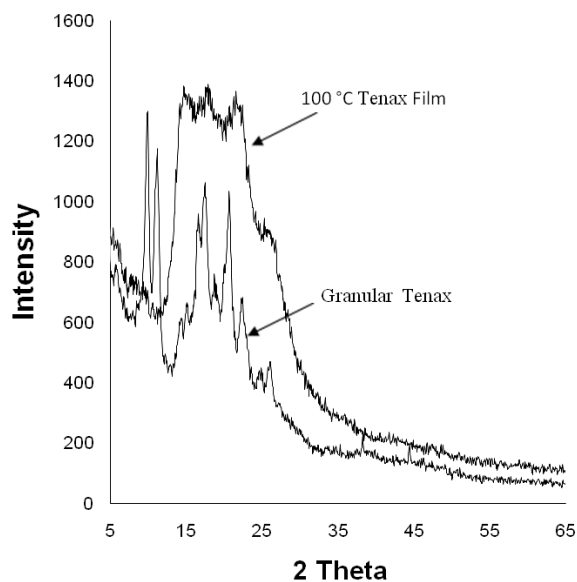
In contrast, 100 °C-deposited films provided little evidence of crystallinity, indicating an amorphous material. The main features of interest in the diffraction data for these samples are the peaks located at 14.7, 17.9, and 21.5 ° $2\theta$ . Moreover, the peaks observed are quite weak and broad. The wide peak at 14.7 ° $2\theta$  was previously described as the amorphous halo by Alentiev *et al.* [41], although here it appears that the amorphous halo is broadly centered at approximately



20  $2\theta$ . The amorphous topography of the 100 °C films is most likely a result of the rapid evaporation of solvent, which prevents polymer crystallization. For the granular sample, maxima are observed at scattering angles of 9.8, 11.2, 17.4, and 20.6  $2\theta$ , again coincident with the amorphous halo region of the scattering data and inconsistent with scattering from the tetragonal crystal topography of Tenax.



**Figure 54 XRD pattern for a Tenax TA film deposited at 20 °C (Peak intensities have been reduced for clarity)**



**Figure 55 XRD patterns from granular Tenax TA and films deposited at 100 °C**

### 7.3.1.2.3 Tenax TA Thermal Characteristics

Thermal stability is a very important property for any adsorbent material for its successful employment in preconcentration devices. Thus, it was necessary to determine the thermal properties of the films in comparison to the granules form of Tenax. This was done by using TGA of the granules and films at identical conditions. The TGA results have shown no weight loss occurs up to 400 °C in all samples. Figure 56 show the TGA results of the 20 °C films. The granules and the 100 °C films exhibited similar profile.

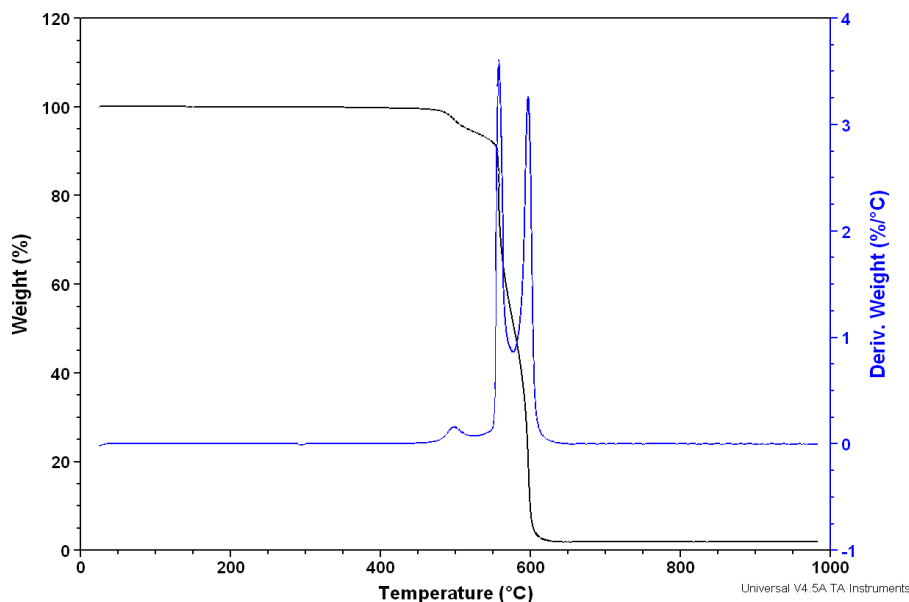


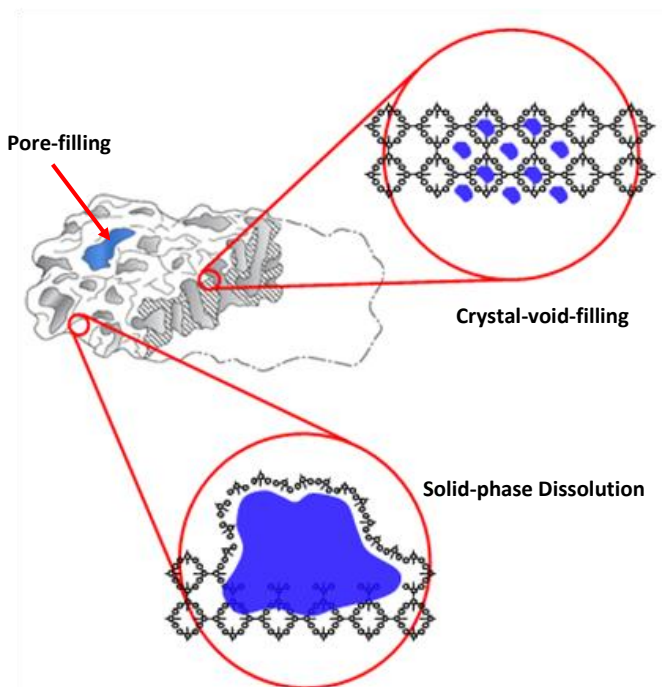
Figure 56 Thermal gravimetric analysis of Tenax films from 0 °C to 1000 °C

## 7.3.2 Tenax TA Adsorbent Films Evaluation

### 7.3.2.1 Modes of Uptake in Tenax TA

There are several mechanisms or combination of mechanisms for organic compound uptake by polymers. Some of these mechanisms are illustrated in Figure 57. A dual-mode sorption mechanism has been proposed for VOCs uptake in Tenax TA [46]. One mode of sorption is solid-phase dissolution and the other is pore-filling. Zhao et al. [25] concluded that the pore-filling mode was much greater than the dissolution mode in Tenax TA beads. It is important to

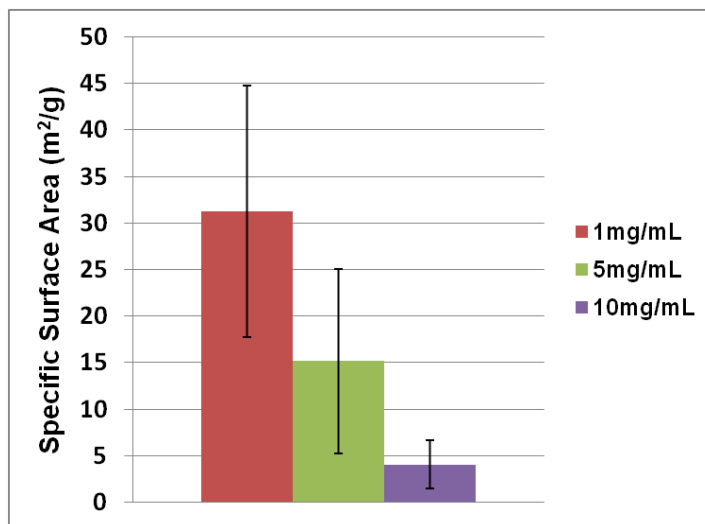
understand the uptake mechanism in Tenax TA film in order to optimize its adsorption performance.



**Figure 57 Mechanisms of organic compound uptake by polymers**

By using a different approach, we studied the solid-phase dissolution in Tenax TA films. We assumed that polymer swelling is proportional to the amount of solid-phase dissolution; thus we used the profilometer to determine if Tenax TA films swelled after exposure to a drop of liquid VOCs. This was tested in the following manner: First, the Tenax film was heated to 300 °C for 3 min to drive out any adsorbed or absorbed molecules from the ambient air. Second, the film thickness was measured immediately after heating and once again after exposing the film to different VOCs such as acetone, propanol, methanol, and n-nonane. Visual inspection under an optical microscope and the surface profiler data showed no significant difference in the specimen before and after exposure to the abovementioned VOCs. The resulting data confirmed that solid-phase dissolution mode was not the dominant mode of sorption by Tenax TA. The pore-filling mode can be studied by examining the film porosity. We utilized BET gas sorption analysis to

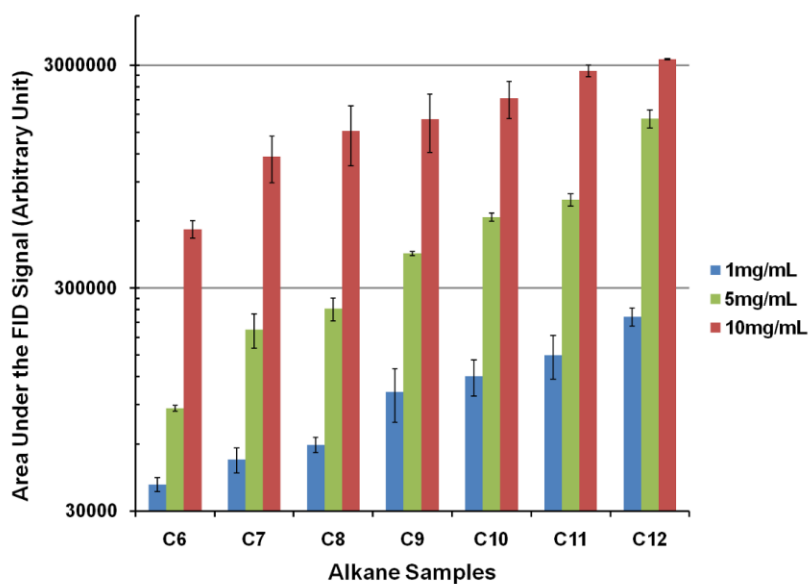
examine the porosity of Tenax TA films at different concentrations. One would expect to see correlation between the specific surface area and porosity. BET analysis of different concentration films prepared under the same conditions is shown in Figure 58. The film thickness varies from few micrometers for the 10 mg/mL concentration to few tens of nanometers for the 1 mg/mL concentration. Results showed that each film's specific surface area is inversely proportional to the solution concentration. When compared to the uncoated surface, the 1 mg/mL film increased the surface area by a factor of 3. In contrast, the 10 mg/mL film decreased the surface area by approximately a factor of 0.5. Since the solvent was assumed to be part of the crystal lattice of Tenax TA, the lower concentration solution produced films with larger surface area than the higher concentration solutions. If pore-filling is the dominant mode, then one would expect that the lower concentration films would have larger adsorption capacities.



**Figure 58 BET surface area analysis of different Tenax TA concentration films prepared under the same conditions**

Representative VOC samples were used to evaluate Tenax TA films as adsorbent material. The samples included n-hexane, n-heptane, n-octane, n-nonane, n-decane, n-undecane, and n-dodecane. To verify if pore-filling was indeed the dominant mode of adsorption, nine  $\mu$ PCs were coated with Tenax TA films under the same conditions. The nine  $\mu$ PCs were divided into three sets of three devices. The three sets were coated with different Tenax TA solutions at

concentrations of 1 mg/mL, 5 mg/mL, and 10 mg/mL. The test was carried out by adsorbing alkane samples at 60 °C with subsequent thermal desorption (250 °C at 100 °C/sec) and FID analysis of the desorbed compounds. The area under the curve of the FID signal was directly proportional to the concentration of the desorbed sample. Each compound was tested three times for every  $\mu$ PC in the three sets of  $\mu$ PCs. The results were averaged for every compound in every set and the uncertainties were calculated as a standard deviation. Figure 59 shows that, on average, the desorbed sample concentration increased in direct proportion to the adsorbent film concentration. This was inconsistent with the BET analysis indicating that pore-filling is not the dominant mode of adsorption in the films tested. Interestingly, it should be noted that BET analysis does not take into account sorption within the crystal voids. The analysis only takes into account the number of molecules required to form a monolayer on the surface. These results suggest that crystal-void-filling is the dominant mode of adsorption in Tenax TA films. This is in agreement with Alentiev et al. conclusions [41].



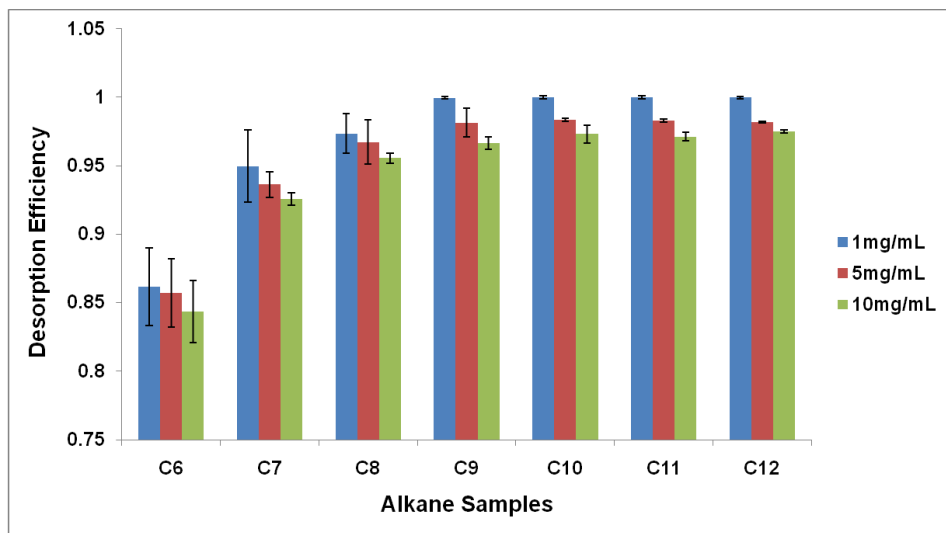
**Figure 59 FID analysis of desorbed alkane samples from Tenax TA films made from different Tenax TA solutions at concentrations of 1 mg/mL, 5 mg/mL, and 10 mg/mL**

Alentiev et al. [41] also reported that film crystallinity is higher than that of the powder and they described the crystalline lattice as loosely packed (large voids can exist inside the crystallites) with a radius of spherical free-volume equal 4.8 Å. Thus, the crystallites can take

part in the gas sorption process. Alentiev et al. [41] finally concluded that crystal phase composition does not affect the permeability and solubility coefficient of the film for several gases (including CH<sub>4</sub>) as much as the film chemical composition. Therefore, with a large free volume within Tenax TA crystallites (crystal voids), the nonporous film can uptake VOCs with little or no swelling.

### 7.3.2.2 Tenax TA Films Desorption Efficiency

The films desorption efficiency was calculated as a percent of desorbed compound during desorption process for the three Tenax TA film concentrations using the alkane samples. For a given compound, the peak area for the first desorption was divided by the sum of the signal of the same compound for the first and second desorption. The second desorption was done without additional adsorption. Calculations obtained were averaged and the uncertainties were calculated as shown in Figure 60. Although there is a small difference among the three Tenax TA film concentrations, it was evident that the desorption efficiency was higher with the lower concentration films. Hereafter,  $\mu$ PCs coated with 10 mg Tenax TA were used to further investigate Tenax TA adsorbent properties.



**Figure 60** Desorption efficiency of alkane samples from Tenax TA films made from different Tenax TA solutions at concentrations of 1 mg/mL, 5 mg/mL, and 10 mg/mL

### 7.3.2.3 Tenax TA Films Affinity to Representative Volatile Organic Compounds

Representative VOC samples were used to evaluate Tenax TA films as adsorbent material. The samples included alkanes (n-hexane, n-heptane, n-octane, n-nonane, n-decane, n-undecane, n-dodecane), aromatic hydrocarbons (benzene, toluene), phosphonates (dimethyl methylphosphonate (DMMP)), ketones (acetone), and alcohols (ethanol, methanol, 1-propanol). Each compound was tested three times in succession on three independent  $\mu$ PCs. The uncertainties were calculated as a standard deviation. When analyzing the Tenax TA films, the data revealed that methanol was adsorbed the least whereas DMMP was adsorbed the most. From Figure 61, it can be concluded that Tenax TA films were more effective in adsorbing phosphonates, and aromatic hydrocarbons samples than alkanes, alcohols, and ketones. The adsorption data is in good agreement with those achieved by Tenax TA particles published elsewhere [34, 38, 40].

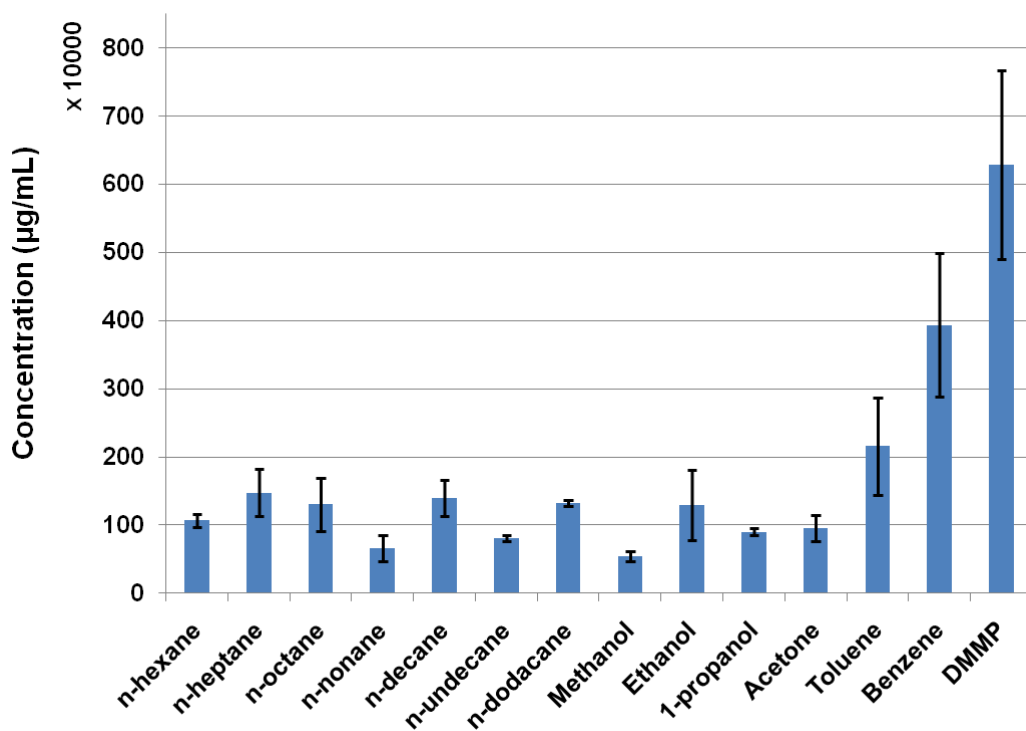


Figure 61 FID analysis of desorbed VOC representative samples on Tenax TA films

#### 7.3.2.4 Tenax TA Films Capacity

To evaluate the adsorption capacity of Tenax TA films, different film-based adsorbent materials such as polydimethylsiloxane (PDMS) and layer-by-layer assembled gold nanoparticles (GNPs) were compared with the adsorbent film in question. PDMS is an all-purpose stationary phase commonly used in GC columns [47]. It is also a common adsorbent used in solid phase microextraction applications [48]. PDMS solution (in dichloromethane) was used to coat the  $\mu$ PCs using inkjet printing method described in our previous publication [49]. GNPs were considered due to their recent application in the field of separation science as a stationary phase material [50, 51]. The interest in GNPs stems from their ability to form self-assembled monolayers (SAM) and functionalize them with different functional groups. This allows customization of the  $\mu$ PCs to specific applications. Monolayer-protected gold nanoparticles (MNP) have been successfully employed as a stationary phase for tubular [52] and microfabricated GC columns [4]. The preparation of GNP coated  $\mu$ PCs is similar to the procedure described elsewhere [4] to coat GC columns with GNP films. Briefly, the  $\mu$ PCs were washed with NaOH to charge the surface with OH-groups., which was then followed by treatment with 2mM solution of aminopropyltrimethoxysilane (APTMS, Sigma-Aldrich Inc., St. Louis, MO) in ethanol. GNPs (Ted Pella Inc., Redding, CA) 20nm in diameter were attached to the amine group of the APTMS by filling the chips with GNP solution. The thiol functional group of alkane was attached to GNPs by introducing a solution of 2mM solution of octadecylthiol ( $C_{18}H_{35}SH$ ) (Sigma-Aldrich Inc., St. Louis, MO) in hexane to the chip.

Table 6 summarizes the results of the comparison study for different adsorbents under similar conditions by loading the chip with 1  $\mu$ L of n-nonane and then thermally desorbing it. Coating the  $\mu$ PC with GNPs increased the adsorption capacity by 2440%. However, it was found that the GNPs experience Ostwald ripening under the extreme temperature ramping (100  $^{\circ}C/sec$ ). Ostwald ripening degrades the performance of GNPs as an adsorbent over time. Coating the  $\mu$ PC with PDMS increased the adsorption capacity by 7892%. Although PDMS added significant adsorption capacity, extreme temperature variations should be avoided with this material. Thus, it is not suitable for applications where the preconcentrator needs to be heated very rapidly to temperatures close to 250  $^{\circ}C$ . Furthermore, exposing PDMS to air or oxygen at elevated temperatures oxidizes it, and consequently degrades its performance. Moreover, some solvents



can swell the PDMS film, possibly change its surface properties, and may cause the film to detach from the substrate [53]. Tenax TA films provided the highest increase, among all adsorbent tested, in performance, especially the 100 °C films (94220%). The high performance of the 100 °C films is attributed to the high porosity of the film along with its amorphous phase property. Tenax TA coating is simpler than PDMS coating as it does not require cross-linking. It also offers many advantages, as discussed in the introduction.

**Table 6 Performance of different adsorbents under similar adsorption/desorption conditions**

<b>Adsorbent</b>	<b>Desorption Peak Concentration (ppm)</b>	<b>% Increase</b>
Uncoated	606	0
GNP	15391	2440
PDMS	48432	7892
Tenax TA 20 °C	190517	31340
Tenax TA 100 °C	571556	94220

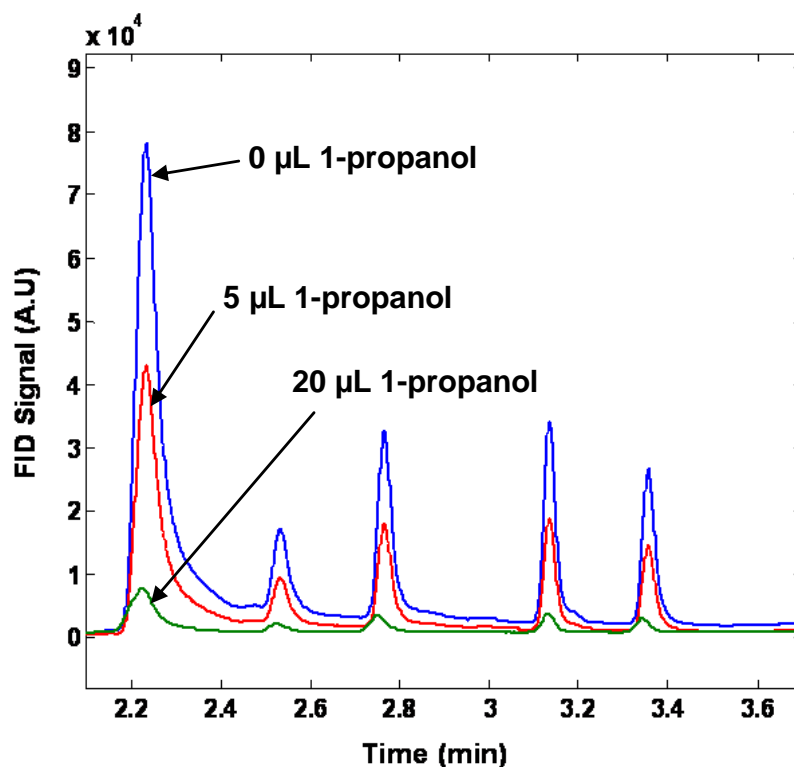
### *7.3.2.5 Analyte Storage Time on Tenax TA Films*

In some air monitoring applications such as compliance with permissible exposure limit, it is necessary to determine the average exposure to analytes over a specified period of time. Or, in some cases, the collected samples are stored for a sometime before they get analyzed. In these applications, the preconcentrator is used as a storage device. Analyte storage time on Tenax TA films within the  $\mu$ PC was studied to determine analyte life time in the Tenax TA coated  $\mu$ PC. This information is valuable in the case where the analysis could not be done immediately after the sample was collected or in case the  $\mu$ PC is to be utilized as analyte micro storage device. This was done by determining the sample amount loss over storage time. For storage periods of one week, one month and three months, the  $\mu$ PC was loaded with fixed amount of n-nonane at room temperature. After each storage period, the analyte in the  $\mu$ PC was desorbed and analyzed by the FID. The analyte concentration in the desorption plug decreased by about 4% per week.

For analyte storage stability, the National Institute for Occupational Health and Safety (NIOSH) recommends that the average quantitative measurements coming from the storage device should not differ from the analysis on day 0 by more than 10% [54]. Conventional Tenax TA preconcentration tubes can hold analytes for up to 14 days according to US EPA method for volatile organic sampling and UK HSE methods for the determination of hazardous substances.

#### *7.3.2.6 Competitive Adsorption on Tenax TA Films*

As noted by Sakodynskii, et al [40] Tenax has a molecular interaction specificity. In fact, it can adsorb both polar and nonpolar compounds. Thus, we investigated the effect of adsorption of a given compound on the adsorption of other compounds (competitive adsorption). It is worth noting that some chemical species are capable of removing already adsorbed species from adsorption sites to take their place. The test was carried out by loading the  $\mu$ PC with three different amounts of 1-propanol (0, 5, 20  $\mu$ L) followed by loading of a fixed volume mixture consisting of toluene, n-octane, n-decane, n-dodecane and n-tridecane. The device was put in series with a 1 m 100% methylpolysiloxane microfabricated column. The initial and final temperatures of the column were 35 °C and 150 °C with temperature programming of 30 °C/min and 1 mL/min flow rate. It should be noted that this stationary phase does not separate 1-propanol. As expected, Figure 62 showed that saturating the  $\mu$ PC with 1-propanol has a negative effect on its performance. This is a typical behavior of high porosity adsorbent. This data is particularly useful in environmental monitoring and/or breath analysis where samples typically contain large amount of water. 1-propanol and water share similar boiling point and polarity. 1-propanol was chosen as a water representative because the available detector (FID) is water insensitive. It should be noted that the retention volume of 1-propanol on Tenax TA is larger than water by a factor of 26 [34].



**Figure 62** FID analysis of competitive adsorption between 1-propanol and toluene, n-octane, n-decane, n-dodecane, and n-tridecane respectively by elution order

#### 7.4 Conclusions

This work contributes to the field of analytical chemistry by giving insight into the nature of Tenax TA films in comparison to the common granular form. Tenax TA films have a complex phase composition that includes crystalline and amorphous phases. The phase composition of the film can be controlled by controlling the film's deposition conditions.

In general, our investigation demonstrated the superiority of Tenax TA films over other possible film-based adsorbents for  $\mu$ PCs. The film form of Tenax TA has several advantages over the granular form, especially in micro preconcentration applications. Tenax TA solution allows a simple way of entraining Tenax TA within the small spaces of  $\mu$ PCs. The film also conforms to the complex microfabricated structures, a commodity that is not possible with granules.

The analysis revealed that Tenax TA beads consist of elongated and entangled particles. Nevertheless, the particles themselves were not porous as suggested in the literature. However, the topography of Tenax TA films depended on the preparation conditions and, even under the same conditions, the films can vary with a wide range. The profilometer results confirmed that solid-phase dissolution is not the dominant mode of sorption in Tenax TA. Comparing the BET analysis with desorption analysis indicated that pore-filling was not the dominant mode of adsorption in Tenax TA films. It is interesting to note that the large variation in the film morphologies was manifested in the large magnitude of the error bars in the BET data but was not reflected in the error bars of the adsorption/desorption data. This is another indication that pore-filling is not the dominant mode of adsorption. The VOCs uptake in films could be attributed to crystal-void-filling.

Moreover, based on the adsorption properties of Tenax TA films investigated here and the published data on Tenax TA granules, it can be concluded that there is no difference in the adsorption properties between the adsorbent polymer in granular and film forms. The effect of phase composition on the properties of the polymer and repeated use on the adsorbent performance as well as long-term sample holdup time will be investigated in future studies.

## References

- [1] B. Alfeeli, L. T. Taylor, and M. Agah, "Evaluation of Tenax Ta Thin Films as Adsorbent Material for Micro Preconcentration Applications," *Microchemical Journal*, vol. 95, 2010, pp. 259-267.
- [2] M. A. Zareian-Jahromi, M. Ashraf-Khorassani, L. T. Taylor, and M. Agah, "Design, Modeling, and Fabrication of Mems-Based Multicapillary Gas Chromatographic Columns," *Journal of Microelectromechanical Systems*, vol. 18, 2009, pp. 28-37.
- [3] I. Elmi, S. Zampolli, L. Masini, G. C. Cardinali, M. Severi, A. Barranco, L. Francioso, and P. Siciliano, "A Miniaturized Gas-Chromatographic System for the Evaluation of Fish Freshness," in *The 7th IEEE Conference on Sensors*, Lecce, Italy, 2008, pp. 1084-1087.
- [4] B. Alfeeli, S. Ali, V. Jain, R. Montazami, J. Heflin, and M. Agah, "Mems-Based Gas Chromatography Columns with Nano-Structured Stationary Phases," in *7th IEEE Conference on Sensors*, Lecce, Italy, 2008, pp. 728-731.
- [5] P. R. Lewis, P. Manginell, D. R. Adkins, R. J. Kottenstette, D. R. Wheeler, S. S. Sokolowski, D. E. Trudell, J. E. Byrnes, M. Okandan, J. M. Bauer, R. G. Manley, and C. Frye-Mason,

- "Recent Advancements in the Gas-Phase Microchemlab," *IEEE Sensors Journal*, vol. 6, 2006, pp. 784-795.
- [6] S. Reidy, D. George, M. Agah, and R. Sacks, "Temperature-Programmed Gc Using Silicon Microfabricated Columns with Integrated Heaters and Temperature Sensors," *Analytical Chemistry*, vol. 79, 2007, pp. 2911-2917.
- [7] V. Camel and M. Caude, "Trace Enrichment Methods for the Determination of Organic Pollutants in Ambient Air," *Journal of Chromatography A*, vol. 710, 1995, pp. 3-19.
- [8] F. Blanco, X. Vilanova, V. Fierro, A. Celzard, P. Ivanov, E. Llobet, N. Cañellas, J. L. Ramírez, and X. Correig, "Fabrication and Characterisation of Microporous Activated Carbon-Based Pre-Concentrators for Benzene Vapours," *Sensors and Actuators B: Chemical*, vol. 132, 2008, pp. 90-98.
- [9] C. E. Davis, C. K. Ho, R. C. Hughes, and M. L. Thomas, "Enhanced Detection of M-Xylene Using a Preconcentrator with a Chemiresistor Sensor," *Sensors and Actuators B: Chemical*, vol. 104, 2005, pp. 207-216.
- [10] I. Gràcia, P. Ivanov, F. Blanco, N. Sabaté, X. Vilanova, X. Correig, L. Fonseca, E. Figueras, J. Santander, and C. Cané, "Sub-Ppm Gas Sensor Detection Via Spiral M-Preconcentrator," *Sensors and Actuators B: Chemical*, vol. 132, 2008, pp. 149-154.
- [11] M. Kim and S. Mitra, "A Microfabricated Microconcentrator for Sensors and Gas Chromatography," *Journal of Chromatography A*, vol. 996, 2003, pp. 1-11.
- [12] S. Li, J. C. Day, J. J. Park, C. P. Cadou, and R. Ghodssi, "A Fast-Response Microfluidic Gas Concentrating Device for Environmental Sensing," *Sensors and Actuators A: Physical*, vol. 136, 2007, pp. 69-79.
- [13] C. J. Lu and E. T. Zellers, "A Dual-Adsorbent Preconcentrator for a Portable Indoor-Voc Microsensor System," *Analytical Chemistry*, vol. 73, July 15, 2001 2001, pp. 3449-3457.
- [14] R. P. Manginell, D. R. Adkins, M. W. Moorman, R. Hadizadeh, D. Copic, D. A. Porter, J. M. Anderson, V. M. Hietala, J. R. Bryan, D. R. Wheeler, K. B. Pfeifer, and A. Rumpf, "Mass-Sensitive Microfabricated Chemical Preconcentrator," *Journal of Microelectromechanical Systems*, vol. 17, 2008, pp. 1396-1407.
- [15] M. Martin, M. Crain, K. Walsh, R. A. McGill, E. Houser, J. Stepnowski, S. Stepnowski, H.-D. Wu, and S. Ross, "Microfabricated Vapor Preconcentrator for Portable Ion Mobility Spectroscopy," *Sensors and Actuators B: Chemical*, vol. 126, 2007, pp. 447-454.
- [16] C. Pijolat, M. Camara, J. Courbat, J. P. Viricelle, D. Briand, and N. F. de Rooij, "Application of Carbon Nano-Powders for a Gas Micro-Preconcentrator," *Sensors and Actuators B: Chemical*, vol. 127, 2007, pp. 179-185.
- [17] Y. Tang, J. Yeom, J. Han, B. Bae, R. I. Masel, and M. A. Shannon, "A Micro-Post Preconcentrator for a Microscale Gas Chromatography System," presented at the International Conference on Miniaturized Systems for Chemistry and Life Sciences, MicroTAS'05, Boston, MA, 2005.

- [18] W.-C. Tian, H. K. L. Chan, L. Chia-Jung, S. W. Pang, and E. T. Zellers, "Multiple-Stage Microfabricated Preconcentrator-Focuser for Micro Gas Chromatography System," *Journal of Microelectromechanical Systems*, vol. 14, 2005, pp. 498-507.
- [19] I. Voiculescu, R. A. McGill, M. E. Zaghoul, D. Mott, J. Stepnowski, S. Stepnowski, H. Summers, V. Nguyen, S. Ross, K. Walsh, and M. Martin, "Micropreconcentrator for Enhanced Trace Detection of Explosives and Chemical Agents," *IEEE Sensors Journal*, vol. 6, 2006, pp. 1094-1104.
- [20] B. Alfeeli and M. Agah, "Micro Preconcentrator with Embedded 3d Pillars for Breath Analysis Applications," presented at the The 7th IEEE Conference on Sensors, Lecce, Italy 2008.
- [21] B. Alfeeli and M. Agah, "Selective Preconcentration by Temperature Manipulation of Cascaded Micro Preconcentrators," presented at the International Solid-State Sensors, Actuators and Microsystems Conference, TRANSDUCERS'09, Denver, CO, 2009.
- [22] S. Jung, S. Ehlert, J.-A. Mora, K. Kraiczek, M. Dittmann, G. P. Rozing, and U. Tallarek, "Packing Density, Permeability, and Separation Efficiency of Packed Microchips at Different Particle-Aspect Ratios," *Journal of Chromatography A*, vol. 1216, 2009, pp. 264-273.
- [23] R. R. Lima, R. A. M. Carvalho, A. P. N. Filho, M. L. P. Silva, and N. R. Demarquette, "Production and Deposition of Adsorbent Films by Plasma Polymerization on Low Cost Micromachined Non-Planar Microchannels for Preconcentration of Organic Compound in Air," *Sensors and Actuators B: Chemical*, vol. 108, 2005, pp. 435-444.
- [24] B. Alfeeli, M. A. Zareian-Jahromi, and M. Agah, "Micro Preconcentrator with Seedless Electroplated Gold as Self-Heating Adsorbent," in *8th IEEE Conference on Sensors*, Chirstchurch, New Zealand, 2009, pp. 1947-1950.
- [25] D. Zhao and J. J. Pignatello, "Model-Aided Characterization of Tenax-Ta for Aromatic Compound Uptake from Water," *Environmental Toxicology and Chemistry*, vol. 23, 2004, pp. 1592-1599.
- [26] A. S. Hay, "Process of Making Poly-(2,6-Diaryl-1,4-Phenylene Ethers)," US Patent 3,432,466, 1969.
- [27] R. van Wijk, "The Use of Poly-Para-2, 6-Diphenyl-Phenylene Oxide as a Porous Polymer in Gas Chromatography," *Journal of Chromatographic Science*, vol. 8, 1970, pp. 418-420.
- [28] W. Bertsch, A. Zlatkis, H. M. Liebich, and H. J. Schneider, "Concentration and Anlalysis of Organic Volatiles in Skylab 4," *Journal of Chromatography A*, vol. 99, 1974, pp. 673-687.
- [29] U04914 Data Sheet, "Tenax-Ta," ed: Alltech Associates Inc., 2007, p. 4.
- [30] M. Harper, "Sorberent Trapping of Volatile Organic Compounds from Air," *Journal of Chromatography A*, vol. 885, 2000, pp. 129-151.
- [31] E. D. Pellizzari, J. E. Bunch, R. E. Berkley, and J. McRae, "Collection and Analysis of Trace Organic Vapor Pollutants in Ambient Atmospheres. The Performance of a Tenax Gc Cartridge Sampler for Hazardous Vapors," *Analytical Letters*, vol. 9, 1976, pp. 45 - 63.

- [32] R. H. Brown and C. J. Purnell, "Collection and Analysis of Trace Organic Vapour Pollutants in Ambient Atmospheres : The Performace of a Tenax-Gc Adsorbent Tube," *Journal of Chromatography A*, vol. 178, 1979, pp. 79-90.
- [33] S. Seshadri and J. W. Bozzelli, "Collection of Vapors of Selected Chlorocarbons and Benzene on Tenax Gc," *Chemosphere*, vol. 12, 1983, pp. 809-820.
- [34] I. Maier and M. Fieber, "Retention Characteristics of Volatile Compounds on Tenax Ta," *Journal of High Resolution Chromatography*, vol. 11, 1988, pp. 566-576.
- [35] K. Ventura, M. Dostál, and J. Churáček, "Retention Characteristics of Some Volatile Compounds on Tenax Gr," *Journal of Chromatography A*, vol. 642, 1993, pp. 379-382.
- [36] V. Simon, M.-L. Riba, A. Waldhart, and L. Torres, "Breakthrough Volume of Monoterpenes on Tenax Ta: Influence of Temperature and Concentration for [Alpha]-Pinene," *Journal of Chromatography A*, vol. 704, 1995, pp. 465-471.
- [37] A. Kroupa, J. Dewulf, H. Van Langenhove, and I. Viden, "Breakthrough Characteristics of Volatile Organic Compounds in the -10 to +170 Oc Temperature Range on Tenax Ta Determined by Microtrap Technology," *Journal of Chromatography A*, vol. 1038, 2004, pp. 215-223.
- [38] R. Borusiewicz and J. Zieba-Palus, "Comparison of the Effectiveness of Tenax Ta and Carbotrap 300 in Concentration of Flammable Liquids Compounds," *Journal of Forensic Sciences*, vol. 52, 2007, pp. 70-74.
- [39] M. Schneider and K.-U. Goss, "Systematic Investigation of the Sorption Properties of Tenax Ta, Chromosorb 106, Porapak N, and Carbopak F," *Analytical Chemistry*, vol. 81, 2009, pp. 3017-3021.
- [40] K. Sakodynskii, L. Panina, and N. Klinskaya, "A Study of Some Properties of Tenax, a Porous Polymer Sorbent," *Chromatographia*, vol. 7, 1974, pp. 339-344.
- [41] A. Alentiev, E. Drioli, M. Gokzhaev, G. Golemme, O. Ilinich, A. Lapkin, V. Volkov, and Y. Yampolskii, "Gas Permeation Properties of Phenylene Oxide Polymers," *Journal of Membrane Science*, vol. 138, 1998, pp. 99-107.
- [42] K. Dettmer and W. Engewald, "Adsorbent Materials Commonly Used in Air Analysis for Adsorptive Enrichment and Thermal Desorption of Volatile Organic Compounds," *Analytical and Bioanalytical Chemistry*, vol. 373, 2002, pp. 490-500.
- [43] "Adsorbent Resins for Trapping Volatiles," Scientific Instrument Services, SIS Catalog: C10-C11, Ringoes, NJ, USA2008.
- [44] J.-M. Guillot, B. Fernandez, and P. Le Cloirec, "Advantages and Limits of Adsorption Sampling for Physico-Chemical Measurements of Odorous Compounds," *Analisis*, vol. 28, 2000, pp. 180-187.
- [45] J. Boon and E. P. Magré, "Structural Studies of Crystalline Poly(*P*-Phenylene Oxides) Ii. Poly(2.6-Diphenyl *P*-Phenylene Oxide)," *Die Makromolekulare Chemie*, vol. 126, 1969, pp. 130-138.

- [46] B. Xing and J. J. Pignatello, "Dual-Mode Sorption of Low-Polarity Compounds in Glassy Poly(Vinyl Chloride) and Soil Organic Matter," *Environmental Science & Technology*, vol. 31, 1997, pp. 792-799.
- [47] M. L. Lee, F. J. Yang, and K. D. Bartle, *Open Tubular Column Gas Chromatography: Theory and Practice* vol. x, 445 p. :. New York: Wiley, 1984.
- [48] D. Budziak, E. Martendal, and E. Carasek, "Preparation and Characterization of New Solid-Phase Microextraction Fibers Obtained by Sol-Gel Technology and Zirconium Oxide Electrodeposited on Niti Alloy," *Journal of Chromatography A*, vol. 1187, 2008, pp. 34-39.
- [49] B. Alfeeli, D. Cho, M. Ashraf-Khorassani, L. T. Taylor, and M. Agah, "Mems-Based Multi-Inlet/Outlet Preconcentrator Coated by Inkjet Printing of Polymer Adsorbents," *Sensors and Actuators B, Chemical*, vol. 133, 2008, pp. 24-32.
- [50] E. Guihen and J. D. Glennon, "Nanoparticles in Separation Science – Recent Developments," *Analytical Letters*, vol. 36, 2003, pp. 3309-3336.
- [51] V. L. Jimenez, M. C. Leopold, C. Mazzitelli, J. W. Jorgenson, and R. W. Murray, "Hplc of Monolayer-Protected Gold Nanoclusters," *Analytical Chemistry*, vol. 75, 2003, pp. 199-206.
- [52] G. M. Gross, D. A. Nelson, J. W. Grate, and R. E. Synovec, "Monolayer-Protected Gold Nanoparticles as a Stationary Phase for Open Tubular Gas Chromatography," *Analytical Chemistry*, vol. 75, 2003, pp. 4558-4564.
- [53] J. N. Lee, C. Park, and G. M. Whitesides, "Solvent Compatibility of Poly(Dimethylsiloxane)-Based Microfluidic Devices," *Analytical Chemistry*, vol. 75, 2003, pp. 6544-6554.
- [54] J. Volden, Y. Thomassen, T. Greibrokk, S. Thorud, and P. Molander, "Stability of Workroom Air Volatile Organic Compounds on Solid Adsorbents for Thermal Desorption Gas Chromatography," *Analytica Chimica Acta*, vol. 530, 2005, pp. 263-271.



## Chapter Eight: Solid-Phase Microextraction Using Silica Fibers Coated with Tenax-Ta Films

Part of this chapter was reproduced from [1] with permission from Elsevier B. V.

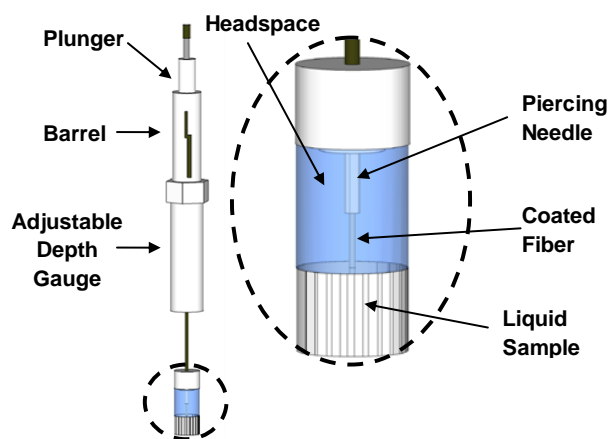
*B. Alfeeli, D. Hogg, and M. Agah, "Solid-Phase Microextraction Using Silica Fibers Coated with Tenax-TA Films," in European Sensors, Actuators, and Microsystems Conference (EUROSENSORS XXIV), Linz, Austria, Procedia Engineering, vol. 5, pp. 1152-1155.*

### 8.1 Introduction

Chemical analyses of organic pollutants, flavor or fragrance components, warfare agents, and many other samples usually begin with extracting and concentrating the target analytes from gaseous or aqueous sample matrices by one or multiple techniques known as sample preparation techniques [2]. Liquid-liquid extraction (LLE), purge-and-trap (P&T), and headspace (HS) are among the established sample preparation techniques in analytical chemistry [3]. These procedures typically require complicated equipment, technical training, excessive time, and/or extravagant use of solvents and reagents. Solid-phase microextraction (SPME) is an extraction technique developed in 1989 [4] to improve the efficiency and to reduce costs associated with sample preparation methods. SPME combines sampling, extraction, concentration and sample introduction into a single solvent-free step [5]. Over the past fifteen years, SPME has become an accepted, standard volatile organic compounds (VOCs) analysis procedure within the food, environmental, pharmaceutical, petroleum/refining, forensic/security, and flavors and fragrances industries [6]. It is commonly used for quick turn-around analysis in analytical laboratories yet it is portable and stable enough for field use.

SPME process relies on sorption trapping of analytes for the extraction and concentration stage and on thermal desorption for the sample introduction stage and subsequent analysis. The sorptive material is immobilized on a 1 cm long, 100  $\mu\text{m}$  in diameter solid support such as silica or metal fibers [7]. Sorptive film thicknesses range from 7 to 100  $\mu\text{m}$ . The fiber is attached to a plunger and is installed in a holder similar to a syringe, as shown in Figure 63. The overall size of the SPME device is about 15 cm long and 2 cm in diameter. The plunger moves the fiber in

and out of a hollow needle. To expose the fiber to a sample or the headspace above a sample, the plunger is depressed allowing the extraction of analytes from the sample matrix. Samples obtained using an SPME device ideally reach a maximum concentration when equilibrium is reached between the sorptive film phase, the headspace above the sample, and the liquid sample phase. Once adsorption equilibrium is attained, the fiber is retracted into the needle, which operates as a protectant mechanism during the insertion, removal, and transportation processes. During thermal desorption, the needle is introduced into the heated inlet of a chromatography system, where the adsorbed analytes are thermally desorbed and delivered to the chromatographic separation column.



**Figure 63 Schematic diagram of standard SPME in headspace sampling mode**

Sorptive film thickness, choice of sampling method (headspace or direct immersion), and diffusive interaction between the sample matrix and the chosen sorptive material influence degree of analyte adsorption and efficiency of desorption [8]. Common sorptive materials include polydimethylsiloxane (PDMS), polyacrylate (PA), carbowax, carboxen, and divinylbenzene (DVB). The sorptive material is chosen to specifically enhance the rate that SPME couples with a desired sample matrix. Choice of fiber coating is often the most influential factor contributing to the ability of SPME to be an effective analytical procedure. Current SPME application is subject to the limitations of commercially available fibers. Currently accepted drawbacks of commercial fibers include poor reproducibility of results from a single fiber and between fibers, instability of fiber coatings in organic solvents, a low thermal stability

(maximum desorption temperature is less 280 °C except for cross-linked PDMS which can be used up to 340 °C), and an inability to effectively target analytes along a broad range of polarities.

Recent innovations and novel SPME fiber coatings have attempted to compensate for these deficiencies and increase the usefulness and ability of SPME as an analytical tool. The implementation of sol-gel technology has allowed for several new fiber coating innovations by chemically bonding the coatings directly on to the silica core support, increasing the porosity, thermal stability and ability to withstand organic solvents [9-12]. Replacement of the traditional silica core with a stronger metal core support has increased fiber lifetime and allowed for coating deposition by electrochemical adhesion, thus creating opportunity to use several conductive fiber coatings that were not previously amenable to SPME [13-16]. Molecular imprinting and tailoring SPME coatings to specific analytes has shown substantial success enhancing the limits of detection, but the application of such coatings are case specific and have limited use in the broad range of chemical analysis [14, 17-19]. Additionally, several highly porous polymers not previously used in SPME have been examined to determine their use as possible fiber coatings [20-22]. In this work, we explore the utilization of Tenax TA films in SPME as a means to increase the versatility and range of SPME techniques in chemical analysis applications.

The carbon based polymer poly-(2,6-diphenyl-p-phenylene oxide) or Tenax TA is a porous adsorbent with a high specific surface area of 35 m<sup>2</sup>/g, a pore volume of 2.4 cc/g, and an average pore size of 200 nm [23]. Tenax TA forms inclusion complexes with dichloromethane solvent creating large voids within the crystal structure of the film which contribute to the high capacity of vapor adsorption in Tenax TA films [24]. Tenax TA films have been recently utilized for chemical micro preconcentration which in turn is used to enhance the sensitivity and selectivity of chemical detection methods. This is especially important for enhancing the performance of chemical sensors and micro analytical systems. Tenax TA, in the granular form, offers several outstanding qualities such as thermal stability up to 400 °C, relatively low water retention, relatively resistant to oxygen, adsorbs both polar and nonpolar compounds, and is soluble only in lower chlorinated hydrocarbons. Our group has pioneered the application of Tenax TA films for

chemical micro preconcentration of hydrocarbons for hand-held devices targeted toward environmental monitoring, medical diagnostics, and forensics applications [25, 26].

## ***8.2 Experimental Section***

### ***8.2.1 Chemicals and Instrumentation***

All VOC samples used in this work were reagent grade (Sigma-Aldrich Inc., St. Louis, MO). Tenax TA (80/100 mesh, Sigma-Aldrich Inc., St. Louis, MO) was dissolved in dichloromethane to create a coating solution. The chromatographic analyses were carried out using 5890 GC system (Agilent Technologies, Inc., Palo Alto, CA) equipped with a flame ionization detector (FID) and an electronic pressure controller. Nitrogen (ultra high purity grade, AirGas Inc., Radnor, PA) was used as carrier gas. SPME 0.75 mm ID inlet liner (Sigma-Aldrich Inc., St. Louis, MO) along with low bleed septa (Thermogreen LB-2, Sigma-Aldrich Inc., St. Louis, MO) were used in the GC inlet system. Thermal gravimetric analysis (TGA) was done using a research-grade thermogravimetric analyzer (Q 500, TA Instruments, New Castle, DE). The samples were heated from 0 °C to 1000 °C with a rate of 20 °C /min in the air atmosphere of 60 ml/min. Scanning electron microscopy was done using field-emission SEM (LEO 1550, Carl Zeiss SMT Inc, Peabody, MA) with 10 kV accelerating potential. Samples were coated with 5 nm gold/palladium alloy.

### ***8.2.2 Tenax TA Fibers Preparation***

1 cm-long silica fibers having a diameter of 125 μm were cleaned with acetone and then dipped in Tenax TA solution. The diameter of the fiber and the length of the coated section were chosen to match those of the commercially available SPME fibers. Tenax TA solution was prepared by dissolving Tenax TA (as received) in dichloromethane at 100 mg/mL concentration. The fibers were then left to dry in ambient air.

### ***8.2.3 Extraction Procedure***

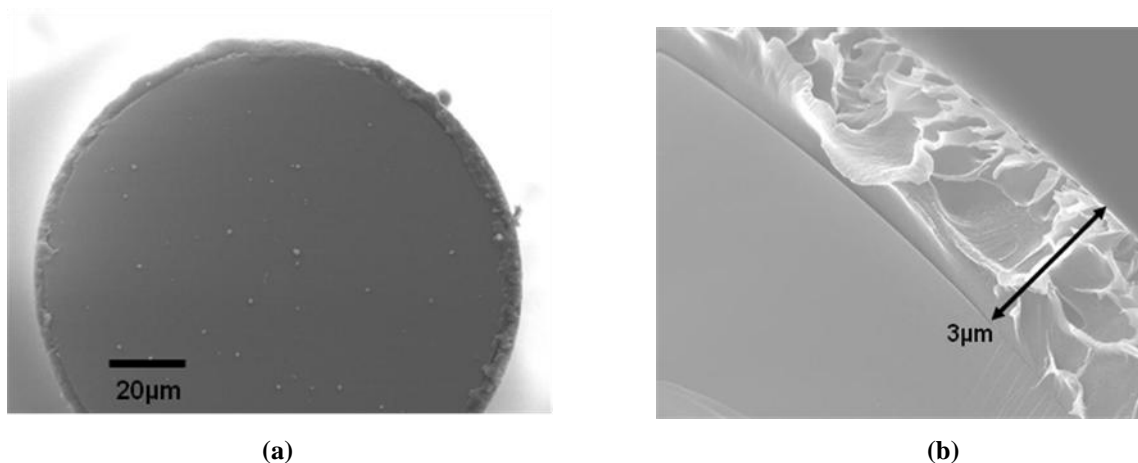
SPME extraction and thermal desorption was carried out using a manual SPME fiber holder (Sigma-Aldrich Inc., St. Louis, MO). Liquid samples of VOCs were placed in septa sealed vials.

Static headspace extraction was performed in all tests at 25 °C and at a fixed position relative to the liquid in the vial.

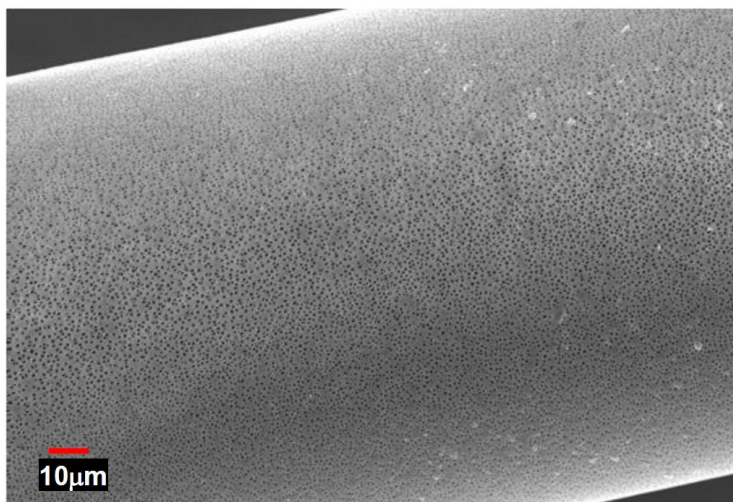
### 8.3 Results and Discussion

#### 8.3.1 Tenax TA Fibers

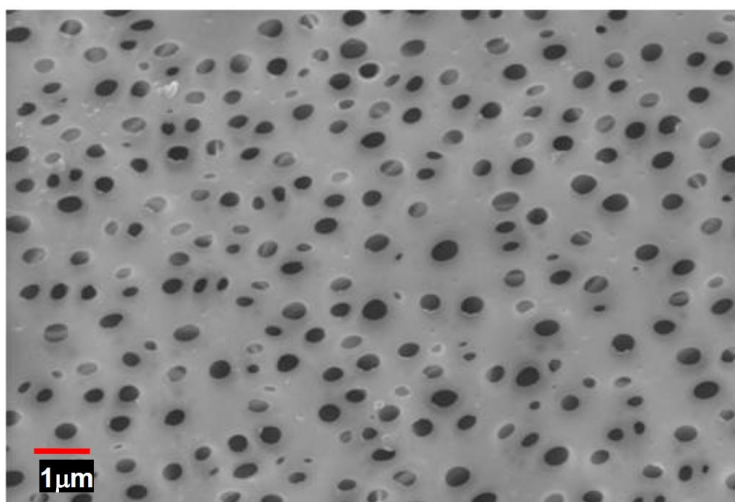
Figure 64 (a) shows a SEM micrograph of Tenax TA coated fiber. The polymer thickness resulted from dipping the 125  $\mu\text{m}$  silica fiber in 100 mg/mL Tenax TA solution at ambient conditions was determined to be about 3  $\mu\text{m}$  as shown in Figure 64 (b). Film thickness is mainly governed by the solution concentration, thus thicker films can be attained with higher concentration solutions. Figure 65 shows a side view of Tenax TA coated fiber. The film has uniform porosity along the fiber. Figure 66 is a higher magnification micrograph of the film. It is evident that the film consists of inter-connected pore network. The pore size was estimated to be between 200-500 nm. It should be noted that porosity of the film depends on the film drying conditions. Clearly, a detailed knowledge of the film pore structure and the factors that affect its porosity is necessary for understanding its behaviour during SPME extraction. However, this information is not readily available. Future work will aim toward better understanding and modelling of Tenax TA porous structure.



**Figure 64 SEM micrographs of (a) silica fiber coated with Tenax TA, (b) higher magnification micrograph showing Tenax TA film thickness resulted from dipping the fiber in 100mg/mL solution**



**Figure 65 SEM micrograph showing side view of Tenax TA coated fiber**



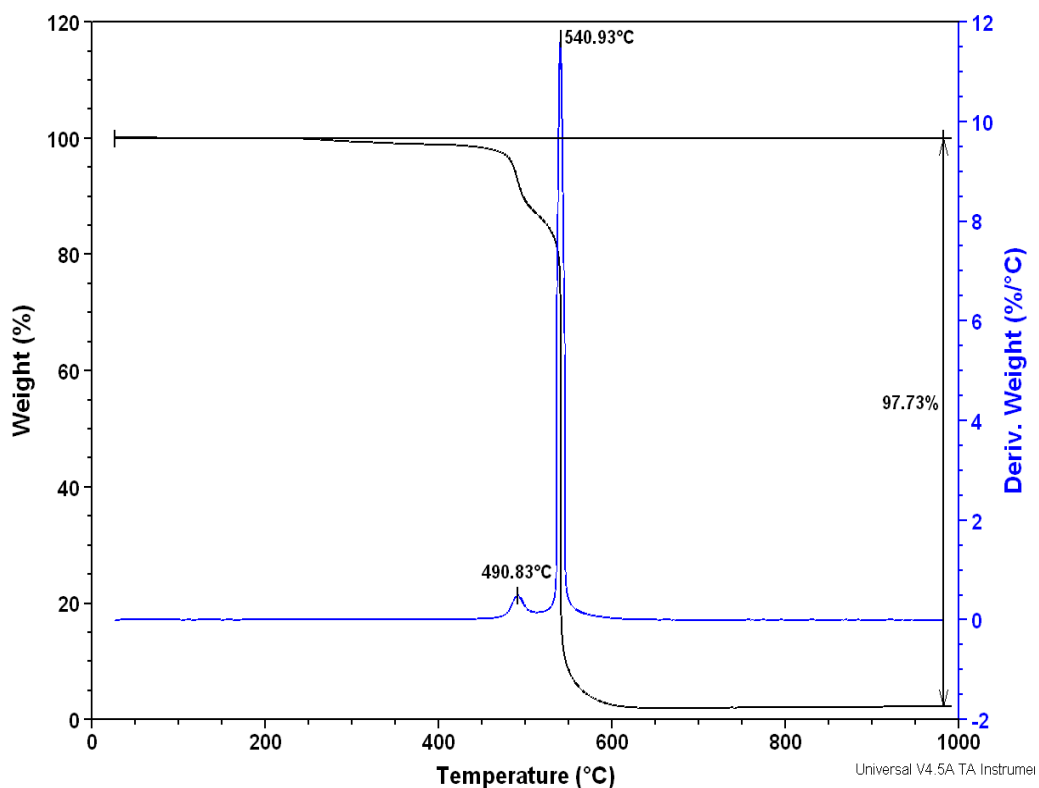
**Figure 66 Higher magnification SEM micrograph of Tenax TA film on a silica fiber**

### ***8.3.2 Tenax TA Film Stability***

Several Tenax TA fibers were subjected to direct immersion in hexane, acetone, methanol, and isopropanol to determine their stability in organic solvents. The fibers showed no signs of degradation in these solvents. However, Tenax TA films showed no stability and disbanded completely in dichloromethane. In addition, identical Tenax TA fibers were exposed to 1 Molar  $\text{H}_2\text{SO}_4$  and 5 Molar NaOH solutions with pH values of 1 and 14, respectively. Tenax TA films remained stable in their respective acidic/basic solutions for 24 hours. SEM imaging before and

after immersion shows no deterioration of either films. The stability of film in various organic solvents along with acidic/basic solutions makes Tenax TA an attractive option for use in HPLC or direct immersion GC in which one or more of the matrix components is an organic solvent, acid, or base. This is an element of SPME that is currently not available with the commercial fibers.

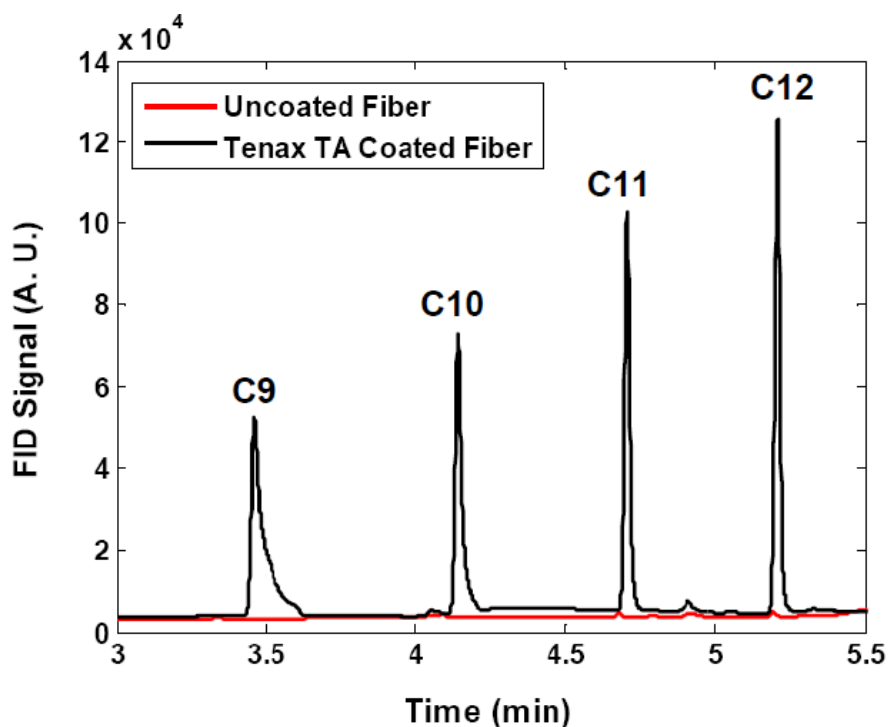
Thermal gravimetric analysis was used to determine the thermal stability of the films. The analysis shown in Figure 67 indicates that negligible weight loss in the film for temperatures as high as 400 °C. At 540 °C, the films shows only 2% weight loss. Tenax TA in the film form is thermally more stable than the granular form. This is significant considering that the maximum operating temperature for most of the commercially available SPME fibers is below 280 °C.



**Figure 67 Thermal gravimetric analysis of Tenax TA film, 98% weight loss occurred at 540°C**

### 8.3.3 Chromatographic Analysis

Static headspace extraction of n-alkanes (n-nonane, n-decane, n-undecane, n-dodecane) was implemented to evaluate Tenax TA fibers. Coated and uncoated fibers along with commercial PDMS/DVB fibers were conditioned for one hour at 280 °C before sampling. The extracted sample was analyzed using a 13 m-long 100% methylpolysiloxane capillary gas chromatography column. The inlet temperature was set to 280 °C to execute thermal desorption. The FID temperature was also set to 280 °C. The column was ramped from 40 °C to 200 °C at a rate of 30 °C/min. The carrier flow rate was set to 1.5 mL/min. A chromatogram of Tenax TA SPME analysis illustrating significant amount of uptake is shown in Figure 68. Extraction from uncoated fibers showed no sign of sample uptake.



**Figure 68** Headspace analysis of n-alkanes extracted by Tenax TA coated silica fiber

The performance of the Tenax TA fiber relative to PDMS/DVB fiber was investigated by comparing the equilibrium time of the two fibers. The extraction time was varied from 2 min to 120 min and was performed at a fixed distance (1 cm) above liquid solutions with no media



agitation. Depicted in Figure 69, the PDMS/DVB fiber saturated after 25 min while Tenax TA saturated after 40 min. The slope of the curves indicates the speed of the uptake in the fiber while the deflection point indicates the capacity of the film. Although the uptake speed in the 65  $\mu\text{m}$ -thick PDMS/DVB film was significantly faster than the 3  $\mu\text{m}$ -thick Tenax TA film, the capacity of Tenax TA was about half of that of PDMS/DVB film as illustrated in Table 7. The uptake speed in Tenax TA film can be enhanced by increasing the porosity of the film. Tenax TA film porosity can be easily altered by changing its deposition conditions.

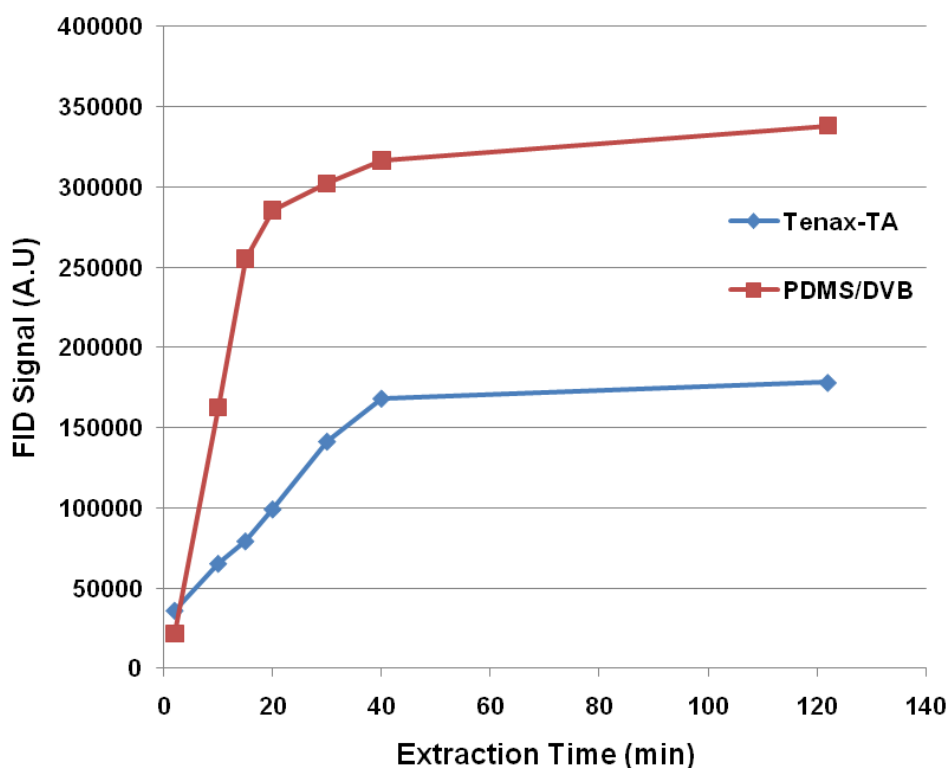


Figure 69 SPME adsorption time profile of 3  $\mu\text{m}$  Tenax TA and 65  $\mu\text{m}$  PDMS/DVB films for Undecane showing uptake saturation time after 25 min for PDMS/DVB and 40 min for Tenax TA

Table 7 Some characteristics of PDMS/DVB and Tenax-TA fibers used in this work

Fiber coating	Film thickness ( $\mu\text{m}$ )	FID area for undecane at saturation time	Uptake saturation time (min)	Max. temp. ( $^{\circ}\text{C}$ )
PDMS/DVB	65	313699	25	270
Tenax-TA	3	168313	40	400

To demonstrate the possibility of employing Tenax TA SPME fibers in chemical analysis of high boiling point VOCs, static headspace extraction of octadecane and pentacosane was carried out. The analysis of pentacosane is not possible with the current commercially available SPME technology. Inlet, oven, and detector temperatures were set to 325 °C and 400 °C for octadecane and pentacosane thermal desorption analysis respectively. The inlet and detector were connected via a 1 m deactivated fused silica capillary. Carrier flow was set to 1.5 mL/min.

Thermal desorption at higher temperatures showed no sign of deterioration of film with continued use, as shown in Table 8. For comparison, reproducibility tests of undecane uptake with no agitation performed using the commercially available Carboxen/PDMS/DVB fiber showed a relative standard deviation of 4.0% as shown in Table 9. Table 10 lists the thermal desorption analysis of pentacosane at 400 °C. The Tenax TA fiber showed an appreciable uptake of this alkane. It should be noted that the ambient boiling point temperature of pentacosane is slightly above 400 °C and it is believed that sample carryover and sample condensation in the inlet, transfer tube, and detector plays a major factor in the deviation of the results.

**Table 8 Static headspace extraction of octadecane showing extraction reproducibility of Tenax TA fiber at a desorption temperature of 325 °C**

Date	7-Jul	9-Jul	9-Jul			
Time (min)	Area	Area	Area	Avg. Area	Std. Deviation	Relative Std. Dev.
2	1.75E+05	1.86E+05	2.62E+05	2.08E+05	47688.6	0.230
15	1.11E+06	1.09E+06	1.09E+06	1.10E+06	10660.5	0.010
30	1.77E+06	1.57E+06	1.60E+06	1.65E+06	110646.6	0.067
40	2.14E+06	1.67E+06	1.76E+06	1.86E+06	249233.9	0.134

**Table 9 Static headspace extraction of undecane using a commercial Carboxen/PDMS/DVB fiber**

Date	21-Jun	26-Jun			
Time (min)	Area	Area	Avg. Area	Std. Deviation	Relative Std. Deviation
2	2.23E+5	2.36E+5	2.29E+5	9372.0	0.041
15	6.29E+5	6.60E+5	6.45E+5	21897.7	0.034
30	8.81E+5	9.03E+5	8.92E+5	15538.0	0.017
40	8.92E+5	9.83E+5	9.38E+5	64114.1	0.068

**Table 10 Static headspace extraction of pentacosane using Tenax TA fiber at a desorption temperature of 400 °C**

<b>Date</b>	<b>19-Jul</b>	<b>19-Jul</b>			
<b>Time (min)</b>	<b>Area</b>	<b>Area</b>	<b>Avg. Area</b>	<b>Std. Deviation</b>	<b>Relative Std. Dev.</b>
2	1.25E+07	6.59E+06	9.57E+06	4216797.3	0.441
10	1.56E+07	8.92E+06	1.22E+07	4696834.5	0.384
15	1.59E+07	9.29E+06	1.26E+07	4658496.5	0.370

#### 8.4 Conclusions

Tenax TA films have demonstrated a competitive ability to extract low molecular weight n-alkanes, with saturation uptake time of undecane peaking at 40 minutes. Tenax TA films offer several advantages over currently available products, including stability in high thermal desorption conditions, stability in acidic and basic conditions, and stability in a variety of organic solvents. Thermal gravimetric analysis shows Tenax TA to maintain stability up to 540°C. 3µm Tenax TA films were found to be thermally stable and capable of extraction of high molecular weight n-alkenes such as octadecane and pentacosane with no sign of polymer deterioration.

#### References

- [1] B. Alfeeli, D. Hogg, and M. Agah, "Solid-Phase Microextraction Using Silica Fibers Coated with Tenax-Ta Films," *Procedia Engineering*, vol. 5, 2010, pp. 1152-1155.
- [2] H.-Å. Lakso and W. F. Ng, "Determination of Chemical Warfare Agents in Natural Water Samples by Solid-Phase Microextraction," *Analytical Chemistry*, vol. 69, 1997, pp. 1866-1872.
- [3] E. Anli, N. Vural, H. Vural, and Y. Gucer, "Application of Solid-Phase Micro-Extraction (Spme) for Determining Residues of Chlorpyrifos and Chlorpyrifos-Methyl in Wine with Gas Chromatography (Gc)," *Journal of the Institute of Brewing*, vol. 113, 2007, pp. 213–218.
- [4] R. P. Belardi and J. B. Pawliszyn, "The Application of Chemically Modified Fused Silica Fibers in the Extraction of Organics from Water Matrix Samples and Their Rapid Transfer to Capillary Columns," *Water Pollution Research Journal of Canada*, vol. 24, 1989, pp. 179-191.
- [5] G. Vas and K. Vékey, "Solid-Phase Microextraction: A Powerful Sample Preparation Tool Prior to Mass Spectrometric Analysis," *Journal of Mass Spectrometry*, vol. 39, 2004, pp. 233-254.

- [6] J. V. Hinshaw, "Solid-Phase Microextraction," *LC-GC Asia Pacific*, vol. 7, 2004, pp. 1056-1061.
- [7] C. L. Arthur and J. Pawliszyn, "Solid Phase Microextraction with Thermal Desorption Using Fused Silica Optical Fibers," *Analytical Chemistry*, vol. 62, 1990, pp. 2145-2148.
- [8] S. A. Scheppers Wercinski, Ed., *Solid Phase Microextraction : A Practical Guide*. New York: Marcel Dekker, 1999.
- [9] T. P. Gbatu, K. L. Sutton, and J. A. Caruso, "Development of New Spme Fibers by Sol-Gel Technology for Spme-Hplc Determination of Organometals," *Analytica Chimica Acta*, vol. 402, 1999, pp. 67-79.
- [10] D. Budziak, E. Martendal, and E. Carasek, "Preparation and Characterization of New Solid-Phase Microextraction Fibers Obtained by Sol-Gel Technology and Zirconium Oxide Electrodeposited on Niti Alloy," *Journal of Chromatography A*, vol. 1187, 2008, pp. 34-39.
- [11] L. Cai, S. Gong, M. Chen, and C. Wu, "Vinyl Crown Ether as a Novel Radical Crosslinked Sol-Gel Spme Fiber for Determination of Organophosphorus Pesticides in Food Samples," *Analytica Chimica Acta*, vol. 559, 2006, pp. 89-96.
- [12] D. Budziak, E. Martendal, and E. Carasek, "New Poly(Ethylene Glycol) Solid-Phase Microextraction Fiber Employing Zirconium Oxide Electrolytically Deposited onto a Niti Alloy as Substrate for Sol-Gel Reactions," *Journal of Chromatography A*, vol. 1198-1199, 2008, pp. 54-58.
- [13] S. Sungkaew, C. Thammakhet, P. Thavarungkul, and P. Kanatharana, "A New Polyethylene Glycol Fiber Prepared by Coating Porous Zinc Electrodeposited onto Silver for Solid-Phase Microextraction of Styrene," *Analytica Chimica Acta*, vol. 664, 2010, pp. 49-55.
- [14] D. Djozan, B. Ebrahimi, M. Mahkam, and M. A. Farajzadeh, "Evaluation of a New Method for Chemical Coating of Aluminum Wire with Molecularly Imprinted Polymer Layer. Application for the Fabrication of Triazines Selective Solid-Phase Microextraction Fiber," *Analytica Chimica Acta*, vol. 674, 2010, pp. 40-48.
- [15] D.-d. Cao, J.-x. Lü, J.-f. Liu, and G.-b. Jiang, "In Situ Fabrication of Nanostructured Titania Coating on the Surface of Titanium Wire: A New Approach for Preparation of Solid-Phase Microextraction Fiber," *Analytica Chimica Acta*, vol. 611, 2008, pp. 56-61.
- [16] N. Alizadeh, H. Zarabadipour, and A. Mohammadi, "Headspace Solid-Phase Microextraction Using an Electrochemically Deposited Dodecylsulfate-Doped Polypyrrole Film to Determine of Phenolic Compounds in Water," *Analytica Chimica Acta*, vol. 605, 2007, pp. 159-165.
- [17] M. Kaykhani, G. W. Dicoski, R. Smedley, J. Pawliszyn, and P. R. Haddad, "Preparation and Evaluation of Solid-Phase Microextraction Fibres Based on Functionalized Latex Nanoparticle Coatings for Trace Analysis of Inorganic Anions," *Journal of Chromatography A*, vol. 1217, 2010, pp. 3452-3456.
- [18] D. Budziak, E. Martendal, and E. Carasek, "Application of Robust Niti-Zro2-Peg Spme Fiber in the Determination of Haloanisoles in Cork Stopper Samples," *Analytica Chimica Acta*, vol. 629, 2008, pp. 92-97.

- [19] P. Olszowy, M. Szultka, P. Fuchs, R. Kegler, R. Mundkowski, W. Miekisch, J. Schubert, and B. Buszewski, "New Coated Spme Fibers for Extraction and Fast Hplc Determination of Selected Drugs in Human Blood," *Journal of Pharmaceutical and Biomedical Analysis*, vol. 53, 2010, pp. 1022-1027.
- [20] J. López-Darias, V. Pino, J. L. Anderson, C. M. Graham, and A. M. Afonso, "Determination of Water Pollutants by Direct-Immersion Solid-Phase Microextraction Using Polymeric Ionic Liquid Coatings," *Journal of Chromatography A*, vol. 1217, 2010, pp. 1236-1243.
- [21] X. Li, C. Li, J. Chen, C. Li, and C. Sun, "Polythiophene as a Novel Fiber Coating for Solid-Phase Microextraction," *Journal of Chromatography A*, vol. 1198-1199, 2008, pp. 7-13.
- [22] W. Chen, J. Zeng, J. Chen, X. Huang, Y. Jiang, Y. Wang, and X. Chen, "High Extraction Efficiency for Polar Aromatic Compounds in Natural Water Samples Using Multiwalled Carbon Nanotubes/Nafion Solid-Phase Microextraction Coating," *Journal of Chromatography A*, vol. 1216, 2009, pp. 9143-9148.
- [23] "Adsorbent Resins for Trapping Volatiles," Scientific Instrument Services, SIS Catalog: C10-C11, Ringoes, NJ, USA2008.
- [24] B. Alfeeli, L. T. Taylor, and M. Agah, "Evaluation of Tenax Ta Thin Films as Adsorbent Material for Micro Preconcentration Applications," *Microchemical Journal*, vol. 95, 2010, pp. 259-267.
- [25] B. Alfeeli, D. Cho, M. Ashraf-Khorassani, L. T. Taylor, and M. Agah, "Mems-Based Multi-Inlet/Outlet Preconcentrator Coated by Inkjet Printing of Polymer Adsorbents," *Sensors and Actuators B, Chemical*, vol. 133, 2008, pp. 24-32.
- [26] B. Alfeeli and M. Agah, "Mems-Based Selective Preconcentration of Trace Level Breath Analytes," *IEEE Sensors Journal*, vol. 9, 2009, pp. 1068-1075.

## Chapter Nine: Summary and Future Directions

### 9.1 Summary

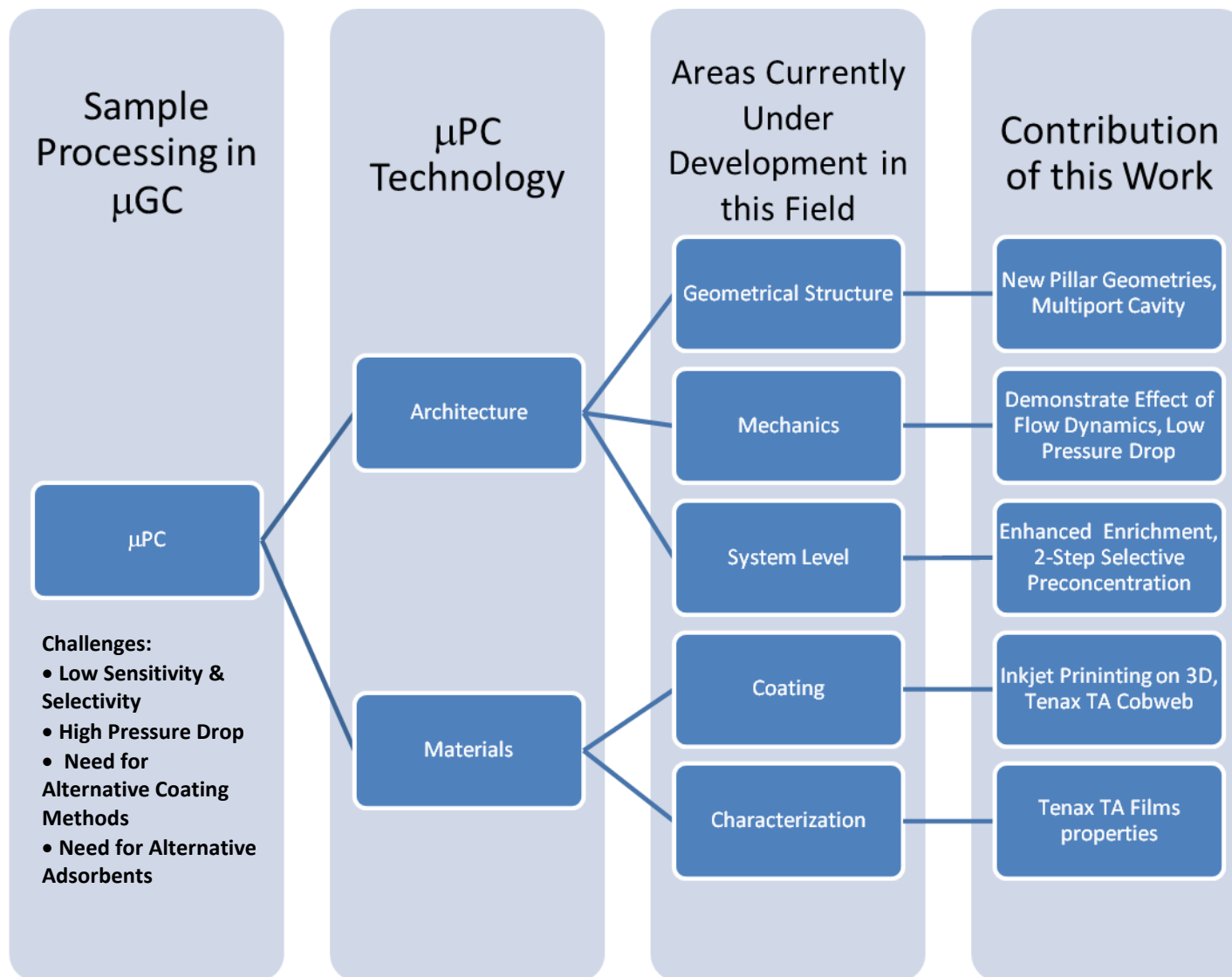
The ultimate goal of developing a  $\mu$ GC is to provide capabilities for quantitative analysis of complex chemical mixtures in the field with very short analysis time and small amounts of consumables. The  $\mu$ GC system performs chemical analysis through three main components which enable the capture, injection, separation, and detection of gaseous mixtures. The first component is the preconcentrator, which serves as the sample collection and injection device. The second component is the separation column, which is responsible for the separation of the chemical mixture to be analyzed. The last component is the detector, which provides a measurable signal that enable data analysis.

Preconcentration methods do not only improve the limits of detection of the system, but can also bridge the gap that exists between the sample collection and analysis.

This dissertation presented the design, fabrication, and experimental evaluation of  $\mu$ PCs all of which were relying on embedded microposts in an etched cavity. The  $\mu$ PCs were evaluated for their practical application in concentrating volatile organic compounds, such as cancer biomarkers, Propofol (anesthetic agent), environmental pollutants, and chemical warfare simulants.

### 9.2 Significance of the Work

Figure 70 shows an overview diagram that maps the different contributions of this work to the  $\mu$ GC technology. There are several areas under development in  $\mu$ PC technology. However, only areas relevant to the contributions of this work are listed.



**Figure 70** An overview diagram mapping the different contributions of this work to the  $\mu$ PC technology

### 9.3 Validation and Scientific Production

As this dissertation is being written, the outcome of this research, stand-alone  $\mu$ PCs are being evaluated independently for their performance by a research group within the Department of Chemistry at the College of William and Mary and for their possible deployment in practical application by a research group within Virginia Tech's Environmental and Water Resources Engineering Program.

The scientific production of this research work included three peer-reviewed original research articles in international journals and nine conference papers in peer-reviewed conference proceedings. Table 11 gives an overview of the major scientific production of this research effort. Moreover, there are three additional journal articles in their final stage of preparation for submission and one conference paper under review. Furthermore, three invention disclosures were assigned to this research work, along with one mutual confidential disclosure agreement with a major analytical chemistry products and services corporation.

**Table 11 Overview of the major scientific production of this research effort**

<b>Type of Production</b>	<b>Name</b>	<b>Metric</b>	<b>Publisher</b>
Journal Article	Sensors & Actuators, B: Chemical	3.1 Impact Factor	Elsevier
Journal Article	IEEE Sensors Journal	1.6 Impact Factor	IEEE
Journal Article	Microchemical Journal	2.6 Impact Factor	Elsevier
Conference Paper (2 papers)	Hilton Head Workshop	35% Acceptance	Transducer Research Foundation
Conference Paper (3 papers)	IEEE Sensors Conference	35% Acceptance	IEEE
Conference Paper	Transducers Conference	35% Acceptance	IEEE
Conference Paper	Engineering in Medicine and Biology Conference	85% Acceptance	IEEE
Conference Paper	$\mu$ TAS Conference	35% Acceptance	The Chemical and Biological Microsystems Society
Conference Paper	Euroensors Conference	70% Acceptance	Elsevier



## *9.4 Future Directions*

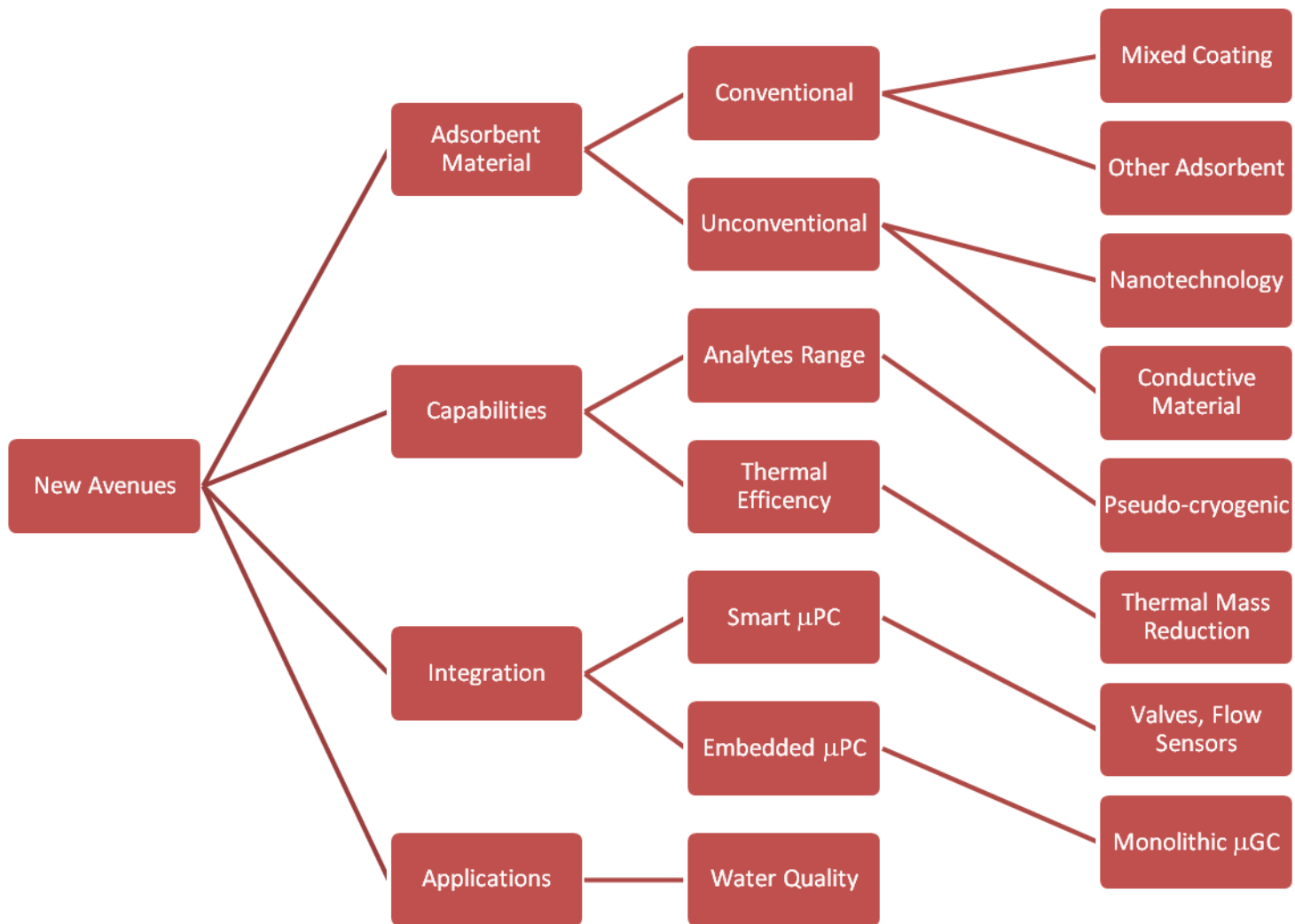
### *9.4.1 General Remarks*

Even with the significant body of work presented in this dissertation, there is plenty of room for additional research and development in  $\mu$ PC technology. Much of the research being reported has focused on proof-of-concept development of  $\mu$ PCs with only preliminary results and limited details on operational parameters and fundamental factors affecting the device performance, which include analyte concentration, interfering analytes, analyte collection time, flow rate, and thermal desorption rate. Even the simplest  $\mu$ PC designs lack a concrete theoretical development, thus, one can foresee the complication when attempting to model the behavior of  $\mu$ PCs with complex 3D structural geometries. One obstacle is that the exact interactions between different molecules and different adsorbent materials are currently unattainable. In equilibrium based 3D  $\mu$ PCs, geometric properties (or surface-to-volume ratio) and flow dynamics increases the complexity of the problem. It is our considered opinion that the designer of  $\mu$ PC should understand that the performance is convoluted with trade-offs among size, capacity, selectivity, pulse width, pressure drop, and power consumption. Moreover, emphasis should be placed on the compatibility of the device under design with the other components of the system.

Thermal desorption in the  $\mu$ PCs presented in this dissertation was not investigated. This, however, is important since it affects the performance of the device. The effect of desorption temperature on the integrity of collected analyte and adsorbent material, as well as the injection pulse width should be investigated to provide a temperature limit for the operation of the device. The heating rate is another important variable to characterize. Maximizing the heating rate is desirable, but it comes at the cost of higher power consumption. Therefore, optimizing desorption conditions for both narrow injection plugs and high desorption efficiency would be the next natural step of this work.

### *9.4.2 New Avenues*

Figure 71 shows an overview diagram that maps new avenues to further improve  $\mu$ PC technology. There are four main avenues that can be pursued in future research. These avenues are discussed in the following subsections.



**Figure 71** An overview diagram mapping new avenues to further improve  $\mu$ PC technology

### *9.4.2.1 Adsorbent Material*

#### *9.4.2.1.1 Conventional Adsorbent*

##### *9.4.2.1.1.1 Tenax TA*

The characterization of Tenax TA presented in this dissertation is not complete. The polymer's physical properties and VOCs adsorption mechanisms are not fully understood. Moreover, the effect of phase composition on the properties of the Tenax TA should be investigated along with film's transport properties. The macromolecular architecture of this polymer should be studied in detail to predict and control its behavior during processing and operation. Knowing the macromolecular architecture also helps in predicting property changes over time and optimization of performance and reliability. Film deposition under different conditions including precipitation from solution using wide range of colligators should also be investigated.

##### *9.4.2.1.1.2 Other Adsorbent Materials*

There are a large number of readily available adsorbent materials besides Tenax TA. Some future studies should be aimed toward the utilization of other commercial adsorbent such as inorganic and carbon based materials in addition to the porous polymeric materials listed in Table 12 in the appendix. Divinylbenzene is particularly of interest due to its superior adsorption characteristics for light VOCs. Furthermore, mixing different adsorbents of different adsorption characteristics can yield an adsorbent film for a wide range of VOCs.

#### *9.4.2.1.2 Unconventional Adsorbent Films*

Functional thin-films created using chemical vapor deposition, atomic layer deposition, colloidal assembly, and molecular beam epitaxy can be explored as alternative adsorbent materials for  $\mu$ PCs. Nanostructured materials are increasingly becoming popular with the development of nano-science and technology. Of many nano-fabrication methods, the water-based layer-by-layer (LbL) assembly technique offers one of the finest control of materials properties and architecture at the nano scale, and is the simplest and easiest method to implement in  $\mu$ PCs.

Conductive materials can also be utilized as adsorbent material. The possibility of using gold as selective and self-heating adsorbent material for high performance and low power consumption has been recently demonstrated. Some preliminary results on this topic are provided in the appendix.

#### *9.4.2.2 Enhancing $\mu$ PC Capabilities*

One exciting possibility to increase the range of analytes adsorption, especially light VOCs, is a  $\mu$ PC with pseudo-cryogenic trapping capabilities using microfabricated thermoelectric coolers in combination with sorbent material. This would enable the trapping of light VOCs ( $C_1$ - $C_5$ ). The current state-of-the-art  $\mu$ PCs can only trap mid-range VOCs ( $C_5$ - $C_{12}$ ) and semi-volatile VOCs ( $>.C_{12}$ ). Temperatures within the  $+10\text{ }^\circ\text{C}$  to  $-30\text{ }^\circ\text{C}$  range can be reached with microfabricated thermoelectric coolers.

The thermal efficiency of the device in terms of thermal cycling time (rapid heating and cooling) and power consumption can be increased by reducing the thermal mass of the device. Creating suspended 3D membranes can reduce the thermal cycle times from minutes to seconds or less. The thermal isolation would also reduce power requirement significantly.

#### *9.4.2.3 Integration*

In addition to heaters and temperature sensors, the overall performance of  $\mu$ PCs is likely to improve with onboard valves and flow sensors to control the sample flow in the device. Thus, integrating such components on the  $\mu$ PC should be considered in future developments. Of course, needless to mention that embedding a  $\mu$ PC in a  $\mu$ GC system monolithically ( $\mu$ PC,  $\mu$ column, and  $\mu$ detector on a single chip) should be tackled as well in the near future.

#### *9.4.2.4 Applications*

$\mu$ PCs can be used in all chemical sensing applications as a single sensor is almost never sufficient in itself. In addition to their normal use in gas sampling,  $\mu$ PCs can be employed to trap VOCs from liquid samples. This would enhance the versatility of  $\mu$ GC systems, especially in

environmental monitoring application. Some preliminary results on this topic are provided in the appendix.

## Appendix

### *A-I. Selective Micro Preconcentration of Propofol for Anesthetic Depth Monitoring by using Seedless Electroplated Gold as Adsorbent*

This section was reproduced from [1] with permission from IEEE

*B. Alfeeli, M. A. Zareian-Jahromi, and M. Agah, "Selective micro preconcentration of propofol for anesthetic depth monitoring by using seedless electroplated gold as adsorbent," in 31st Annual International Conference of IEEE Engineering in Medicine and Biology Society, September 2-6, 2009, pp. 2763-2766.*

#### *a. Introduction*

Depth of anesthesia assessment is a persistent challenge for anesthesiologists [2]. Conventional clinical signs of inadequate anesthetic depth include changes in blood pressure, heart rate, movement, lacrimation, sweating, and pupil size which often are inconsistent and unreliable [3-5]. More accurate methods of assessing depth of anesthesia is needed especially when using newer intravenous anesthetic compounds such as Propofol (2,6-diisopropylphenol) whose effective dosages vary greatly across patients [6]. Propofol is an aromatic compound with a distinct smell used for induction and maintenance of anesthesia in the intensive care unit [7]. It has been reported that the expiratory measurement of Propofol in human breath is a suitable procedure for non-invasive monitoring of patients undergoing anesthesia [8]. However, normal human breath contains a complex mixture of more than 1200 volatile organic compounds (VOCs) [9] at very low concentrations typically in the parts per billion (ppb) range [10] which are hardly detectable by conventional sensors. Consequently sample preconcentration along with gas chromatographic (GC) analysis are used for accurate and precision detection of complex gas mixtures [11]. However, current GC systems are large, require highly trained technicians and intensive maintenance, and are expensive table-top instruments with high power consumptions [12].

Miniaturization of GC systems was enabled by microelectromechanical systems (MEMS) technology and, recently, various designs of micro separation columns and preconcentrators (PC) for sensing and monitoring applications have been reported [12-18]. Nevertheless, the success of

micro analytical systems ( $\mu$ TAS) in breath analysis applications rely on the ability to remove water vapor from the sample and selectively preconcentrate analytes of interest in the mixture that can later be processed  $\mu$ GC column and micro detector [19]. The use of selective adsorbent is one possible way to attain selective micro preconcentration ( $\mu$ PC). This article reports, for the first time, electrodeposited-gold thin films as a selective adsorbent for Propofol in  $\mu$ PCs.

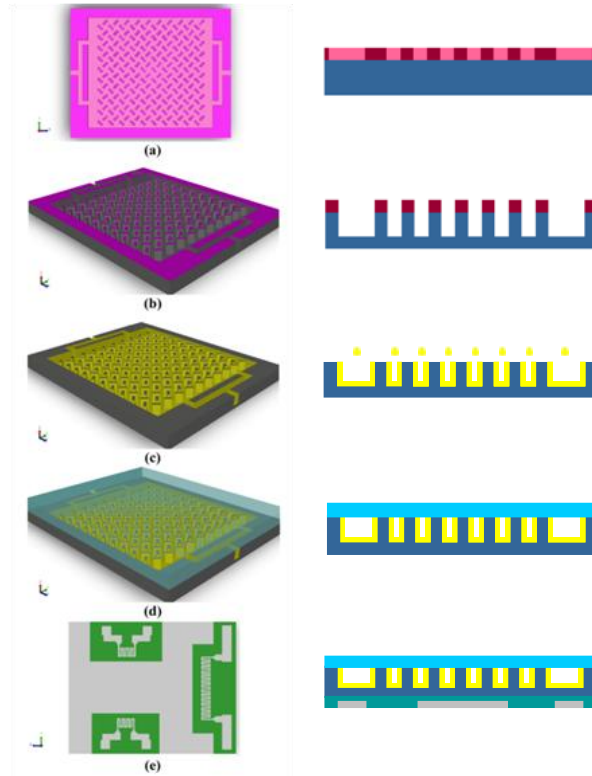
### ***b. Fabrication***

The  $\mu$ PCs used in this study contain an array of 3D micro pillars and is similar to our previously reported work [20]. Figure 72 summarizes the fabrication process of the  $\mu$ PC. First, the single mask design pattern was transferred to a silicon wafer via standard photolithography as shown in Figure 72 (a). Second, the silicon wafer was etched by deep reactive ion etching (DRIE) process (Figure 72 (b)) followed by oxygen plasma clean step to remove any residual fluorocarbon on the etched surface. The devices were then coated with the adsorbent material via electrodeposition technology as shown in Figure 72 (c). Pulsed electroplating technique was used to directly deposit a thin layer of gold on heavily phosphorous-doped ( $n^+$ ) silicon microstructures. Seedless gold electroplating of silicon surfaces provides simple method of realizing large surface area gold films (Figure 73 inset) with low adhesion strength. The weak gold-to-silicon adhesion is advantageous at this step as it allows post deposition patterning of the gold films as reported previously [21] and shown in Figure 73. The film can be stabilized by thermal annealing at a later stage. The pulse duration and time period for pulse electroplating were adjusted to achieve a desired thickness (350 nm) on the micro pillars. Phosphorous diffusion was done at 950 °C for 6 hours to achieve 2  $\mu$ m-deep doped region below the silicon surface. The electroplating bath was maintained at 55 °C with a stirring rate of 200 rpm to provide a uniform distribution of gold ions in the bath. Acidic gold electroplating solution and a platinized Ti grid (anode) were used to complete the electroplating circuit. The anode is placed at a distance of 2 cm from the cathode and has a size at least twice that of the cathode to afford a uniform electric field on the silicon wafer. The current between the platinized Ti grid anode and doped silicon cathode was controlled by a square current pulse. After gold deposition and patterning, the silicon wafer was anodically bonded to the Pyrex 7740 substrate (Figure 72 (d)). The bonding temperature and pressure were 350 °C and 2 kPa, respectively. Thermal annealing

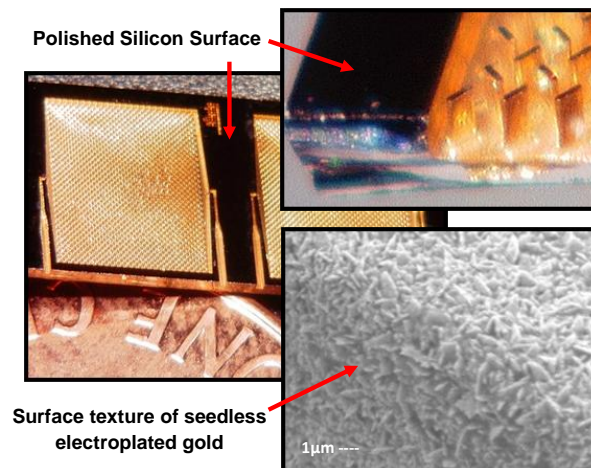


during the bonding process at temperatures less than the Si-Au eutectic temperature (365 °C) stabilizes the electroplated gold by significantly improving its adhesion to the doped silicon surface. The gold coating was proved to be stable under GC operating temperature (350 °C) and flow conditions (1 mL/min) [22]. The final step of  $\mu$ PCs fabrication was patterning thin film Ti/Pt resistive heaters and temperature sensors over plasma enhanced chemical vapor deposition (PECVD) oxide on the backside of the silicon wafer as shown in Figure 72 (e). The wafer was then diced and fused silica capillary tubing with 167  $\mu$ m O.D. and 100  $\mu$ m I.D. was attached to fluidic ports.

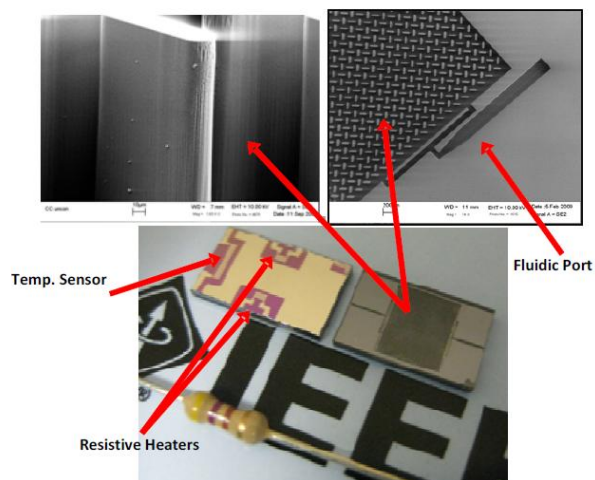
The fabrication process described above produced high quality  $\mu$ PCs. The silicon-glass chips have outer dimensions of 7 mm  $\times$  7 mm  $\times$  1 mm, specific surface area of 10 m<sup>2</sup>/g (gas sorption method), and an inner volume of about 6.5  $\mu$ L. The dimensions of the high-aspect-ratio pillars were 30  $\mu$ m  $\times$  120  $\mu$ m  $\times$  240  $\mu$ m. Figure 74 illustrates the top and bottom views of the  $\mu$ PC placed in front of a resistor to give a size prospective.



**Figure 72 (a) Photolithography (b) Deep reactive-ion etching (DRIE) (c) Electrodeposition and patterning of the adsorbent material (d) Sealing the device with Pyrex by anodic bonding (e) Patterning of resistive heaters and temperature sensors over PECVD oxide at the back of the device, © [2009] IEEE. Reprinted, with permission, from [1]**



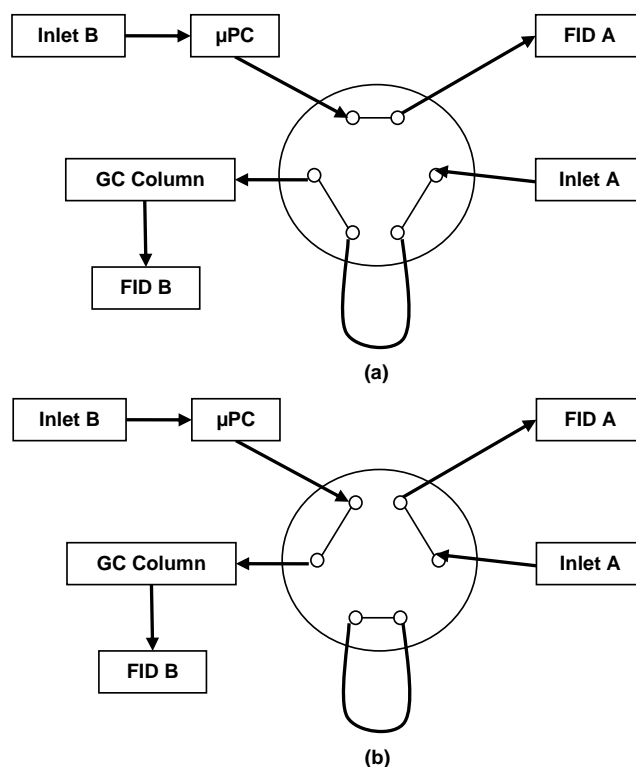
**Figure 73 Optical images showing the the uniform and conformal coverage coating of electroplated gold. The top flat surfaces including the top of the posts are polished and smooth for anodic bonding. The porouse surface texture of the gold layer maximizes the adsorbent surface area, © [2009] IEEE. Reprinted, with permission, from [1]**



**Figure 74 Optical images of the  $\mu$ PC showing the front and back sides of the device, insets are SEM monographs of the etched microstructures and the fluidic ports, © [2009] IEEE. Reprinted, with permission, from [1]**

### *c. Testing Setup*

To maintain isothermal temperature conditions, the testing setup was installed inside the oven of a commercial dual inlet and dual detector GC system. Moreover, the built-in auxiliary systems such as a gas flow controller and flame ionization detectors (FIDs) were also utilized to ensure consistent testing parameters. Carrier gas was supplied via the GC inlets and controlled by the flow controller. The testing setup consisted of a six-port zero-dead-volume valve, commercial methylpolysiloxane phase GC column, and deactivated fused silica transfer lines configured as shown in Figure 75. The inlet pressure was adjusted to achieve 1mL/min flow rate through the  $\mu$ PC and column. During the loading stage the valve is set in the “loading position” to load the  $\mu$ PC as shown in Figure 75 (a). The loading was done by supplying the breath representative mixture into the GC inlet-B and monitored by FID-A. Figure 75 (b) illustrates the valves set in the “injection position.” In this configuration, the GC column was connected to the preconcentrator. The  $\mu$ PC was then heated rapidly to 250 °C at 100 °C/sec to inject the collected sample into the column. As soon as the injection step was completed, the valves set back to the “separation position” (Figure 75 (a)). Here, the column was heated to 150 °C from 35 °C at 30 °C/min to separate the injected sample.



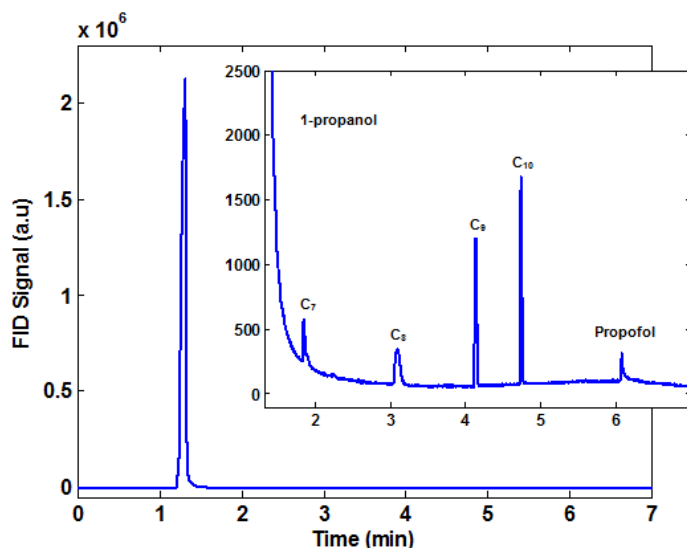
**Figure 75**  $\mu$ PC test setup with the valves set in the (a) loading or separation position (b) injection position, © [2009] IEEE. Reprinted, with permission, from [1]

#### *d. Results and Discussion*

For the preliminary evaluation of the presented device, a 125 ppm of Propofol was added to a mixture of n-heptane ( $C_7$ ) at 250 ppm, n-octane ( $C_8$ ) at 250 ppm, n-nonane ( $C_9$ ) at 500 ppm, and n-decane ( $C_{10}$ ) at 750 ppm, which are some of the VOCs found in normal human breath [9] diluted in 1-propanol. The choice of 1-propanol as solvent instead of water vapor present in breath was dictated mainly by the available water insensitive detector (FID).

Figure 76 shows the separation of the breath representative mixture without preconcentration as a reference. The large 1-propanol content in injected sample is evident. 1-propanol (or water vapor in breath) could impose premature saturation in the collection process by saturating the adsorbent material. It can also saturate the detector as well during the detection process. It should be noted that most gas detectors are sensitive to water [23]. As a result, eliminating any

interfering compounds by means of selective preconcentration is essential for high performance analysis.



**Figure 76 Chromatogram of breath representative mixture without  $\mu$ PC showing the large amount of 1-Propano, inset is zoom-in of the separated VOCs, © [2009] IEEE. Reprinted, with permission, from [1]**

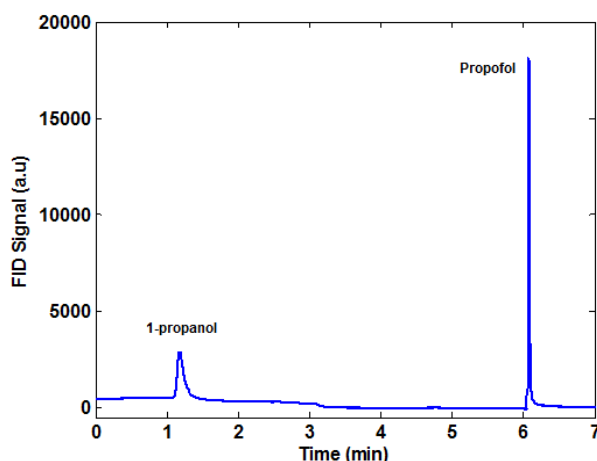
Figure 77 demonstrates the results of selective preconcentration of trace Propofol in the breath representative mixture. The electrodeposited gold thin film demonstrated preferential adsorption characteristics over the other compounds which are non-polar. We considered polar adsorption as possible mechanism since the electrodeposited gold showed high affinity to polar compounds. Thus, the adsorption of Propofol on the electrodeposited gold could be attributed to the polar nature of both the phenol derivative anesthetic agent [24] and the gold film. The polar nature of the electrodeposited gold can be explained by the formation of gold oxide layer on the gold electrode surface [25]. Gold oxides are known to be polar [26]. Determining the exact mechanism responsible for Propofol adsorption on electrodeposited gold films will be the subject of future investigation.

The performance of the presented adsorbent can be evaluated by a figure of merit known as the preconcentration factor (PF). This figure of merit can be defined as the ratio of peak height of the detector's signal with and without the presence of the  $\mu$ PC. Using the gold electroplated  $\mu$ PC and

under the testing conditions presented here, the PF factor for Propofol was determined to be about 100.

Propofol measurements in human breath, which are not yet possible to monitor on-line, could be used to monitor depth of anesthesia to prevent accidental awakening of patients during surgery. Additionally, the demand for cost-effective Propofol monitoring devices is expected to increase as many surgical procedures are now being shifted from hospitals to outpatient surgical centers and physician's offices.

This paper reported the utilization of MEMS technology to develop  $\mu$ PCs which is selective to a target chemical species for breath analysis. The elimination of unwanted species by selective preconcentration allowed more adsorption surface for the target compound on the adsorbent material and alleviated stringent requirements on the separation and detection stages.



**Figure 77 Chromatogram of selective preconcentration of propofol. VOCs were not preconcentrated in the  $\mu$ PC, © [2009] IEEE. Reprinted, with permission, from [1]**

### *e. References*

- [1] B. Alfeeli, M. A. Zareian-Jahromi, and M. Agah, "Selective Micro Preconcentration of Propofol for Anesthetic Depth Monitoring by Using Seedless Electroplated Gold as Adsorbent," in *International Conference of IEEE Engineering in Medicine and Biology Society, EMBC'09*, 2009, pp. 2763-2766.
- [2] H. L. Kaul and N. Bharti, "Monitoring Depth of Anaesthesia," *INDIAN JOURNAL OF ANAESTHESIA*, vol. 46, 2002, pp. 323-332.

- [3] N. Moerman, B. Bonke, and J. Oosting, "Awareness and Recall During General Anesthesia. Facts and Feelings," *Anesthesiology*, vol. 79, 1993, pp. 454–464.
- [4] J. Bruhn, P. S. Myles, R. Sneyd, and M. M. R. F. Struys, "Depth of Anaesthesia Monitoring: What's Available, What's Validated and What's Next?," *British Journal of Anaesthesia*, vol. 97, July 1, 2006 2006, pp. 85-94.
- [5] C. J. D. Pomfrett. (2000) Monitoring Depth of Anaesthesia. *Bulletin of The Royal College of Anaesthetists*.
- [6] R. Flaishon, A. Windsor, J. Sigl, and P. S. Sebel, "Recovery of Consciousness after Thiopental or Propofol. Bispectral Index and Isolated Forearm Technique," *Anesthesiology*, vol. 86, 1997, pp. 613–619.
- [7] C. Hornuss, S. Praun, J. Villinger, A. Dornauer, P. Moehnle, M. Dolch, E. Weninger, A. Chouker, C. Feil, J. Briegel, M. Thiel, and G. Schelling, "Real-Time Monitoring of Propofol in Expired Air in Humans Undergoing Total Intravenous Anesthesia," *Anesthesiology*, vol. 106, 2007, pp. 665-674.
- [8] E. D. Kharasch, "Every Breath You Take, We'll Be Watching You," *Anesthesiology*, vol. 106, 2007, pp. 652-654.
- [9] M. Phillips, "Method for the Collection and Assay of Volatile Organic Compounds in Breath," *Analytical Biochemistry*, vol. 247, 1997, pp. 272-278.
- [10] P. Spanel, K. Dryahina, and D. Smith, "The Concentration Distributions of Some Metabolites in the Exhaled Breath of Young Adults," *Journal of Breath Research*, vol. 1, 2007, p. 026001.
- [11] D. Helmig, "Air Analysis by Gas Chromatography," *Journal of Chromatography A*, vol. 843, 1999, pp. 129-146.
- [12] M. Agah and K. D. Wise, "Low-Mass Pecvd Oxynitride Gas Chromatographic Columns," *Journal of Microelectromechanical Systems*, vol. 16, 2007, pp. 853-860.
- [13] B. Alfeeli, S. Ali, V. Jain, R. Montazami, J. Heflin, and M. Agah, "Mems-Based Gas Chromatography Columns with Nano-Structured Stationary Phases," in *7th IEEE Conference on Sensors*, Lecce, Italy, 2008, pp. 728-731.
- [14] I. Gràcia, P. Ivanov, F. Blanco, N. Sabaté, X. Vilanova, X. Correig, L. Fonseca, E. Figueras, J. Santander, and C. Cané, "Sub-Ppm Gas Sensor Detection Via Spiral M-Preconcentrator," *Sensors and Actuators B: Chemical*, vol. 132, 2008, pp. 149-154.
- [15] S. Li, J. C. Day, J. J. Park, C. P. Cadou, and R. Ghodssi, "A Fast-Response Microfluidic Gas Concentrating Device for Environmental Sensing," *Sensors and Actuators A: Physical*, vol. 136, 2007, pp. 69-79.
- [16] F. Blanco, X. Vilanova, V. Fierro, A. Celzard, P. Ivanov, E. Llobet, N. Cañellas, J. L. Ramírez, and X. Correig, "Fabrication and Characterisation of Microporous Activated Carbon-Based Pre-Concentrators for Benzene Vapours," *Sensors and Actuators B: Chemical*, vol. 132, 2008, pp. 90-98.

- [17] M. A. Zareian-Jahromi, M. Ashraf-Khorassani, L. T. Taylor, and M. Agah, "Design, Modeling, and Fabrication of Mems-Based Multicapillary Gas Chromatographic Columns," *Journal of Microelectromechanical Systems*, vol. 18, 2009, pp. 28-37.
- [18] B. Alfeeli, S. Ali, V. Jain, R. Montazami, J. Heflin, and M. Agah, "Mems-Based Gas Chromatography Columns with Nano-Structured Stationary Phases," in *Sensors, 2008 IEEE*, 2008, pp. 728-731.
- [19] B. Alfeeli and M. Agah, "Selective Preconcentration by Temperature Manipulation of Cascaded Micro Preconcentrators," presented at the International Solid-State Sensors, Actuators and Microsystems Conference, TRANSDUCERS'09, Denver, CO, 2009.
- [20] B. Alfeeli, D. Cho, M. Ashraf-Khorassani, L. T. Taylor, and M. Agah, "Mems-Based Multi-Inlet/Outlet Preconcentrator Coated by Inkjet Printing of Polymer Adsorbents," *Sensors and Actuators B: Chemical*, vol. 133, 2008, pp. 24-32.
- [21] M. A. Zareian-Jahromi and M. Agah, "Micro Gas Chromatography Multicapillary Columns with Mono-Layer Protected Gold as a Stationary," in *International Conference on Micro Electro Mechanical Systems, MEMS'09*, Italy, 2009, pp. 288-291.
- [22] M. A. Zareian-Jahromi and M. Agah, "Self-Patterned Seedless Gold Electroplating in High-Aspect-Ratio Channels for Gc Application," presented at the International Solid-State Sensors, Actuators and Microsystems Conference, TRANSDUCERS'09, Denver, CO, 2009.
- [23] S. M. Cho, Y. J. Kim, G. S. Heo, and S.-M. Shin, "Two-Step Preconcentration for Analysis of Exhaled Gas of Human Breath with Electronic Nose," *Sensors and Actuators B: Chemical*, vol. 117, 2006, pp. 50-57.
- [24] M. Barann, I. Linden, S. Witten, and B. W. Urban, "Molecular Actions of Propofol on Human 5-Ht3a Receptors: Enhancement as Well as Inhibition by Closely Related Phenol Derivatives," *Anesthesia & Analgesia*, vol. 106, March 1, 2008 2008, pp. 846-857.
- [25] K. Juodkazis, J. Juodkazyte, V. Jasulaitiene, A. Lukinskas, and B. Sebek, "Xps Studies on the Gold Oxide Surface Layer Formation," *Electrochemistry Communications*, vol. 2, 2000, pp. 503-507.
- [26] N. Cioffi, I. Farella, L. Torsi, A. Valentini, and A. Tafuri, "Correlation between Surface Chemical Composition and Vapor Sensing Properties of Gold-Fluorocarbon Nanocomposites," *Sensors and Actuators B: Chemical*, vol. 84, 2002, pp. 49-54.



## A-II. Micro Preconcentrator for Handheld Monitoring of Water Quality

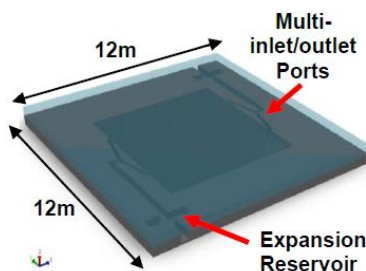
This section was reproduced from [1] with permission from the Chemical and Biological Microsystems Society

*B. Alfeeli and M. Agah, "Micro Preconcentrator for Handheld Monitoring of Water Quality," in 14th International Conference on Miniaturized Systems for Chemistry and Life Sciences, Groningen, The Netherlands, 3-7 October 2010, pp. 1721-1723.*

### a. Introduction

Water resources are susceptible to both natural and man-made contamination. Water contaminants are grouped into microbiological, radioactive, inorganic, synthetic organic, and volatile organic compounds (VOCs) [2]. These contaminants, specifically VOCs, pose serious health effects which include liver and nervous system diseases and cancer [3]. Chemical analysis of water supplies requires samples to be transported to off-site laboratories. The cost of such analysis can range between \$100 to \$1000 per sample and the integrity of the analyses can be compromised during sample collection, transport, and storage [2]. Thus, there is a need for inexpensive and accurate handheld water monitoring systems.

Several technologies for handheld environmental monitoring have been reported which include spectroscopic [4, 5] and chromatographic systems [6-10] for analyzing gaseous and liquid samples on-site. However, reports on systems that can process liquid samples are very limited. This paper report on the development of micro preconcentrator ( $\mu$ PC) consisting of square shaped  $\mu$ -pillar structures embedded within a microcavity, as shown in Figure 78, aimed for handheld water quality monitoring systems.

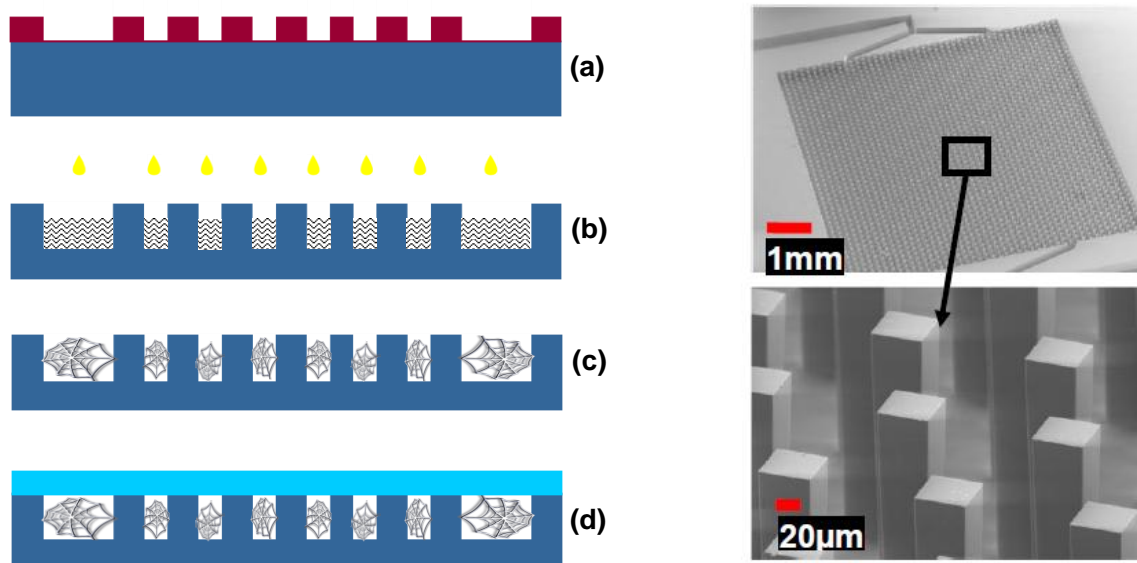


**Figure 78 3D rendering of the silicon-glass  $\mu$ PC**

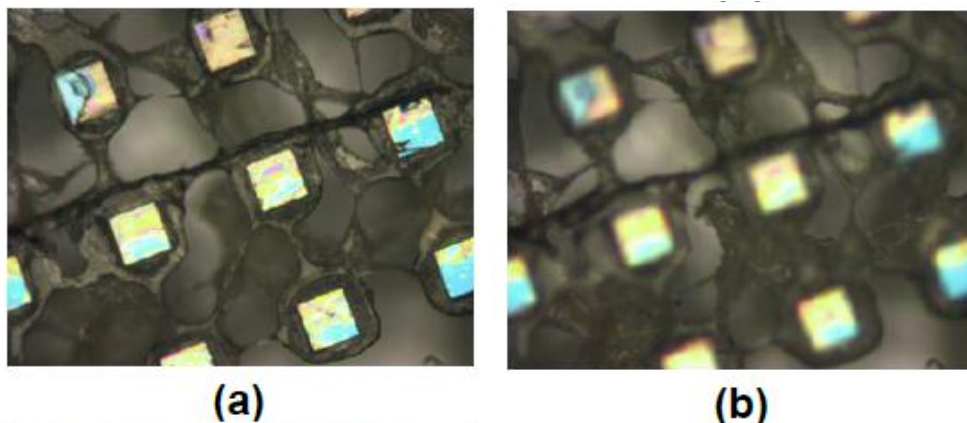
## *b. Fabrication*

The fabrication process of the presented device is shown in Figure 79. A 6  $\mu\text{m}$ -thick layer of AZ9260 photoresist was used to pattern a 500  $\mu\text{m}$  silicon wafer with the  $\mu\text{PC}$  layout. Then, the wafer was anisotropically etched using deep reactive ion etching (DRIE) technique to achieve vertical microstructures (pillars). The etching process parameters were configured to achieve a depth of 300  $\mu\text{m}$ . The wafer was then exposed to oxygen plasma for 20 minutes to remove any residual passivation polymers from the etching process. This is an important step since any fluorocarbon residuals on the sidewall can compromise the adsorbent coating stability.

Adsorbent deposition was achieved by utilizing our recently reported adsorbent deposition method to deposit Tenax-TA on the  $\mu$ -pillars [11]. The cavity was filled with Tenax-TA solution (25 mg/mL in dichloromethane). Then, before the solvent evaporates, drops of 2-propanol were added into the cavity. Cobweb Tenax-TA evolves when 2-propanol contacts Tenax-TA solution. The cobweb structure anchors to the  $\mu$ -pillars once the solvent evaporates as shown in Figure 80. The  $\mu\text{PC}$  was then sealed by anodic bonding the silicon substrate to a Pyrex wafer under 1250 V of applied electric field at 250  $^{\circ}\text{C}$  to avoid damaging the polymer.



**Figure 79**  $\mu\text{PC}$  fabrication process flow, (a) photolithography on silicon wafer using PR9260 followed by etching using DRIE (b) adsorbent deposition, (c) formation of cobweb, (d) anodic bonding, Right, SEM micrographs of the fabricated  $\mu\text{PC}$  showing the square shaped  $\mu$ -pillars



**Figure 80** Optical image of the cobweb Tenax TA, (a) and (b) are a different focal points showing that the cobweb extends in all direction between the  $\mu$ -pillars

### *c. Experimenta*

The  $\mu$ PC was evaluated experimentally by flowing water samples spiked with benzene through it. It is noteworthy that benzene has been classified by the US Department of Health and Human Services (DHHS) as a human carcinogen. Benzene has 0.8 g/L solubility in water at room temperature. Thus, benzene was added to deionized water and the solution was left for 24 hours to equilibrate. Then, water samples were extracted from the bottom of the container to avoid the insoluble benzene floating on the top of the water surface. A 1  $\mu$ L sample of the solution was injected directly to a flame ionization detector (FID) to determine the detector response to the unpreconcentrated sample. It should be noted that the FID is water insensitive detector. Subsequently, the  $\mu$ PCs chip was connected to the FID through a zero dead volume valve. While the valve in waste position, the chip was loaded with three water samples volumes (1, 5, and 10 mL) at room temperature. After every load, the chip was dried by purging it with helium for 5 min. Then, the valve was switched to FID position and the device was heated to 250 °C at 100 °C/sec to desorb the collected benzene from the different volumes of the water sample. The flow rate through the  $\mu$ PC was set to 1 mL/min.

### *d. Results and Discussion*

Figure 81 shows the FID response to the concentrated benzene from the 10 mL water sample. The area under the curve of the FID signal is directly proportional to the concentration of the desorbed sample. The peak width at half height was about 10 seconds. Figure 82 compares the

FID response to the three different sample volumes including the 1  $\mu\text{L}$  sample of unpreconcentrated water sample. The amount of benzene collected by the device was proportional to water volume flown through it. The experimental results showed that the  $\mu\text{PC}$  was capable of extracting and concentrating benzene from water samples.

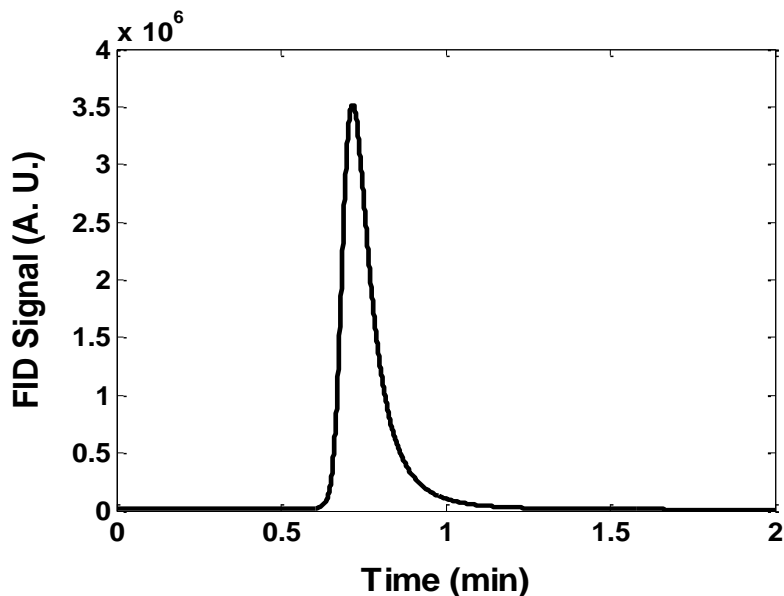


Figure 81 FID response to the concentrated benzene from the 10mL water sample.

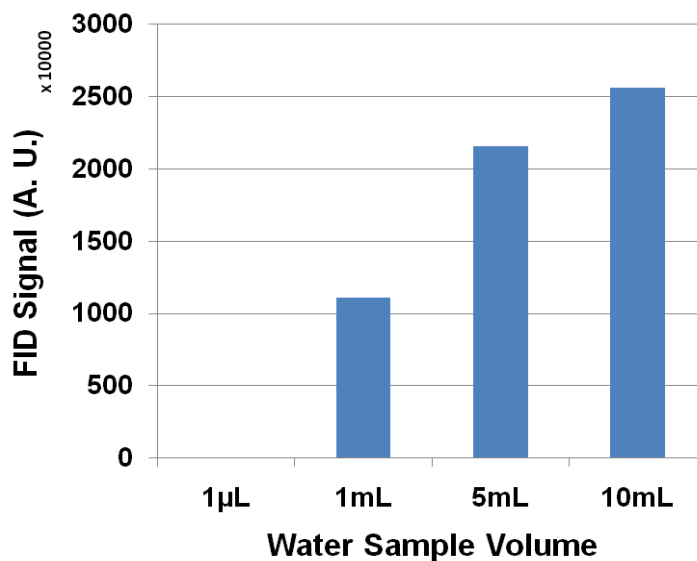


Figure 82 FID response (peak area) to the three different sample volumes along with the 1 $\mu\text{L}$  sample of unpreconcentrated water sample

The reported MEMS device was capable of capturing VOCs from water. This development would be of significant benefit to local authorities, environmental agencies, and environmental researchers as it promises sensitive and quantitative on-site monitoring at a low cost.

### *e. References*

- [1] B. Alfeeli and M. Agah, "Micro Preconcentrator for Handheld Monitoring of Water Quality," in *International Conference on Miniaturized Systems for Chemistry and Life Sciences, MicroTAS'10*, Groningen, The Netherlands, 2010, pp. 1721-1723.
- [2] C. K. Ho, A. Robinson, D. R. Miller, and M. J. Davis, "Overview of Sensors and Needs for Environmental Monitoring," *Sensors*, vol. 5, 2005, pp. 4-37.
- [3] L. Zhu, D. Meier, Z. Boger, C. Montgomery, S. Semancik, and D. L. DeVoe, "Development of a Water Monitoring System Based on Integrated Polymer Microfluidics," in *Solid-State Sensors, Actuators, and Microsystems Workshop, Hilton Head'06*, Hilton Head Island, SC, 2006, pp. 163-166.
- [4] D. S. Blair, "Evaluation of an Evanescent Fiber Optic Chemical Sensor for Monitoring Aqueous Volatile Organic Compounds," Sandia National Laboratories, Albuquerque, NM1997.
- [5] B. Alfeeli, G. Pickrell, and A. Wang, "Sub-Nanoliter Spectroscopic Gas Sensor," *Sensors*, vol. 6, 2006, pp. 1308-1320.
- [6] P. Nolan, "Sandia National Laboratories Annual Report 2003-2004," Sandia National Laboratories, Albuquerque, NM2004.
- [7] P. R. Lewis, P. Manginell, D. R. Adkins, R. J. Kottenstette, D. R. Wheeler, S. S. Sokolowski, D. E. Trudell, J. E. Byrnes, M. Okandan, J. M. Bauer, R. G. Manley, and C. Frye-Mason, "Recent Advancements in the Gas-Phase Microchemlab," *IEEE Sensors Journal*, vol. 6, 2006, pp. 784-795.
- [8] M. Agah and K. D. Wise, "Low-Mass Pecvd Oxynitride Gas Chromatographic Columns," *Journal of Microelectromechanical Systems*, vol. 16, 2007, pp. 853-860.
- [9] S. Ali, M. Ashraf-Khorassani, L. T. Taylor, and M. Agah, "Mems-Based Semi-Packed Gas Chromatography Columns," *Sensors and Actuators B, Chemical*, vol. 141, 2009, pp. 309-315.
- [10] M. A. Zareian-Jahromi and M. Agah, "Microfabricated Gas Chromatography Columns with Mono-Layer Protected Gold Stationary Phases," *Journal of Microelectromechanical Systems*, vol. 19, 2010, pp. 294-304.
- [11] B. Alfeeli and M. Agah, "Low Pressure Drop Micro Preconcentrators with a Cobweb Tenax-Ta Film," in *Solid-State Sensors, Actuators, and Microsystems Workshop, Hilton Head'10*, Hilton Head Island, South Carolina, 2010, pp. 166-169.

A-III. Adsorbent Material Selection

Table 12 Porous Polymer Adsorbent Selection Chart

Physical Properties		Adsorbent		Applications and Selection Guide			
Surface Area	Max Temp	Commercial Name (equivalent or replaceable)	Type	Volatility Range (Carbon & BP)	Suitable Analytes	Features	Weakness/Caution
35	350	Tenax TA	Poly(2,6-diphenyl-p-phenylenoxide)	C6 ~ C26 100 ~ 400°C	Aromatics, nonpolars (BP>150°C), semi volatile polars (BP>150°C). Note: Tenax TA has replaced Tenax GC for lower background signals	Poly (2,6-diphenyl-p-phenylenoxide) polymer. Low surface area, within optimum range, will readily / efficiently release what it adsorbs and can be easily cleaned to a very low background. Inert and does not react with labile compounds. Low inherent artifacts (<1ng). Low affinity for water, hydrophobic	Low breakthrough volume. May form some artifacts when heated, reported sources are: CO2, benzene, toluene, benzaldehyde, acetophenone
24	350	Tenax GR	Poly(2,6-diphenyl-p-phenylenoxide)	C7 ~ C30 100 ~ 450°C	Alkyl benzenes, PAH's (polycyclic aromatic hydrocarbons), PCB's (polychlorobiphenols)	Low surface area. Lower affinity for water than Tenax-TA. Chemical composition: 30% graphite carbon & 70% Tenax TA	Low breakthrough volume
350	250	Chromosorb 102	Styrene/divinylbenzene copolymer	C5 ~ C12 50 ~ 200°C	Wide range of VOCs, oxygenated compounds, haloforms and chlorinecontaining pesticides that has a BP >40°C (less volatile than methylene chloride). Some functional similarities to Amberlite XAD-2	Styrene/ Divinylbenzene (DVB) copolymer. Hydrophobic, inert. Some background at high temp (> 200°C). Note: The polarity of sorbents: Chromosorb 106 < Porapak Q < Chromosorb 102 < Porapak R = Chromosorb 105 < Porapak N < Chromosorb 101 < Porapak P < Chromosorb 103 < Chromosorb 104	Low temperature limit. High artifacts (10ng)
400	250	Chromosorb 107	Polyacrylic ester resin	Up to 150°C	Vinyl acetate, formaldehyde from water and acetylene from lower hydrocarbons. Sulfur compounds. Not recommended for glycols and amines	Cross-linked acrylic ester polymer. Hydrophobic and polar. Note: The polarity of Chromosorb 107/108 increases with their exposure to high temperature (~ 200°C, for example)	Low temperature limit
100	250	Chromosorb 108	Cross-linked acrylic ester	Up to 150°C	Polar small molecules such as alcohols, water, aldehydes and glycols	Cross-linked acrylic. Hydrophobic and polar. See the note above	Low temperature limit
405	165	HayeSep N (Porapak N)	Divinyl benzene/vinyl pyrrolidinone	C5 ~ C8 50 ~ 150°C	Volatile nitriles, e.g. acrylonitrile, acetonitrile, propionitrile. Pyridine, volatile alcohols, ethanol, methyl ethyl ketone	DVB and ethylene glycolmethacrylate (EGDM) copolymer. Polarity 9/10, highly hydrophilic. Porapak polymers are in order of increasing polarity as types P, PS, Q, QS, R, S, N, and T	Low temperature limit. High artifacts ~10ng)
795	290	HayeSep D	High purity Divinyl benzene	Up to 160°C	Low molecular weight compounds, esp. acetylene, halogen, and sulfur groups. CO and CO2 analysis	DVB polymer. Polarity 1/10, highly hydrophobic. Backup for Tenax where carbon based adsorbents are unsuitable. Retains low boiling compounds that breakthrough Tenax, esp. in saturated atmosphere	Low temperature limit. Moderate artifact level at upper temperature limit. High pressure drop

Physical Properties		Adsorbent		Applications and Selection Guide			
Surface Area	Max Temp	Commercial Name (equivalent or replaceable)	Type	Volatility Range (Carbon & BP)	Suitable Analytes	Features	Weakness/Caution
165	250	HayeSep P (Porapak P)	Styrene/divinyl benzene copolymer	Up to 200°C	Esters, ethers, ketones, alcohols, Hydrocarbons, fatty acids, aldehydes and glycols. Not recommended for amines and anilines	DVB/Styrene copolymer. Polarity 3/10. Porapak polymers are in order of increasing polarity as types P, PS, Q, QS, R, S, N, and T	Low temperature limit
582	275	HayeSep Q (Porapak Q)	Ethylvinyl benzene/divinyl benzene	C5 ~ C12 50 ~ 200°C	Some similarities to Chromosorb 106. Not for amines and anilines, not for nitric oxides	DVB polymer. Polarity 2/10, hydrophobic. Porapak polymers are in order of increasing polarity as types P, PS, Q, QS, R, S, N, and T	Low temperature limit. High artifacts, nitrated by nitrogen oxide gases
344	250	HayeSep R (Porapak R)	Divinyl benzene/vinyl pyrrolidinone	Up to 200°C	Match the polarity of the analyte to the polarity of the sorbent, while covering the boiling temperature. Esters, ethers, nitriles and nitro compounds. Not recommended for glycols and amines	DVB/N-vinyl2-pyrrolidone (NV2P) copolymer. Polarity 5/10, both hydrophobic and hydrophilic. Porapak polymers are in order of increasing polarity as types P, PS, Q, QS, R, S, N, and T	Low temperature limit
583	250	HayeSep S (Porapak S)	Divinyl benzene/vinyl pyridine	Up to 200°C	Match the polarity of the analyte to the polarity of the sorbent, while covering the boiling temperature (Amines, amides, alcohols, aldehydes, hydrazines and ketones, Not for acids, glycols and nitriles)	DVB/4-vinyl-pyridine (4VP) copolymer. Polarity 4/10, both hydrophobic and hydrophilic. Porapak polymers are in order of increasing polarity as types P, PS, Q, QS, R, S, N, and T	Low temperature limit. Reacts with nitroalkanes